Development and application of bundle-valued forms in the hybrid mimetic spectral element method

Applications to linear elasticity

Revanth Kollegala Sharma

Delft University of Technology

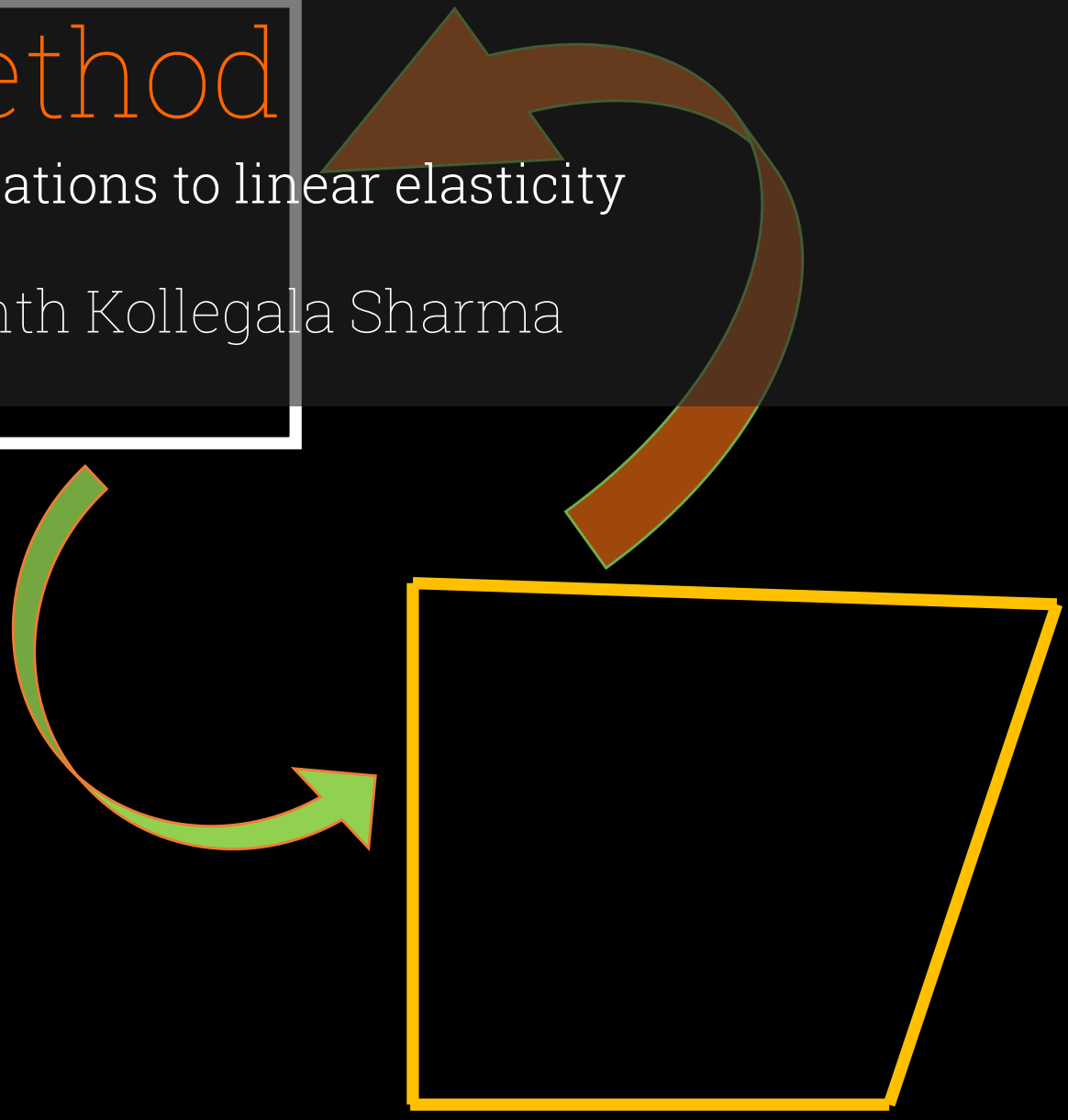

TU Delft

Development and application of bundle-valued forms in the hybrid mimetic spectral element method

Applications to linear elasticity

by

Revanth Kollegala Sharma

to obtain the degree of Master of Science
at the Delft University of Technology,
to be defended publicly on September 22, 2023 at 10:00 AM

Student Number:	5250587	
Project Duration:	August 1, 2022 – September 22, 2023	
Faculty:	Faculty of Aerospace Engineering, Delft	
Supervisor:	Dr.ir. M.I. Gerritsma	TU Delft
Thesis Committee :	Dr. A. Palha	TU Delft, External
	Dr. B. Chen	TU Delft
	Dr.ir. A.H. van Zuijlen	TU Delft

TU Delft

Acknowledgements

This thesis would not have happened if I was not made aware of how fundamental aspects of aerodynamics could be looked at with a different perspective, through the course on mimetic discretizations for computational fluid dynamics taught by Dr. Marc Gerritsma. All of his motivation, and dedication throughout the online classes motivated me to work with mimetic methods for my thesis work.

Dr. Marc Gerritsma has always been supportive throughout. He was always willing to help, there whenever I was stuck. This thesis work would not have been possible without his dedication and him nurturing and developing my creativity throughout, with great enthusiasm too. I thank him for his guidance, both for this work and beyond.

My parents, Shobha & Sharma have always been the kind who believe that no amount is caution is too much, especially when it comes to their kids. Thanks Appa and Amma for being supportive throughout my studies and all my adventures during my Masters. I am convinced that my sister, Revathi, is the best elder sister in the universe, not only for being a source of inspiration and a companion on several of these adventures but also because of how bold and fearless she is. Thanks Akka for everything. I would also like to thank all my aunts, uncles, grandma and my brother-in-law Michael for making home feel truly like home.

Srijit, Pratik, and Siddharth were the first like-minded people I encountered, where we managed to turn assignment-stress into fun and laughter. I want to thank them for all these times, but also for the fun and chaotic times we had playing cricket and enjoying some heavenly dishes, also because I wouldn't be able to graduate without all the work we put in, and the knowledge we gained together.

I would also like to thank all the exchange students I met during the Autumn and Summer of 2023, although I may have graduated earlier if not for all the fun we had. Special mention to Chiara, Nico and Carmen for being legends, and everyone else for bringing their creativity and wit into all interesting discussions we had at odd times. Thanks for all the movie nights, and making this time memorable.

Special mention to my legendary roommates Luís, Naeem, Sara, Filippo, Simona and Ariele. I have become used to dinner being so fun, and I can't remember a time when I did not look forward to coming back to my comfort place, even when it was pouring outside. Thanks for all the Catan games, and all the singing and dancing in the kitchen.

Anish, Iva, Tarun and Ansh have been a constant part of my Masters journey. I want to thank them for all the times we played board games even with online classes and went on trips across the continent. Along with Vivek, there were a lot of times when memories were made over train journeys and amazing food. Thanks for everything.

Lastly, I would like to thank Parinith and Keerthi for confirming that not only can friendships last years, but also that they remain halfway across the world, while bringing a slice of home to life in the Netherlands. Thanks to also all my friends in India, who treated me the same way as before when I briefly went back.

I am truly happy at this moment and am excited to see what is in store for me in the future.

Revanth Kollegala Sharma
Delft, September 2023

Abstract

One of the novel methodologies in computational physics research is to use mimetic discretisation techniques. Among these, the mimetic spectral element method holds special promise as it not only has the benefits of mimetic methods but also the additional benefit of higher-order discretisations using higher polynomial degrees. These methods are aided by the development of algebraic dual polynomials, resulting in a sparser system for better computational efficiency. This combination was used to develop a formulation that would result in topological relations for equilibrium of forces as well as the symmetry of the stress tensor for linear elasticity as well as the first steps for Stokes flows in an orthogonal domain. As a result, this study was extended to look at how a modified formulation would behave for an unsteady linear elastic solid, with the intention to extend this method to Fluid-Structure Interaction cases. However, the choice of both primal and nodal basis functions makes it impossible to undertake this challenge, demanding a rethink in strategy towards looking at linear elastic solids when the physical domain is not orthogonal. With the use of bundle-valued forms to represent physical quantities, a new hybrid formulation is developed where the equivalent of the physical problem is computed on a reference domain, which is orthogonal and thus can utilise the spectral bases defined before. The physical problem is defined on a skewed domain, where partial transformation of components results in a formulation that can conserve linear momentum point-wise, but not conservation of angular momentum, although angular momentum does converge on refinement of polynomial degree and mesh parameters. A change in bases with partial transformation aiming to make angular momentum conservation topological is not fruitful, although the value of the error decreases in the process. The final attempt is through full transformation, which results in a formulation with an inherent error in the formulation, owing to erroneous assumptions.

Contents

List of Figures

1 Introduction

With the development of computer hardware and improvements in accessibility and availability of this computational resource, numerical simulations are taking the forefront in simulation and engineering [55]. For development of technology across various fields, experiments are usually much more expensive, and may not be accessible to everyone, compared to computational approaches. However, experimental verification is still a necessity owing to the various errors with numerical approaches that results in losses in accuracy of various proportions. Some of these errors can be so large that they might not even make physical sense. In an effort to conserve the underlying physics of a problem, there has been a increase in various techniques of discretisation which are mimetic, that is mimicking the physics, like in [2, 27, 49]. By considering how the physics of the problem can be associated to the geometric content within the problem, these methods try to convert these into solvable equations. In such a discretisation, the quantities are connected to the geometry by representing the integrated values over various geometrical quantities, and not just a random representation at a point. As a result of these, the discrete representation of these quantities should still be able to conserve the physical relations just like their continuous counterparts [27], which will lead to improvements in accuracy and a better approximation of the physics behind the problem. However, the accuracy can still be improved if the geometric component that the physical quantity is associated to, is complicated to model on its own. In an attempt to further improve accuracies, there is an option to convert all these quantities into a reference or computational domain, where computational properties of the method can be exploited. With spectral elements to give a high-order method, mimetic spectral element method finds one application here.

1.1. Motivation

Taking the example of linear elasticity, the problem can be separated into physical relations and constitutive relations. For linear elasticity,

$$\nabla \cdot \underline{\underline{\boldsymbol{\sigma}}} + \mathbf{f} = 0, \tag{1.1}$$

$$\underline{\underline{\boldsymbol{\sigma}}} = \underline{\underline{\boldsymbol{\sigma}}}^T, \tag{1.2}$$

$$\nabla \mathbf{u} = \frac{1}{2}\left(\nabla \mathbf{u} + (\nabla \mathbf{u})^T\right) + \frac{1}{2}\left(\nabla \mathbf{u} - (\nabla \mathbf{u})^T\right) = \underline{\underline{\epsilon}} + \omega, \tag{1.3}$$

where $\underline{\underline{\boldsymbol{\sigma}}}$ represents the Cauchy stress tensor, $\mathbf{f}$ represents the body force, and $\mathbf{u}$ denotes the displacement vector. The first equation denotes the conservation of linear momentum, which when combined with the second equation will also conserve angular momentum. The third equation represents the compatibility relation between the gradient of displacement with the strains and the rotation tensor. All of these are physical laws, which need to be conserved. On the other hand, there is another relation used in linear elasticity, which relates quantities in these equations,

$$\underline{\underline{\mathbf{C}}}\underline{\underline{\boldsymbol{\sigma}}} = \underline{\underline{\epsilon}}, \tag{1.4}$$

which is called the constitutional law for linear elastic solids, where $\underline{\underline{\mathbf{C}}}$ is the compliance tensor. This is a relation that was obtained empirically. An empirical relation will also have tolerances from the experiment built

into the relation, and would be the source of the error in the formulation. On the other hand, the divergence of the stress tensor is a mathematical quantity that cannot be different whether the formulation is discrete or continuous. Similarly, the symmetry of the stress tensor, and the operations of gradient of displacement do not change in the discrete formulation too. Similarly, the body forces mentioned may not be exact, as it is defined on a point. The boundary conditions too may be approximated.

Thus, an ideal discretisation would separate the two different kinds of equations, the ones which are exact and metric-independent, and the constitutional laws themselves. However, this is not a prerequisite to design methods to solve partial differential equations which model continuum phenomena. With the finite difference method, the idea begins with a conveniently-drawn, structured stencil that is used to approximate derivatives from values at various points in this stencil. Taylor expansions are used to analyse the discretisation error from different schemes, while nowhere it is suggested to look at how the physics can be maintained discretely. A finite volume method deals with fluxes through the edges of the cell, and although it is a great way to approximate the divergence theorem more naturally (by balancing the fluxes through the cell), exact relations may not be maintained when the constitutive relations are introduced, such as for example, the calculation of the fluxes themselves. Even in finite element methods, although this can be applied to a wider selection of meshes and structures, there might not be separation of exact quantities and the ones which contain the metric. The reason can be attributed to physical quantities not being associated to relevant geometrical elements [27]. In case of the finite element method, arbitrary test and basis functions should not be used to model physical quantities, when these quantities have natural structures [63]. These representations can also lead to non-physical modes, which are numerical errors caused by formulations which cannot mimic the continuous operators in the discrete scenario. All of these reasons are the motivation to work on methods which will try to enforce those relations which should be satisfied, regardless of whether the problem is formulated in the physical domain or the computational domain.

1.2. Thesis outline

The aim of this research is to look at extending the mimetic spectral element method towards unsteady methods, starting with linear elasticity. This would be the first step taken towards looking at Fluid-Structure Interaction problems, in particular, looking at the linear elasticity problem through the Lagrangian perspective. The main question that will be answered is:

> **"Is it possible to extend the hybrid mimetic spectral element method towards broader applications, by transforming physical problems into computations on a reference domain, such that both linear momentum and angular momentum is strongly conserved?"**

This thesis involves taking several steps toward something new, as well as several steps backwards to understand the causes for the errors. Who built the framework, and what was the reasoning behind it? What are the mathematical and physical concepts behind the mimetic spectral element method? What problems were successfully solved, and which ones could not be formulated accurately? Which formulations were successfully hybridized, and how? Could the quantities and equations be transformed accurately onto a computational domain for better calculations, and if so, what are the considerations for a feasible transformation? In each part of the thesis, answers to many of these questions are found. Overview of the thesis is shown in Figure 1.1.

The work starts with looking at an overview of how the mimetic methods came into being, by understanding concepts from exterior calculus, algebraic topology, which along with vector- and covector-valued forms lead to a mimetic discretisation. A brief look through some of the research conducted in this domain is presented and its relevance to the topic is explained in Chapter 2. This also includes a brief history of the research conducted using the mimetic spectral element method.

With the motivation and the previous research understood, the mathematics behind several concepts in the thesis should be understood. Starting from the notation and the basic operators used in the mimetic spectral element method, the applications of these are explained using a test example. The use of mappings are also explained, along with the use of Lagrangian functional to set up problems. The grid generation and how components of the Jacobian are computed are also mentioned. These concepts are mentioned in Chapter 3.

The research into extending the formulation in [65] is undertaken with the first foray into Unsteady Linear Elasticity, in Chapter 4. Then, a new way to look at the Poisson problem is looked at in Chapter 5. Using ideas from the Poisson problem, several different formulations of Linear Elasticity are tested in Chapter 6, Chapter 7 and Chapter 8. In all these chapters, the quantities are described first in the physical domain, and how they are transformed when in the computational domain. A similar comparison is done for the conservation laws. Results are analysed and error analysis is done for every chapter, with detailed observations in every case study. In the end, there are directions to continue this thesis work for future applications.

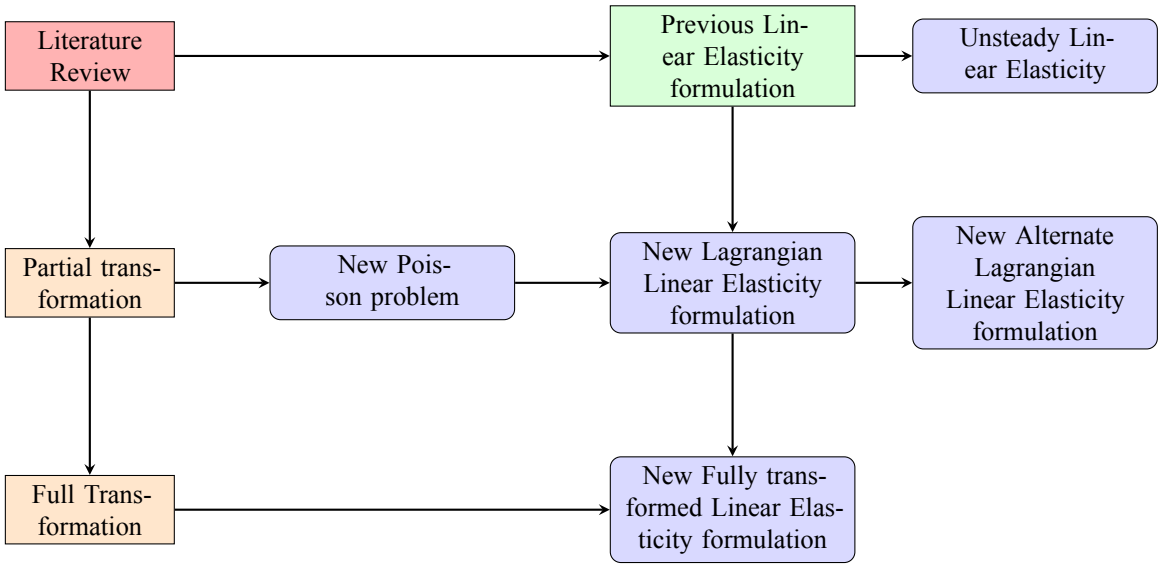

Figure 1.1: Outline of the thesis

2

Literature review

This chapter looks at why concepts from exterior calculus and algebraic topology are applied to physics. In this way, the ideas leading to the birth of mimetic discretisation are looked at. How algebraic topology provides answers for extension of theories from the continuous domain to the discrete environment is answered. More questions on how a mimetic spectral element method fulfills the requirements for a mimetic discretisation, and why this method was chosen are explained. The history of the mimetic spectral element method is also scrutinised, with choices for future formulations being made along the way.

2.1. Motivation for development of Mimetic methods

This section helps to identify why mimetic discretizations were conceived, and what motivated the process. This starts from the application of concepts learnt in algebraic topology and exterior calculus to physics. In particular, how to extend the application of algebraic topology to discrete applications is discussed. The operations on differential forms then lead to the ingredients for a mimetic discretization. More details are given on these areas with the backdrop of how they are implemented in the mimetic spectral element method. To extend these ideas into Fluid-Structure interactions and other unsteady problems like Navier-Stokes equations, there are several nuances discussed with respect to each case study that needs to be performed.

2.1.1. Overview

Connecting the description of physics to notion of exterior calculus was performed initially by [61] and [20]. It is through these ideas that methods of mimetic discretisation came into being. The concepts have been improved and motivated recently through [10] and [58], Mattiussi used these to extend theories into electromagnetism [43]. Further, [5] looks into the mathematical theory of differential operators, along with [34], which works on the Hodge operator, and [54] which is on applying these concepts to tensors. Several implementations were made using these, some of which are [2, 3, 13, 39, 41, 48, 49, 65] among others.

Research into exterior calculus was performed through Grassmann (in exterior or Grassmann algebra), Poincaré (homology and duality), and Cartan (differential geometry). The connection between physics and exterior calculus was conceptualised early on through [24].

Exterior calculus deals with differential forms, which are field quantities associated to geometry. This gives rise to a geometric description of physics. The argument put forward is that this description of physics is advantageous to actually deal with vector or tensor calculus for fluids. The language of algebraic topology is readily available to write down the concepts in exterior calculus as a discrete method [5].

This chapter thus will look at the various findings and how this leads or motivated the search and development of new mimetic methods. The first part looks at how new ideas originated and why they provided a better alternative to the vector calculus, as argued by [63]. Following this, there is a discussion on the use of differential forms, and an overview of the construction of De Rham complexes. The final piece of the puzzle is to make a connection between algebraic topology and discrete methods.

2.1.2. Physics using Geometry

When dealing with differential equations, it is easy to see that for simple cases an exact analytical solution can be computed. When doing this, it is implicitly assumed that these are happening in the mathematical notion of a limit,

which is how the differential equations are formulated in the first place. However, numerical computations are always approximations and thus any numerical method deals with set tolerances. This means that it is impossible to reach the idealised mathematical notion of a limit when numerically calculating solutions.

However, one should not be discouraged by this complication. In fact, as mentioned in [63] all experimental measurements made are in fact discrete in nature, not just those made in computational experiments. This is why there is an experimental *tolerance* not a limit when running experiments. In this scenario, it is implied that the error from running virtual experiments should be lower than the tolerances used by similar experiments conducted in the real world. It should also be noted that the limiting process, is also a something done mentally, that takes us away from real measurements. Thus, it makes sense to remain in the algebraic domain, as suggested by [63].

To put theories into practice, [63] suggests that instead of looking at variables as *field* quantities, where the quantities are defined at a point, it is better to look at *global* variables. While the field variables are obtained after applying the limiting process to adapt to the differential formulation, the global variables are easy to understand as they are associated with a geometrical aspect of space, which can be lines, surfaces or volumes. The field variables are used only because the differential equations are easy to define and written that way, which is under the mathematical limit. The usage of global variables for computational physics is akin to taking physical measurements, in the sense that there is a finite tolerance that is taken into the measurement by design. [63] also argues that the association between geometrical elements and the global physical variables themselves are essential for computational physics. In fact, it is important to look at the development of these aspects *before* the application of the limiting process and writing down the differential formulation.

To do this, one should look at how to define separate global quantities into *source* and *configuration* quantities as well. The source variables are those which are the causes of a phenomenon, like forces are the sources of displacement and deformation, while the configuration variables are those which shows how the system has changed due to the action of the source variable (here the positions of particles change due to the action of the force). This simplifies procedures when tackling physical problems, because the source variables are related to other source variables through differentials or integrals or by finding out the density, and without the need for any physical constant. Thus, similar source variables can be related to each other topologically. Similarly, configuration variables can also be related topologically. However, the relation between a source variable and a configuration variable is not topological and results in the use of a metric, as seen in [27].

The idea of coupling physical computations to geometry could be attributed to Tonti [61], who discusses the similarities between existing physical theories to geometrical aspects. These physical theories need not be limited to mechanics or fluid dynamics, but can also have applications in electromagnetism. The quantities to be computed based on these physical theories, can be assigned to two different geometrical sets, also called as cell complexes. These are referred to as the primal and dual complexes as mentioned in [63]. There is still the need to understand how various physical quantities are represented on geometric components. For a better visual representation, the positioning of these quantities are written in a classification diagram (or Tonti diagram). Note that the variables on the dual domain are represented with a tilde, while the variables on the primal domain are without one. If these diagrams already have physical laws written in them, it is called a factorisation diagram, as compiled by [43], which is shown in Figure 2.1. Several physical phenomena can be represented using these diagrams, with most of them mentioned in [62]. These diagrams help us to understand that there are symmetries that already exist in the physical system. The important part these diagrams play is that topological relations can be used when you are working with quantities on either primal or dual complexes, which means that these relations will be exact. Only when you are relating the primal complex with the dual complex (using constitutive relations) that you see the metric approximations playing a role. If source variables would be represented on the primal components and the configuration variables on the dual components (or vice versa), these properties of the domains can be used to mimic physical laws as well.

Regarding these complexes, one should also consider how these complexes are *oriented*. Tonti [63] shows that this orientation of complexes plays an important role in classifying physical variables. There are two kinds of orientation of these complexes, inner and outer. The inner orientation concerns the direction within or along geometric objects, while the outer orientation concerns directions through and around objects. These two orientations are assigned to a primal and dual complexes. The choice for the orientation for the cell complexes are arbitrary, however they should be consistent and distinguished from each other. Although there is no predefined order, [63] recommends using the outer orientation for source variables, while the configuration variables will then be on the inner orientation. The depictions of these orientations on geometric objects are shown in Figure 2.2.

Note that for $\mathbb{R}^3$, the fluxes will be assigned to a surface, which is different to the circulation which is assigned to lines. There is also a difference between values in points, like temperature or displacement, and values that are assigned to the volume, like total energy or mass [49]. From a fluid dynamics perspective, it is important to note

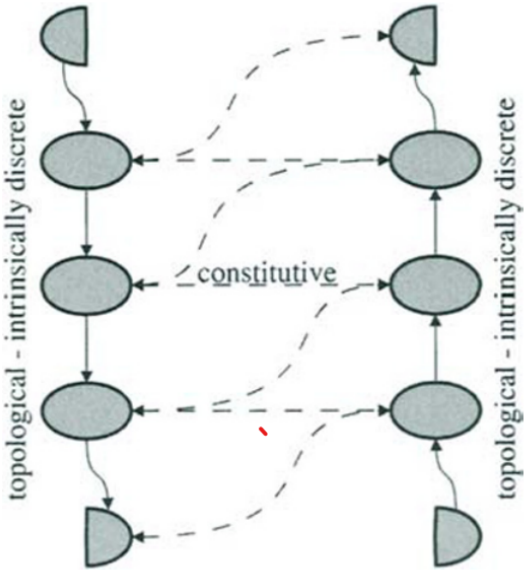

Figure 2.1: Factorisation diagram as in [43]

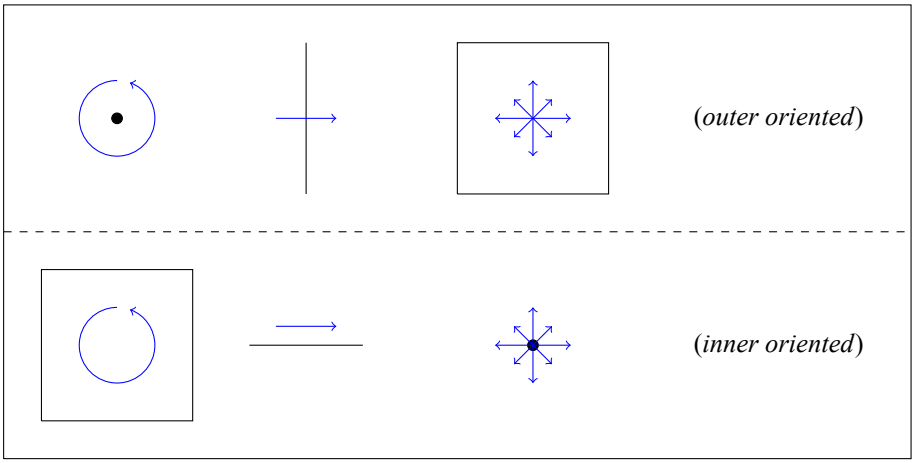

Figure 2.2: Denoting the two different orientations of geometric objects in $\mathbb{R}^2$

that the velocity can be viewed in inner orientation as the circulation, which is the integral of the velocity along a line. Alternatively, the velocity is also written as the flux in the outer orientation, where it is integrated over the surface. This shows that the orientation can be used as a device to find the correct interpretation of physical quantities.

It can be that seen different quantities are represented using different orientations, but can be related to the same velocity as mentioned. For example, the sum of the circulations around an enclosed surface will be the rotation or vorticity, which is in the inner orientation. However, the sum of the fluxes through an enclosed volume will be the divergence of the velocity, which is determined using the outer orientation. For solid statics or solid dynamics, the displacement acts as the analogue to velocity for fluid dynamics, and the displacement can be integrated over a line in the inner orientation, or over a surface to get to the outer orientation.

It is also important to note that this is not the only way that velocity can be assigned to geometrical components. A better representation, which is used in most of the thesis work, is when displacement or velocity is assigned to points, depending on which vector component it belongs to. In this scenario, there are n different outer-oriented and n corresponding inner-oriented cell complexes, each for a different component of the vector in n dimensions. Thus, the displacement vector $\mathbf{u}$ in $\mathbb{R}^2$ having components u_x and u_y along x- and y- directions respectively, will have u_x and u_y on points, but not along the same points. Keep in mind that this is not just the scalar part u_x that is assigned to the points, but it is also the direction that is assigned to these points. These are called fibres of the vector, that is assigned to these points. Since this involves two different representations in $\mathbb{R}^2$, this is called a *vector-valued* representation. In this case, the vectors whose value is incorporated into the cell-complexes are the cartesian basis vectors themselves. Unlike displacements mentioned here, these vector fibres can be assigned to other geometrical components, For example, later you will see how fibres of the stress tensor are assigned to surfaces in linear elasticity formulations. There is more on these vector-valued representations in [26]. In particular, this representation can be helpful in representing tensors like the stress tensor, where for each vector component in $\mathbb{R}^n$, the tensor components can be associated with different surfaces. With this, the component of the divergence of stress along that vector component can be easily calculated as the sum of the fluxes through those surfaces. This can be carried out for other components of the divergence of the stress as mentioned in [26, p. 618].

2.1.3. Forms for physics

While it is easy to explain how quantities can be associated with geometrical objects, it is also necessary to make a clear distinction between the physical quantities and the geometries they are linked to. This relationship between quantities and geometric objects is crucial to designing a mimetic discretization framework or problem. There is no need for a distinction when you are considering conventional vector calculus, which makes it more important to write down the distinction for computational methods.

Flanders [25, p. 1] introduces differential forms as "the things which occur under integral signs". However, these are better explained by Hiptmair [34, p. 266], as "mappings assigning values to oriented manifolds of different dimensions". The reason for using manifolds here is that there is no strict constraint on a manifold, apart from it being a n-dimensional description of space. The Euclidean space is the familiar, but particular kind of manifold, as mentioned in [26, p. 3]. When dealing with manifolds, there is no need to define a metric associated with it [26, p. 18]. That is why forms are associated with manifolds, instead of the Euclidean space. Thus, the relations between forms are metric-independent. A form is represented by all quantities of the same dimension, and cannot be isolated to a single component of geometry. For example, a form can be represented by all lines, or all surfaces, or all points etc., as mentioned in [48]. To describe these forms, functions are associated to the geometric basis, which are called *vector proxies*. These proxies are the only parts considered in vector calculus, as mentioned in [27].

There is a subtle difference between these exterior forms and differential forms, which are used to describe physical quantities. Exterior k-forms are k-linear and anti-symmetric mappings from k-dimensional vector space to the space of real numbers [6]. That is, if $\alpha^{(k)}$ is a k-form on a vector field $\mathcal{V}$, then

$$\alpha^{(k)} : \underbrace{\mathcal{V} \times \cdots \times \mathcal{V}}_{k \text{ copies}} \to \mathbb{R},$$

with

$$\alpha^{(k)}(\ldots, v_i, \ldots, v_j, \ldots) = -\alpha^{(k)}(\ldots, v_j, \ldots, v_i, \ldots), \quad v_i \in \mathcal{V},\ i = 1, \ldots, k.$$

Because these forms are linear, addition and subtraction are easily done. Using the exterior product, the

multiplication of these forms can also be accomplished, however, one should keep in mind that the resulting forms will have $k \leq n$. The wedge product uses two forms to produce another form. For example, a multiplication between a k-form and an l-form results in a $(k+l)$ form. Keep in mind that for this operation to happen, $1 \leq (k+l) \leq n$.

$$\left(\alpha^{(k)} + \beta^{(l)}\right) \wedge \gamma^{(m)} = \alpha^{(k)} \wedge \gamma^{(m)} + \beta^{(l)} \wedge \gamma^{(m)}, \quad \text{(Distributivity)}$$

$$\left(\alpha^{(k)} \wedge \beta^{(l)}\right) \wedge \gamma^{(m)} = \alpha^{(k)} \wedge \left(\beta^{(l)} \wedge \gamma^{(m)}\right) = \alpha^{(k)} \wedge \beta^{(l)} \wedge \gamma^{(m)}, \quad \text{(Associativity)}$$

$$a\alpha^{(k)} \wedge \beta^{(l)} = \alpha^{(k)} \wedge a\beta^{(l)} = a\left(\alpha^{(k)} \wedge \beta^{(l)}\right), \quad \text{(Multiplication by functions)}$$

$$\alpha^{(k)} \wedge \beta^{(l)} = (-1)^{kl}\beta^{(l)} \wedge \alpha^{(k)}. \quad \text{(Skew symmetry)}$$

These exterior forms represent components of geometry spanned by vectors in the Euclidean space $\mathbb{R}^n$. Differential forms, however, are an application of these exterior forms to more general differentiable manifolds through the definition of the tangent vector. This means that the differential forms inherit the properties of the exterior forms too. The differential form possesses an exterior form part, that transforms combinations of tangent vectors to values, and a proxy part that applies a spatially varying modification of the value [6]. Apart from these operators, the differential form also introduces the operations of differentiation and integration. We should keep in mind that these forms cannot be 'seen' directly. Only its action on elements can be observed. In this case, $\alpha^{(k)}$ can be better understood by applying to various elements b which belong to the vector space. A similar analogy applies to physical variables too, only the action of the force is observed. Nobody has seen 'force' without looking at how work is done by it. This is also one of the reasons why it is natural to represent physical variables using forms.

Differential forms, as explained in [48] are summarised here. Any vector $\mathbf{v}$ in a vector space $\mathcal{V}$, located on a point p in a manifold $\mathcal{M}$ can be expanded using a linearly independent basis, using basis vectors from a vector space. The tangent vector is the derivative at p on a curve through p contained within $\mathcal{M}$. With an n-dimensional manifold, a basis of n tangent vectors can be constructed through this point, associated to n curves. These form the tangent space $\mathcal{T}_p\mathcal{M}$, which is also a linear vector space. By collecting all the tangent spaces $\mathcal{T}_p\mathcal{M}$ at all points p in $\mathcal{M}$, a tangent bundle $\mathcal{T}\mathcal{M}$ can be constructed.

A dual vector space $\mathcal{V}'$ can be associated to the vector space $\mathcal{V}$. This dual space contains co-vectors $\gamma \in \mathcal{V}'$, which are linear functionals acting on vectors $\mathbf{v} \in \mathcal{V}$. These are nothing but the exterior forms acting on the basis vectors. These co-vectors can be formulated in the dual of the tangent space, in a similar way as done for the vector space $\mathcal{V}$, since the tangent space $\mathcal{T}_p\mathcal{M}$ is always a linear vector space. This is then called the cotangent space, $\mathcal{T}_p^*\mathcal{M}$. The collection of these cotangent spaces at all points results in the cotangent bundle. A section of this cotangent bundle is the differentiable 1-form or basic 1-form [48], denoted in this report as $\mathrm{d}x$ and $\mathrm{d}y$ in $\mathbb{R}^2$.

A differential form which is defined at every point in $\mathcal{M}$ for an associated geometrical element of dimension k, is called a k-form on $\mathcal{M}$ [6]. These forms are anti-symmetric tensors. Starting from the basic 1-forms, the wedge product is used to construct higher-order forms. The space of k-forms is denoted by $\Lambda^{(k)}(\Omega, \mathbb{R})$, where the $\mathbb{R}$ indicates that the form is real-valued. The 2-form is created by the wedge product of two basic 1-forms. Starting from the 0-forms, there are thus $(n+1)$ different differential forms possible in n dimensions.

For simplicity, let us assume that Ω denotes a manifold. When basis forms are 'wedged' together, the operation can be assumed to be a mapping, where the $\wedge$ operator takes two different forms and produces another form [27]. Thus,

$$\wedge : \Lambda^{(k)}(\Omega, \mathbb{R}) \times \Lambda^{(l)}(\Omega, \mathbb{R}) \to \Lambda^{(k+l)}(\Omega, \mathbb{R}).$$

This wedge operation is metric-independent if it is performed on the same manifold. As mentioned before, the wedge product is skew-symmetric, which means that the sign changes if the order changes. The anti-symmetry also means that the wedge product of two equal components is zero. Specifically for basis forms, it can be written as [27]

$$\mathrm{d}x \wedge \mathrm{d}x = -\mathrm{d}x \wedge \mathrm{d}x = 0,$$
$$\mathrm{d}x \wedge \mathrm{d}y = -\mathrm{d}y \wedge \mathrm{d}x.$$

With this work being restricted to $\mathbb{R}^2$, the inner-oriented forms (as mentioned in [27]) are denoted using the basis forms for $k = 0, 1, 2$ respectively as,

$$\begin{aligned}\alpha'^{(0)} &= \overline{a}(x,y),\\ \beta'^{(1)} &= \overline{b_1}(x,y)\mathrm{d}x + \overline{b_2}(x,y)\mathrm{d}y,\\ \gamma'^{(2)} &= \overline{c}(x,y)\mathrm{d}x\mathrm{d}y.\end{aligned}$$

Note that $\mathrm{d}x \wedge \mathrm{d}y$ is shortened to $\mathrm{d}x\mathrm{d}y$ The prime indicates that the inner-oriented forms are taken to be in the dual space here. The functions of (x, y) are the vector proxies mentioned previously. These are just written to denote the analogy to vector calculus, where these represent physical quantities. The geometrical connection can be further understood when you look at integrating these forms, which shows the concept of *duality pairing*. The integration of these forms are done over points $\mathcal{P}$, a line $\mathcal{L}$ or a surface $\mathcal{S}$ respectively, as written in [27].

$$\begin{aligned}\int_{\mathcal{P}} \alpha'^{(0)} &= \sum_{\mathcal{P}} \overline{a} = \left\langle \alpha'^{(0)}, \mathcal{P} \right\rangle,\\ \int_{\mathcal{L}} \beta'^{(1)} &= \int_{\mathcal{L}} \overline{b_1}(x,y)\mathrm{d}x + \overline{b_2}(x,y)\mathrm{d}y = \left\langle \beta'^{(1)}, \mathcal{L} \right\rangle,\\ \int_{\mathcal{S}} \gamma'^{(2)} &= \int_{\mathcal{S}} \overline{c}(x,y)\mathrm{d}x\mathrm{d}y = \left\langle \gamma'^{(2)}, \mathcal{S} \right\rangle.\end{aligned}$$

The idea can be extended further by assigning vector fibres instead of vector proxies to these forms. These result in the vector-valued forms mentioned in the previous section [52]. Similar to the representation for real-valued forms, the space of vector-valued k-forms is written as $\Lambda^{(k)}(\Omega, \mathcal{T}\Omega)$. As an example, let $e_x = \frac{\partial}{\partial x}$ be a vector in the x-direction. Then the inner-oriented forms in the x-direction can be written as

$$\begin{aligned}\alpha'^{(0)}_x &= \frac{\partial}{\partial x} \otimes \overline{a}(x,y),\\ \beta'^{(1)}_x &= \frac{\partial}{\partial x} \otimes \left(\overline{b_1}(x,y)\mathrm{d}x + \overline{b_2}(x,y)\mathrm{d}y\right),\\ \gamma'^{(2)}_x &= \frac{\partial}{\partial x} \otimes \overline{c}(x,y)\mathrm{d}x\mathrm{d}y.\end{aligned}$$

where $\otimes$ indicates the tensor product. Similarly, vector-valued forms with $e_y = \frac{\partial}{\partial y}$ as the vector-value can also be assigned to points, lines and surfaces respectively.

With the assumption of assigning vector fibres to geometrical quantities, the idea of assigning fibres of covectors (defined previously) naturally follows [52]. Let the basic 1-forms or covectors be denoted as $e^x = \mathrm{d}x$, along the x-direction. Then, the corresponding inner-oriented *covector*-valued forms can be written down as,

$$\begin{aligned}\left(\alpha'^{(0)}\right)^x &= \mathrm{d}x \otimes \overline{a}(x,y),\\ \left(\beta'^{(1)}\right)^x &= \mathrm{d}x \otimes \left(\overline{b_1}(x,y)\mathrm{d}x + \overline{b_2}(x,y)\mathrm{d}y\right),\\ \left(\gamma'^{(2)}\right)^x &= \mathrm{d}x \otimes \overline{c}(x,y)\mathrm{d}x\mathrm{d}y.\end{aligned}$$

Similarly, covector-valued forms with $e^y = \mathrm{d}y$ as the covector-value can be constructed. In general, the space of covector-valued k-forms can be represented by $\Lambda^{(k)}(\Omega, \mathcal{T}^*\Omega)$. These vector-valued forms and covector-valued forms are collectively referred to as bundle-valued forms.

2.1.4. De-Rham complexes

The first step to show that these differential forms and bundle-valued forms can be related to the theory from Tonti, is by defining how forms can be differentiated. This can be accomplished using the *exterior derivative*, which is maps forms as [27],

$$\mathrm{d} : \Lambda^{(k)}(\Omega) \to \Lambda^{(k+1)}(\Omega)\ , k < n.$$

Depending on the value of k, the exterior derivative can behave like the gradient, curl or divergence operator. This comes from the duality pairing of a form on the boundary and its derivative in the enclosed manifold by this boundary [48],

$$\int_{\mathcal{M}_{k+1}} \mathrm{d}\lambda^{(k)} = \int_{\partial\mathcal{M}_{k+1}} \lambda^{(k)}.$$

This relation is better known as the (Generalised) Stokes Theorem [27], also written in [24, p. 2] as the general Stokes' formula. This relationship is also seen in the use of the exterior derivative, where it is linked to the geometry through the duality pairing as [27, 48]

$$\left\langle \mathrm{d}\lambda^{(k)}, \Omega \right\rangle = \left\langle \lambda^{(k)}, \partial\Omega \right\rangle.$$

Some of the applications of this theorem are the well-known Newton-Leibniz or Gradient theorem, Gauss' or Divergence theorem, and the Kelvin-Stokes or Curl theorem. The generalised Stokes theorem thus unifies all of these relations in a single theorem [39]. The exterior derivative is also metric-independent and nilpotent [48]. This means for any differential form $a^{(k)}$, $\mathrm{d}\mathrm{d}a^{(k)} = 0$, which are analogous to $\nabla \cdot \nabla \times \mathbf{a} = 0$ or $\nabla \times \nabla a = 0$, depending on what k is, thus obeying these well-known identities from vector calculus.

This means that the exterior derivatives of the inner-oriented differential forms introduced before can be written as

$$\begin{aligned}
\mathrm{d}\alpha'^{(0)} &= \frac{\partial \overline{a}}{\partial x}\mathrm{d}x + \frac{\partial \overline{a}}{\partial y}\mathrm{d}y, \\
\mathrm{d}\beta'^{(1)} &= \left(-\frac{\partial \overline{b_1}}{\partial y} + \frac{\partial \overline{b_2}}{\partial x}\right)\mathrm{d}x\mathrm{d}y, \\
\mathrm{d}\gamma'^{(2)} &= 0.
\end{aligned}$$

The result of the exterior derivative on forms is the same as how scalars, vectors and pseudo-vectors are transformed by the gradient, curl and divergence operations. For the exterior derivative, like the wedge-product, $(k+1) < n$. This means that the derivative on a n-form will lead to the null space.

A similar operation can be performed on vector- and covector-valued forms too. However, there is a small difference from the exterior derivative itself. Because there is a value that the form is associated with, for vector- and covector-valued forms, the operator acts only on the form part, ignoring the value part. This results in the *exterior covariant derivative*, whose actions on vector-valued and covector-valued forms in $\mathbb{R}^2$ are mentioned below.

$$\begin{aligned}
\mathrm{d}\alpha'^{(0)}_x &= \frac{\partial}{\partial x} \otimes \left(\frac{\partial \overline{a}}{\partial x}\mathrm{d}x + \frac{\partial \overline{a}}{\partial y}\mathrm{d}y\right), \\
\mathrm{d}\beta'^{(1)}_x &= \frac{\partial}{\partial x} \otimes \left(-\frac{\partial \overline{b_1}}{\partial y} + \frac{\partial \overline{b_2}}{\partial x}\right)\mathrm{d}x\mathrm{d}y, \\
\mathrm{d}\gamma'^{(2)}_x &= 0,
\end{aligned}$$

and

$$\begin{aligned}
\mathrm{d}\left(\alpha'^{(0)}\right)^x &= \mathrm{d}x \otimes \left(\frac{\partial \overline{a}}{\partial x}\mathrm{d}x + \frac{\partial \overline{a}}{\partial y}\mathrm{d}y\right), \\
\mathrm{d}\left(\beta'^{(1)}\right)^x &= \mathrm{d}x \otimes \left(-\frac{\partial \overline{b_1}}{\partial y} + \frac{\partial \overline{b_2}}{\partial x}\right)\mathrm{d}x\mathrm{d}y, \\
\mathrm{d}\left(\gamma'^{(2)}\right)^x &= 0.
\end{aligned}$$

Note that unlike for differential forms, consecutive application of the exterior covariant derivative on vector-valued and covector-valued forms yields zero if and only if the curvature is zero, which is defined in [26, p. 251]. Thus, to make use of the exterior covariant derivative, these forms are applied only in instances where the curvature is zero.

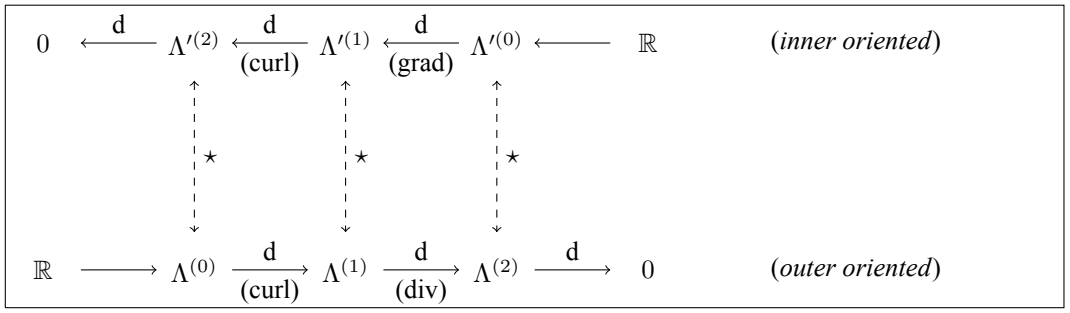

Figure 2.3: Double De Rham complex summarising the forms and operators in $\mathbb{R}^2$ [27]

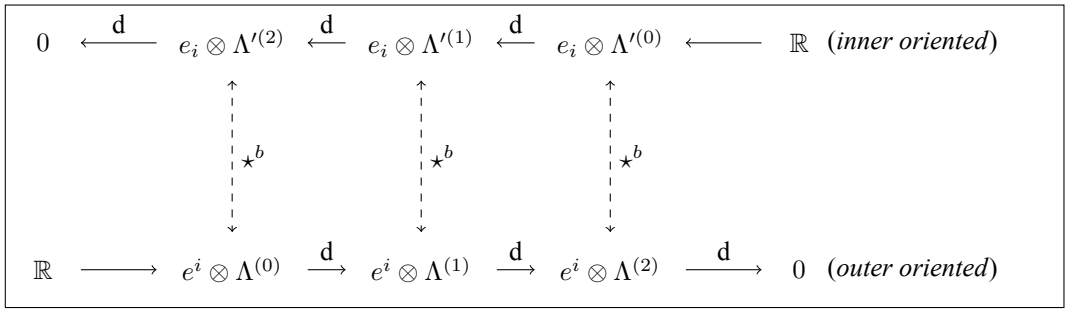

Figure 2.4: Double De Rham complex summarising the vector- and covector-valued forms and operators in $\mathbb{R}^2$ [52]

The *Hodge operator* relates differential forms which are on two complexes having different orientations. This operator represents a constitutive law of physics [62]. This is the part of the formulation that is approximate in the discrete setting, as the Hodge is metric-dependent. Thus, this is also the part of the formulation that introduces the discretisation error into equations. It can be represented as an operator that maps k-forms into $(n-k)$-forms.

$$\star : \Lambda'^{(k)}(\Omega, \mathbb{R}) \to \Lambda^{(n-k)}(\Omega, \mathbb{R}).$$

The prime indicates that this is in the dual space of the latter form. For the rest of the thesis, the outer-oriented space is taken as the primal space (which is also the recommendation in [63]), which means that the inner-oriented space becomes the dual space. This is why all the forms mentioned were indicated with a prime. For more information and a more detailed definition of the Hodge operator, one can check out [59, p. 436], where it is defined using the exterior product. When working in $\mathbb{R}^2$, the important results are $\star \mathrm{d}x = \mathrm{d}y$, $\star \mathrm{d}y = -\mathrm{d}x$, $\star \mathrm{d}x\mathrm{d}y = 1$ and $\star 1 = \mathrm{d}x\mathrm{d}y$. With this, the previously written inner-oriented forms can be associated to the outer-oriented forms as

$$\begin{aligned}
\star\alpha'^{(0)} &= \overline{a}(x,y)\mathrm{d}x\mathrm{d}y = \alpha^{(2)}, \\
\star\beta'^{(1)} &= \overline{b_1}(x,y)\mathrm{d}y - \overline{b_2}(x,y)\mathrm{d}x = \beta^{(1)}, \\
\star\gamma'^{(2)} &= \overline{c}(x,y) = \gamma^{(0)}.
\end{aligned}$$

Vector proxies can thus be chosen to be described in either orientation and in a form that is of relevant order [34]. The example of velocity from fluid dynamics shows that you can represent it as a 1-form in the inner-orientation, or as a 2-form in the outer-orientation. Starting from points, a *De Rham complex* can be drawn, with two such complexes shown in Figure 2.3 signifying the two different orientations. Here, you can also see the effect of the Hodge operators.

There is an equivalent of the Hodge operator for vector-valued and covector-valued forms. This is called the Hodge-star operator, as mentioned in [52]. This maps vector-valued forms to covector-valued pseudo-forms. This involves a Hodge operator on the form part, while the value part undergoes duality pairing. This means that only the vector-valued form that has a value of $\frac{\partial}{\partial x} = e_x$ interacts with the covector-valued form that has the value of $\mathrm{d}x = e^x$, and similarly for the vector and covector along y, or in other words it follows the Kronecker-Delta property. This operation is denoted by $\star^b$, and

$$\star^b\left(\alpha_x'^{(0)}\right) = \mathrm{d}x \otimes \overline{a}(x,y)\mathrm{d}x\mathrm{d}y,$$
$$\star^b\left(\beta_x'^{(1)}\right) = \mathrm{d}x \otimes \left(-\overline{b_1}(x,y)\mathrm{d}y + \overline{b_2}(x,y)\mathrm{d}x\right),$$
$$\star^b\left(\gamma_x'^{(2)}\right) = \mathrm{d}x \otimes \overline{c}(x,y).$$

A similar relation can be written down for the covector-valued forms mentioned before too. Similarly, a double De Rham complex can be written down with the Hodge-star operation instead of the Hodge operation for the relation between two orientations, one of which is composed of vector-valued forms, and the other composed of covector-valued forms. This is shown in Figure 2.4, where e_i denote vector-values and e^i denote covector-values. Note that it is only for reference that vector-values are on the inner-oriented complex and covector-values are on the outer-oriented complex. The outer-oriented complex could also be vector-valued, in which case the inner-oriented complex immediately is covector-valued, to ensure duality pairing.

2.1.5. Bringing together algebraic topology and exterior calculus

There needs to be a leap made to connect the knowledge of differential (and vector-valued/covector-valued) forms to how Tonti describes quantities being associated with geometrical objects. [9] does exactly this, introducing the problem as a network of first-order differential equations. Constitutive relations are clearly separated from the metric-free balance equations. Using the connectivity of the geometric components, a concept from algebraic topology, the topological equations inducing the exterior derivative can be described. The introduction of the idea of a second mesh also happens here. For triangular meshes, the dual mesh will be polygonal, where the cell centers can be taken as barycentric or by taking the dual mesh edges normal to the primal mesh edges. The result is the barycentric and Voronoi-Delaunay dual meshes respectively. For the mimetic spectral element, there is still no certainty on where the dual mesh should be. Because there is a metric involved when switching from a primal to a dual mesh, there is no unique way to construct the dual mesh [9].

The connectivity of the components of the discrete mesh, just like in network theory, defines chains of these components as discussed in [43]. The discrete projection of differential forms on these chains is called co-chains. Co-chains represent the integrated values over these components since co-chains act as weights on these chains. [26, p. 638] notes that ”chains correspond to vectors while co-chains correspond to covectors or 1-forms”.

Mattiussi also kept Tonti’s theory in mind when looking at methods to solve problems numerically, taking electromagnetism in particular. Physical systems should behave similarly, no matter the context. To ensure this, [43] makes a deviation from Tonti’s diagram to show there is a difference between chains and co-chains, that while the former is the discrete representation of geometry, the latter will be a discrete representation of the physics of the problem. In this context, popular numerical methods used for partial differential equations are compared with the mimetic approach. He concludes that numerical methods have the tendency to evolve techniques similar to the mimetic approach, like using the staggered grid for the finite volume method. If the topological and constitutive relations are separated, this would be similar to combining the best features of each popular numerical method. When looking at how the error behaves in a mimetic approach, the error in the model present in the constitutive relations can be considered the discretisation error itself. The co-chain-based field function approximation used in mimetic methods makes it natural to look at global errors too. The boundary conditions and sources in a problem are external effects that are modelled and are ignored in the problem description. The conclusion drawn from this is that boundary conditions and sources can be described in terms of topological and constitutive laws by physical reasoning [43].

These are the basic ideas which gave birth to mimetic methods.

2.2. Mimetic discretisation

This section describes how exterior calculus is ideal to describe physics and its laws in the continuous domain. Here one learns that the classical vector calculus operations of gradient, curl and divergence are topological relations and directly discretisable with the quantities to which they relate. These relations are exact because there is a discrete projection of forms (co-chains) onto the geometric components of a discretised domain thus making it exact in the discrete environment. This enables us to write exact versions of these operators.

With this property, the metric part can be separated from the conservation laws, allowing topological relations to be metric-free at the discrete level. This also allows the error to be introduced in the constitutive laws, which are also the approximate parts of the model. This chapter discusses these operations, in order to set up a mimetic

discretisation method following these ideas. Starting with the requirements for having mimetic discretisation, to then looking at discrete Hodge operators, an overview is provided for mimetic discretisation methods.

2.2.1. Requirements

In [6], the essential considerations for making a mimetic discretisation method are given. These five requirements are [54]:

- a discretisation of integrals over geometry components,
- a discrete analog of the fundamental theorems of calculus,
- a discretisation of differential operators,
- a discrete analog of commuting diagrams,
- a discrete analog of product rules.

The first requirement is the discretisation of differential forms to co-chains associated to chains. The forms are mapped to co-chains using the reduction operation [5], and this requires discretisation of those field variables which would be the given quantities in a problem. The computed quantities are discrete integral quantities, which are not usually the quantities of interest anyway. These quantities of interest can be determined by ”reconstructing” using the degrees of freedom. This is how the reconstruction operator is defined, which maps the computed integral quantities back to get the field variables [5]. In the context of the mimetic spectral element method, reconstruction is nothing but interpolation over the domain using the weighted basis functions.

The second requirement is connected with the generalised Stokes theorem, which should hold in the discrete setting with co-chains as well. Related to this, the third requirement means the co-boundary operator needs to be defined, which will be the analog for the exterior derivative and the exterior covariant derivative within the discrete framework. The co-boundary operator relates co-chains in such a way that within a complex, the exact derivative of the associated form is obtained. This operation can be compared to Kirchhoff’s laws in circuit analysis [26, p. 643]. This operation is done by the incidence matrices, which consist of plus one, minus one and zeros only [5, 27]. Thus the incidence matrices are sparse by construction, which is a strong point of mimetic methods when you look at it from the computational perspective too. As mentioned before, the incidence matrices are exact and do not depend on any kind of metric (like lengths and areas), but only on the connectivity of the mesh. This means that it can be generated for any kind of mesh, and also that the incidence matrices remain the same regardless of how the mesh looks, as long as the connectivity remains the same.

A *commutation diagram* is used to show that the application of many operations in different orders ends up yielding the same result, which is a property that is ideally also maintained at the discrete level. This brings us to the fourth requirement, that the co-boundary operator defined above should commute with the projection operator, which is the combination of both reduction and reconstruction mentioned before. All of these result in a discrete double De Rham complex that involves the co-boundary operator and the Hodge operator mentioned before. Care should be taken when defining the reduction and the reconstruction as their consequent applications on a co-chain should result in the same co-chain [5, 27].

The last requirement is when you look at the wedge product, which should also have a discrete version. This takes the form of products between co-chains, which should resemble the wedge product between forms. Thus, a choice is made to define a discrete inner product. However, this leads to a dilemma. The goal of the discrete operators on forms mimicking their continuous counterparts can be hard to achieve and depends on the choice of reduction and reconstruction. The choice of the primary operation, for instance, the inner product or the discrete Hodge operator, affects whether the other operations are derived from this operation. The inner product is however easier to construct and leads to well-behaved discrete structures [5], which is why this is done for the mimetic spectral element method in this thesis too.

2.2.2. Discrete Hodge operators

One of the important aspects when dealing with numerical methods used for elliptic second-order partial differential equations is separating the metric part from the topological part. One of the ways to do this is by using a mixed formulation, like in the mixed finite element method. The other way can be to solve these equations directly (after elimination of one of the first order equations) using a dual grid that is explicitly defined like in a staggered finite volume method. Both of these cases involve the use of a discrete Hodge operator. This operator appears in the definition of the inner product (and thus in the mass matrices) which acts as the relation between the primal and the (implicitly-defined) dual variables. In the second case, there are Hodge matrices which map from the primal to the dual grid and vice versa, which of course act as discrete Hodge operators [48].

One of the ways to distinguish between mimetic methods is to see how the Hodge operator is discretised in that method. Unlike the co-boundary operator, the Hodge operator cannot be constructed using algebraic topology [27], and will be different depending on the discretisation being used. With many options to choose from to define the discrete Hodge operator, [34] states that the choice of dual mesh is irrelevant and that the use of elimination results in a loss of information. The mixed formulation leads to a saddle-point problem with a unique solution. [58] gives the relationship between the explicit definition of the Hodge operator or introduction by the Galerkin method, and says although the mass matrix and the Hodge matrices may be different, both of them represent the discrete Hodge operator.

The Hodge matrices need to be square, symmetric, and positive definite [34]. In addition, they should also follow the property of the skew-symmetry of the wedge product when switching arguments, and they should satisfy the discrete integration by parts rule. When using the mimetic spectral element method, the introduction of discrete Hodge operators results in diagonal or full square, symmetric, positive definite matrices. The mimetic spectral element method also ensures that the inner product between a form and a form on which the co-differential acts, which is a combination of the exterior derivative and the Hodge operator, satisfies the integration by parts rule [48]. The discrete wedge product constructed in the mimetic spectral element method also satisfies the skew-symmetry property [48].

The mass matrices are thus dependent on the metric and have to be generated again when the mesh is changed. However, this is not necessary when the metrics are defined in a reference domain. The pull-back operator and the exterior derivative commute, so all the operations on the forms can then be performed in the reference domain. Once computations are performed, the result can be mapped back into the physical domain. This means that the mass matrix can be constructed in general, and can then be multiplied by the local pull-back operator for every part of the physical domain.

With this, the ingredients required for the mimetic spectral element method to be implemented are made available. These are the mass matrices, the incidence matrices, and the reduction and reconstruction operations.

2.2.3. Development of related mimetic discretisation methods

Some of the applications include unstructured triangular staggered meshes preserving symmetries considered, like in [50], and extensions to general polyhedral meshes like in [8, 12]. There are geometric approaches that include discrete exterior calculus [19], covolume methods [44] and mimetic isogeometric discretisations [14, 22, 33]. However these are small contributions compared to the extensive developments in finite element exterior calculus and mimetic finite difference methods.

The finite element exterior calculus [2, 3] is born out of the conventional finite element method. It aims at ”the development of finite element subcomplexes of certain elliptic differential complexes and co-chain projections onto them, and their implications and applications in numerical PDEs” [2, p. 4]. While finite element de Rham subcomplexes and co-chain projections are seen as key parts of the method, the main ingredients for the method come from differential geometry, algebraic topology and homological algebra. The domain is usually divided into an unstructured mesh of elements and, just like in a conventional finite element method, the solution is characterised by a weak or variational formulation. The solution exists in suitable function spaces, which are decomposed in finite-dimensional subspaces, allowing for direct comparison to the exact solution through the same mathematical tools such as norms or functionals. The Kozsul operator and Koszul complex play a key role in constructing, as well as analysing the finite element subspaces. More specifically, features of exact complexes like co-homology are inherited through co-chains by only considering solutions within the finite-dimensional subspaces of the space in which the exact solution would be [2]. Recent work on the method is for example on the effect of lower order terms on stability and convergence rates for both scalar and vector Laplacian problems [1], and even a semi-Lagrangian method used to solve the incompressible Navier-Stokes equation[60].

Mimetic finite differences are not new either, with its 50-year history being reviewed in [41]. Finite difference methods contain support operators, which have a discrete version of tensor and vector calculus, that perform the discrete analogs of operations like gradient, curl and divergence. The mimetic version is also born out of these support operator methods [36, 56]. The mesh objects in these methods are associated with the degrees of freedom, which can represent a scalar, vector or tensor field. Collections of these degrees of freedom are called grid functions, which have either a nodal or an edge basis. Algebraic topology helps us understand this association of the degrees of freedom to mesh objects. Because it is directly discretised when working with conservation laws, the differential operators can ensure, for example, that the conservation of mass is ensured by the framework. This is also aided by the fact that gradient and divergence operators are negatively adjoint. However, there is the introduction of parasitic or spurious modes that, in general for all discretisation methods, can be attributed to the differential operators having null spaces that are too large [41]. This mimetic finite

difference method also has symmetric discretisation, which makes convergence analysis easier. This method is also shown to be almost identical to hybrid and mixed (staggered) finite volume methods [21]. It is applied to elliptic problems on polyhedral meshes in [41]. Other recent work includes the application of a modified mimetic finite difference method which is written in a tensor-train format to act as a low-rank approximation for the time-dependent Maxwell wave propagation equations [42], and also to model two-dimensional resistivity, which is essential to monitor earth's subsurface using geoelectric methods [57].

2.3. Applications of mimetic spectral element method

Once the basic idea behind the mimetic spectral method is explained, the current state of research needs to be looked at. This motivates a short look back at how it has evolved, which will be presented in this section. The applications to linear elasticity will be discussed with an ending note on the hybrid methods.

2.3.1. Overview

The work on mimetic spectral element methods is relatively new, with it essentially trying to achieve exact conservation for topological relations while being a high-order mixed finite element method with optimal convergence. Here, basis functions are used to project quantities of interest on components of the mesh. For this purpose, a nodal basis, which is constructed from Lagrange polynomials, and an edge basis, constructed from the edge functions proposed in [28] is used. These functions satisfy the Kronecker-delta property for their respective dimensions, the nodal basis on nodes and the edge basis on the edges. These are constructed on a quadrilateral structured mesh and can be extended from one dimension to multiple using the tensor product. A more detailed description of the ideas involved in the mimetic spectral element method is given in [27].

The conference papers [11, 28, 40, 46] were some of the first works to look at this method. The Poisson equation was first solved on multiple continuous spectral elements. Journal papers [33, 39, 48] complete the full overview of the method, with applications to (anisotropic) diffusion and Stokes flow. An extension to advection is also discussed in [47], while momentum conservation is considered in [64]. Convection terms were also modelled using a discrete Lie derivative, which was proposed in [29, 40, 46]. Algebraic dual polynomials have been derived and applied in papers like [37, 30]. The polynomials allow for the setup of sparse systems, such as in [65, 68], with the system still having a topological discretisation of conservation laws and a single mesh being defined. [67] also looks at incompressible Navier-Stokes equations, with mimetic discretisation to enforce conservation properties.

One of the developments is to extend this method to hybrid elements with domain decomposition, as in [65, 66]. This makes the mimetic spectral element method easier as the domain is divided into several sub-domains, with each sub-domain being solved independently. This means that the operators used for this method need to be set up to account for the boundaries too, to ensure that the conservation laws hold at these locations. Because they are divided into several sub-domains, each sub-domain can be solved for in parallel once the interface relations are computed. This makes it attractive as a computational method because it can give high accuracy as well.

2.3.2. Linear elasticity

For linear elasticity, a better representation would be if tensor quantities could themselves be written down instead of vectors, using first-order equations like in Poisson's equation. One of the first to use tensors to enforce the equilibrium of forces was [45], although the symmetry of the stress tensor was not strongly enforced. Enforcing symmetry of the stress tensor strongly is something that this study can be extended to.

Linear elasticity is a widely used theory for the analysis of solid structures and materials, although it is only applicable to small displacements. In [45, 65], a formulation with the mixed spectral element method for linear elasticity is proposed, with stress components being the primary variables. The rotation tensor is used as a Lagrange multiplier to enforce the symmetry of the stress tensor, while the components of the displacement are used to enforce the conservation of linear momentum. In both these papers, the equilibrium of forces is satisfied point-wise. However, it is noted that for curvilinear domains, the formulation used in [45] weakly enforces the symmetry of the stress tensor, while [65] builds on this to have a formulation that strongly enforces symmetry of the stress tensor, with the trick to have the same number of degrees of freedom to represent both the shear components of the stress tensor. Another point to note is that the number of degrees of freedom is much larger than if it was a first-order equation, but the advantage of using this formulation is that there is no post-processing necessary to calculate the tractions at surfaces, as these are readily available.

[65] introduces a new mixed hybrid mimetic spectral method, where the linear elasticity problem is written as a saddle-point problem. This results in the system solving for two quantities simultaneously. For linear elasticity

problems, both the stresses and the displacements are solved for at the same time. Because the formulation is a minimisation problem, the Lagrange multipliers which are introduced in between lead to a mixed formulation.

There are two methods to set up mixed methods, classified on whether they circumvent or satisfy the Ladyshenskaya-Babuška-Brezzi stability condition, also called the inf-sup condition. You can circumvent this condition by using stabilized methods or least-squares methods. Compatible methods are those which satisfy the inf-sup condition. This involves the construction of discrete vector spaces which satisfy this condition, which include Nedelec spaces (curl-conforming), Raviart-Thomas spaces (divergence-conforming), and Brezzi-Douglas-Marini spaces (also divergence-conforming). The mimetic methods act as a subclass of these compatible methods, which lead to stable solutions for elliptic problems.

2.3.3. The hybrid method

The mimetic spectral element method was extended to form a hybrid method in [65, 66], which will be better for large-scale computations as mentioned before. The hybrid method is further explained here, and comparisons between this and other popular methods are considered.

In [65, 66], the hybrid method means that the physical domain is divided into multiple elements, and each element incorporates a formulation of the mimetic spectral element method, with Lagrange multipliers coupling elements together. For comparison, the similarities between this approach and continuous Galerkin methods and discontinuous Galerkin methods, which also look at dividing the domain into multiple elements, are looked at here.

For continuous Galerkin methods, there are basis functions defined only within the element, with the domain containing multiple elements. The boundaries of the element contain a single unknown, which is shared by all the neighbouring elements. The numbering of these elements and edges will determine the structure of the sparse matrix. These methods are conforming, that is the solutions derived from a subset of the original solution space of the continuous problem. The conservation properties of these methods are examined in [35].

The discontinuous Galerkin methods divide the domain into sub-problems using domain decomposition, unlike continuous Galerkin methods. The degrees of freedom are thus numbered as if the edges of the elements are disconnected.

These methods are summarised in [4]. The methods are distinguished from each other based on how the numerical fluxes are imposed between elements. These fluxes are not necessarily physical relations, but are purely numerical. Because this flux plays a big role in the stability, accuracy and sparsity and symmetry of the stiffness matrix, each choice made at this stage results in a different method. The motivation for using these methods is given in [16], which also highlights why this could be a finite element alternative to high-resolution finite difference and finite volume methods when dealing with convection-dominated problems with physical discontinuities. Another strength of these discontinuous Galerkin methods is that they are highly parallelisable, can accommodate complex geometries through high mesh flexibility, and are easily compatible with adaptive refinement strategies.

The discontinuous Petrov-Galerkin method has improved stability [18], because it looks for optimal test function spaces for each problem before using these test functions. This step can be computed during the set-up of the element matrices and does not need any extra steps during the computation of solutions. However, the discontinuous Petrov-Galerkin method does not, in general, conserve laws at the element level. There is, however, an alternative proposed in [18] that makes it possible to conserve laws by introducing another scalar unknown. This method is more expensive than continuous Galerkin or other discontinuous Galerkin methods, but it is also a stable method. Another alternative is the hybridisable discontinuous Galerkin method [15], which combines ideas from the hybrid finite element method and the discontinuous Galerkin method. These methods are, by construction, discontinuous Galerkin methods that allow for static condensation as seen in [15].

[66] uses a hybrid method that separates elements, while continuity at the boundaries is enforced with the help of interface operators using Lagrange multipliers. Thus, the solution will remain continuous across the boundary even though the boundary itself will have two degrees of freedom. This is inherently different from the discontinuous Galerkin methods, where there is no continuity maintained at the boundaries, with the solution jumping at the boundaries. The Lagrange multipliers are also a way to see physical boundary conditions for each element, which can be comparable to primal hybrid finite element methods [53].

Higher-order methods like these have a high number of unknowns inside the elements, so even if there are extra unknowns at the edges this will not pose a problem. There are separate degrees of freedom at the element edges, which separates elements and results in independent blocks for each element in the system matrix. This requires an interface operator (which results in new equations) that will pair the degrees of freedom at the boundary of neighbouring elements. For example, the Steklov-Poincaré operator is used in a similar way for boundary-value

problems [51]. Using the method of static condensation, the interface quantity can be computed separately [7, p. 429]. With this, the resulting system is parallelisable for computation especially when the number of unknowns is really high, as the domains can be solved independently afterwards. All these methods lead to a block diagonal mass matrix, that can be solved in parallel for every element [15].

Thus, the discontinuous Galerkin and hybrid mimetic methods benefit from being parallelisable due to domain decomposition. While the discontinuous Galerkin method deals with numerical fluxes, the hybrid mimetic spectral element method uses the continuity of fluxes and also has physical meaning for its Lagrange multipliers. This bodes well for the mimetic spectral element method for elliptic problems.

3

Theoretical basics

This chapter will contain a brief overview of the theoretical (mainly mathematical) background needed to better understand and work with the mimetic spectral element method and vector- and covector-valued forms. It can also be interpreted as a way to understand the basics for those who are not familiar with the ideas.

3.1. Basics

This section will describe the notation used throughout this thesis work. This will also simplify the problem of multiple notations used in literature. There is also a brief review of the relevant operations performed as part of the mimetic spectral element method, and the implications of these operations.

3.1.1. Notation

The following symbols and specific notation are common across different case studies in this work, which is why it is specified here. As usual, n denotes the dimension of ambient space and is limited to two dimensions throughout the thesis. N is used to denote the degree of polynomial interpolation used in the numerical method. N_t is used for the same, but when you are integrating in the time dimension. k is used to denote the dimension of a form. For numerical integration and interpolation, N_x is a suitable number that is large enough for the numerical error in numerical integration and interpolation to be negligible.

In general, vectors are denoted in boldface, for example as $\mathbf{X}$. Tensors are denoted as boldface doubly underlined quantities, like $\underline{\underline{\boldsymbol{\sigma}}}$. Dual spaces and functions are denoted with a prime, e.g. $h'(\xi)$. System vectors, or unknowns in computations are written in boldface with a superscript, e.g. $\mathbf{X}^h$. Reconstructed fields are written with an over-line, e.g. $\overline{X}$. Test functions are written down with a tilde, like $\widetilde{\sigma_{xx}}$. In this chapter, k-forms will also be denoted with their specific dimension, for example, $\omega^{(0)}$.

3.1.2. Projection onto a mesh

To make the differential forms act like continuous quantities, they must be discretized judiciously. The aim, specifically, is that they satisfy the relationships that their continuous counterparts satisfy. A basic implementation of this can be seen in the figure below. Because this is a two-dimensional setup, there are three different k-cells. The 0-cell comprises of all the $(N+1)^2$ points, the 1-cell all $2N(N+1)$ edges, and the 2-cell comprises all N^2 surfaces. The variables represented by (for example) $\omega^{(0)}$, $q^{(1)}$ and $p^{(2)}$ is represented on these discrete cells. To arrive at this discrete representation of differential forms, two operators are required, projection and reconstruction, explained better in [48].

Reduction or integration is the first operation, which involves reducing continuous forms to a mesh and is symbolized by the mathematical symbol $\mathcal{R}$. Every form passes through reduction, producing a co-chain that is linked to a chain of mesh elements. This is a unique operation. The co-chains are values that are associated with components of the discrete geometry. A better representation would be that these are the weights of the solution's representation, while the basis representing the mesh can be formed by a basis. These basis functions are a choice, making them well-defined. The discretisation of field variables can be performed by means of integration over the geometric element, with the unknowns being defined as the integral quantities themselves. Of course, the reduction of any continuous field results in a loss of resolution from its continuous counterpart. This is the source of interpolation error that is observed when reconstructing the reduced field.

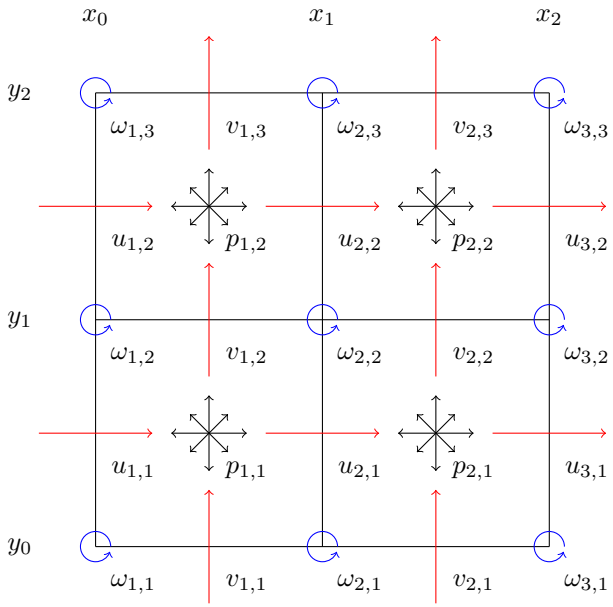

Figure 3.1: Outer-oriented cell complex ($N = 2$), with components of $\omega^{(0)}$, $q^{(1)}$, $p^{(2)}$ indicated

The second operation is the reconstruction or interpolation operator $\mathcal{I}$, which interpolates the values from the degrees of freedom with their weighted basis. Together with reduction, reconstruction results in the projection operation, denoted by $\pi_h = \mathcal{I}\mathcal{R}$. The operation $\mathcal{I}$ must be the right inverse of the reduction operation, since then the condition $\mathcal{R}\mathcal{I} = I$ holds, where I is the identity matrix. This will hold as long as you are reconstructing with the correct weighted basis. Vice versa, the reduction followed by the reconstruction will always lead to an interpolation error, $\mathcal{I}\mathcal{R} = I + \mathcal{O}(h^P)$, which will be the main contributor to the error if the convergence is optimal [48].

In two dimensions, there are three possible co-chains. The components of the co-chains are numbered using indices (i, j) along x and y respectively. $\omega^{(0)}$ is situated on the $(N + 1)^2$ nodes or 0-cells, with components ω_{ij}. The reduction for 0-forms is direct nodal sampling at the defined nodes. The next co-chain $q^{(1)}$ is situated on the $2N(N + 1)$ edges or 1-cells, which comprises of two sets of components, u_{ij} and v_{ij}. A 1-form is reduced onto this cell by integrating the value over the edge. The co-chain $p^{(2)}$ is associated to a chain of N^2 surfaces or 2-cells, such that each quantity represents an integral over the surface. Of course, this means that this is obtained by integrating over the surface.

For example, the nodal value of $\omega_{3,1}$ in Figure 3.1, can be determined as $\omega_{3,1} = \omega(x_2, y_0)$. $u_{2,1}$ can be determined using $\int_{y_0}^{y_1} u(x_1, y)\mathrm{d}y$, and $v_{1,2}$ is calculated as $\int_{x_0}^{x_1} v(x, y_1)\mathrm{d}x$. $p_{2,2}$, being a 2-cell, is the surface integral $\int_{y_1}^{y_2}\int_{x_1}^{x_2} p(x, y)\mathrm{d}x\mathrm{d}y$

3.1.3. The discrete exterior derivative

To compute exterior derivatives (operator d), the co-boundary operator δ can be utilised, while it acts on co-chains instead of acting on differential forms themselves. However, it relates co-chains in the same way that the exterior derivative relates differential forms in a De Rham complex. It is important to note that this operator commutes with both components of the projection [48],

$$\pi_h \mathrm{d} = \mathcal{I}\mathcal{R}\mathrm{d} = \mathcal{I}\delta\mathcal{R} = \mathrm{d}\mathcal{I}\mathcal{R} = \mathrm{d}\pi_h.$$

The discrete exterior derivative is constructed and written down as incidence matrices, which depends on what co-chain it is acting on. Let us take an example, how to arrive at the co-chain on the 1-cells from the co-chain on the 0-cells. While writing down the operator, the positive or negative action of the 0-cells on a 1-cell is considered. To illustrate this, let us consider the cell-complex in Figure 3.1. $\boldsymbol{\omega}$ is defined as a counter-clockwise positive quantity here, which means that the action of $\omega_{1,1}$ on $u_{1,1}$ is negative, while it is positive on $v_{1,1}$. In a similar way, $\mathbf{p}$ is defined source-like, which means that the action of $u_{1,1}$ on $p_{1,1}$ is negative, while the action of $v_{1,1}$ on $p_{1,1}$ is also negative. All of these contributions can be written down in an incidence matrix. Note that while the numbering and definition of a positive sign is free to choose since it does not impact the sparsity

properties of the incidence matrix, it is important that it be kept consistent everywhere in the setup of the system.

With this in mind, the incidence matrix $\mathbb{E}^{(1,0)}$ for Figure 3.1 is denoted for x-lexicographic numbering of the edges, with the vertical edges followed by the horizontal edges as

$$\mathbb{E}^{(1,0)} = \begin{bmatrix} -1 & 0 & 0 & 1 & 0 & 0 & 0 & 0 & 0 \\ 0 & -1 & 0 & 0 & 1 & 0 & 0 & 0 & 0 \\ 0 & 0 & -1 & 0 & 0 & 1 & 0 & 0 & 0 \\ 0 & 0 & 0 & -1 & 0 & 0 & 1 & 0 & 0 \\ 0 & 0 & 0 & 0 & -1 & 0 & 0 & 1 & 0 \\ 0 & 0 & 0 & 0 & 0 & -1 & 0 & 0 & 1 \\ 1 & -1 & 0 & 0 & 0 & 0 & 0 & 0 & 0 \\ 0 & 1 & -1 & 0 & 0 & 0 & 0 & 0 & 0 \\ 0 & 0 & 0 & 1 & -1 & 0 & 0 & 0 & 0 \\ 0 & 0 & 0 & 0 & 1 & -1 & 0 & 0 & 0 \\ 0 & 0 & 0 & 0 & 0 & 0 & 1 & -1 & 0 \\ 0 & 0 & 0 & 0 & 0 & 0 & 0 & 1 & -1 \end{bmatrix} \tag{3.1}$$

With $N = 2$, there are $(N + 1)^2 = 9$ unknowns $\omega_{i,j}$ for $\omega^{(0)}$, and $N(N + 1) = 6$ unknowns for $u_{i,j}$ and another $N(N+1) = 6$ for $v_{i,j}$, which totals to 12 unknowns for $q^{(1)}$. For $\omega_{i,j}$, x-lexicographic numbering is used, that is it is represented as a single vector ω_k, with $k = i+(j-1)(N+1)\ \forall i, j \in [1, N+1]$. Because this incidence matrix relates the 0-form to the 1-form, the indices of ω_k are in the horizontal direction. Similarly, $u_{i,j}$ and $v_{i,j}$ is written down in a x-lexicographic order to get a vector u_k with $k = i+(j-1)(N+1)\ \forall i \in [1, N+1],\ j \in [1, N]$, and v_k with $k = i + (j - 1)N\ \forall i \in [1, N],\ j \in [1, N + 1]$. The indices of u_k followed by v_k are in the vertical direction of this matrix.

Similarly, the incidence matrix $\mathbb{E}^{(2,1)}$ can be written down as

$$\mathbb{E}^{(2,1)} = \begin{bmatrix} -1 & 1 & 0 & 0 & 0 & 0 & -1 & 0 & 1 & 0 & 0 & 0 \\ 0 & -1 & 1 & 0 & 0 & 0 & 0 & -1 & 0 & 1 & 0 & 0 \\ 0 & 0 & 0 & -1 & 1 & 0 & 0 & 0 & -1 & 0 & 1 & 0 \\ 0 & 0 & 0 & 0 & -1 & 1 & 0 & 0 & 0 & -1 & 0 & 1 \end{bmatrix} \tag{3.2}$$

There are $N^2 = 4$ unknowns $p_{i,j}$ for $p^{(2)}$, which is represented as p_k, where $k = i + (j - 1)N\ \forall i, j\,\epsilon[1, N]$. The indices of u_k and then v_k are in the horizontal direction, while the indices of p_k are in the vertical direction.

It is important to keep in mind that these matrices act as the discrete equivalent of differential operators. In this case, the incidence matrix $\mathbb{E}^{(2,1)}$ matrix acts as the discrete equivalent of the divergence operator, while the incidence matrix $\mathbb{E}^{(1,0)}$ acts as the discrete equivalent of the perpendicular gradient operator. This shows the sparsity of these matrices. Of course, one can notice that $\mathbb{E}^{(2,1)} \cdot \mathbb{E}^{(1,0)} \equiv 0$, which is what is suggested by vector laws.

3.2. Basis

By definition of the co-chains, they are associated to mesh cells of different dimensions. To represent these co-chains, a basis is necessary, one which has special properties. One way to do this is to select a primal grid where these mesh elements can be represented. Then, a basis for this primal grid is selected. Using the primal grid and basis, the algebraic dual basis can be constructed.

3.2.1. Reference grid construction

For the grid, a Gauss-Lobatto-Legendre grid is used in all case studies as the reference domain. This is based on the root locations of the Legendre polynomial

$$\phi_{GLL} = \left(1 - \xi^2\right) \frac{\partial L_p(\xi)}{\partial \xi},$$

where $L_p(\xi)$ is a Legendre polynomial of degree p. This polynomial solves the Legendre's differential equation

$$\frac{\partial}{\partial \xi}\left((1 - \xi^2)\frac{\partial L_p(\xi)}{\partial \xi}\right) + p(p + 1)L_p(\xi) = 0.$$

To obtain the points, instead of algebraically or numerically solving the ordinary differential equation, Bonnet's recurrence relation for the Legendre polynomials can be used, with $L_1(\xi) = 1$ and $L_2(\xi) = \xi$ and for $k > 2$,

$$(k+1)L_{k+1}(\xi) = (2k+1)\xi L_k(\xi) - kL_{k-1}(\xi).$$

Using an iterative method for root finding (like the Newton-Raphson method), the roots of ξ_i of $L_p(\xi)$ can be found for any p.

3.2.2. Primal basis

Before basis functions are derived, it is useful to define the nodal and edge degrees of freedom as $\mathcal{N}_i^0$ and $\mathcal{N}_i^1$ respectively. Any 0-form $\phi^{(0)}$ or 1-form $\chi^{(1)}$ can be expanded using their corresponding degrees of freedom and basis as

$$\phi^{(0)}(\xi) = \sum_{i=1}^{N+1} \mathcal{N}_i^0(\phi) h_i(\xi), \quad \chi^{(1)}(\xi) = \sum_{i=1}^{N} \mathcal{N}_i^1(\chi) e_i(\xi),$$

Given the Gauss-Lobatto-Legendre nodes, where $-1 = \xi_1 \leq \xi_2 \ldots \leq \xi_{N+1} = 1$, the nodal and edge degrees of freedom are defined as [37],

$$\mathcal{N}_i^0(\phi) \equiv \phi^{(0)}(\xi_i), \quad \mathcal{N}_i^1(\chi) \equiv \int_{\xi_i}^{i+1} \chi^{(1)}(\xi).$$

Here, $\mathcal{N}_i$ are linear functionals, called local degrees of freedom, or co-chains, that act on the elements, which evaluate them on one node i. Thus, these $\mathcal{N}_i$ denote the reduction $\mathcal{R}$ from a continuous function. Note that this is well-defined for smooth functions, and the $\phi = \phi^{(0)}$ is written as a 0-form. With this criterion, the nodal basis functions should satisfy

$$h_j(\xi_i) = \delta_{ij} = \begin{cases} 1 & \text{if } j = i \\ 0 & \text{if } j \neq i \end{cases}, \forall i, j \in [1, N+1],$$

since then each nodal basis function corresponds to the individual contribution of the node in question. Thus, the Lagrange polynomials are used, which are constructed from $N+1$ data points with

$$h_i(\xi) = \prod_{k=1, k\neq i}^{N+1} \frac{\xi - \xi_k}{\xi_i - \xi_k}.$$

These basis functions are shown in Figure 3.2a. It can be seen that at each node only one basis function has the value one, while the others are zero. It can be noted expansion using these basis functions denotes the reconstruction operation $\mathcal{I}$.

Similarly, the edge basis functions should satisfy the property

$$\int_{\xi_i}^{\xi_{i+1}} e_j(\xi) = \delta_{ij} = \begin{cases} 1 & \text{if } j = i \\ 0 & \text{if } j \neq i \end{cases}, \forall i, j \in [1, N],$$

The functions for the edge basis that will be used are the functions $e_j(\xi)$ called the edge functions, from [28]. On the same GLL points, they are defined as the sum of the derivatives of the nodal basis functions over the grid,

$$e_j(\xi) = -\sum_{k=1}^{j} \mathrm{d}h_k(\xi),$$

as these have the property that [28]

$$\int_{\xi_i}^{\xi_{i+1}} e_j(\xi) = -\sum_{k=1}^{j} \int_{\xi_i}^{\xi_{i+1}} \mathrm{d}h_k(\xi) = -\sum_{k=1}^{j} [h_k(\xi_{i+1}) - h_k(\xi_i)] = \delta_{ij}, \ \ \forall i, j \ \epsilon [1, N].$$

An important detail to note is that the edge basis functions actually include the basis form (i.e. the edge function is actually a 1-form), since

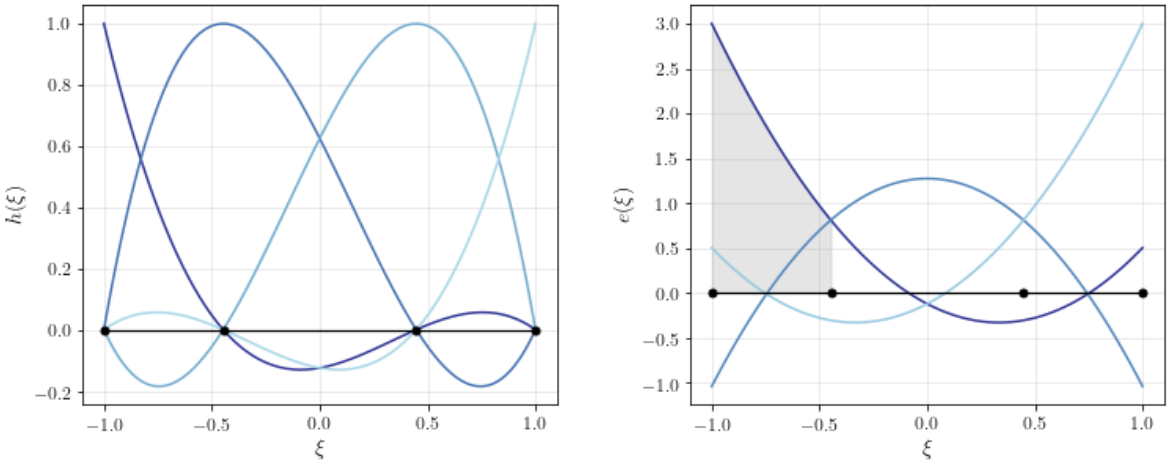

(a) Nodal basis function of order N

(b) Edge basis functions, of lower order $(N-1)$

Figure 3.2: The primal basis functions for an element in $\mathbb{R}^1$ of $N = 3$

$$e_j(\xi) = -\sum_{k=1}^{j} \mathrm{d}h_k(\xi) = -\sum_{k=1}^{j} \frac{\mathrm{d}h_k(\xi)}{\mathrm{d}\xi}\mathrm{d}\xi = \varepsilon_j(\xi)\mathrm{d}\xi.$$

Hence the edge functions e_j are in fact only the vector proxy part ε_j of the true edge functions, which are derived in [28]. These edge functions are also depicted in Figure 3.2b. It can be observed that the shaded area equals one, while the integrals of the other edge functions over this area are zero.

3.2.3. Dual basis

The idea for the generation of the dual basis is to generate another algebraic basis that is orthonormal to the primal basis. This eliminates the need for too many mass matrices in the formulation, as the dual basis helps define an alternate basis on which the degrees of freedom can be solved. In actual implementations, there is no need to derive these dual polynomials, although it can be done explicitly. A detailed discussion on the proofs for the derivation of these algebraic dual functions is discussed in [37].

Any polynomial $\phi\,\epsilon\mathcal{P}$, with $\mathcal{P}$ the space of polynomials of degree N, can be represented by $(N+1)$ nodal degrees of freedom, i.e.

$$\phi(\xi) = \sum_{i=1}^{N+1} \mathcal{N}_i^0(\phi) h_i(\xi) = \Psi^0(\xi)\mathcal{N}^0(\phi).$$

where matrices holding the function values at each node for each function are defined.

$$\Psi^0(\xi) = \left[h_1(\xi), h_2(\xi) \dots h_{N+1}(\xi)\right], \qquad \left[\mathcal{N}^0(\phi)\right]^T = \left[\mathcal{N}_1^0(\phi), \mathcal{N}_2^0(\phi) \dots \mathcal{N}_{N+1}^0(\phi)\right].$$

If the one-dimensional mass matrix is defined as

$$\mathbb{M}_{1D}^{(0)} = \int_\Omega \left(\Psi^0(\xi)\right)^T \Psi^0(\xi)\mathrm{d}\Omega.$$

the $\mathcal{L}^2$ inner product of two elements $\phi, \pi\ \epsilon\mathcal{P}$ leads to

$$(\phi, \pi)_{\mathcal{L}^2(\Omega)} = \int_\Omega \phi\pi\ \mathrm{d}\Omega = \int_\Omega \left(\mathcal{N}^0(\phi)\right)^T \left[\Psi^0(\xi)\right]^T \Psi^0(\xi)\mathcal{N}^0(\pi) = \left(\mathcal{N}^0(\phi)\right)^T \mathbb{M}_{1D}^{(0)}\mathcal{N}^0(\pi).$$

Then, if the dual edge degrees of freedom are defined as $\mathcal{N}'^1(\pi)$, with

$$\left(\mathcal{N}^0(\phi)\right)^T \mathcal{N}'^1(\pi) \equiv \left(\mathcal{N}^0(\phi)\right)^T \mathbb{M}_{1D}^{(0)}\mathcal{N}^0(\pi),$$

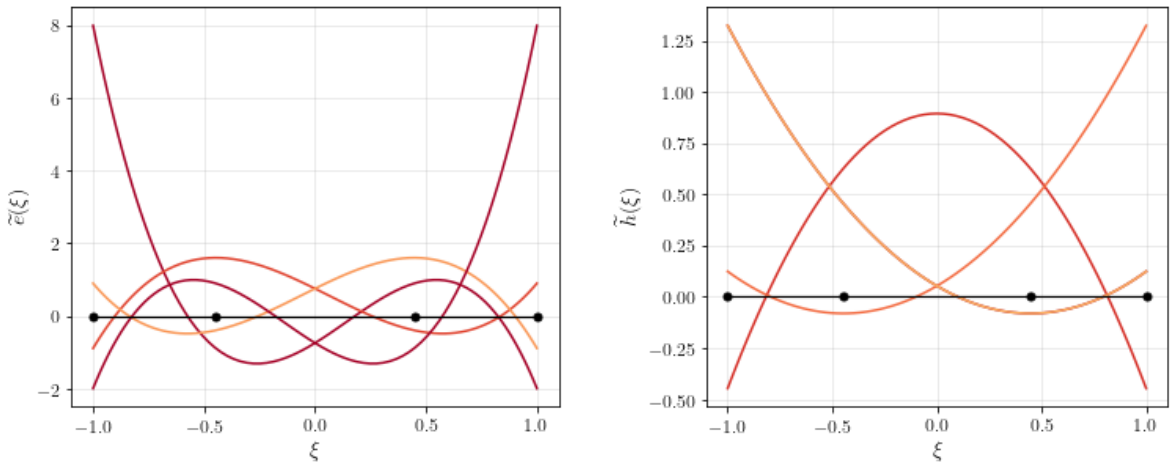

(a) Dual edge basis function of order N

(b) Dual nodal basis functions, of lower order $N-1$

Figure 3.3: The dual basis functions for an element in $\mathbb{R}^1$ of $N=3$

the dual basis functions $h'_j(\xi)$ must again satisfy the Kronecker-delta property, i.e. $\mathcal{N}'^1_i(h'_j)=\delta_{ij}$, hence they are found to be

$$\Psi'^1(\xi)=\Psi^0(\xi)\left(\mathbb{M}^{(0)}_{1D}\right)^{-1},$$

where

$$\Psi'^1(\xi)=\left[e'_1(\xi),e'_2(\xi)\dots e'_{N+1}(\xi)\right].$$

It can be seen in Figure 3.3 that while the Lagrange polynomials are nodal, the corresponding dual polynomials derived from them are more like edge polynomials.

Expressing the edge degrees of freedom again for any $\chi\ \epsilon\mathcal{Q}$, with $\mathcal{Q}$ the space of polynomials of degree $N-1$,

$$\chi(\xi)=\sum_{i=1}^{N}\mathcal{N}^1_i(\chi)e_i(\xi)=\Psi^1(\xi)\mathcal{N}^1(\chi),$$

where

$$\Psi^1(\xi)=\left[e_1(\xi),e_2(\xi)\dots e_N(\xi)\right],\qquad \left[\mathcal{N}^1(\chi)\right]^T=\left[\mathcal{N}^1_1(\chi),\mathcal{N}^1_2(\chi)\dots\mathcal{N}^1_N(\chi)\right].$$

Then, similar to the nodal basis, the $\mathcal{L}^2$-inner product of two elements $\chi,\gamma\ \epsilon\mathcal{Q}$ leads again to a mass matrix written as

$$\mathbb{M}^{(1)}_{1D}=\int_\Omega\left(\Psi^1(\xi)\right)^T\Psi^1(\xi)\mathrm{d}\Omega,$$

and the dual of the edge functions are given by

$$\Psi'^0(\xi)=\Psi^1(\xi)\left(\mathbb{M}^{(1)}_{1D}\right)^{-1},$$

where

$$\Psi'^0(\xi)=\left[h'_1(\xi),h'_2(\xi)\dots h'_N(\xi)\right].$$

These polynomials are also shown in Figure 3.3. It can be seen that the dual polynomials derived from the edge functions look more like (weighted) nodal polynomials.

3.2.4. Tensor products of basis functions

In higher dimensions, the co-chains are expanded as tensor products of the basis [48]. 0-forms in two dimensions will have the basis of

$$P(\xi,\eta) = \Psi^0(\xi) \otimes \Psi^0(\eta),$$

with individual components

$$P_{i,j}(\xi,\eta) = h_i(\xi)h_j(\eta).$$

Then, the basis of a projected 1-form is constructed from a mix of nodal and edge basis, for lines in ξ- and η-direction respectively. For example,

$$\mathbf{L}(\xi,\eta) = \begin{bmatrix} L_x(\xi,\eta) & 0 \\ 0 & L_y(\xi,\eta) \end{bmatrix} = \begin{bmatrix} \Psi^1(\xi) \otimes \Psi^0(\eta) & 0 \\ 0 & \Psi^0(\xi) \otimes \Psi^1(\eta) \end{bmatrix},$$

with individual components written as

$$\begin{aligned}(L_x)_{i,j}(\xi,\eta) &= e_i(\xi)h_j(\eta),\\ (L_y)_{i,j}(\xi,\eta) &= h_i(\xi)e_j(\eta).\end{aligned}$$

Similarly, the basis of a 2-form is written as

$$S(\xi,\eta) = \Psi^1(\xi) \otimes \Psi^1(\eta),$$

with components,

$$S_{i,j}(\xi,\eta) = e_i(\xi)e_j(\eta).$$

Similar to the construction of the dual basis for a single dimension, the algebraic dual polynomials in $\mathbb{R}^2$ is constructed using the basis for the primal functions. Writing down the mass matrices as

$$\mathbb{M}^{(0)} = \int_\Omega P^T P \mathrm{d}\Omega, \qquad \mathbb{M}^{(1)} = \int_\Omega \mathbf{L}^T \mathbf{L} \mathrm{d}\Omega, \qquad \mathbb{M}^{(2)} = \int_\Omega S^T S \mathrm{d}\Omega,$$

For the polynomials of polynomial space of order N, denoted again by $\mathcal{P}^N$, with $\phi \in \mathcal{P}^N \otimes \mathcal{P}^N$, $\boldsymbol{\pi} \in \left(\mathcal{P}^N \otimes \mathcal{P}^{N-1}\right) \times \left(\mathcal{P}^{N-1} \otimes \mathcal{P}^N\right)$, and $\chi \in \mathcal{P}^{N-1} \otimes \mathcal{P}^{N-1}$, then the nodal, edge, and surface degrees of freedom are given by

$$\mathcal{N}'^2(\phi) = \mathbb{M}^{(0)}\mathcal{N}^0(\phi), \qquad \mathcal{N}'^1(\boldsymbol{\pi}) = \mathbb{M}^{(1)}\mathcal{N}^1(\boldsymbol{\pi}), \qquad \mathcal{N}'^0(\chi) = \mathbb{M}^{(2)}\mathcal{N}^2(\chi).$$

and the corresponding basis can be constructed using

$$P' = P^T \left(\mathbb{M}^{(0)}\right)^{-1}, \qquad \mathbf{L}' = \mathbf{L}^T \left(\mathbb{M}^{(1)}\right)^{-1}, \qquad S' = S^T \left(\mathbb{M}^{(2)}\right)^{-1}.$$

Note that by this definition the algebraic dual of a tensor product, need not be the tensor product of the algebraic duals of functions. This is only the case when the coordinates are orthogonal.

3.3. Mapping

The motivation behind the mapping is to simplify the computations, as well as make it easier to visualise complex geometries. It is much more convenient to compute quantities to do all computations on a nice, orthogonal (*reference*) domain, and then transfer the results onto the physical domain. Let $(\xi,\eta) \in \hat{\Omega}$ be the coordinates in the reference domain, while the physical domain be denoted by $(x,y) \in \Omega$. The mapping of coordinates is in fact an operator on the coordinates in the reference domain, which yields the coordinates in the physical domain, i.e. $\Phi : \hat{\Omega} \to \Omega$, such that $(x,y) = (f_1(\xi,\eta), f_2(\xi,\eta))$. This mapping is in general not invertible.

The k-forms themselves have the desired property that they are independent of metric, that is [39]

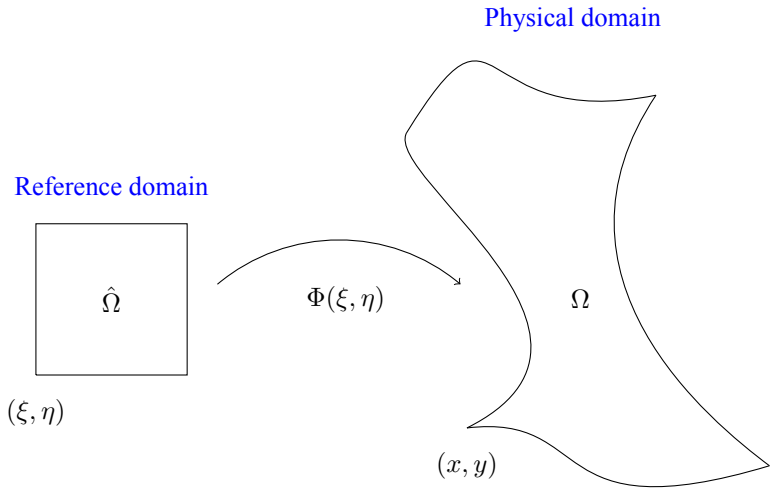

Figure 3.4: The Mapping between reference and physical domain

$$\int_{\hat{\Omega}} \hat{a}^{(k)} = \int_{\Omega} a^{(k)}.$$

With this, the pull-back operator Φ^* is defined by [39]

$$\int_{\Omega} a^{(k)} = \int_{\Phi(\hat{\Omega})} a^{(k)} = \int_{\hat{\Omega}} \Phi^* a^{(k)} = \int_{\hat{\Omega}} \hat{a}^{(k)}.$$

The pull-back commutes with the wedge product $\wedge$, as

$$\Phi\left(a^{(k)} \wedge b^{(k)}\right) = \Phi\left(a^{(k)}\right) \wedge \Phi * \left(b^{(k)}\right),$$

and with the exterior derivative d [39, 48], that is

$$\Phi^* \mathrm{d} = \mathrm{d}\Phi^*.$$

It also commutes with the projection operation π_h [39]. These properties will be used extensively to derive the corresponding terms for mapped forms. In general, the pull-back operator involves the use of the components of the Jacobian matrix and its inverse. That is,

$$\mathcal{J} = \begin{bmatrix} \frac{\partial x}{\partial \xi} & \frac{\partial x}{\partial \eta} \\ \frac{\partial y}{\partial \xi} & \frac{\partial y}{\partial \eta} \end{bmatrix}$$

The determinant can then be written as

$$|\mathcal{J}| = \det \mathcal{J} = \left(\frac{\partial x}{\partial \xi}\frac{\partial y}{\partial \eta} - \frac{\partial x}{\partial \eta}\frac{\partial y}{\partial \xi}\right).$$

The components of the inverse of the pull-back operation (push-forward), the one-to-one correspondence is used. This results in

$$\mathcal{J}^{-1} = \begin{bmatrix} \frac{\partial \xi}{\partial x} & \frac{\partial \xi}{\partial y} \\ \frac{\partial \eta}{\partial x} & \frac{\partial \eta}{\partial y} \end{bmatrix} = \frac{1}{|\mathcal{J}|} \begin{bmatrix} \frac{\partial y}{\partial \eta} & -\frac{\partial x}{\partial \eta} \\ -\frac{\partial y}{\partial \xi} & \frac{\partial x}{\partial \xi} \end{bmatrix}.$$

0-forms remain invariant under transformation, as they are values sampled at that point. The pull-back can be applied to the physical differential basis dx and dy as

$$\Phi^*(\mathrm{d}x) = \frac{\partial x}{\partial \xi}\mathrm{d}\xi + \frac{\partial x}{\partial \eta}\mathrm{d}\eta, \qquad \Phi^*(\mathrm{d}y) = \frac{\partial y}{\partial \xi}\mathrm{d}\xi + \frac{\partial y}{\partial \eta}\mathrm{d}\eta.$$

Similarly, the push-forward can be applied to the reference differential basis $\mathrm{d}\xi$ and $\mathrm{d}\eta$ as

$$\Phi^{-*}(\mathrm{d}\xi) = \frac{\partial \xi}{\partial x}\mathrm{d}x + \frac{\partial \xi}{\partial y}\mathrm{d}y = \frac{1}{|\mathcal{J}|}\left(\frac{\partial y}{\partial \eta}\mathrm{d}x - \frac{\partial x}{\partial \eta}\mathrm{d}y\right),$$
$$\Phi^{-*}(\mathrm{d}\eta) = \frac{\partial \eta}{\partial x}\mathrm{d}x + \frac{\partial \eta}{\partial y}\mathrm{d}y = \frac{1}{|\mathcal{J}|}\left(-\frac{\partial y}{\partial \xi}\mathrm{d}x + \frac{\partial x}{\partial \xi}\mathrm{d}y\right).$$

When looking at 2-forms, the metric is involved. For example,

$$\mathrm{d}x \wedge \mathrm{d}y = \left(\frac{\partial x}{\partial \xi}\mathrm{d}\xi + \frac{\partial x}{\partial \eta}\mathrm{d}\eta\right) \wedge \left(\frac{\partial y}{\partial \xi}\mathrm{d}\xi + \frac{\partial y}{\partial \eta}\mathrm{d}\eta\right) = \left(\frac{\partial x}{\partial \xi}\frac{\partial y}{\partial \eta} - \frac{\partial x}{\partial \eta}\frac{\partial y}{\partial \xi}\right)\mathrm{d}\xi \wedge \mathrm{d}\eta = |\mathcal{J}|\mathrm{d}\xi \wedge \mathrm{d}\eta.$$

Another important consequence of using the mapping is that the solution is represented on the quadrature points present in the reference domain, which are labels for points in the physical domain. Transfinite mappings (mentioned in [31, 32]) from the reference domain are used when arbitrary domains are involved for such calculations.

3.4. Minimisation problems

One of the important steps in using forms to develop a numerical method is to arrive at a weak formulation that can be solved. An example would be the Galerkin method, where any partial differential equation is multiplied by a test function, and integrated over the domain. To introduce the boundary conditions, integration by parts is introduced [7, p. 1-3]. In our case, a different formulation is used, which will result in a weak-form. This involves a (constrained) minimisation problem, where the minimum of a given functional is sought after. The solution is constrained beforehand by the essential boundary conditions on the variables. Variations, or calculus of variations is used for this minimisation. On taking variations of the problem formulations, the weak formulations are obtained [38, p.75-77]. If the exact solution and the variations are smooth enough, the weak formulation leads to the partial differential equations to solve, which can be done by adding explicitly additional boundary conditions, called natural boundary conditions.

Let us understand the procedure to derive weak forms

3.4.1. Getting to the weak forms

The goal, when starting from the minimisation problem is to get a resulting set of equations that will lead to a symmetric matrix to be solved. It is possible to write the Poisson problem, as well as the linear elasticity problem in this manner. This is because all of these can be written in terms of energy in the system, and the energy can be minimised. Let us take the Poisson problem as an example. With $\mathbf{q} = \nabla p$, the energy in the system is written as

$$\mathcal{E}(p) = \int_\Omega \left(\frac{1}{2}|\mathbf{q}|^2 - pf\right)\mathrm{d}\Omega = \int_\Omega \left(\frac{1}{2}|\nabla p|^2 - pf\right)\mathrm{d}\Omega.$$

The pressure p is prescribed as 0 at the boundaries. The minimum energy can be found using variations of the problem. Considering a small change α in the direction $\tilde{p}$, the derivative of the energy is taken with respect to this α, and set to zero. Thus,

$$\begin{aligned}
0 = \left.\frac{\mathrm{d}\mathcal{E}(p+\alpha\tilde{p})}{\mathrm{d}\alpha}\right|_{\alpha=0} &= \int_\Omega \left.\frac{\mathrm{d}\left\{\frac{1}{2}|\nabla p + \alpha\nabla\tilde{p}|^2 - f(p+\alpha\tilde{p})\right\}}{\mathrm{d}\alpha}\right|_{\alpha=0}\mathrm{d}\Omega, \\
&= \int_\Omega \left\{\frac{1}{2}\left(2\nabla\tilde{p}\cdot(\nabla p + \alpha\nabla\tilde{p})\right) - \tilde{p}f\right\}\mathrm{d}\Omega, \\
&= \int_\Omega (\nabla\tilde{p}\cdot\nabla p) - \tilde{p}f\mathrm{d}\Omega, \\
&= (\nabla\tilde{p}, \nabla p)_\Omega - (\tilde{p}, f)_\Omega,
\end{aligned}$$

where α is set to zero and the inner product is written down. This is how the variation with respect to p is taken in the problem.

Since $p = 0$ at the boundaries, on integrating by parts,

$$(\nabla\tilde{p}, \nabla p)_\Omega - (\tilde{p}, f)_\Omega = -(\tilde{p}, \nabla \cdot (\nabla p))_\Omega - (\tilde{p}, f)_\Omega = 0.$$

Because the choice for function $\tilde{p}$ is arbitrary, the result is the Poisson equation

$$-\nabla \cdot (\nabla p) = -\Delta p = f.$$

Additional constraints can also be introduced to the problem. This procedure, called constrained minimisation, involves the use of one or more Lagrange multipliers. Using λ as another Lagrange multiplier, the functional to be minimised becomes

$$\mathcal{E}(\mathbf{q}, \lambda) = \int_\Omega \left(\frac{1}{2}|\mathbf{q}|^2\right) \mathrm{d}\Omega + \int_\Omega (\lambda \mathcal{L}(\mathbf{q}))\, \mathrm{d}\Omega.$$

Here, $\mathcal{L}(\mathbf{q}) = \nabla \cdot \mathbf{q} - f$ is a linear operator. Applying minimisation to such formulations will lead to a mixed formulation. In such cases if a physical constraint is enforced by a Lagrange multiplier, the Lagrange multiplier itself will also have a physical meaning. In this example, when you take the variational derivative with respect to q, the resulting equation is

$$0 = \int_\Omega |\tilde{\mathbf{q}}||\mathbf{q}|\mathrm{d}\Omega + \int_\Omega \lambda \nabla \cdot \tilde{\mathbf{q}} \mathrm{d}\Omega.$$

If you use integration by parts, and the fact that $p = 0$ at the boundaries,

$$0 = \int_\Omega \tilde{\mathbf{q}}\mathbf{q}\mathrm{d}\Omega - \int_\Omega \tilde{\mathbf{q}} \nabla \lambda \mathrm{d}\Omega.$$

With an arbitrary $\tilde{\mathbf{q}}$, the equation reduces to

$$\mathbf{q} - \nabla\lambda = 0$$

Since it is known that $\mathbf{q} = \nabla p$, it can be seen that the Lagrange multiplier λ is nothing but p. This shows that it has a physical meaning. For a deeper discussion of various properties of unconstrained and constrained optimisation problems derived using the Galerkin method, one can check out [6].

3.4.2. The inner product

Weak-form based solutions cannot be formulated, unless the inner product is defined in terms of the exterior product and a Hodge operator [34]. The inner product on forms on the same oriented manifold is always metric dependent.

For two k-forms $a^{(k)}$ and $b^{(k)}$ associated to the same geometry, the inner product is defined as [39, 48]

$$\left(a^{(k)}, b^{(k)}\right)_\Omega = \int_\Omega a^{(k)} \wedge \star b^{(k)}.$$

The inner product is a bilinear form, mapping two differential forms to a scalar. This is symmetric and results in a symmetric mass matrix. In cases where the two forms are in dual spaces to one another, the inner product becomes metric-free, since the wedge product between two forms in the same space will be metric free [27].

Another property of the inner product is that

$$\left(a^{(k-1)}, \mathrm{d}^\star b^{(k)}\right)_\Omega = \left(\mathrm{d}a^{(k-1)}, b^{(k)}\right) - \int_{\partial\Omega} \mathrm{tr}\left(a^{(k-1)}\right) \wedge \mathrm{tr}\left(b^{(k)}\right).$$

where $\mathrm{d}^\star = (-1)^{n(k+1)+1} \star \mathrm{d} \star$ [48] is the co-differential operator and d is the exterior derivative. This property is similar to the Green's formula [5] and integration by parts [39].

3.5. Error Computation

In this report there are many instances where it is beneficial to look at by how much the point-wise evaluation of the solution in contour plots differ from the exact solution at these points. Thus, these errors are computed using several different kinds of norms. This measurement also helps to quantitatively determine how the convergence of different formulations.

3.5.1. Norms

The most commonly used norm is the L^2-error norm, which for a scalar (here p) is given by

$$\|\epsilon_p\|_{L^2(\Omega)} = \sqrt{\int_\Omega \left(p^{ex}(x,y) - p^h(x,y)\right)^2 \mathrm{d}\Omega}, \tag{3.3}$$

Since $x(\xi,\eta)$ and $y(\xi,\eta)$ are functions of ξ and η (i.e. the reference coordinates), especially since the point-wise evaluations happen at the points when (ξ,η) is mapped on to its respective physical coordinates, it is better to write the norm in terms of ξ,η instead of x,y. Thus,

$$\|\epsilon_p\|_{L^2(\Omega)} = \sqrt{\int_\Omega \left(p^{ex}\left(x(\xi,\eta),y(\xi,\eta)\right) - p^h(\xi,\eta)\right)^2 \mathrm{d}\Omega}.$$

Note that the reconstructed solution is already in represented at the reference coordinates. Further, the integral can be simplified using Gaussian quadrature as

$$\|\epsilon_p\|_{L^2(\Omega)} = \sum_r \sum_s \left(p^{ex}\left(x(\xi_r,\eta_s),y(\xi_r,\eta_s)\right) - p^h(\xi_r,\eta_s)\right)^2 \left(\det \mathcal{J}(\xi_r,\eta_s)\right) w_r\, w_s. \tag{3.4}$$

where w_r and w_s are the integration weights for the quadrature. Additionally, the function $\det \mathcal{J}$ enters as the integration weights operate in the reference domain, while the actual integration needs to take place in the physical domain (where the error is calculated).

For a vector (here the flux $\mathbf{q}$), which is represented as a 1-form on the grid, the Pythagorean sum of the errors of both representative components should be taken. That is

$$\|\epsilon_{\mathbf{q}}\|^2_{L^2(\Omega)} = \|\epsilon_{q_x}\|^2_{L^2(\Omega)} + \left\|\epsilon_{q_y}\right\|^2_{L^2(\Omega)},$$

when in $\mathbb{R}^2$. For the stress tensor,

$$\left\|\epsilon_{\underline{\boldsymbol{\sigma}}}\right\|^2_{L^2(\Omega)} = \|\epsilon_{\sigma_{xx}}\|^2_{L^2(\Omega)} + \left\|\epsilon_{\sigma_{yy}}\right\|^2_{L^2(\Omega)} + \left\|\epsilon_{\sigma_{xy}}\right\|^2_{L^2(\Omega)} + \left\|\epsilon_{\sigma_{yx}}\right\|^2_{L^2(\Omega)}.$$

Apart from the L^2-norm, the L^∞ can additionally be used to identify or rule out the presence of local (large) oscillations in the solution. This norm is defined as

$$\|\epsilon_p\|_{L^\infty(\Omega)} = \max_{r,s} \left|p^{ex}\left(x(\xi_r,\eta_s),y(\xi_r,\eta_s)\right) - p^h(\xi_r,\eta_s)\right|. \tag{3.5}$$

This error emphasises the cases where a single point has a high error, which would be weighted out in the case of an L^2-norm. This is especially useful when proving that the error for topological relations is indeed exact.

3.5.2. Convergence

The interpolation error can be expressed as

$$\epsilon = Ch^{\alpha p} \tag{3.6}$$

where C and α are positive non-zero constants, $0 < \alpha < 1$. On increasing the polynomial degree p, there is an expected exponential decrease in the error, which should be easy to see in a plot with a linear scale for p but a logarithmic scale for the error. On increasing the number of elements the convergence will be of the order of αp, as h is the inverse of the mesh width. A graph where both the error and the mesh width are in the logarithmic scale shows optimal convergence, which shows a straight line with slope p. The constant C only determines the height of the line in this plot, which is influenced by the quality of the mesh.

It is valuable to compare the error of the solution to the interpolation error. This indirectly indicates sub-optimal performance, for example, $\alpha < \alpha_{opt} < 1$. This interpolation error, with the exact solution projected on the mesh denoted by $\left(f^{ex}\right)^h$, is computed with

$$\|\epsilon_{\mathcal{I}}\|^2_{\mathcal{L}^2(\Omega)} = \int_\Omega \left(f^{ex}(x,y) - \left(f^{ex}\right)^h(x,y)\right)^2 \mathrm{d}\Omega. \tag{3.7}$$

3.6. Grid construction

With the reference domain and physical domain already defined, there is a need to map the points on the reference domain to ones on the physical domain. Thus, grid generation on the physical domain is very important, which is also used to generate the components of the Jacobian, as seen in section 3.7.

As a simplification and to convert (ξ, η) from $[-1,1]\times[-1,1]$ to $[0,1]\times[0,1]$, another mapping is introduced,

$$s = \frac{1+\xi}{2}, \qquad t = \frac{1+\eta}{2}.$$

The idea behind grid construction is that the physical boundaries are known. Keeping this in mind, the first step would be to write down the coordinates of each physical boundary as a function of the boundaries in the reference domain. For instance, if the "bottom" boundary is denoted by (x_b, y_b), then these coordinates should be written as a function of the variable coordinate in the bottom boundary of the reference domain, which is s. That is

$$x_b \equiv x_b(s), \qquad y_b \equiv y_b(s).$$

Similarly, if (x_t, y_t), (x_l, y_l) and (x_r, y_r) denote the "top", "left" and "right" boundaries respectively, then

$$\begin{aligned} x_t &\equiv x_t(s), & y_t &\equiv y_t(s),\\ x_l &\equiv x_l(t), & y_l &\equiv y_l(t),\\ x_r &\equiv x_r(t), & y_r &\equiv y_r(t). \end{aligned}$$

Keep in mind that the corners should also be at the same position, regardless of which boundary function you are using. This means that there are several consistency conditions which need to be kept in mind, which are

$$\begin{aligned} x_t(s=1) &= x_r(t=1), & y_t(s=1) &= y_r(t=1),\\ x_t(s=0) &= x_l(t=1), & y_t(s=0) &= y_l(t=1),\\ x_b(s=1) &= x_r(t=0), & y_b(s=1) &= y_r(t=0),\\ x_b(s=0) &= x_l(t=0), & y_b(s=0) &= y_r(t=0). \end{aligned}$$

With this in mind, the grid can be generated for the physical domain as [31, 32]

$$\begin{aligned} x(s,t) =& (1-t)x_b(s) + t x_t(s) + (1-s)x_t(t) + s x_r(t)\\ &- \left[st\, x_t(1) + s(1-t)x_b(1) + t(1-s)x_t(0) + (1-s)(1-t)x_b(0)\right],\\ y(s,t) =& (1-t)y_b(s) + t y_t(s) + (1-s)y_t(t) + s y_r(t)\\ &- \left[st\, y_t(1) + s(1-t)y_b(1) + t(1-s)y_t(0) + (1-s)(1-t)y_b(0)\right]. \end{aligned}$$

This is how the grid is generated for values of (s,t) (and thus (ξ,η)).

In order to separate the domain into several elements, the first step is to generate a low-resolution grid, which corresponds to how many elements are needed in both dimensions. These would become the boundaries of the respective elements. Then, it is only needed to generate the grid for every element assuming that it is a physical domain on its own, with the boundaries of this physical domain being the boundaries of the element in question.

3.7. Components of Jacobian

One of the important parts of the formulations where the physical domain is mapped onto the reference domain is to determine the components of the Jacobian between the two domains, given by

$$\mathcal{J} = \begin{bmatrix} \frac{\partial x}{\partial \xi} & \frac{\partial x}{\partial \eta} \\ \frac{\partial y}{\partial \xi} & \frac{\partial y}{\partial \eta} \end{bmatrix}.$$

It is necessary to calculate these components for any arbitrary physical domain, to map it into the physical domain (for example, when prescribing the boundary conditions), as well as to map it back from the reference domain to the physical domain (when reconstructing results for example). This is especially a problem when meshes are constructed as they are in Chapter 5-Chapter 8.

For example, usually, the boundaries of the physical domain are prescribed as functions of (ξ, η) at the boundaries, along with the values at the corners of the (reference) domain. Transfinite mappings are used to construct the interior points of the domain. While the functions at the boundaries are available, the components of the Jacobian can be analytically calculated at the boundaries. However, the interior of the domain also needs good approximations of these components.

There is an easy way to compute these when the physical coordinates are known, using the primal basis functions mentioned in subsection 3.2.2. Let us assume that there are N_x number of points on the mesh in each direction in the reference domain. This will translate to the physical domain containing $(N_x)^2$ points which are mapped onto the nodes in the reference domain. If the x and y coordinates are determined using transfinite mappings, then you can also write

$$\begin{aligned} x &= \sum_{r}^{N_x} \sum_{s}^{N_y} x(\xi_r, \eta_s) h_r(\xi) h_s(\eta), \\ y &= \sum_{r}^{N_x} \sum_{s}^{N_y} y(\xi_r, \eta_s) h_r(\xi) h_s(\eta), \end{aligned}$$

This is just another way to write the coordinates, as the property of the primal basis function is that $h_r(\xi)$ is zero at all other nodes except when $\xi = \xi_r$, and similarly for $h_s(\eta)$. Note that this representation will generate a polynomial representation of x and y. In general, this generates an error in the representation, but as long as N_x and N_y are high enough values that the error is of the order of machine precision, then this representation can be used. Even for a circular boundary, the idea is the number of nodes is chosen such that the boundary can be represented as a polynomial using primal bases.

With this approximation for the physical coordinates, the primal edge functions can be used to compute the components of the Jacobian, as

$$\begin{aligned} \frac{\partial x}{\partial \xi} &= \sum_{r}^{N_x - 1} \sum_{s}^{N_y} \left(x(\xi_{r+1}, \eta_s) - x(\xi_r, \eta_s) \right) e_r(\xi) h_s(\eta), \\ \frac{\partial x}{\partial \eta} &= \sum_{r}^{N_x} \sum_{s}^{N_y - 1} \left(x(\xi_r, \eta_{s+1}) - x(\xi_r, \eta_s) \right) h_r(\xi) e_s(\eta), \\ \frac{\partial y}{\partial \xi} &= \sum_{r}^{N_x - 1} \sum_{s}^{N_y} \left(y(\xi_{r+1}, \eta_s) - y(\xi_r, \eta_s) \right) e_r(\xi) h_s(\eta), \\ \frac{\partial y}{\partial \eta} &= \sum_{r}^{N_x} \sum_{s}^{N_y - 1} \left(y(\xi_r, \eta_{s+1}) - y(\xi_r, \eta_s) \right) h_r(\xi) e_s(\eta). \end{aligned}$$

These operations can accomplished using incidence matrices, one for the derivative with respect to ξ, and one for the derivative with respect to η. If the physical coordinates are written as a vector in x-lexicographic order, then the components of the matrices for $N_x = 4$ is

$$\mathbb{E}_\xi = \begin{bmatrix} -1 & 1 & 0 & 0 & 0 & 0 & 0 & 0 & 0 & 0 & 0 & 0 & 0 & 0 & 0 & 0 \\ 0 & -1 & 1 & 0 & 0 & 0 & 0 & 0 & 0 & 0 & 0 & 0 & 0 & 0 & 0 & 0 \\ 0 & 0 & -1 & 1 & 0 & 0 & 0 & 0 & 0 & 0 & 0 & 0 & 0 & 0 & 0 & 0 \\ 0 & 0 & 0 & 0 & -1 & 1 & 0 & 0 & 0 & 0 & 0 & 0 & 0 & 0 & 0 & 0 \\ 0 & 0 & 0 & 0 & 0 & -1 & 1 & 0 & 0 & 0 & 0 & 0 & 0 & 0 & 0 & 0 \\ 0 & 0 & 0 & 0 & 0 & 0 & -1 & 1 & 0 & 0 & 0 & 0 & 0 & 0 & 0 & 0 \\ 0 & 0 & 0 & 0 & 0 & 0 & 0 & 0 & -1 & 1 & 0 & 0 & 0 & 0 & 0 & 0 \\ 0 & 0 & 0 & 0 & 0 & 0 & 0 & 0 & 0 & -1 & 1 & 0 & 0 & 0 & 0 & 0 \\ 0 & 0 & 0 & 0 & 0 & 0 & 0 & 0 & 0 & 0 & -1 & 1 & 0 & 0 & 0 & 0 \\ 0 & 0 & 0 & 0 & 0 & 0 & 0 & 0 & 0 & 0 & 0 & 0 & -1 & 1 & 0 & 0 \\ 0 & 0 & 0 & 0 & 0 & 0 & 0 & 0 & 0 & 0 & 0 & 0 & 0 & -1 & 1 & 0 \\ 0 & 0 & 0 & 0 & 0 & 0 & 0 & 0 & 0 & 0 & 0 & 0 & 0 & 0 & -1 & 1 \end{bmatrix},$$

and

$$\mathbb{E}_\eta = \begin{bmatrix} -1 & 0 & 0 & 0 & 1 & 0 & 0 & 0 & 0 & 0 & 0 & 0 & 0 & 0 & 0 & 0 \\ 0 & -1 & 0 & 0 & 0 & 1 & 0 & 0 & 0 & 0 & 0 & 0 & 0 & 0 & 0 & 0 \\ 0 & 0 & -1 & 0 & 0 & 0 & 1 & 0 & 0 & 0 & 0 & 0 & 0 & 0 & 0 & 0 \\ 0 & 0 & 0 & -1 & 0 & 0 & 0 & 1 & 0 & 0 & 0 & 0 & 0 & 0 & 0 & 0 \\ 0 & 0 & 0 & 0 & -1 & 0 & 0 & 0 & 1 & 0 & 0 & 0 & 0 & 0 & 0 & 0 \\ 0 & 0 & 0 & 0 & 0 & -1 & 0 & 0 & 0 & 1 & 0 & 0 & 0 & 0 & 0 & 0 \\ 0 & 0 & 0 & 0 & 0 & 0 & -1 & 0 & 0 & 0 & 1 & 0 & 0 & 0 & 0 & 0 \\ 0 & 0 & 0 & 0 & 0 & 0 & 0 & -1 & 0 & 0 & 0 & 1 & 0 & 0 & 0 & 0 \\ 0 & 0 & 0 & 0 & 0 & 0 & 0 & 0 & -1 & 0 & 0 & 0 & 1 & 0 & 0 & 0 \\ 0 & 0 & 0 & 0 & 0 & 0 & 0 & 0 & 0 & -1 & 0 & 0 & 0 & 1 & 0 & 0 \\ 0 & 0 & 0 & 0 & 0 & 0 & 0 & 0 & 0 & 0 & -1 & 0 & 0 & 0 & 1 & 0 \\ 0 & 0 & 0 & 0 & 0 & 0 & 0 & 0 & 0 & 0 & 0 & -1 & 0 & 0 & 0 & 1 \end{bmatrix}.$$

For all further applications, $N_x = N_y = 50$ is used to make the mesh on the reference domain, which should also make the interpolation error up to machine precision for the domains being used in this thesis.

3.8. Mixed formulation

This thesis involves the use of mixed basis functions. These are a combination of primal basis functions in one direction, along with other dual functions, when you consider primal basis in 1-dimension. For example, one of the formulations that is used is

$$\overline{\sigma_{\xi x}} = \sum_{i=1}^{N+1}\sum_{j=1}^{N+1}(\sigma_{\xi x})_{ij}\; h_i(\xi)\; e'_j(\eta)\;,$$
$$\overline{\sigma_{\eta x}} = \sum_{i=1}^{N}\sum_{j=1}^{N}(\sigma_{\eta x})_{ij}\; e_i(\xi)\; h'_j(\eta)\;,$$

where

$$e'_k(\eta_j) = h_i(\eta_j)\left(\mathbb{M}^{(0)}\right)^{-1}_{ik}, \qquad h'_l(\eta_j) = e_i(\eta_j)\left(\mathbb{M}^{(1)}\right)^{-1}_{il}.$$

These expressions denote how the dual basis are constructed in 1-dimension. The tensor product can be used to construct the mixed basis, using either the nodal or edge functions which can be either primal or dual. However, do note that the dual of the tensor product of basis functions need not be equal to the tensor product of the dual functions. This means that

$$\widetilde{h_i(x)e'_j}(y) \neq e'_i(x)h_j(y).$$

The equality is only valid when an orthogonal domain is used, and is thus necessary to convert all quantities into ξ, η coordinates using the mapping. Thus,

$$\widetilde{h_i(\xi)e'_j}(\eta) = e'_i(\xi)h_j(\eta).$$

3.9. Summary

By defining the generation of grids, calculating the components of the Jacobian, how to project continuous quantities and writing down the discrete exterior derivative for an example, as well as defining the basis functions, and the notion of inner product, it is possible to construct the matrices required for the mimetic spectral element method. The mapping helps to translate these quantities in the reference domain to those in the physical domain and vice versa. The notion of the error and how to calculate it is now known too, allowing a quantitative analysis of the results. With this, implementations can be tested.

4

Unsteady Linear Elasticity

The first step towards using the Mimetic Spectral element method for Fluid-Structure Interaction problems involves the use of the mimetic spectral element method for unsteady solid problems. So far, the hybrid version of the mimetic spectral element method behaved great when there is an orthogonal domain involved, when both linear momentum and angular momentum are conserved. A natural extension to this would be to look at how this is affected when an unsteady problem (where an additional unsteady force in the equilibrium of forces) is considered.

At least that was the intended goal. However, there are several problems encountered during implementation, which are mentioned in Section 4.4. These issues will be looked at in subsequent chapters, so this chapter serves as a motivation for further studies.

4.1. Representation of physical quantities

In order to have topological relations for the divergence of stress and gradient of the displacement (for example), it is important to write down the relevant quantities in terms of vector-valued or covector-valued forms. Further, if the covector- and vector-values are in the same coordinate system, then their duality pairing will nullify the value part itself. With this representation, the goal is to make use of these identities to construct a Lagrangian formulation.

4.1.1. Stress tensor

The stress tensor is represented as a covector-valued $(n-1)$-form (in 2 dimensions, this is a 1-form), and it is written down as a pseudo-form. The stress tensor is also written as 1-form in the time dimension. With this in mind, the stress is represented as

$$\underline{\underline{\boldsymbol{\sigma}}} = \mathrm{d}x \otimes (\sigma_{xx}\mathrm{d}y - \sigma_{yx}\mathrm{d}x)\,\mathrm{d}t + \mathrm{d}y \otimes (\sigma_{xy}\mathrm{d}y - \sigma_{yy}\mathrm{d}x)\,\mathrm{d}t. \tag{4.1}$$

Thus, the divergence of stress can be easily written down as

$$\boldsymbol{\nabla} \cdot \underline{\underline{\boldsymbol{\sigma}}} = \left[\mathrm{d}x \otimes \left(\frac{\partial \sigma_{xx}}{\partial x} + \frac{\partial \sigma_{yx}}{\partial y}\right)\mathrm{d}x\mathrm{d}y \wedge \mathrm{d}t\right] + \left[\mathrm{d}y \otimes \left(\frac{\partial \sigma_{xy}}{\partial x} + \frac{\partial \sigma_{yy}}{\partial y}\right)\mathrm{d}x\mathrm{d}y \wedge \mathrm{d}t\right],$$

becomes a covector-valued 2-form (in general, n-form) in space, and the signs of the respective components in the representation of the divergence is accurate. Also note that for this to hold, the covector-values themselves should be invariant in that coordinate system, i.e. the gradient of the covector-values should be zero. With this formulation where the covectors are basic 1-forms made out of coordinate bases, this criterion is satisfied.

4.1.2. Position

Position is defined as a vector-valued 0-form (0 form in time as well). It can be represented as

$$\mathbf{X} = \frac{\partial}{\partial x} \otimes X + \frac{\partial}{\partial y} \otimes Y. \tag{4.2}$$

The idea to represent the position as a vector-valued quantity is so that whenever there is a duality pairing between the displacement and the stress, it results in no contribution from the value part. This way, the form parts are the only ones that take part in the calculations, which can be computed in the reference domain itself.

4.1.3. Rotation tensor

The rotation is defined as the antisymmetric part of the displacement gradient tensor. In order to easily represent this quantity, it is easier to represent this in terms of scalar ω, written as

$$\underline{\underline{\boldsymbol{\omega}}} = \omega \begin{bmatrix} 0 & -1 \\ 1 & 0 \end{bmatrix}, \tag{4.3}$$

4.1.4. Momentum

The momentum is represented as a covector-valued n-form in space (2-form in this case), and as a 0-form in time. Thus,

$$\boldsymbol{\phi} = (\mathrm{d}x \otimes \phi_x \mathrm{d}x\mathrm{d}y) + (\mathrm{d}y \otimes \phi_y \mathrm{d}x\mathrm{d}y)\,. \tag{4.4}$$

This definition enables the time derivative of momentum (which is the force) to have the same values and forms as the divergence of stress, as

$$\frac{\partial \boldsymbol{\phi}}{\partial t} = \left(\mathrm{d}x \otimes \frac{\partial \phi_x}{\partial t}\mathrm{d}x\mathrm{d}y \wedge \mathrm{d}t\right) + \left(\mathrm{d}y \otimes \frac{\partial \phi_y}{\partial t}\mathrm{d}x\mathrm{d}y \wedge \mathrm{d}t\right).$$

This is under the assumption that the covector-values themselves don't change with time, which should hold as they are based on the coordinate system.

4.2. Lagrangian formulation

The idea to solve the unsteady solid problem with the mimetic spectral element method begins with the Lagrangian problem formulation. The idea is to minimise the Lagrangian formulation using variational calculus. This process cannot be understated and ideally should be done in a way that the variational derivatives of the formulation themselves denote conservation laws or constitutive equations.

With this in mind, the theoretical Lagrangian problem formulation can be written as

$$\begin{aligned}
\mathcal{L}\Big(\mathbf{X}, \underline{\underline{\boldsymbol{\sigma}}}, \boldsymbol{\omega}, \boldsymbol{\phi}; \underline{\underline{\mathbf{C}}}, \boldsymbol{\rho}, \mathbf{X_0}, \mathbf{f}\Big) = \; & \int_{\Omega_t}\int_{\Omega} \left(\omega(\sigma_{xy} - \sigma_{yx})\right) \mathrm{d}\Omega\mathrm{d}t \\
& + \int_{\Omega_t}\int_{\Omega} \Big((X - X_0)\tfrac{\partial \sigma_{xx}}{\partial x} - \tfrac{\partial (X - X_0)}{\partial y}\sigma_{yx} - \tfrac{\partial (Y - Y_0)}{\partial x}\sigma_{xy} + (Y - Y_0)\tfrac{\partial \sigma_{yy}}{\partial y}\Big)\mathrm{d}\Omega\mathrm{d}t \\
& + \int_{\Omega_t}\int_{\Omega} \Big(\big(-X\tfrac{\partial \phi_x}{\partial t} - Y\tfrac{\partial \phi_y}{\partial t}\big) + (X - X_0)\, f_x + (Y - Y_0)\, f_y\Big)\mathrm{d}\Omega\mathrm{d}t \\
& + \int_{\Omega_t}\int_{\Omega} \Big(\tfrac{1}{2}\underline{\underline{\boldsymbol{\sigma}}}^T\big(\underline{\underline{\mathbf{C}}}\big)\underline{\underline{\boldsymbol{\sigma}}}\Big)\mathrm{d}\Omega\mathrm{d}t \\
& - \int_{\Omega_t}\int_{\Omega} \Big(\tfrac{1}{2}\boldsymbol{\phi}^T\tfrac{1}{\boldsymbol{\rho}}\boldsymbol{\phi}\Big)\mathrm{d}\Omega\mathrm{d}t \\
& - \int_{\Omega_t}\oint_{\partial\Omega} \left((X - X_0)_P\sigma_{xx}n_x + (Y - Y_0)_P\sigma_{yy}n_y\right)\mathrm{d}\Gamma\mathrm{d}t \\
& + \int_{\Omega_t}\oint_{\partial\Omega} \left(X(\sigma_{yx})_P n_y + Y(\sigma_{xy})_P n_x\right)\mathrm{d}\Gamma\mathrm{d}t \\
& - \int_{\Omega} \left(\phi_x X_0 + \phi_y Y_0\right)\mathrm{d}\Omega
\end{aligned} \tag{4.5}$$

Note that the symbols represent the quantities already defined in Section 4.1. Also note that $(\sigma_{xy})_P$ indicates the prescribed value of the quantity, in this case σ_{xy}, at the relevant boundaries. This sign convention will be used to denote the values prescribed at the boundaries in the following chapters.

Further, Ω denotes the physical domain for the problem, while Ω_t denotes the time interval considered. $\mathbf{X_0}$ is the initial position and $\mathbf{f}$ is the body force. ρ and $\underline{\underline{\mathbf{C}}}$ indicate the density and the compliance tensor for the material respectively.

Now, let us look at what the variational derivatives (and thus the equations involving the unknowns in this formulation) shape up to be.

4.2.1. Constitutive relation

The variational derivative of the Lagrangian formulation with respect to $\underline{\underline{\boldsymbol{\sigma}}}$, when equated to zero, reduces to

$$\begin{array}{l} \int_{\Omega_t}\int_{\Omega}\left(\omega(\widetilde{\sigma_{xy}}-\widetilde{\sigma_{yx}})\right)\mathrm{d}\Omega\mathrm{d}t \\ +\int_{\Omega_t}\int_{\Omega}\Big((X-X_0)\frac{\partial\widetilde{\sigma_{xx}}}{\partial x}-\frac{\partial(X-X_0)}{\partial y}\widetilde{\sigma_{yx}}-\frac{\partial(Y-Y_0)}{\partial x}\widetilde{\sigma_{xy}}+(Y-Y_0)\frac{\partial\widetilde{\sigma_{yy}}}{\partial y}\Big)\mathrm{d}\Omega\mathrm{d}t \\ +\int_{\Omega_t}\int_{\Omega}\Big(\underline{\underline{\widetilde{\boldsymbol{\sigma}}}}^T(\underline{\underline{\mathbf{C}}})\underline{\underline{\boldsymbol{\sigma}}}\Big)\mathrm{d}\Omega\mathrm{d}t \end{array} = \mathcal{B}_\sigma, \tag{4.6}$$

where

$$\mathcal{B}_\sigma = \int_{\Omega_t}\oint_{\partial\Omega}\left((X-X_0)_P\widetilde{\sigma_{xx}}n_x+(Y-Y_0)_P\widetilde{\sigma_{yy}}n_y\right)\mathrm{d}\Gamma\mathrm{d}t. \tag{4.7}$$

This boundary term shows the displacement (with respect to the initial position $\mathbf{X_0}$) that is being prescribed at the normal boundaries. Using integration by parts on this boundary term, the relation can be reduced to

$$\begin{array}{l} \int_{\Omega_t}\int_{\Omega}\left(\omega(\widetilde{\sigma_{xy}}-\widetilde{\sigma_{yx}})\right)\mathrm{d}\Omega\mathrm{d}t \\ +\int_{\Omega_t}\int_{\Omega}\Big(-\frac{\partial(X-X_0)}{\partial x}\widetilde{\sigma_{xx}}-\frac{\partial(X-X_0)}{\partial y}\widetilde{\sigma_{yx}}-\frac{\partial(Y-Y_0)}{\partial x}\widetilde{\sigma_{xy}}-\frac{\partial(Y-Y_0)}{\partial y}\widetilde{\sigma_{yy}}\Big)\mathrm{d}\Omega\mathrm{d}t \\ +\int_{\Omega_t}\int_{\Omega}\Big(\underline{\underline{\widetilde{\boldsymbol{\sigma}}}}^T\underline{\underline{\mathbf{C}\boldsymbol{\sigma}}}\Big)\mathrm{d}\Omega\mathrm{d}t \end{array} = 0.$$

With $\underline{\underline{\boldsymbol{\sigma}}}$ being arbitrary, the resulting relation can be written down as

$$\underline{\underline{\mathbf{C}\boldsymbol{\sigma}}} = \frac{1}{2}\left[\boldsymbol{\nabla}\left(\mathbf{X}-\mathbf{X_0}\right)+\boldsymbol{\nabla}\left(\mathbf{X}-\mathbf{X_0}\right)^T\right],$$

because

$$\boldsymbol{\omega} = \frac{1}{2}\left[\boldsymbol{\nabla}\left(\mathbf{X}-\mathbf{X_0}\right)-\boldsymbol{\nabla}\left(\mathbf{X}-\mathbf{X_0}\right)^T\right].$$

This is the relation used in Hooke's law for linear elastic solids. This is the way the constitutive law for the material is enforced.

In this study (and all further studies in this document), the compliance tensor $\underline{\underline{\mathbf{C}}}$ for an isotropic material is used.

$$\begin{aligned} C_{11}\sigma_{xx}+C_{14}\sigma_{yy} &= \frac{\partial(X-X_0)}{\partial x} \\ C_{22}\sigma_{yx} &= \frac{\partial(X-X_0)}{\partial y}+\omega \\ C_{33}\sigma_{xy} &= \frac{\partial(Y-Y_0)}{\partial x}-\omega \\ C_{41}\sigma_{xx}+C_{44}\sigma_{yy} &= \frac{\partial(Y-Y_0)}{\partial y}, \end{aligned}$$

where

$$\begin{aligned} C_{11} = C_{44} &= \frac{1}{E} \\ C_{14} = C_{41} &= -\frac{\nu}{E} \\ C_{22} = C_{33} &= \frac{1+\nu}{E}. \end{aligned}$$

with ν being Poisson's ratio of the material and E being Young's modulus of elasticity.

4.2.2. Conservation of linear momentum

If you take the variational derivative with respect to $\mathbf{X}$ and equate it to zero,

$$\begin{array}{l} \int_{\Omega_t}\int_{\Omega}\Big(\widetilde{X}\frac{\partial\sigma_{xx}}{\partial x}-\frac{\partial\widetilde{X}}{\partial y}\sigma_{yx}-\frac{\partial\widetilde{Y}}{\partial x}\sigma_{xy}+\widetilde{Y}\frac{\partial\sigma_{yy}}{\partial y}\Big)\mathrm{d}\Omega\mathrm{d}t \\ +\int_{\Omega_t}\int_{\Omega}\Big(\big(-\widetilde{X}\frac{\partial\phi_x}{\partial t}-\widetilde{Y}\frac{\partial\phi_y}{\partial t}\big)+\widetilde{X}f_x+\widetilde{Y}f_y\Big)\mathrm{d}\Omega\mathrm{d}t \end{array} = -\mathcal{B}_{\mathbf{X}}, \tag{4.8}$$

with

$$\mathcal{B}_{\mathbf{X}} = \int_{\Omega_t} \oint_{\partial\Omega} \left(\widetilde{X}(\sigma_{yx})_P n_y + \widetilde{Y}(\sigma_{xy})_P n_x \right) \mathrm{d}\Gamma \mathrm{d}t. \tag{4.9}$$

Using integration by parts on the boundary term results in

$$\begin{array}{l} \int_{\Omega_t} \int_{\Omega} \left(\widetilde{X} \frac{\partial \sigma_{xx}}{\partial x} + \widetilde{X} \frac{\partial \sigma_{yx}}{\partial y} + \widetilde{Y} \frac{\partial \sigma_{xy}}{\partial x} + \widetilde{Y} \frac{\partial \sigma_{yy}}{\partial y} \right) \mathrm{d}\Omega \mathrm{d}t \\ + \int_{\Omega_t} \int_{\Omega} \left(\left(- \widetilde{X} \frac{\partial \phi_x}{\partial t} - \widetilde{Y} \frac{\partial \phi_y}{\partial t} \right) + \widetilde{X} f_x + \widetilde{Y} f_y \right) \mathrm{d}\Omega \mathrm{d}t \end{array} = 0.$$

With the assumption that this should hold for arbitrary $\widetilde{X}$ and $\widetilde{Y}$, the resulting equations are

$$\begin{aligned} \frac{\partial \sigma_{xx}}{\partial x} + \frac{\partial \sigma_{yx}}{\partial y} - \frac{\partial \phi_x}{\partial t} + f_x &= 0 \\ \frac{\partial \sigma_{xy}}{\partial x} + \frac{\partial \sigma_{yy}}{\partial y} - \frac{\partial \phi_y}{\partial t} + f_y &= 0, \end{aligned}$$

which is the conservation of linear momentum for a body undergoing unsteady motion.

4.2.3. Conservation of angular momentum

Taking the variational derivative with respect to $\boldsymbol{\omega}$, and equating the remaining terms in the Lagrangian formulation to zero,

$$\int_{\Omega_t} \int_{\Omega} (\widetilde{\omega}(\sigma_{xy} - \sigma_{yx})) \, \mathrm{d}\Omega \mathrm{d}t = 0 \tag{4.10}$$

Assuming that this holds for arbitrary $\widetilde{\omega}$, then

$$\sigma_{xy} - \sigma_{yx} = 0$$

This equation, if linear momentum is conserved exactly, should also conserve angular momentum exactly.

4.2.4. Momentum-velocity correlation

Taking the variational derivative with respect to $\boldsymbol{\phi}$, and equating the remaining terms in the Lagrangian formulation to zero,

$$\int_{\Omega_t} \int_{\Omega} \left(- X \frac{\partial \widetilde{\phi_x}}{\partial t} - Y \frac{\partial \widetilde{\phi_y}}{\partial t} \right) \mathrm{d}\Omega \mathrm{d}t - \int_{\Omega_t} \int_{\Omega} \left(\widetilde{\boldsymbol{\phi}}^T \frac{1}{\boldsymbol{\rho}} \boldsymbol{\phi} \right) \mathrm{d}\Omega \mathrm{d}t = -\mathcal{I}_{\boldsymbol{\phi}} \tag{4.11}$$

$$\mathcal{I}_{\boldsymbol{\phi}} = \int_{\Omega} \left(\widetilde{\phi_x} X_0 + \widetilde{\phi_y} Y_0 \right) \mathrm{d}\Omega \tag{4.12}$$

Using integration by parts, this equation can be simplified into

$$\int_{\Omega_t} \int_{\Omega} \left(\frac{\partial X}{\partial t} \widetilde{\phi_x} + \frac{\partial Y}{\partial t} \widetilde{\phi_y} \right) \mathrm{d}\Omega \mathrm{d}t - \int_{\Omega_t} \int_{\Omega} \left(\widetilde{\boldsymbol{\phi}}^T \frac{1}{\boldsymbol{\rho}} \boldsymbol{\phi} \right) \mathrm{d}\Omega \mathrm{d}t = 0$$

Assuming that $\widetilde{\boldsymbol{\phi}}$ is arbitrary, then the equation can be reduced to

$$\begin{aligned} \frac{\partial X}{\partial t} - \frac{1}{\rho} \phi_x &= 0 \\ \frac{\partial Y}{\partial t} - \frac{1}{\rho} \phi_y &= 0 \end{aligned}$$

This equation shows the relation between velocity and momentum. This can be considered another constitutive relation used in this formulation.

4.3. Spectral bases

As part of the spectral element method, the idea is to discretise the quantities in terms of spectral bases. The availability of the dual polynomials is beneficial, as the dual quantities can be directly represented using its dual polynomial representation. With this in mind, the stress components are written as

$$\begin{aligned}
\overline{\sigma_{xx}} &= \sum_{i=1}^{N+1}\sum_{j=1}^{N+1}\sum_{k=1}^{N_t}(\sigma_{xx})_{ijk}\; h_i(x)\; e'_j(y)\; e_k(t),\\
\overline{\sigma_{yx}} &= \sum_{i=1}^{N}\sum_{j=1}^{N}\sum_{k=1}^{N_t}(\sigma_{yx})_{ijk}\; e_i(x)\; h'_j(y)\; e_k(t),\\
\overline{\sigma_{xy}} &= \sum_{i=1}^{N}\sum_{j=1}^{N}\sum_{k=1}^{N_t}(\sigma_{xy})_{ijk}\; h'_i(x)\; e_j(y)\; e_k(t),\\
\overline{\sigma_{yy}} &= \sum_{i=1}^{N+1}\sum_{j=1}^{N+1}\sum_{k=1}^{N_t}(\sigma_{yy})_{ijk}\; e'_i(x)\; h_j(y)\; e_k(t).
\end{aligned}$$

Using these bases, the conservation of linear momentum can be written as

$$\begin{aligned}
\frac{\partial\overline{\sigma_{xx}}}{\partial x}+\frac{\partial\overline{\sigma_{yx}}}{\partial y} = {} & \textstyle\sum_{i=1}^{N}\sum_{j=1}^{N+1}\sum_{k=1}^{N_t}\Big((\sigma_{xx})_{i+1,j,k}-(\sigma_{xx})_{i,j,k}\Big)\; e_i(x)\; e'_j(y)\; e_k(t)+\\
& \textstyle\sum_{i=1}^{N}\sum_{j=1}^{N+1}\sum_{k=1}^{N_t}\Big((\sigma_{yx})_{i,j,k}-(\sigma_{yx})_{i,j-1,k}\Big)\; e_i(x)\; e'_j(y)\; e_k(t),\\
\frac{\partial\overline{\sigma_{xy}}}{\partial x}+\frac{\partial\overline{\sigma_{yy}}}{\partial y} = {} & \textstyle\sum_{i=1}^{N+1}\sum_{j=1}^{N}\sum_{k=1}^{N_t}\Big((\sigma_{xy})_{i,j,k}-(\sigma_{xy})_{i-1,j,k}\Big)\; e'_i(x)\; e_j(y)\; e_k(t)+\\
& \textstyle\sum_{i=1}^{N+1}\sum_{j=1}^{N}\sum_{k=1}^{N_t}\Big((\sigma_{yy})_{i,j+1,k}-(\sigma_{yy})_{i,j,k}\Big)\; e'_i(x)\; e_j(y)\; e_k(t).
\end{aligned}$$

including the boundary conditions $(\sigma_{yx})_{i,0,k}$ and $(\sigma_{yx})_{i,N+1,k}$ for the equation along x, and $(\sigma_{xy})_{0,j,k}$ and $(\sigma_{xy})_{N+1,j,k}$ for the equation along y. Thus, these equations ensure that the derivatives of the stress components in the x- and y-directions can be represented by the same bases.

The displacements act as the Lagrange multiplier for these equations. Hence, it makes sense to write them as the dual to the basis function used to write the divergence of stresses. This means that

$$\begin{aligned}
\overline{X-X_0} &= \sum_{i=1}^{N}\sum_{j=1}^{N+1}\sum_{k=1}^{N_t}((X)_{ijk}-(X_0)_{ijk})\;\widetilde{e_i(x)e'_j}(y)\; h'_k(t)\\
\overline{Y-Y_0} &= \sum_{i=1}^{N+1}\sum_{j=1}^{N}\sum_{k=1}^{N_t}((Y)_{ijk}-(Y_0)_{ijk})\;\widetilde{e'_i(x)e_j}(y)\; h'_k(t)
\end{aligned}$$

The rotation is assumed to be completely contained within the element, and thus it is expanded as

$$\overline{\omega} = \sum_{i=1}^{N}\sum_{j=1}^{N}\sum_{k=1}^{N_t}(\omega)_{ijk}\; h'_i(x)\; h'_j(y)\; h'_k(t)$$

The time-derivative of momentum should have the same basis as the divergence of the stresses. Thus, it can be written as

$$\begin{aligned}
\overline{\phi_x} &= \sum_{i=1}^{N}\sum_{j=1}^{N+1}\sum_{k=1}^{N_t+1}(\phi_x)_{ijk}\; e_i(x)\; e'_j(y)\; h_k(t)\\
\overline{\phi_y} &= \sum_{i=1}^{N+1}\sum_{j=1}^{N}\sum_{k=1}^{N_t+1}(\phi_y)_{ijk}\; e'_i(x)\; e_j(y)\; h_k(t)
\end{aligned}$$

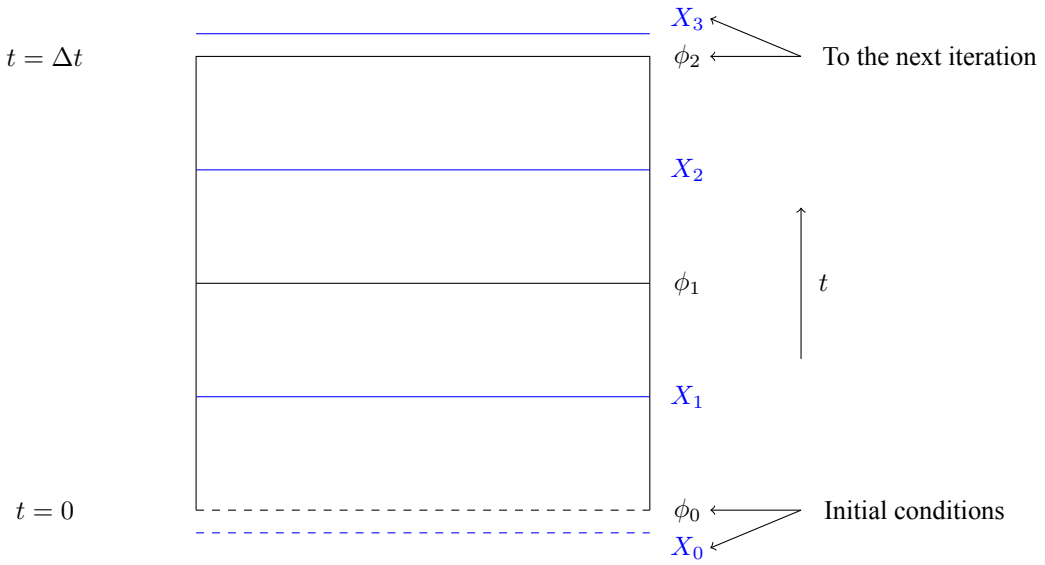

Figure 4.1: Figure showing the time stepping method for $N_t = 2$, and the initial conditions along with the unknowns

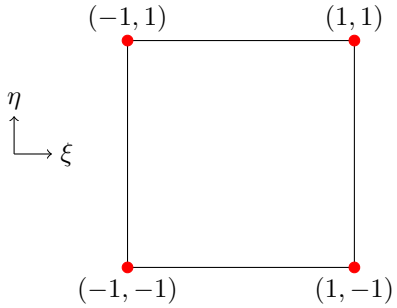

Figure 4.2: The reference domain

Something important that has to be noted is that the momentum is defined in $N_t + 1$ levels, while the position/displacement is defined only at N_t levels. That is because the spectral bases are used to expand the position unknowns at those time levels. The initial displacement is provided as a projection in the time direction at all points in the domain. A pictorial representation for $N_t = 2$ is seen in Figure 4.1.

The idea is to construct the polynomials using nodes constructed in a square domain, using Gauss-Lobatto nodes. This is called as the reference domain, and all the incidence matrices used in the formulation are a result of the properties of the Lagrange polynomials which are constructed in this domain. This domain is shown in Figure 4.2.

The values of momentum at $k = 1$ are also known and is provided as an initial condition. Since there are $N_t + 1$ equations where momentum acts as the Lagrange multiplier and N_t equations where the position acts as the Lagrange multiplier, while the unknowns for momentum are in N_t time levels, the extra equation produces the positions for another time level, which are the positions when projected on to the time step.

With this information in hand, a system can be written to find the unknown degrees of freedom

$$\begin{bmatrix} \mathbb{M}_\sigma & \mathbb{E}_\sigma^T & 0 & \mathbb{R}_\sigma^T \\ \mathbb{E}_\sigma & 0 & \mathbb{E}_\phi & 0 \\ 0 & \mathbb{E}_\phi & \mathbb{M}_\phi & 0 \\ \mathbb{R}_\sigma & 0 & 0 & 0 \end{bmatrix} \begin{bmatrix} \boldsymbol{\sigma}^h \\ \mathbf{X}^h \\ \boldsymbol{\phi}^h \\ \boldsymbol{\omega}^h \end{bmatrix} = \begin{bmatrix} -\mathbf{g}_\sigma^h \\ -\mathbf{f}^h - \mathbf{g}_X^h - \mathbf{i}_\phi^h \\ -\mathbf{i}_X^h \\ 0 \end{bmatrix} \tag{4.13}$$

Here, the terms $\mathbf{g}_X^h$ and $\mathbf{g}_\sigma^h$ indicate the boundary conditions, which are values of shear stresses and the normal displacements from the initial positions respectively. $\mathbf{i}_\phi^h$ and $\mathbf{i}_X^h$ indicate the initial conditions for the momentum and the position respectively. $\mathbf{f}^h$ indicates the contribution from the forcing function.

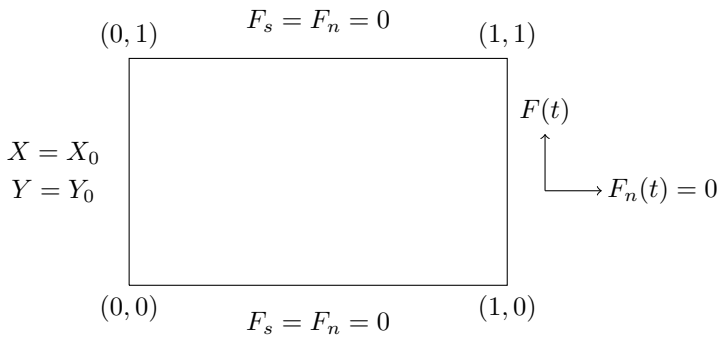

Figure 4.3: The sample problem, with boundary conditions

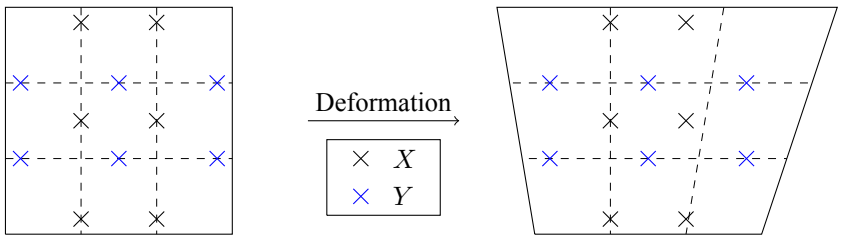

Figure 4.4: Approximate locations of degrees of freedom for X and Y before and after deformation, for $N = 2$

4.4. Results

This formulation was tested against a Cantilever beam, undergoing alternating shear stress as shown in Figure 4.3, with $F(t) = A \sin \omega_f t$, with F_s and F_n indicating the normal and shear tractions at every surface of the beam. There is no forcing assumed, and the initial displacement and momentum are assumed to be zero. However, the result was that the problem would diverge no matter how stiff the parameters (with high E and low A), were after one iteration/time-step.

The problem was that the formulation uses basis functions constructed in the reference domain, while the deformation happens in the physical domain. As long as the mapping between the reference domain and the physical domain is orthogonal, that is when the x-coordinate of a particle depends only on the ξ value of the corresponding particle's representation in the reference domain (similarly with y-coordinate and η), this formulation can be applied, and these expansions for the reconstructed functions hold. However, upon deformation, the reference domain remains the same, while the physical domain changes. This means that the particle's x-coordinate cannot be limited to be a function of only ξ, and similarly for the y-coordinate and η.

What this entails is that incidence matrices written here will no longer be calculating the gradients in the physical domain but in the reference domain. This means that the expansions written down will not represent the physical laws. For example, instead of calculating the divergence of the stress (in the x-direction) in the physical domain, the incidence matrix will instead be calculating $\frac{\partial \sigma_{xx}}{\partial \xi} + \frac{\partial \sigma_{yx}}{\partial \eta}$. This leads to the system blowing up after a few iterations. Another problem that arises out of this is that angular momentum is automatically not conserved, because linear momentum is not conserved. Symmetry of stress tensor ensures the conservation of angular momentum if and only if linear momentum is conserved. To illustrate this, how the degrees of freedom for X and Y look before and after (an arbitrary) deformation is shown in Figure 4.4. Ideally, the degrees of freedom should lie on the dashed lines, like how they are before deformation.

Another perspective to this problem can be represented using the idea of the mimetic methods themselves. If you look at how σ_{xx} is defined, it is the value of the traction in the x-direction when the surface under observation has a normal in the x-direction, and similarly σ_{yx} is the traction in the x-direction when the surface under observation has a normal in the y-direction. Thus, only when the geometry is a rectangle can σ_{xx} and σ_{yx} can be associated to the horizontal and vertical boundaries respectively, such that algebraic topology will allow us to calculate the net flux through the enclosed geometry, which will be the integrated force in the x-direction. When the geometry is deformed however, the normal at the horizontal boundaries may no longer be in the x-direction, thus it cannot denote σ_{xx} anymore. This is why this formulation with these values cannot be used anymore.

In order to further analyse this, there needs to be further analyses on how the constitutive equations need to be solved on a skewed domain. Once angular momentum is conserved in such a domain, this problem can be

solved later.

4.5. Summary

In this section, there is an attempt to take the mimetic spectral element method towards solving fluid-structure interaction problems by trying out a formulation for unsteady linear elastic solids. Here, the stress and position are used as covector- and vector-valued quantities respectively to create a duality pairing. A Lagrangian problem formulation is constructed in such a way that variational derivatives of the variables result in two constitutive relations, one which relates the stress tensor with the strain tensor (Hooke's law) and another to relate momentum with velocity, and two conservation laws for linear momentum and angular momentum respectively. For this formulation, the conservation of linear momentum is constructed to be topological (including the rate of change of momentum), and for point-wise conservation of angular momentum, the symmetry of the Cauchy stress tensor is enforced which will conserve angular momentum in combination with the equilibrium of forces. To perform computations, the spectral bases are constructed using Lagrange polynomials on the reference domain, which itself is constructed using Gauss-Lobatto nodes. Using this method, the results show that for the first timestep, the results are as expected. But the solution diverges as soon as there is deformation in the domain when the physical domain is not orthogonal anymore. This is attributed to how the basis for the problem is constructed in the reference domain, and implicitly assumes that for this formulation to work the relationship between the coordinates in the reference domain and the physical (cartesian) coordinates is diagonal, i.e. x depends on ξ and y depends on η only. Thus, it is concluded that the constitutive equations, as well as the quantities themselves need to be transformed into the reference domain first, before attempting to perform computations. This needs to be tested especially for skewed domains.

5

Poisson problem

The failure to successfully use mimetic spectral elements to write down the unsteady linear elasticity problem meant that we had to focus on how we could solve a steady linear elasticity problem for a skewed domain. This prompted us to look at a simpler problem.

The linear elasticity problem can be written down as two Poisson equations in two linearly independent directions, with a constraint of angular momentum conservation enforced between them. Thus, it was decided that we would look for a formulation for the Poisson problem that could also be extended to a linear elasticity in a similar way but would also produce optimal convergence for a skewed domain.

5.1. Introduction

The Poisson problem has been one of the basic numerical test cases for a long time. It has always been customary to use other weak formulation approaches to solve the Poisson problem. One of the popular approaches is to use the gradient of pressure in weak formulations. This can be given by

$$(\nabla\tilde{p}, \nabla p)_\Omega - (\tilde{p}, f)_\Omega = 0,$$

where $\tilde{p}$ is the test function. Another formulation for the Poisson problem is using constrained minimisation, with another Lagrange multiplier λ, where the problem formulation is written as

$$\mathcal{E}(\mathbf{q}, \lambda) = \int_\Omega \frac{1}{2}|\mathbf{q}|^2 \mathrm{d}\Omega + \int_\Omega \lambda\mathcal{L}(\mathbf{q})\mathrm{d}\Omega.$$

where $\lambda\mathcal{L}(\mathbf{q}) = \nabla\cdot\mathbf{q} - f$. As you can see this has the divergence of velocity in the formulation. These have already been mentioned in Section 3.4.1.

A novel formulation is proposed, with part of the derivatives on p and the other half of the derivatives on $\mathbf{q}$. The idea is to make this formulation similar to what is planned for linear elasticity formulations, and this is why the velocities are written down in a mixed basis (with both primal and dual bases). Additionally, how the hybridisation works when the Poisson problem is formulated this way is an object of curiosity.

5.1.1. Defining the problem

Here, the Poisson problem is looked at, with the pressure being the scalar quantity while the velocity $\mathbf{q}$ is the vector quantity. With this in mind, the problem can be formulated as

$$\begin{aligned} u_x - \frac{\partial p}{\partial x} &= 0, \\ u_y - \frac{\partial p}{\partial y} &= 0, \\ \frac{\partial u_x}{\partial x} + \frac{\partial u_y}{\partial y} &= f. \end{aligned}$$

These equations show the problem that is being solved in the physical domain. These are further transformed into the reference domain so that the quantities can be solved in the reference domain. After all computations are made in the reference domain, it can be transformed back into the physical domain.

5.2. Components in the reference domain

In this section, we will deal with how the components of the quantities are represented in the reference domain. This will help to map the quantities into the reference domain and back, as well as apply the boundary conditions to the problem.

5.2.1. Reference domain

In this scenario, the reference domain is chosen to be $[-1,1]\times[-1,1]$ 2-dimensional square, with the independent dimensions being ξ and η, as shown in Figure 4.2.

This is ideal because the Gauss-Lobatto points which are used to construct the spectral bases lie in this domain.

5.2.2. Velocity

The velocity is described as a (scalar-valued) 1-form.

$$\underline{\mathbf{q}} = u_x \mathrm{d}y - u_y \mathrm{d}x. \tag{5.1}$$

When fully transformed into the reference domain, this would look like

$$\underline{\mathbf{q}} = u_\xi \mathrm{d}\eta - u_\eta \mathrm{d}\xi. \tag{5.2}$$

Thus, we can convert between the two domains as

$$\begin{aligned} u_x &= u_\xi \frac{\partial \eta}{\partial y} - u_\eta \frac{\partial \xi}{\partial y}, \\ u_y &= -u_\xi \frac{\partial \eta}{\partial x} + u_\eta \frac{\partial \xi}{\partial x}, \end{aligned}$$

and

$$\begin{aligned} u_\xi &= u_x \frac{\partial y}{\partial \eta} - u_y \frac{\partial x}{\partial \eta}, \\ u_\eta &= -u_x \frac{\partial y}{\partial \xi} + u_y \frac{\partial x}{\partial \xi}. \end{aligned}$$

Using these transformations, the velocities in the physical space can be converted into their respective velocities in the reference domain.

5.2.3. Pressure

The pressure is written down as a scalar 0-form. Thus, it does not change whether it is represented in the reference domain or in the physical domain.

$$\mathbf{p} = p. \tag{5.3}$$

5.2.4. Body force

The body force/ forcing function is described as a 2-form. Thus, in the physical domain

$$\mathbf{f} = f \mathrm{d}x \wedge \mathrm{d}y, \tag{5.4}$$

while in the reference domain, it is seen as

$$\mathbf{f} = f' \mathrm{d}\xi \wedge \mathrm{d}\eta. \tag{5.5}$$

Thus, we can convert between the two domains as

$$\begin{aligned} f &= \frac{f'}{(\det \mathcal{J})}, \\ f' &= f\,(\det \mathcal{J})\,. \end{aligned}$$

5.3. Equations in the reference domain

In this section, the equations in the physical domain are translated into equivalent equations in the reference domain. By doing this, the resulting equations should be such that the solution obtained using the equations in the reference domain should be analogous to how the solution would be had the equations from the physical domain been used.

5.3.1. Velocity-pressure relation

The velocity is written as the gradient of the pressure. In the physical space, this is written as

$$u_x = \frac{\partial p}{\partial x},$$
$$u_y = \frac{\partial p}{\partial y}.$$

However, these relations change when you consider the reference domain. For example, the components of the gradient in the reference coordinates can be obtained, not those in the physical coordinates. And the velocities themselves are represented in a different way in the reference domain.

The components of the gradient in the reference domain can be written as

$$\frac{\partial p}{\partial \xi} = \frac{\partial p}{\partial x}\frac{\partial x}{\partial \xi} + \frac{\partial p}{\partial y}\frac{\partial y}{\partial \xi},$$
$$\frac{\partial p}{\partial \eta} = \frac{\partial p}{\partial x}\frac{\partial x}{\partial \eta} + \frac{\partial p}{\partial y}\frac{\partial y}{\partial \eta}.$$

$$\frac{\partial p}{\partial \xi} = u_x\frac{\partial x}{\partial \xi} + u_y\frac{\partial y}{\partial \xi},$$
$$\frac{\partial p}{\partial \eta} = u_x\frac{\partial x}{\partial \eta} + u_y\frac{\partial y}{\partial \eta}.$$

Thus,

$$\begin{bmatrix} C'_{11} & C'_{12} \\ C'_{21} & C'_{22} \end{bmatrix} \begin{bmatrix} u_\xi \\ u_\eta \end{bmatrix} = \begin{bmatrix} \frac{\partial p}{\partial \xi} \\ \frac{\partial p}{\partial \eta} \end{bmatrix}, \tag{5.6}$$

where

$$C'_{11} = \frac{1}{\det \mathcal{J}}\left[\frac{\partial x}{\partial \xi}\frac{\partial x}{\partial \xi} + \frac{\partial y}{\partial \xi}\frac{\partial y}{\partial \xi}\right],$$
$$C'_{12} = \frac{1}{\det \mathcal{J}}\left[\frac{\partial x}{\partial \eta}\frac{\partial x}{\partial \xi} + \frac{\partial y}{\partial \eta}\frac{\partial y}{\partial \xi}\right],$$
$$C'_{21} = \frac{1}{\det \mathcal{J}}\left[\frac{\partial x}{\partial \xi}\frac{\partial x}{\partial \eta} + \frac{\partial y}{\partial \xi}\frac{\partial y}{\partial \eta}\right],$$
$$C'_{22} = \frac{1}{\det \mathcal{J}}\left[\frac{\partial x}{\partial \eta}\frac{\partial x}{\partial \eta} + \frac{\partial y}{\partial \eta}\frac{\partial y}{\partial \eta}\right].$$

These equations can be used for assigning values to the matrices associated with the velocity mass matrix.

5.3.2. Divergence equation

In the physical coordinates, this equation can be written as

$$\frac{\partial u_x}{\partial x} + \frac{\partial u_y}{\partial y} + f = 0.$$

Therefore,

$$\frac{\partial u_x}{\partial \xi}\frac{\partial \xi}{\partial x} + \frac{\partial u_x}{\partial \eta}\frac{\partial \eta}{\partial x} + \frac{\partial u_y}{\partial \xi}\frac{\partial \xi}{\partial y} + \frac{\partial u_y}{\partial \eta}\frac{\partial \eta}{\partial y} + f = 0.$$

$$\frac{\partial u_\xi}{\partial \xi}\left(\frac{\partial \eta}{\partial y}\frac{\partial \xi}{\partial x}-\frac{\partial \eta}{\partial x}\frac{\partial \xi}{\partial y}\right)+\frac{\partial u_\xi}{\partial \eta}\left(\cancel{\frac{\partial \eta}{\partial x}\frac{\partial \eta}{\partial y}}-\cancel{\frac{\partial \eta}{\partial y}\frac{\partial \eta}{\partial x}}\right)+\frac{\partial u_\eta}{\partial \xi}\left(\cancel{-\frac{\partial \xi}{\partial x}\frac{\partial \xi}{\partial y}}+\cancel{\frac{\partial \xi}{\partial y}\frac{\partial \xi}{\partial x}}\right)+\frac{\partial u_\eta}{\partial \eta}\left(-\frac{\partial \eta}{\partial x}\frac{\partial \xi}{\partial y}+\frac{\partial \eta}{\partial y}\frac{\partial \xi}{\partial x}\right)+f=0.$$

Therefore,

$$\frac{\partial u_\xi}{\partial \xi}+\frac{\partial u_\eta}{\partial \eta}+f'=0. \tag{5.7}$$

This shows that the divergence is invariant under transformation if the coordinate basis vectors are used. This is also the main reason to use coordinate basis vectors, other basis vectors may not result in the same expression for the divergence.

5.4. Lagrangian formulation

By converting the velocities and pressures to their respective components in the reference domain, the idea is to solve these equations completely in the reference domain.

For this, the theoretical formulation (in the reference domain) can be written as

$$\mathcal{L}\left(\underline{\mathbf{u}},\mathbf{p},\underline{\underline{\mathbf{C}'}}\right)=\begin{array}{l}\int_{\hat{\Omega}}\left(\left(p\frac{\partial u_\xi}{\partial \xi}-\frac{\partial p}{\partial \eta}u_\eta\right)+p\,f\,(\det\mathcal{J})\right)\mathrm{d}\hat{\Omega}\\ +\int_{\hat{\Omega}}\left(\frac{1}{2}\underline{\mathbf{u}}^T\left(\underline{\underline{\mathbf{C}'}}\right)\underline{\mathbf{u}}\right)\mathrm{d}\hat{\Omega}\\ -\oint_{\partial\hat{\Omega}}(p)_P u_\xi n_\xi \mathrm{d}\Gamma\\ +\oint_{\partial\hat{\Omega}}p(u_\eta)_P n_\eta \mathrm{d}\Gamma\end{array}, \tag{5.8}$$

where $\underline{\mathbf{u}}=[u_\xi\ u_\eta]^T$, and

$$\underline{\underline{\mathbf{C}'}}=\begin{bmatrix}C'_{11} & C'_{12}\\ C'_{21} & C'_{22}\end{bmatrix},$$

whose values are mentioned in (5.6). Also, note that $\hat{\Omega}$ denotes the reference domain, and the boundary integrals written down are at the boundaries of the reference domain, in the ξ- and η- directions.

5.4.1. Velocity-Pressure relation

On taking the variational derivative of the functional with respect to $\underline{\mathbf{u}}$ and equating it to 0, the functional reduces to

$$\begin{array}{l}\int_{\hat{\Omega}}\left(p\frac{\partial \widetilde{u_\xi}}{\partial \xi}-\frac{\partial p}{\partial \eta}\widetilde{u_\eta}\right)\mathrm{d}\hat{\Omega}\\ +\int_{\hat{\Omega}}\left(\underline{\widetilde{\mathbf{u}}}^T\left(\underline{\underline{\mathbf{C}'}}\right)\underline{\mathbf{u}}\right)\mathrm{d}\hat{\Omega}\end{array}=\mathcal{B}_{\mathbf{u}}. \tag{5.9}$$

This is the formulation that is being solved for. To verify that this is indeed the correct relation, integration by parts can be used to see that it leads to

$$\begin{array}{l}\int_{\hat{\Omega}}\left(-\frac{\partial p}{\partial \xi}\widetilde{u_\xi}-\frac{\partial p}{\partial \eta}\widetilde{u_\eta}\right)\mathrm{d}\hat{\Omega}\\ +\int_{\hat{\Omega}}\left(\underline{\widetilde{\mathbf{u}}}^T\left(\underline{\underline{\mathbf{C}'}}\right)\underline{\mathbf{u}}\right)\mathrm{d}\hat{\Omega}\end{array}=0.$$

Assuming that this holds for any arbitrary value of $\underline{\widetilde{\mathbf{u}}}$, this will give the formulation derived in (5.6).

Important consideration is that

$$\mathcal{B}_{\mathbf{u}}=\oint_{\partial\hat{\Omega}}(p)_P\widetilde{u_\xi}n_\xi \mathrm{d}\Gamma, \tag{5.10}$$

where $(p)_P$ is the pressure prescribed at the horizontal boundaries in the reference domain. This boundary integral makes sure that the correct constitutive relation is solved.

5.4.2. Divergence equation

On taking the variational derivative of the functional with respect to p and equating it to 0, the functional reduces to

$$\int_{\hat{\Omega}} \Big((\widetilde{p}\frac{\partial u_\xi}{\partial \xi} - \frac{\partial \widetilde{p}}{\partial \eta} u_\eta) + \widetilde{p}\, f\, (\det \mathcal{J}) \Big) \mathrm{d}\hat{\Omega} = -\mathcal{B}_p, \tag{5.11}$$

where

$$\mathcal{B}_p = \oint_{\partial\hat{\Omega}} \widetilde{p}(u_\eta)_P n_\eta \mathrm{d}\Gamma. \tag{5.12}$$

With an arbitrary $\widetilde{p}$ and assuming this holds for any arbitrary domain, this equation is the same as the diffusion equation in the reference domain in (5.7). This can be verified by including the boundary terms in the equation and using integration by parts.

5.5. Spectral bases

In this section, the expansion of the quantities in the reference domain is shown. The overhead bar indicates that they are reconstructed (using the spectral bases functions).

$$\overline{u_\xi} = \sum_{i=1}^{N+1} \sum_{j=1}^{N+1} (u_\xi)_{ij}\ h_i(\xi)\ e'_j(\eta)\ ,$$
$$\overline{u_\eta} = \sum_{i=1}^{N} \sum_{j=1}^{N} (u_\eta)_{ij}\ e_i(\xi)\ h'_j(\eta)\ .$$

With these bases, one of the terms in the weak formulation for the diffusion equation is

$$\widetilde{p}\frac{\partial \overline{u_\xi}}{\partial \xi} = \widetilde{p} \left[\sum_{i=1}^{N} \sum_{j=1}^{N+1} \Big((u_\xi)_{i+1,j} - (u_\xi)_{i,j} \Big)\ e_i(\xi)\ e'_j(\eta) \right],$$

The idea with this expansion is to make it topological, with $\widetilde{p}$ acting as the test function. This can be done by making $\widetilde{p}$ dual to $e_i(\xi)\ e'_j(\eta)$. This results in pressure being expanded as

$$\overline{p} = \sum_{i=1}^{N} \sum_{j=1}^{N+1} (p)_{ij}\ h'_i(\xi) h_j(\eta)\ .$$

Note that this expansion holds true as the expansion is in the reference domain, where the dual of the tensor product will also be the tensor product of the dual.

With this the other term in the weak formulation for the diffusion equation $-\frac{\partial \widetilde{p}}{\partial \eta} u_\eta$ would also be topological. This makes the diffusion equation a topological relation.

With these spectral bases, the system can be written to find the unknown degrees of freedom as

$$\begin{bmatrix} \mathbb{M}_{\mathbf{u}} & \mathbb{E}_{\mathbf{u}}^T \\ \mathbb{E}_{\mathbf{u}} & 0 \end{bmatrix} \begin{bmatrix} \mathbf{u}^h \\ \mathbf{p}^h \end{bmatrix} = \begin{bmatrix} -\mathbf{g}_u^h \\ -\mathbf{f}^h - \mathbf{g}_p^h \end{bmatrix}. \tag{5.13}$$

In this representation, let

$$\mathbf{u}^h = \left[(u_\xi)^h\ (u_\eta)^h \right]^T. \tag{5.14}$$

Making it easier to arrange the unknowns for the tensor and vector quantities. In addition, it should be easier to construct matrices if the quantities are arranged in this order.

5.6. Incidence matrix

The divergence equation is designed to be topological in the computational (reference) domain. With this, the matrix that needs to be made should not involve any terms other than ± 1 or 0.

With the degrees of freedom for velocity arranged as in (5.14), and if the degrees of freedom are arranged in the x-lexicographic order, the components of $\mathbb{E}_{\mathbf{u}}$ (for $N = 2$) are given below.

$$(\mathbb{E}_{\mathbf{u}}) = \begin{bmatrix} 1 & -1 & 0 & 0 & 0 & 0 & 0 & 0 & 0 & -1 & 0 & 0 & 0 \\ 0 & 1 & -1 & 0 & 0 & 0 & 0 & 0 & 0 & 0 & -1 & 0 & 0 \\ 0 & 0 & 0 & 1 & -1 & 0 & 0 & 0 & 0 & 1 & 0 & -1 & 0 \\ 0 & 0 & 0 & 0 & 1 & -1 & 0 & 0 & 0 & 0 & 1 & 0 & -1 \\ 0 & 0 & 0 & 0 & 0 & 0 & 1 & -1 & 0 & 0 & 0 & 1 & 0 \\ 0 & 0 & 0 & 0 & 0 & 0 & 0 & 1 & -1 & 0 & 0 & 0 & 1 \end{bmatrix}.$$

5.7. Mass matrix

The mass matrix is referred to the equations in this formulation where the velocity components themselves act as the Lagrange multipliers.

Because there are 2 velocity components in the two-dimensional formulation, there are also 2 equations enforcing the constitutive relation. In general, the mass matrix can be written as $\left[(\widetilde{\mathbf{u}}^h)^T \mathbb{M}_\sigma \mathbf{u}^h\right]$. To make it easier to write it down, $\mathbb{M}_\sigma$ can be separated into two horizontal matrices, representing each of the constitutive equations, as

$$\mathbb{M}_\sigma = \begin{bmatrix} \mathbb{M}_1 \\ \mathbb{M}_2 \end{bmatrix},$$

Let us look at how the different components are computed.

5.7.1. Constitutive relation 1

This relation has $\widetilde{u_\xi}$ as the test function. For this constitutive relation, the integral that needs to be represented is

$$\int \widetilde{u_\xi}\,(C'_{11}\,u_\xi + C'_{12}\,u_\eta)\,\mathrm{d}\xi \wedge \mathrm{d}\eta.$$

Let $\mathbb{M}_{11}$ represent the first term in the integral. Writing down the bases for the components,

$$\int \widetilde{u_\xi}\,C'_{11}\,u_\xi \mathrm{d}\xi \wedge \mathrm{d}\eta = \int \sum_{i=1}^{N_x+1}\sum_{j=1}^{N_x+1}\sum_{k=1}^{N_x+1}\sum_{l=1}^{N_x+1} (\widetilde{u_\xi})_{kl} C'_{11}(\xi,\eta)(u_\xi)_{ij} h_i(\xi)\; e'_j(\eta)\; h_k(\xi)\; e'_l(\eta)\; \mathrm{d}\xi \wedge \mathrm{d}\eta.$$

This means that

$$(\mathbb{M}_{11})_{ijkl} = \sum_{r=1}^{N_x}\sum_{s=1}^{N_x} C'_{11}\,(\xi_r,\eta_s)\,h_i(\xi_r)\;e'_j(\eta_s)\;h_k(\xi_r)\;e'_l(\eta_s)\,w_r\,w_s, \tag{5.15}$$

where w_r and w_s are the integration weights associated with the nodes at ξ_r and η_s using Gaussian quadrature, and N_x denotes the number of Gauss-Lobatto nodes used for quadrature.

Similarly,

$$(\mathbb{M}_{12})_{ijkl} = \sum_{r=1}^{N_x}\sum_{s=1}^{N_x} C'_{12}\,(\xi_r,\eta_s)\,e_i(\xi_r)\;h'_j(\eta_s)\;h_k(\xi_r)\;e'_l(\eta_s)\,w_r\,w_s, \tag{5.16}$$

where the components of $\underline{\underline{\boldsymbol{C'}}}$ are what were derived in (5.6).

Once these matrices are formed $\mathbb{M}_1 = [\mathbb{M}_{11}\;\;\mathbb{M}_{12}]$.

5.7.2. Constitutive relation 2

A similar method to the way the matrices are derived can be used to determine the matrices for the second constitutive relation, with the test function being $\widetilde{u_\eta}$. The expressions are given below.

$$(\mathbb{M}_{21})_{ijkl} = \sum_{r=1}^{N_x}\sum_{s=1}^{N_x} C'_{21}\,(\xi_r,\eta_s)\,h_i(\xi_r)\;e'_j(\eta_s)\;e_k(\xi_r)\;h'_l(\eta_s)\,w_r\,w_s. \tag{5.17}$$

$$(\mathbb{M}_{22})_{ijkl} = \sum_{r=1}^{N_x}\sum_{s=1}^{N_x} C'_{22}\left(\xi_r,\eta_s\right) e_i(\xi_r)\; h'_j(\eta_s)\; e_k(\xi_r)\; h'_l(\eta_s)\, w_r\, w_s. \tag{5.18}$$

where the components of $\underline{\underline{\boldsymbol{C'}}}$ are what were derived in (5.6).
Then we get $\mathbb{M}_2 = [\mathbb{M}_{21}\ \ \mathbb{M}_{22}]$.
With these components, the mass matrix can be set up by vertically stacking $\mathbb{M}_1$ and $\mathbb{M}_2$ respectively.

5.8. Boundary conditions

The boundary conditions can be enforced using a trick arising from the definition of the dual basis functions themselves.

5.8.1. Pressures for velocity-pressure relation

The boundary condition for the constitutive relation with $\widetilde{u_\xi}$ shall be considered first. When looking at the reference domain, the pressure at the left and right boundaries is prescribed.

On the boundary, the prescribed pressure is expanded as

$$\int_{\partial\hat{\Omega}} p^{ex}\left(\xi,\eta\right)\mathrm{d}\eta \approx \int_{\partial\hat{\Omega}} \sum_{l=1}^{N+1} (p_P)_l h_l\left(\eta\right)\mathrm{d}\eta.$$

Using the dual polynomials, this integral can be reformulated as

$$\int_{\partial\hat{\Omega}} \sum_{j=1}^{N+1}\sum_{l=1}^{N+1} (p_P)_l h_l(\eta) e'_j(\eta)\mathrm{d}\eta \approx \int_{\partial\hat{\Omega}} \sum_{j=1}^{N+1} p^{ex}(\xi,\eta) e'_j(\eta)\mathrm{d}\eta = p_{a,j}.$$

where $a = 0$ or $a = N+1$ depending on whether it is the left or the right boundary respectively.
Thus, the boundary condition becomes

$$\int_{\partial\hat{\Omega}} p_P \widetilde{u_\xi} n_\xi \mathrm{d}\Gamma = \int_{\partial\hat{\Omega}} \sum_{j=1}^{N+1}\sum_{l=1}^{N+1} \left(\widetilde{u_\xi}\right)_{a,l} p^{ex}\left(\xi,\eta\right) e'_j(\eta)\mathrm{d}\eta = \sum_{j=1}^{N+1}\sum_{l=1}^{N+1} \left(\widetilde{u_\xi}\right)_{a,l} p_{a,j}. \tag{5.19}$$

Note that the boundary conditions do not require the use of basis functions, and only require the degrees of freedom, adding to the plus points of the method.

5.8.2. 'Vertical' velocity for diffusion equation

Considering the diffusion equation (where $\widetilde{p}$ acts as the test function) the vertical velocity (in the reference domain) needs to be prescribed at the top and bottom boundaries.

This velocity component can be expanded as

$$\int_{\partial\hat{\Omega}} u_\eta^{ex}\left(\xi,\eta\right)\mathrm{d}\xi \approx \int_{\partial\hat{\Omega}} \sum_{l=1}^{N} (u_\eta)_P e_l(\xi)\mathrm{d}\xi.$$

Using dual polynomials, this can be modified as

$$\int_{\partial\hat{\Omega}} \sum_{j=1}^{N}\sum_{l=1}^{N} (u_\eta)_P e_l(\xi) h'_j(\xi)\mathrm{d}\xi \approx \int_{\partial\hat{\Omega}} \sum_{j=1}^{N} u_\eta^{ex}\left(\xi,\eta\right) h'_j(\xi)\mathrm{d}\xi = (u_\eta)_{j,a}.$$

where $a = 0$ and $a = N+1$ respectively for the bottom and top boundaries.
Thus, the boundary integral can be reformulated as

$$\int_{\partial\hat{\Omega}} \widetilde{p}\left(u_\eta\right)_P n_\eta \mathrm{d}\Gamma = \int_{\partial\hat{\Omega}} \sum_{j=1}^{N}\sum_{l=1}^{N} (\widetilde{p})_{l,a} u_\eta^{ex}\left(\xi,\eta\right) h'_j(\xi)\mathrm{d}\xi = \sum_{j=1}^{N}\sum_{l=1}^{N} (\widetilde{p})_{l,a} (u_\eta)_{j,a} \tag{5.20}$$

Again, these boundary conditions involve only the degrees of freedom and not the basis functions.

An important observation with the boundary condition is that the velocity at the boundary that needs to be prescribed is the normal velocity to the top and bottom boundary, unlike the pressure boundary condition which is just a scalar.

5.8.3. Contributions from the forcing function

The forcing function needs to have the same basis as the derivatives of the velocities, i.e.

$$\overline{f} = \sum_{i=1}^{N} \sum_{j=1}^{N+1} (f)_{i,j} e_i(\xi) e'_j(\eta)$$

Similar to the boundary conditions, the degrees of freedom for the body forces can be computed using property of the dual basis functions.

$$\begin{aligned}(f)_{k,l} &= \int_{\hat{\Omega}} \sum_{i=1}^{N} \sum_{j=1}^{N+1} (f)_{i,j} e_i(\xi) e'_j(\eta) h'_k(\xi) h_l(\eta) \mathrm{d}\xi \wedge \mathrm{d}\eta \\ &= \int_{\hat{\Omega}} f^{ex}\left(x(\xi,\eta), y(\xi,\eta)\right) \det \mathcal{J}(\xi_r, \eta_s) h'_k(\xi) h_l(\eta) \mathrm{d}\xi \wedge \mathrm{d}\eta.\end{aligned}$$

Note that these transformations derived are the same ones mentioned in Section 5.2.

5.9. Hybridized system

In a hybridized system, the physical domain is subdivided into several elements. Then each of the elements is treated as a separate problem on its own, with the physical domain being mapped to the reference domain and all computations being performed in that domain. Then, each element will have its own mapping, which may not be the same as the mapping associated to any other element.

In order to not overdefine the problem, the Lagrange multipliers at the internal boundaries of different elements are used to constrain the values on neighbouring elements to be the same. This will result in a system matrix of the form

$$\begin{bmatrix} \mathbb{A} & \mathbb{B}^T \\ \mathbb{B} & 0 \end{bmatrix} \begin{bmatrix} \mathbf{x}^h \\ \boldsymbol{\lambda}^h \end{bmatrix} = \begin{bmatrix} \mathbf{f}^h \\ 0 \end{bmatrix}. \tag{5.21}$$

Here $\mathbb{A}$ contains mass and incidence matrices of each element as mentioned in (5.13), with elements arranged in (again) x-lexicographic order. This enables it to be ordered in a block-diagonal matrix.

$\mathbb{B}$ contains the relations which impose the desired continuity at the boundaries between elements when it does not lie on the physical boundary of the entire domain. With this formulation, the relations used at the *horizontal* boundaries are

$$\widetilde{u_\xi}\,|_l = \widetilde{u_\xi}\,|_r\,,$$

where l and r indicate values at the left and right boundaries respectively, and at the *vertical* boundaries,

$$\widetilde{p}\,|_b = \widetilde{p}\,|_t\,,$$

where b and t indicate values at the bottom and top boundaries respectively. This is shown in Figure 5.1, for $K_x = K_y = N = 2$.

5.10. Results

This formulation is tested against a manufactured solution. Here, the pressure is assumed to be

$$p^{ex}(x,y) = \sin(2\pi x)\sin(2\pi y),$$

Then, the velocities will be

$$\begin{aligned}u_x^{ex}(x,y) &= 2\pi\cos(2\pi x)\sin(2\pi y), \\ u_y^{ex}(x,y) &= 2\pi\sin(2\pi x)\cos(2\pi y).\end{aligned}$$

With this, the derivatives of the velocities are

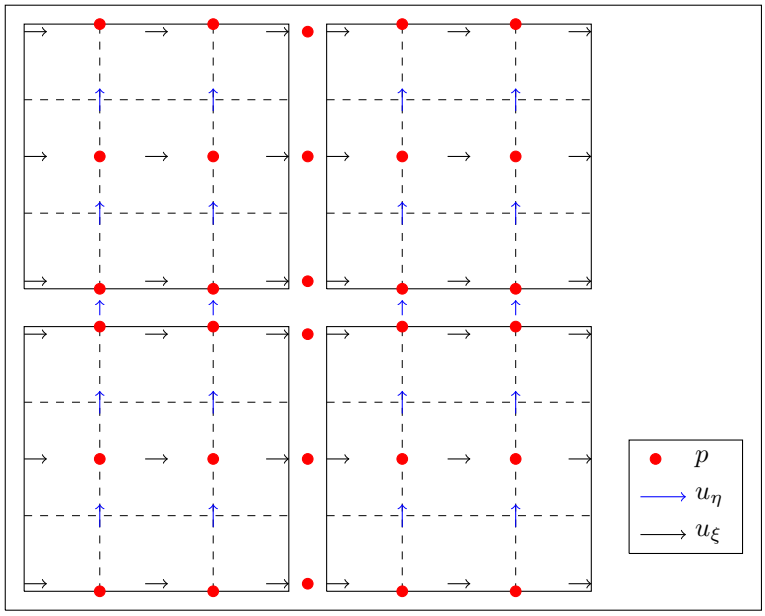

Figure 5.1: Degrees of freedom of quantities for the hybrid formulation on the reference domain with $K_x = K_y = 2$, $N = 2$

$$\frac{\partial u_x^{ex}}{\partial x} = -4\pi^2 \sin(2\pi x)\sin(2\pi y),$$
$$\frac{\partial u_y^{ex}}{\partial y} = -4\pi^2 \sin(2\pi x)\sin(2\pi y),$$

and the forcing function is

$$f^{ex}(x,y) = -8\pi^2 \sin(2\pi x)\sin(2\pi y),$$

5.10.1. Domain

A trapezoid domain is chosen for this problem. The slope of the skewed edge (m) is chosen to be a variable, and studies are conducted over multiple m, each of which results in a different domain. A sample domain with $m = 2$ is shown in Figure 5.2. Results with $m = 2$ are discussed in Section 5.10.2.

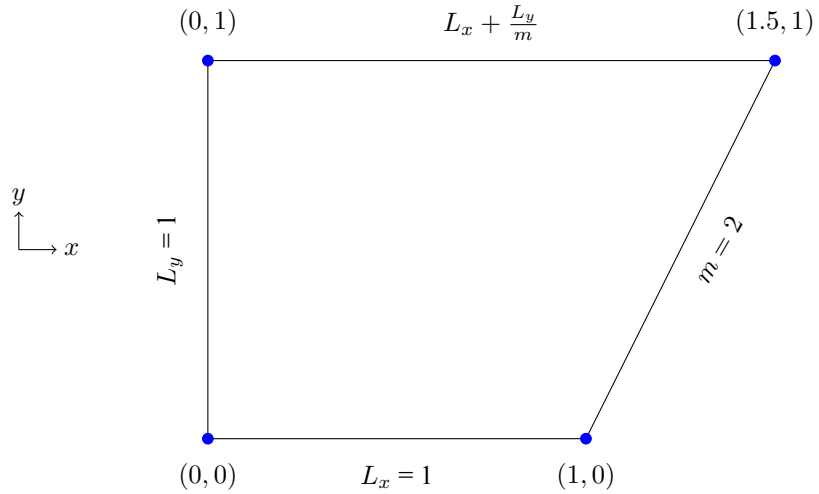

Figure 5.2: Domain with $m = 2$

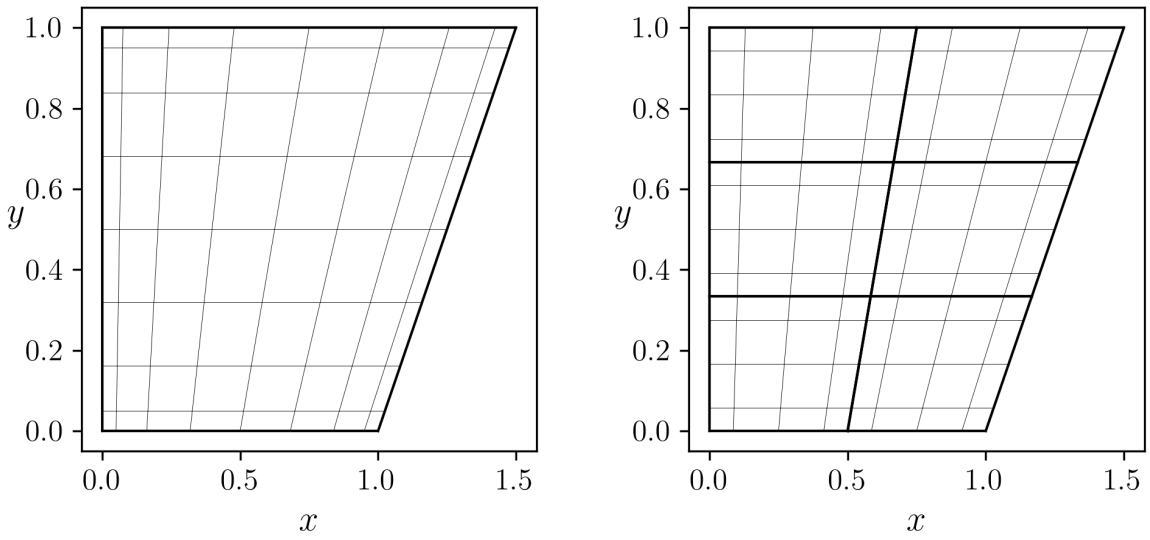

(a) $K_x = 1, K_y = 1, N = 8$ **(b)** $K_x = 2, K_y = 3, N = 4$

Figure 5.3: The Meshes in the physical domain for two different scenarios

The points on this domain are mapped onto the points in the reference domain (Figure 4.2) using bilinear transfinite mapping. The Gauss-Lobatto points on the reference domain are then mapped onto the physical domain. When the domain is divided into several elements, the boundaries of the elements are first calculated using a bilinear transfinite mapping, and using these maps the Gauss-Lobatto points are mapped onto the physical domain. Note that the maps for each element can be different. These can be visualised in Figure 5.3. Note that K_x and K_y used in the pictures indicate the number of elements used along the x- and $y-$ directions respectively, and this notation will be used in the subsequent chapters too.

On these domains, the pressure p^{ex} is prescribed on the left and right boundary, and the velocity u_η^{ex} is prescribed at the bottom and top boundary.

5.10.2. Observations and Conclusions

The aim of this formulation is to study how the Poisson problem would be transformed when you are mapping the physical domain onto the reference domain, and performing your calculations there. Since this formulation is new, containing both the pressure and a component of velocity as Lagrange multipliers, this study for a skewed domain would be essential. In addition, like the previous studies, a mixed formulation is used, where the spectral bases functions are a combination of both primal and dual basis functions. This helps to understand the intricacies of the formulation and the limitations of the problem at hand. As mentioned before, linear elasticity is essentially two Poisson problems coupled together using the conservation of angular momentum, which means that tackling the Poisson problem for a skewed domain is the first step towards extending this theory to elasticity formulations.

With this in mind, let us look at the results. The results for u_x as shown in Figure 5.4 look consistent for the different number of elements and polynomial degree when compared to the exact solution. When comparing the results for u_x with u_y in Figure 5.5, it can be seen that the results for u_x have a higher resolution. This can be understood y looking at the polynomial representation of each of these quantities. For example, since u_x has a higher contribution from u_ξ, which is represented on the reference domain using $\mathcal{P}^{(N+1,N+1)}$ degrees of freedom, the error in this quantity is much lesser than u_y which has a major contribution from u_η, represented using $\mathcal{P}^{(N,N)}$ degrees of freedom. There is also an error associated at the boundaries of elements in u_x and u_y, because the elements are continuous at the left and right boundaries in u_ξ, and not in the quantities in the physical space. The polynomial degree of the solutions for u_x and u_y are not exactly $\mathcal{P}^{(N+1,N+1)}$ and $\mathcal{P}^{(N,N)}$ respectively. Both their polynomial degrees are somewhere in between $\mathcal{P}^{(N+1,N+1)}$ and $\mathcal{P}^{(N,N)}$ because u_ξ is of the polynomial degree $\mathcal{P}^{(N+1,N+1)}$, while u_η is of polynomial degree $\mathcal{P}^{(N,N)}$.

Looking at the results for p in Figure 5.6, it is consistent like u_x and u_y. Additionally, it is observed that p is constrained to be continuous only at the top and bottom boundaries of the element, and thus the error in p is seen at the left and right boundaries of the element. p has a degree of freedom of $\mathcal{P}^{(N,N+1)}$.

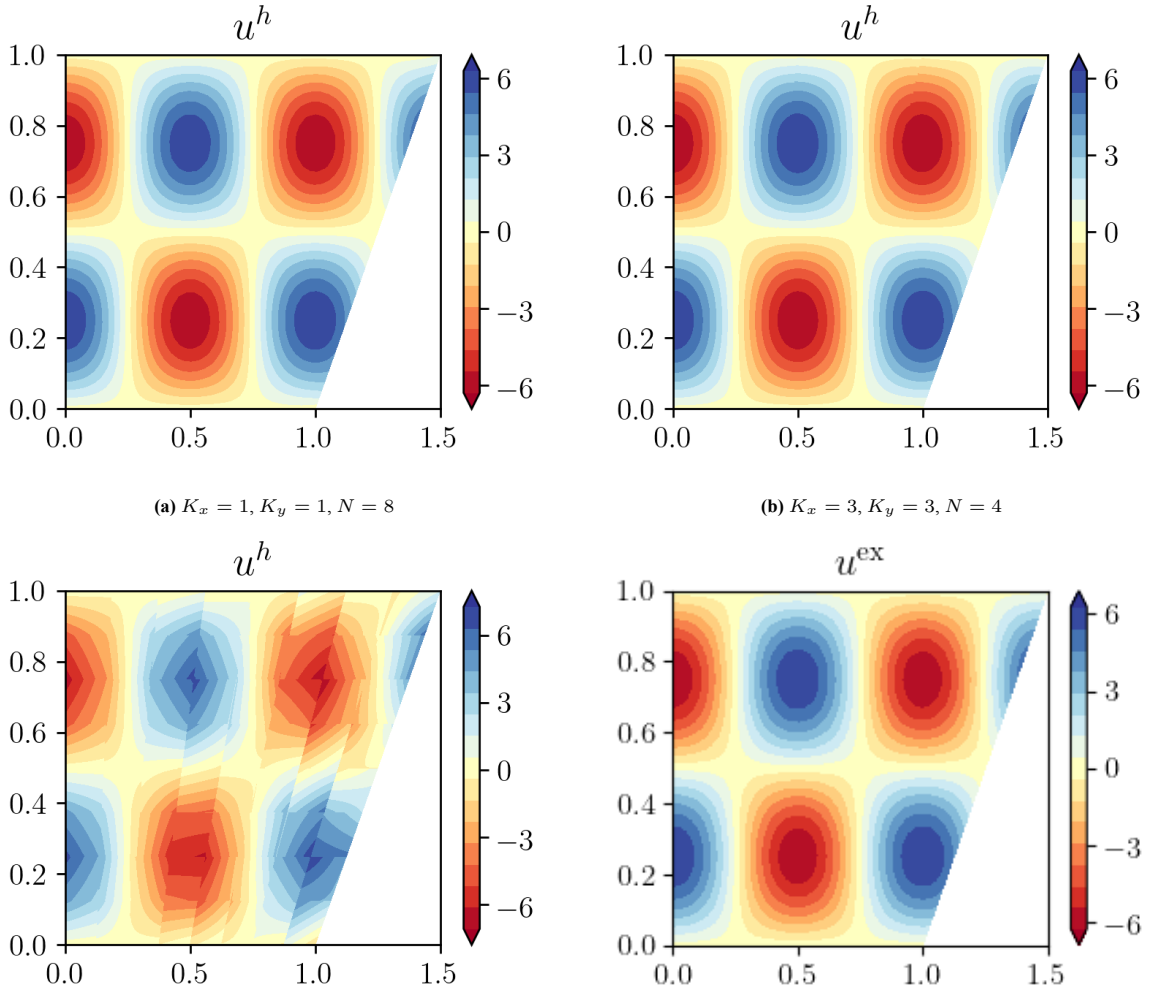

(a) $K_x = 1, K_y = 1, N = 8$

(b) $K_x = 3, K_y = 3, N = 4$

(c) $K_x = 8, K_y = 8, N = 1$

(d) Exact solution

Figure 5.4: Results for u^h in the physical domain

These discontinuities contribute to the numerical error of the system. However, the error

$$\epsilon_{lin} = \frac{\partial u_\xi}{\partial \xi} + \frac{\partial u_\eta}{\partial \eta} - f \det J,$$

shown in Figure 5.7 divergence equation is still a topological relation, with the error in the equation only due to the projection of f. This means that the errors in u_x, u_y and p are due to the error in the constitutive relation, which is where the error should be. But the errors in all quantities and equations do converge as expected, and optimal convergence is seen with increasing number of elements (Figure 5.9). Figure 5.10 shows exponential convergence with polynomial degree.

A similar trend can be seen for all these quantities for a different skewed domain in section B.1

5.11. Summary

In this section, a new formulation is tested for the Poisson equation. Here, the pressure (since it is a scalar) does not change its representation, but the velocity is represented with its equivalent components in the reference domain. The constitutive law and the divergence equation are rewritten in terms of these components, and the solution is computed and compared to a reference manufactured solution. Once the results obtained from this formulation have been converted back into the physical domain, the deviation from the exact solution is calculated. The error shows convergence as expected, both on increasing polynomial degree and increase in number of elements.

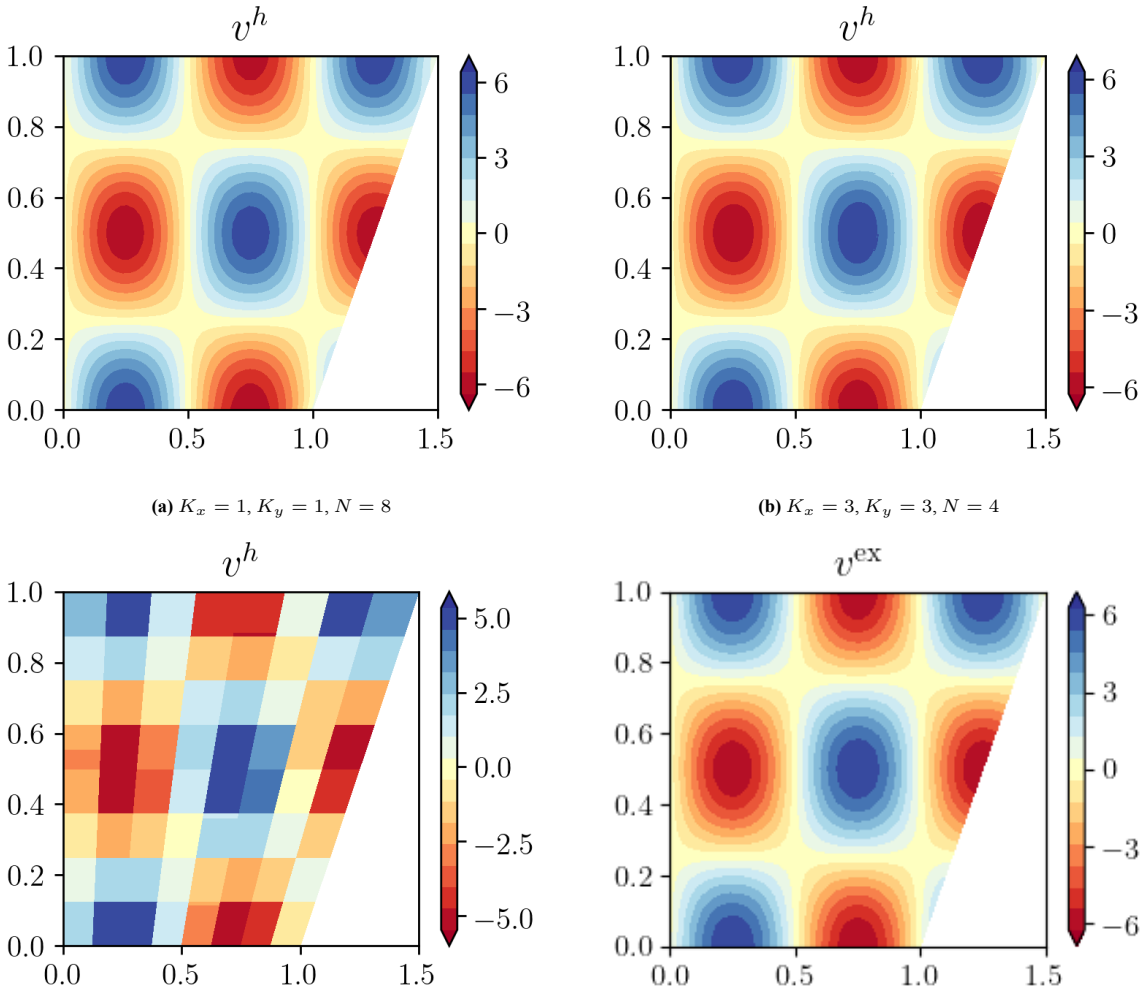

(a) $K_x = 1, K_y = 1, N = 8$

(b) $K_x = 3, K_y = 3, N = 4$

(c) $K_x = 8, K_y = 8, N = 1$

(d) Exact solution

Figure 5.5: Results for v^h in the physical domain

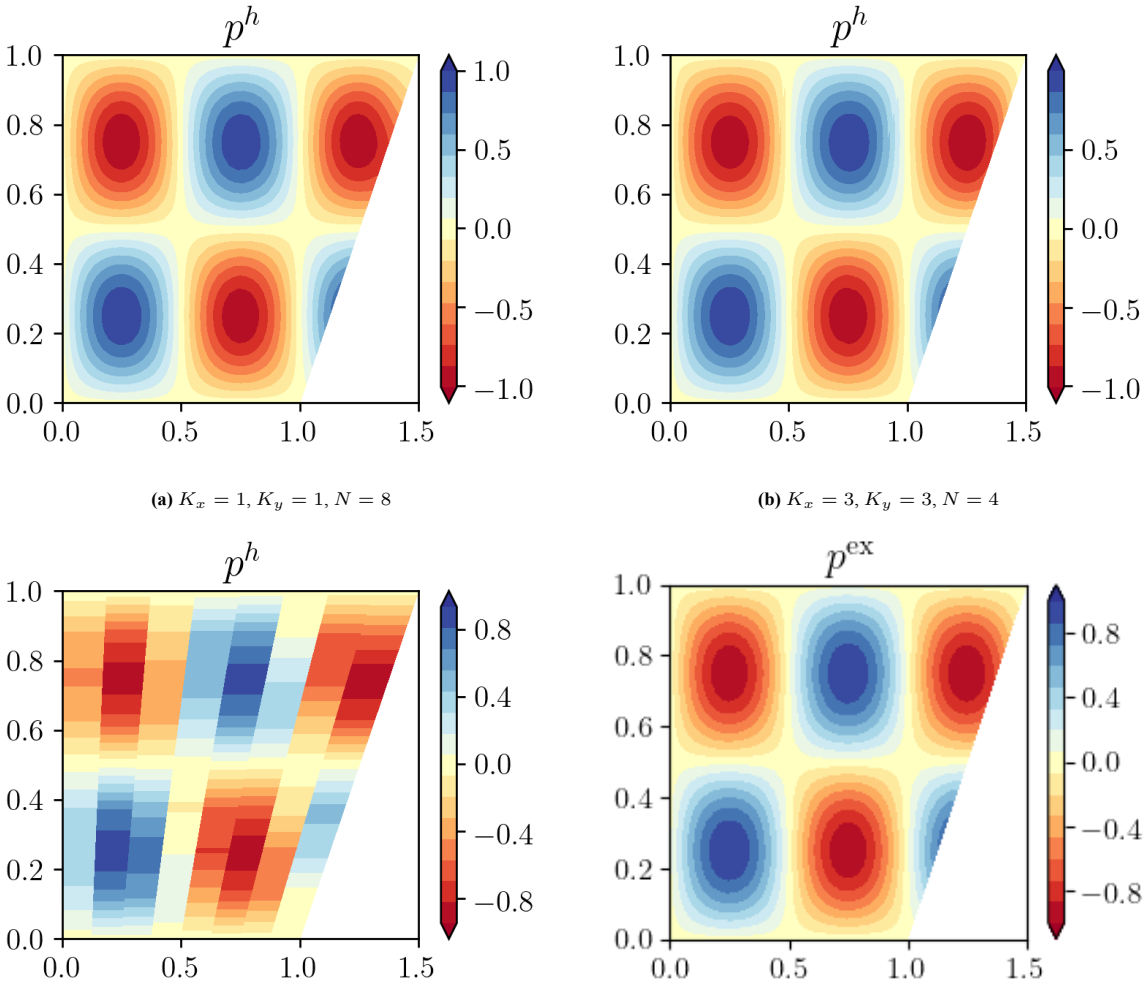

(a) $K_x = 1, K_y = 1, N = 8$

(b) $K_x = 3, K_y = 3, N = 4$

(c) $K_x = 8, K_y = 8, N = 1$

(d) Exact solution

Figure 5.6: Results for p^h in the physical domain

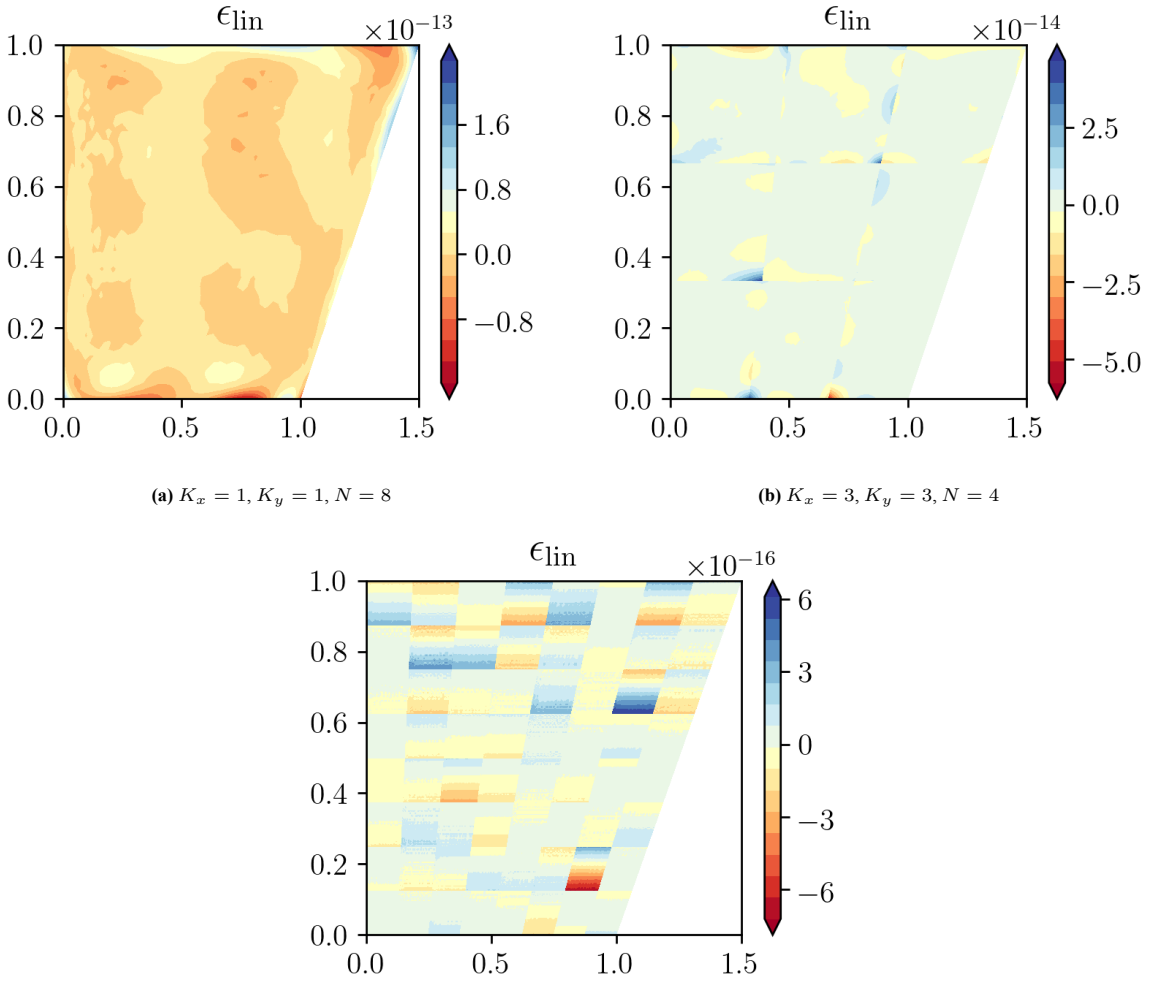

(a) $K_x = 1, K_y = 1, N = 8$

(b) $K_x = 3, K_y = 3, N = 4$

(c) $K_x = 8, K_y = 8, N = 1$

Figure 5.7: Results for the error in the divergence equation in the physical domain

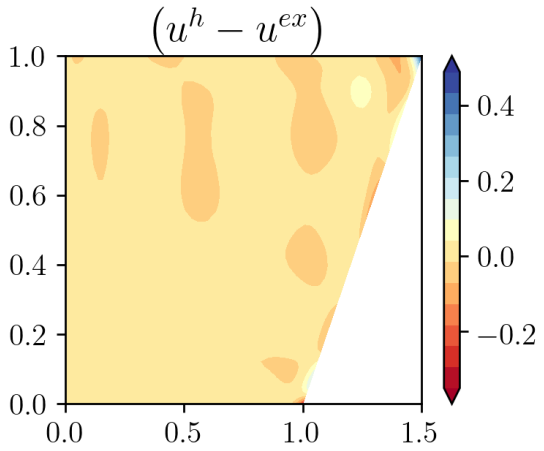

(a) $u_x^h - u_x^{ex}$ for $K_x = 1, K_y = 1, N = 8$

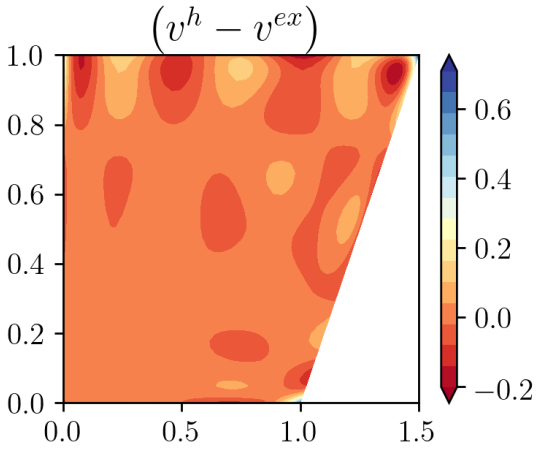

(b) $u_y^h - u_y^{ex}$ for $K_x = 1, K_y = 1, N = 8$

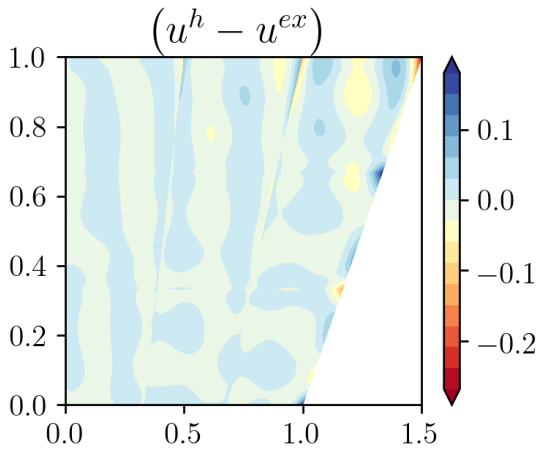

(c) $u_x^h - u_x^{ex}$ for $K_x = 3, K_y = 3, N = 4$

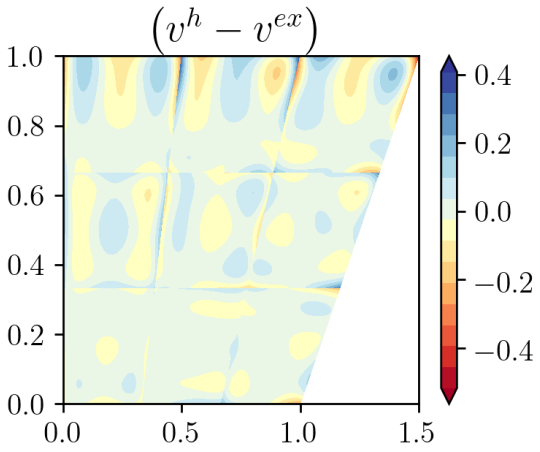

(d) $u_y^h - u_y^{ex}$ for $K_x = 3, K_y = 3, N = 4$

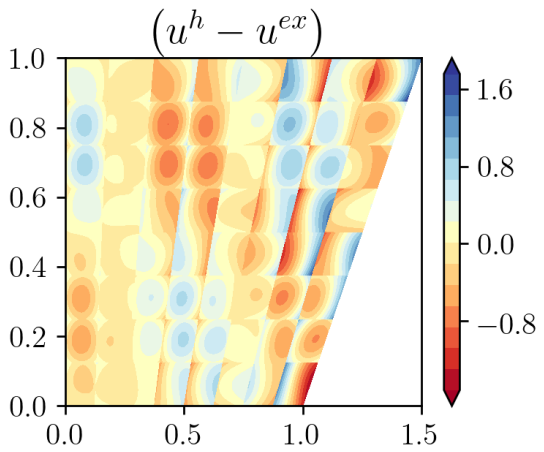

(e) $u_x^h - u_x^{ex}$ for $K_x = 8, K_y = 8, N = 1$

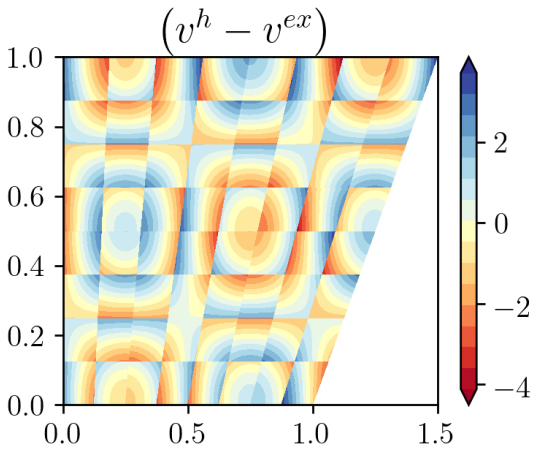

(f) $u_y^h - u_y^{ex}$ for $K_x = 8, K_y = 8, N = 1$

Figure 5.8: Errors in u_y and u_x for different configurations

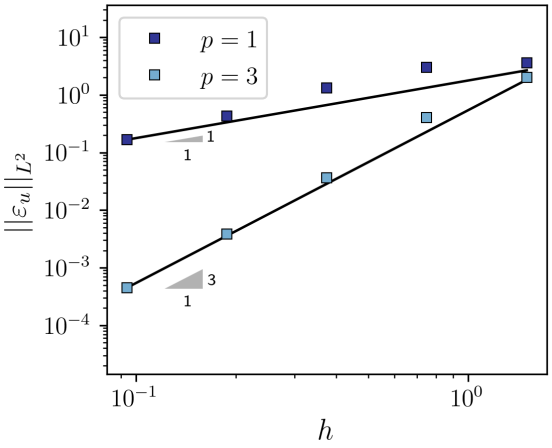

(a) Convergence with mesh width of L^2 error for u^h

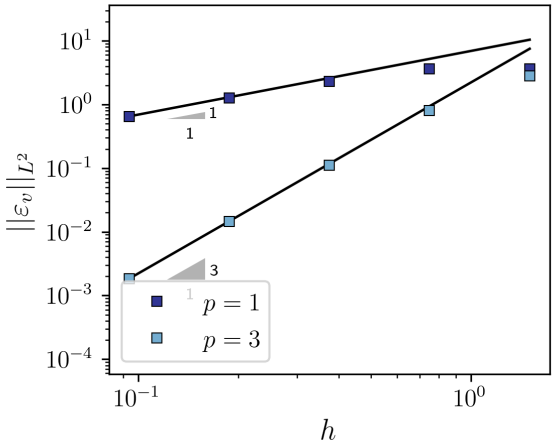

(b) Convergence with mesh width of L^2 error for v^h

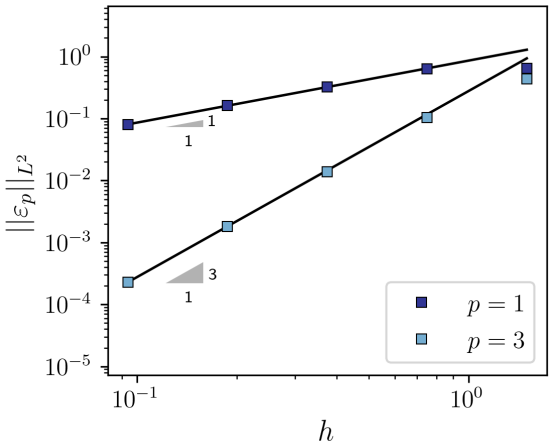

(c) Convergence with mesh width of L^2 error for p^h

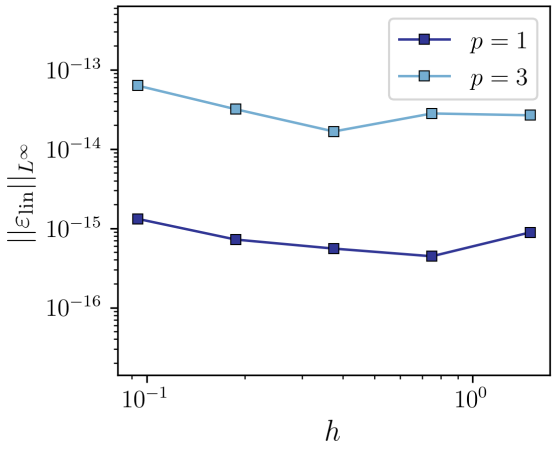

(d) Convergence with mesh width of L^∞ error for the error in the divergence equation

Figure 5.9: Results from the h-convergence study

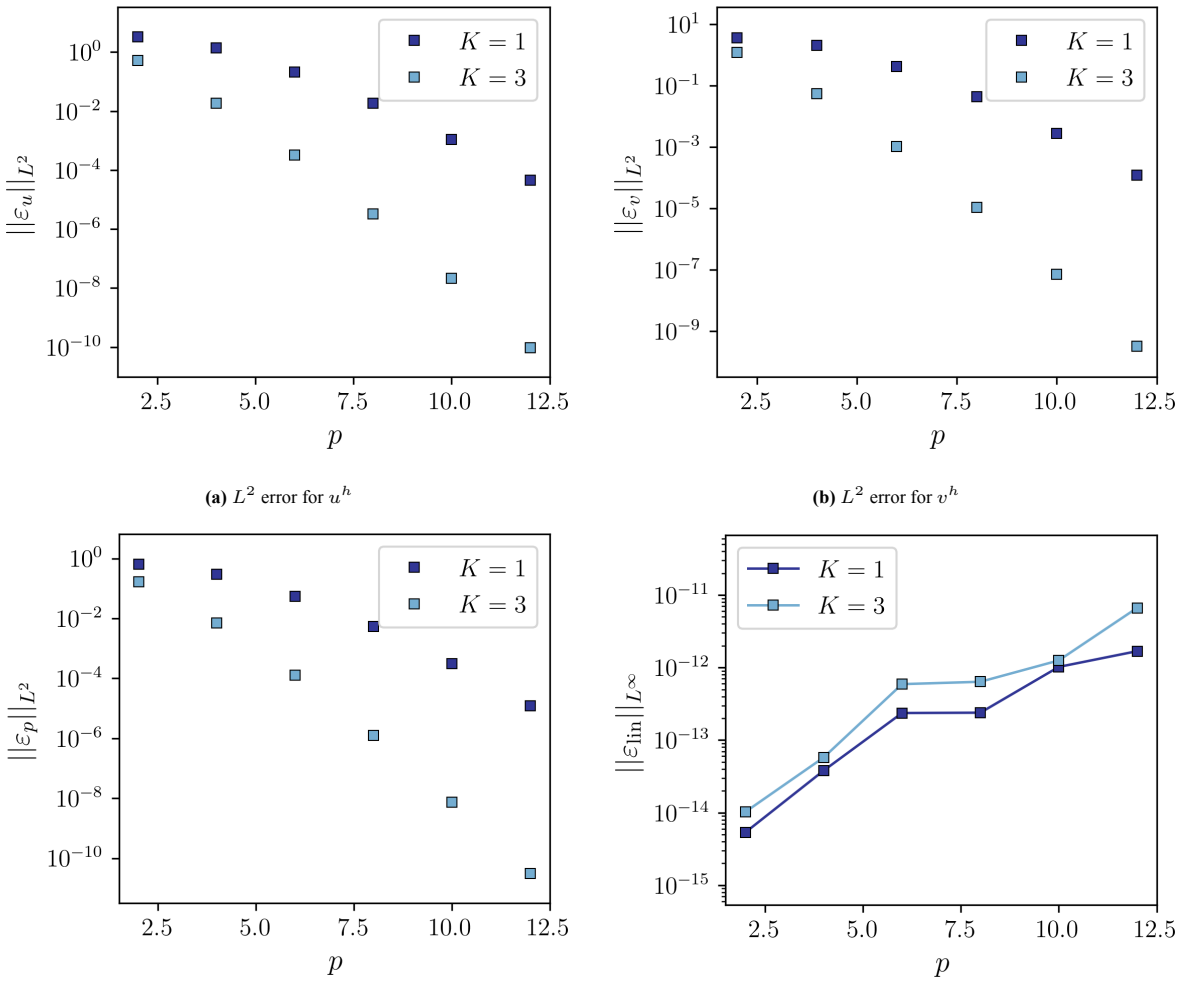

(a) L^2 error for u^h

(b) L^2 error for v^h

(c) L^2 error for p^h

(d) L^∞ error for the divergence equation

Figure 5.10: Results from the polynomial convergence study

6

Original Lagrangian formulation

The Poisson problem was looked at with a new perspective. With success in maintaining the topological relationship by using differential forms, the next step is to come back to linear elasticity and look at it using bundle-valued forms in the reference domain. This idea is tested in this chapter.

6.1. Introduction

Compared to the Poisson problem, the linear elasticity problem essentially is a combination of two Poisson problems, which are coupled using the conservation of angular momentum (or the symmetry of the Cauchy stresses).

The goal is to still perform calculations on the reference domain, like in the previous chapter, by converting all physical quantities into the reference domain. However, in this formulation, the idea is to not convert all parts of the quantities into the reference domain. Since the incidence matrices used in the formulation result only in the change of the form parts of quantities, it is sufficient to convert to form parts of quantities into their respective reference-domain counterparts. A formulation that does this is explained in this chapter.

6.2. Components in the reference domain

In this section, we will deal with how the components of different quantities are represented in the reference domain. This will help to map the quantities into the reference domain and back, as well as apply the boundary conditions to the problem.

6.2.1. Reference domain

In this scenario, the reference domain is chosen to be $\left[-1,1\right] \times \left[-1,1\right]$ 2-dimensional square, with the independent dimensions being ξ and η, the same one in Figure 4.2.

This is ideal because the Gauss-Lobatto points which are used to construct the spectral bases lie in this domain.

6.2.2. Stress

The stress is described as a covector-valued 1-form. In the physical domain, it is represented as

$$\underline{\underline{\boldsymbol{\sigma}}} = \mathrm{d}x \otimes \left(\sigma_{xx}\mathrm{d}y - \sigma_{yx}\mathrm{d}x\right) + \mathrm{d}y \otimes \left(\sigma_{xy}\mathrm{d}y - \sigma_{yy}\mathrm{d}x\right). \tag{6.1}$$

In the reference domain, this would look like

$$\underline{\underline{\boldsymbol{\sigma}}} = \mathrm{d}x \otimes \left(\sigma_{\xi x}\mathrm{d}\eta - \sigma_{\eta x}\mathrm{d}\xi\right) + \mathrm{d}y \otimes \left(\sigma_{\xi y}\mathrm{d}\eta - \sigma_{\eta y}\mathrm{d}\xi\right). \tag{6.2}$$

It should be noted that even in the reference domain, the covector value part is not converted to its counterparts in the reference domain. That is, it is not converted into $\mathrm{d}\xi$ and $\mathrm{d}\eta$.

With these representations for the stress, we can convert between the two domains as

$$\sigma_{xx} = \frac{1}{\det \mathcal{J}} \left[\sigma_{\xi x} \frac{\partial x}{\partial \xi} + \sigma_{\eta x} \frac{\partial x}{\partial \eta} \right], \qquad \sigma_{xy} = \frac{1}{\det \mathcal{J}} \left[\sigma_{\xi y} \frac{\partial x}{\partial \xi} + \sigma_{\eta y} \frac{\partial x}{\partial \eta} \right],$$
$$\sigma_{yx} = \frac{1}{\det \mathcal{J}} \left[\sigma_{\xi x} \frac{\partial y}{\partial \xi} + \sigma_{\eta x} \frac{\partial y}{\partial \eta} \right], \qquad \sigma_{yy} = \frac{1}{\det \mathcal{J}} \left[\sigma_{\xi y} \frac{\partial y}{\partial \xi} + \sigma_{\eta y} \frac{\partial y}{\partial \eta} \right].$$

where $\det \mathcal{J} = \left(\frac{\partial x}{\partial \xi} \frac{\partial y}{\partial \eta} - \frac{\partial x}{\partial \eta} \frac{\partial y}{\partial \xi} \right)$ and

$$\sigma_{\xi x} = \sigma_{xx} \frac{\partial y}{\partial \eta} - \sigma_{yx} \frac{\partial x}{\partial \eta}, \qquad \sigma_{\xi y} = \sigma_{xy} \frac{\partial y}{\partial \eta} - \sigma_{yy} \frac{\partial x}{\partial \eta},$$
$$\sigma_{\eta x} = -\sigma_{xx} \frac{\partial y}{\partial \xi} + \sigma_{yx} \frac{\partial x}{\partial \xi}, \qquad \sigma_{\eta y} = -\sigma_{xy} \frac{\partial y}{\partial \xi} + \sigma_{yy} \frac{\partial x}{\partial \xi}.$$

With the way the stress tensor is defined, the resulting traction force on a surface will always be represented in the components of the physical coordinate system. This is helpful especially when the physical domain is severely skewed, the location of the boundaries in the reference domain will still be easy to locate, and the resulting traction can be imposed in the reference domain with the same directional components as in the physical domain.

6.2.3. Displacement

The displacement is described as a vector-valued 0-form, written as

$$\mathbf{u} = \frac{\partial}{\partial x} \otimes u + \frac{\partial}{\partial y} \otimes v. \tag{6.3}$$

This representation ensures that the displacement does not need to be mapped from the reference domain to the physical domain, or vice versa.

The reason for this representation stems from the fact that the goal of this method is to still make all computations in the reference domain. With the vector-valued part for the displacement and the covector-valued part present in the components of the stress tensor, there is a duality pairing between the stress components and the displacement components.

6.2.4. Rotation

The rotation is defined as the antisymmetric part of the displacement gradient. Thus, it is a second-order tensor. It is described as a scalar-valued 0-form. This means that it remains the same irrespective of the domain, similar to the displacement.

$$\boldsymbol{\omega} = \omega \begin{bmatrix} 0 & 1 \\ -1 & 1 \end{bmatrix} \tag{6.4}$$

6.2.5. Body force

The body force/ forcing function is described as a covector-valued 2-form. In the physical domain, this can be written as

$$\mathbf{f} = \mathrm{d}x \otimes f_x \mathrm{d}x\mathrm{d}y + \mathrm{d}y \otimes f_y \mathrm{d}x\mathrm{d}y, \tag{6.5}$$

while in the reference domain

$$\mathbf{f} = \mathrm{d}x \otimes f_1 \mathrm{d}\xi\mathrm{d}\eta + \mathrm{d}y \otimes f_2 \mathrm{d}\xi\mathrm{d}\eta. \tag{6.6}$$

Thus, we can convert between the two domains as

$$f_x = f_1 / \det \mathcal{J}, \qquad f_1 = f_x \det \mathcal{J},$$
$$f_y = f_2 / \det \mathcal{J}, \qquad f_2 = f_y \det \mathcal{J}.$$

where $\det \mathcal{J} = \left(\frac{\partial x}{\partial \xi} \frac{\partial y}{\partial \eta} - \frac{\partial x}{\partial \eta} \frac{\partial y}{\partial \xi} \right)$, and

$$\mathcal{J} = \begin{bmatrix} \frac{\partial x}{\partial \xi} & \frac{\partial x}{\partial \eta} \\ \frac{\partial y}{\partial \xi} & \frac{\partial y}{\partial \eta} \end{bmatrix}.$$

6.3. Equations in the reference domain

The aim of this section is to translate the equations which were already derived in the physical/cartesian domain into the reference domain. By doing this, the result should be such that the solution obtained in the reference domain should be analogous to how the solution would be had the equations been solved for in the physical domain itself.

6.3.1. Constitutive law

For isotropic linear elastic materials, the compliance tensor can be described using only the elastic modulus E and the Poisson's ratio ν. This means that the constitutive relations can be written as

$$\begin{aligned}
\frac{1}{E}\sigma_{xx} - \frac{\nu}{E}\sigma_{yy} &= \frac{\partial u_x}{\partial x}, \\
\frac{(1+\nu)}{E}\sigma_{yx} &= \frac{\partial u_x}{\partial y} + \omega, \\
\frac{(1+\nu)}{E}\sigma_{xy} &= \frac{\partial u_y}{\partial x} - \omega, \\
\frac{1}{E}\sigma_{yy} - \frac{\nu}{E}\sigma_{xx} &= \frac{\partial u_y}{\partial y}.
\end{aligned}$$

To convert this in the reference domain, we need to rewrite the stress components in the physical domain into their respective counterparts in the reference domain. In addition, the derivatives can be rewritten as

$$\begin{aligned}
\frac{\partial}{\partial x} &= \frac{\partial \xi}{\partial x}\frac{\partial}{\partial \xi} + \frac{\partial \eta}{\partial x}\frac{\partial}{\partial \eta}, \\
\frac{\partial}{\partial y} &= \frac{\partial \xi}{\partial y}\frac{\partial}{\partial \xi} + \frac{\partial \eta}{\partial y}\frac{\partial}{\partial \eta}.
\end{aligned}$$

Thus the equations become

$$\begin{aligned}
\frac{1}{E}\sigma_{\xi x}\frac{\partial \eta}{\partial y} - \frac{1}{E}\sigma_{\eta x}\frac{\partial \xi}{\partial y} - \frac{\nu}{E}\sigma_{\eta y}\frac{\partial \xi}{\partial x} + \frac{\nu}{E}\sigma_{\xi y}\frac{\partial \eta}{\partial x} &= \frac{\partial u_x}{\partial \xi}\frac{\partial \xi}{\partial x} + \frac{\partial u_x}{\partial \eta}\frac{\partial \eta}{\partial x}, \\
\frac{(1+\nu)}{E}\sigma_{\eta x}\frac{\partial \xi}{\partial x} - \frac{(1+\nu)}{E}\sigma_{\xi x}\frac{\partial \eta}{\partial x} &= \frac{\partial u_x}{\partial \xi}\frac{\partial \xi}{\partial y} + \frac{\partial u_x}{\partial \eta}\frac{\partial \eta}{\partial y} + \omega, \\
\frac{(1+\nu)}{E}\sigma_{\xi y}\frac{\partial \eta}{\partial y} - \frac{(1+\nu)}{E}\sigma_{\eta y}\frac{\partial \xi}{\partial y} &= \frac{\partial u_y}{\partial \xi}\frac{\partial \xi}{\partial x} + \frac{\partial u_y}{\partial \eta}\frac{\partial \eta}{\partial x} - \omega, \\
\frac{1}{E}\sigma_{\eta y}\frac{\partial \xi}{\partial x} - \frac{1}{E}\sigma_{\xi y}\frac{\partial \eta}{\partial x} - \frac{\nu}{E}\sigma_{\xi x}\frac{\partial \eta}{\partial y} + \frac{\nu}{E}\sigma_{\eta x}\frac{\partial \xi}{\partial y} &= \frac{\partial u_y}{\partial \xi}\frac{\partial \xi}{\partial y} + \frac{\partial u_y}{\partial \eta}\frac{\partial \eta}{\partial y}.
\end{aligned}$$

Eliminating $\frac{\partial u_x}{\partial \eta}$ from the first two equations, and multiplying the result with $\det \mathcal{J}$, we get

$$\frac{\partial u_x}{\partial \xi} + \omega\frac{\partial y}{\partial \xi} = \begin{cases}
\sigma_{\xi x}\left[\left(\frac{\partial x}{\partial \xi}\right)^2\left(\frac{1}{E}\right) + \left(\frac{\partial y}{\partial \xi}\right)^2\left(\frac{1+\nu}{E}\right)\right]\left(\frac{1}{\det \mathcal{J}}\right) + \\
\sigma_{\eta x}\left[\left(\frac{\partial x}{\partial \xi}\frac{\partial x}{\partial \eta}\right)\left(\frac{1}{E}\right) + \left(\frac{\partial y}{\partial \xi}\frac{\partial y}{\partial \eta}\right)\left(\frac{1+\nu}{E}\right)\right]\left(\frac{1}{\det \mathcal{J}}\right) + \\
\sigma_{\xi y}\left[\frac{\partial y}{\partial \xi}\frac{\partial x}{\partial \xi}\left(-\frac{\nu}{E}\right)\right]\left(\frac{1}{\det \mathcal{J}}\right) + \\
\sigma_{\eta y}\left[\frac{\partial x}{\partial \xi}\frac{\partial y}{\partial \eta}\left(-\frac{\nu}{E}\right)\right]\left(\frac{1}{\det \mathcal{J}}\right)
\end{cases}. \tag{6.7}$$

Similarly, by eliminating $\frac{\partial u_x}{\partial \xi}$ from the first two equations, and multiplying the result with $\det \mathcal{J}$, we get

$$\frac{\partial u_x}{\partial \eta} + \omega\frac{\partial y}{\partial \eta} = \begin{cases}
\sigma_{\xi x}\left[\left(\frac{\partial x}{\partial \xi}\frac{\partial x}{\partial \eta}\right)\left(\frac{1}{E}\right) + \left(\frac{\partial y}{\partial \xi}\frac{\partial y}{\partial \eta}\right)\left(\frac{1+\nu}{E}\right)\right]\left(\frac{1}{\det \mathcal{J}}\right) + \\
\sigma_{\eta x}\left[\left(\frac{\partial x}{\partial \xi}\frac{\partial x}{\partial \xi}\right)\left(\frac{1}{E}\right) + \left(\frac{\partial y}{\partial \xi}\frac{\partial y}{\partial \xi}\right)\left(\frac{1+\nu}{E}\right)\right]\left(\frac{1}{\det \mathcal{J}}\right) + \\
\sigma_{\xi y}\left[\frac{\partial y}{\partial \xi}\frac{\partial x}{\partial \eta}\left(-\frac{\nu}{E}\right)\right]\left(\frac{1}{\det \mathcal{J}}\right) + \\
\sigma_{\eta y}\left[\frac{\partial x}{\partial \eta}\frac{\partial y}{\partial \eta}\left(-\frac{\nu}{E}\right)\right]\left(\frac{1}{\det \mathcal{J}}\right)
\end{cases}. \tag{6.8}$$

Eliminating $\frac{\partial u_y}{\partial \eta}$ from the last two relations results in

$$\boxed{\frac{\partial u_y}{\partial \xi} - \omega \frac{\partial x}{\partial \xi} = \begin{cases} \sigma_{\xi x}\Big[\frac{\partial y}{\partial \xi}\frac{\partial x}{\partial \xi}\big(-\frac{\nu}{E}\big)\Big]\big(\frac{1}{\det \mathcal{J}}\big) + \\ \sigma_{\eta x}\Big[\frac{\partial y}{\partial \xi}\frac{\partial x}{\partial \eta}\big(-\frac{\nu}{E}\big)\Big]\big(\frac{1}{\det \mathcal{J}}\big) + \\ \sigma_{\xi y}\Big[\big(\frac{\partial x}{\partial \xi}\frac{\partial x}{\partial \xi}\big)\big(\frac{1+\nu}{E}\big) + \big(\frac{\partial y}{\partial \xi}\frac{\partial y}{\partial \xi}\big)\big(\frac{1}{E}\big)\Big]\big(\frac{1}{\det \mathcal{J}}\big) + \\ \sigma_{\eta y}\Big[\big(-\frac{\partial \eta}{\partial y}\frac{\partial \xi}{\partial y}\big)\big(\frac{1+\nu}{E}\big) + \big(-\frac{\partial \eta}{\partial x}\frac{\partial \xi}{\partial x}\big)\big(\frac{1}{E}\big)\Big]\big(\frac{1}{\det \mathcal{J}}\big) \end{cases}}. \tag{6.9}$$

Eliminating $\frac{\partial u_y}{\partial \xi}$ from the last two relations, we obtain

$$\boxed{\frac{\partial u_y}{\partial \eta} - \omega \frac{\partial x}{\partial \eta} = \begin{cases} \sigma_{\xi x}\Big[\frac{\partial y}{\partial \eta}\frac{\partial x}{\partial \xi}\big(-\frac{\nu}{E}\big)\Big]\big(\frac{1}{\det \mathcal{J}}\big) + \\ \sigma_{\eta x}\Big[\frac{\partial y}{\partial \eta}\frac{\partial x}{\partial \eta}\big(-\frac{\nu}{E}\big)\Big] + \\ \sigma_{\xi y}\Big[\big(\frac{\partial x}{\partial \xi}\frac{\partial x}{\partial \eta}\big)\big(\frac{1+\nu}{E}\big) + \big(\frac{\partial y}{\partial \xi}\frac{\partial y}{\partial \eta}\big)\big(\frac{1}{E}\big)\Big]\big(\frac{1}{\det \mathcal{J}}\big) + \\ \sigma_{\eta y}\Big[\big(\frac{\partial x}{\partial \eta}\frac{\partial x}{\partial \eta}\big)\big(\frac{1+\nu}{E}\big) + \big(\frac{\partial y}{\partial \eta}\frac{\partial y}{\partial \eta}\big)\big(\frac{1}{E}\big)\Big]\big(\frac{1}{\det \mathcal{J}}\big) \end{cases}}. \tag{6.10}$$

These equations can be used for assigning values to the matrices associated with the stress mass matrix, and the mass matrix corresponding to the rotation tensor.

6.3.2. Conservation of linear momentum

The conservation of linear momentum for a steady state, written in the cartesian coordinates, is

$$\Big(\frac{\partial \sigma_{xx}}{\partial x} + \frac{\partial \sigma_{yx}}{\partial y} + f_x\Big)\mathrm{d}x\mathrm{d}y = 0,$$
$$\Big(\frac{\partial \sigma_{xy}}{\partial x} + \frac{\partial \sigma_{yy}}{\partial y} + f_y\Big)\mathrm{d}x\mathrm{d}y = 0.$$

Rewriting these in terms of the reference components,

$$\Big(\frac{\partial \sigma_{\xi x}}{\partial x}\frac{\partial \eta}{\partial y} - \frac{\partial \sigma_{\eta x}}{\partial x}\frac{\partial \xi}{\partial y} - \frac{\partial \sigma_{\xi x}}{\partial y}\frac{\partial \eta}{\partial x} + \frac{\partial \sigma_{\eta x}}{\partial y}\frac{\partial \xi}{\partial x}\Big) + \sigma_{\xi x}\Big(\frac{\partial}{\partial x}\frac{\partial \eta}{\partial y} - \frac{\partial}{\partial y}\frac{\partial \eta}{\partial x}\Big) + \sigma_{\eta x}\Big(-\frac{\partial}{\partial x}\frac{\partial \xi}{\partial y} + \frac{\partial}{\partial y}\frac{\partial \xi}{\partial x}\Big) = 0,$$
$$\Big(\frac{\partial \sigma_{\xi y}}{\partial x}\frac{\partial \eta}{\partial y} - \frac{\partial \sigma_{\eta y}}{\partial x}\frac{\partial \xi}{\partial y} - \frac{\partial \sigma_{\xi y}}{\partial y}\frac{\partial \eta}{\partial x} + \frac{\partial \sigma_{\eta y}}{\partial y}\frac{\partial \xi}{\partial x}\Big) + \sigma_{\xi y}\Big(\frac{\partial}{\partial x}\frac{\partial \eta}{\partial y} - \frac{\partial}{\partial y}\frac{\partial \eta}{\partial x}\Big) + \sigma_{\eta y}\Big(-\frac{\partial}{\partial x}\frac{\partial \xi}{\partial y} + \frac{\partial}{\partial y}\frac{\partial \xi}{\partial x}\Big) = 0.$$

Assuming that the coordinate transformations are continuous enough, the mixed partial derivatives are nullified. In addition, we have

$$\frac{\partial}{\partial x} = \frac{\partial \xi}{\partial x}\frac{\partial}{\partial \xi} + \frac{\partial \eta}{\partial x}\frac{\partial}{\partial \eta},$$
$$\frac{\partial}{\partial y} = \frac{\partial \xi}{\partial y}\frac{\partial}{\partial \xi} + \frac{\partial \eta}{\partial y}\frac{\partial}{\partial \eta}.$$

Thus, the equations become

$$\frac{\partial \sigma_{\xi x}}{\partial \xi}\Big(\frac{1}{\det \mathcal{J}}\Big) + \frac{\partial \sigma_{\eta x}}{\partial \eta}\Big(\frac{1}{\det \mathcal{J}}\Big) + f_x = 0,$$
$$\frac{\partial \sigma_{\xi y}}{\partial \xi}\Big(\frac{1}{\det \mathcal{J}}\Big) + \frac{\partial \sigma_{\eta y}}{\partial \eta}\Big(\frac{1}{\det \mathcal{J}}\Big) + f_y = 0.$$

$$\frac{\partial \sigma_{\xi x}}{\partial \xi} + \frac{\partial \sigma_{\eta x}}{\partial \eta} + f_1 = 0,$$
$$\frac{\partial \sigma_{\xi y}}{\partial \xi} + \frac{\partial \sigma_{\eta y}}{\partial \eta} + f_2 = 0.$$

This is the topological relation used for the conservation of linear momentum. This is also the reason the coordinate basis is used for the divergence of stress, as other bases result in extra terms for the divergence.

6.4. Theoretical formulation

The theoretical formulation can be written as

$$\mathcal{L}\Big(\underline{\underline{\boldsymbol{\sigma}}}, \mathbf{u}, \boldsymbol{\omega}; \underline{\underline{\mathbf{C}}}\Big) = \begin{array}{l} \int_{\hat{\Omega}} \boldsymbol{\omega}\Big(\sigma_{\xi y}\frac{\partial \eta}{\partial y} - \sigma_{\eta y}\frac{\partial \xi}{\partial y} - \sigma_{\eta x}\frac{\partial \xi}{\partial x} + \sigma_{\xi x}\frac{\partial \eta}{\partial x}\Big)\mathrm{d}\hat{\Omega} \\ + \int_{\hat{\Omega}} \Big((u\frac{\partial \sigma_{\xi x}}{\partial \xi} - \frac{\partial u}{\partial \eta}\sigma_{\eta x} - \frac{\partial v}{\partial \xi}\sigma_{\xi y} + v\frac{\partial \sigma_{\eta y}}{\partial \eta})\frac{1}{\det \mathcal{J}} + u\, f_x + v\, f_y\Big)\mathrm{d}\hat{\Omega} \\ + \int_{\hat{\Omega}} \Big(\frac{1}{2}\underline{\underline{\boldsymbol{\sigma}}}^T\big(\mathbf{F}^T\underline{\underline{\mathbf{C}}}\mathbf{F}\big)\underline{\underline{\boldsymbol{\sigma}}}\Big)\mathrm{d}\hat{\Omega} \\ - \oint_{\partial\hat{\Omega}} \big(u_P\sigma_{\xi x}n_\xi + v_P\sigma_{\eta y}n_\eta\big)\frac{1}{\det \mathcal{J}}\mathrm{d}\Gamma \\ + \oint_{\partial\hat{\Omega}} \big(u(\sigma_{\eta x})_P n_\eta + v(\sigma_{\xi y})_P n_\xi\big)\frac{1}{\det \mathcal{J}}\mathrm{d}\Gamma \end{array} \tag{6.11}$$

where $\mathbf{F}$ denotes the transformation tensor for the components of the Cauchy stress into the reference stresses as mentioned previously. Thus,

$$\begin{bmatrix} \sigma_{xx} \\ \sigma_{yx} \\ \sigma_{xy} \\ \sigma_{yy} \end{bmatrix} = \frac{1}{\det \mathcal{J}} \begin{bmatrix} \frac{\partial x}{\partial \xi} & \frac{\partial x}{\partial \eta} & 0 & 0 \\ \frac{\partial y}{\partial \xi} & \frac{\partial y}{\partial \eta} & 0 & 0 \\ 0 & 0 & \frac{\partial x}{\partial \xi} & \frac{\partial x}{\partial \eta} \\ 0 & 0 & \frac{\partial y}{\partial \xi} & \frac{\partial y}{\partial \eta} \end{bmatrix} \begin{bmatrix} \sigma_{\xi x} \\ \sigma_{\eta x} \\ \sigma_{\xi y} \\ \sigma_{\eta y} \end{bmatrix},$$

and

$$\mathbf{F} = \frac{1}{\det \mathcal{J}} \begin{bmatrix} \frac{\partial x}{\partial \xi} & \frac{\partial x}{\partial \eta} & 0 & 0 \\ \frac{\partial y}{\partial \xi} & \frac{\partial y}{\partial \eta} & 0 & 0 \\ 0 & 0 & \frac{\partial x}{\partial \xi} & \frac{\partial x}{\partial \eta} \\ 0 & 0 & \frac{\partial y}{\partial \xi} & \frac{\partial y}{\partial \eta} \end{bmatrix}.$$

6.4.1. Constitutional Law

On taking the variational derivative of the functional with respect to $\underline{\underline{\boldsymbol{\sigma}}}$ and equating it to 0, the functional reduces to

$$\begin{array}{l} \int_{\hat{\Omega}} \Big(\boldsymbol{\omega}\Big(\widetilde{\sigma_{\xi y}}\frac{\partial \eta}{\partial y} - \widetilde{\sigma_{\eta y}}\frac{\partial \xi}{\partial y} - \widetilde{\sigma_{\eta x}}\frac{\partial \xi}{\partial x} + \widetilde{\sigma_{\xi x}}\frac{\partial \eta}{\partial x}\Big)\mathrm{d}\hat{\Omega} \\ + \int_{\hat{\Omega}} \Big((u\frac{\partial \widetilde{\sigma_{\xi x}}}{\partial \xi} - \frac{\partial u}{\partial \eta}\widetilde{\sigma_{\eta x}} - \frac{\partial v}{\partial \xi}\widetilde{\sigma_{\xi y}} + v\frac{\partial \widetilde{\sigma_{\eta y}}}{\partial \eta})\frac{1}{\det \mathcal{J}}\Big)\mathrm{d}\hat{\Omega} \quad = B_\sigma. \\ + \int_{\hat{\Omega}} \underline{\underline{\widetilde{\boldsymbol{\sigma}}}}^T(\mathbf{F}^T\underline{\underline{\mathbf{C}}}\mathbf{F})\underline{\underline{\boldsymbol{\sigma}}}\Big)\mathrm{d}\hat{\Omega} \end{array} \tag{6.12}$$

To understand what this equation represents, if integration by parts is used this results in

$$\begin{array}{l} \int_{\hat{\Omega}} \Big(\boldsymbol{\omega}(\det \mathcal{J})\Big(\widetilde{\sigma_{\xi y}}\frac{\partial \eta}{\partial y} - \widetilde{\sigma_{\eta y}}\frac{\partial \xi}{\partial y} - \widetilde{\sigma_{\eta x}}\frac{\partial \xi}{\partial x} + \widetilde{\sigma_{\xi x}}\frac{\partial \eta}{\partial x}\Big)\mathrm{d}\hat{\Omega} \\ + \int_{\hat{\Omega}} \Big(\big(-\frac{\partial u}{\partial \xi}\widetilde{\sigma_{\xi x}} - \frac{\partial u}{\partial \eta}\widetilde{\sigma_{\eta x}} - \frac{\partial v}{\partial \xi}\widetilde{\sigma_{\xi y}} - \frac{\partial v}{\partial \eta}\widetilde{\sigma_{\eta y}}\big)\Big)\mathrm{d}\hat{\Omega} \qquad = 0. \\ + \int_{\hat{\Omega}} \underline{\underline{\widetilde{\boldsymbol{\sigma}}}}^T\big((\det \mathcal{J})\mathbf{F}^T\underline{\underline{\mathbf{C}}}\mathbf{F}\big)\underline{\underline{\boldsymbol{\sigma}}}\Big)\mathrm{d}\hat{\Omega} \end{array}$$

Since $\underline{\underline{\widetilde{\boldsymbol{\sigma}}}}$ is an arbitrary function, the result reduces to the constitutive laws derived in the section before. This means that with the variational derivative of $\underline{\underline{\boldsymbol{\sigma}}}$ the equations that need to be satisfied are the constitutive relations for the material.

Important consideration is that for this to hold, the term $\mathcal{B}_\sigma$ should be

$$\mathcal{B}_\sigma = \oint_{\partial\hat{\Omega}} \big(u_P\widetilde{\sigma_{\xi x}}n_\xi + v_P\widetilde{\sigma_{\eta y}}n_\eta\big)\mathrm{d}\Gamma, \tag{6.13}$$

which makes sure that the correct constitutive relation is solved, using the prescribed values of displacement at the normal boundaries.

6.4.2. Conservation of linear momentum

On taking the variational derivative of the functional with respect to $\mathbf{u}$ and equating it to 0, the functional reduces to

$$\int_{\hat{\Omega}} \Big((\widetilde{u}\frac{\partial \sigma_{\xi x}}{\partial \xi} - \frac{\partial \widetilde{u}}{\partial \eta}\sigma_{\eta x} - \frac{\partial \widetilde{v}}{\partial \xi}\sigma_{\xi y} + \widetilde{v}\frac{\partial \sigma_{\eta y}}{\partial \eta}) + (\widetilde{u}\, f_x + \widetilde{v}\, f_y)(\det \mathcal{J}) \Big) \mathrm{d}\hat{\Omega} = -B_{\mathbf{u}}, \tag{6.14}$$

where

$$B_{\mathbf{u}} = \oint_{\partial\hat{\Omega}} \big(\widetilde{u}(\sigma_{\eta x})_P n_\eta + \widetilde{v}(\sigma_{\xi y})_P n_\xi \big) \mathrm{d}\Gamma. \tag{6.15}$$

It can be verified that if integration by parts is used to include the boundary terms, this results in the same equations used to conserve linear momentum that were derived earlier. (Assuming that $\widetilde{u}$ and $\widetilde{v}$ are arbitrary and hold for any arbitrary domain).

6.4.3. Conservation of angular momentum

On taking the variational derivative of the functional with respect to $\boldsymbol{\omega}$ and equating it to 0, the functional reduces to

$$\int_{\hat{\Omega}} \widetilde{\boldsymbol{\omega}} \Big(\sigma_{\xi y}\frac{\partial \eta}{\partial y} - \sigma_{\eta y}\frac{\partial \xi}{\partial y} - \sigma_{\eta x}\frac{\partial \xi}{\partial x} + \sigma_{\xi x}\frac{\partial \eta}{\partial x} \Big) \mathrm{d}\hat{\Omega} = 0 \tag{6.16}$$

With an arbitrary $\widetilde{\boldsymbol{\omega}}$ and assuming this holds for any arbitrary domain, the symmetry of the stress tensor is achieved. If linear momentum is conserved, then the symmetry of the Cauchy stress tensor results in the conservation of angular momentum too.

With these variations equated to zero, the solution obtained using these equations will be a saddle point of the original Lagrangian functional.

6.5. Spectral bases

In this section, the expansion of the quantities in the reference domain are shown. The overhead bar indicates that they are reconstructed (using the spectral bases functions).

$$\begin{aligned}
\overline{\sigma_{\xi x}} &= \sum_{i=1}^{N+1}\sum_{j=1}^{N+1} (\sigma_{\xi x})_{ij}\; h_i(\xi)\; e'_j(\eta)\;, \\
\overline{\sigma_{\eta x}} &= \sum_{i=1}^{N}\sum_{j=1}^{N} (\sigma_{\eta x})_{ij}\; e_i(\xi)\; h'_j(\eta)\;, \\
\overline{\sigma_{\xi y}} &= \sum_{i=1}^{N}\sum_{j=1}^{N} (\sigma_{\xi y})_{ij}\; h'_i(\xi)\; e_j(\eta)\;, \\
\overline{\sigma_{\eta y}} &= \sum_{i=1}^{N+1}\sum_{j=1}^{N+1} (\sigma_{\eta y})_{ij}\; e'_i(\xi)\; h_j(\eta)\;.
\end{aligned}$$

Using these bases, if we write the conservation of linear momentum in the reference domain, we get

$$\begin{aligned}
\frac{\partial \overline{\sigma_{\xi x}}}{\partial \xi} + \frac{\partial \overline{\sigma_{\eta x}}}{\partial \eta} &= \sum_{i=1}^{N}\sum_{j=1}^{N+1} \Big((\sigma_{\xi x})_{i+1,j} - (\sigma_{\xi x})_{i,j} \Big)\; e_i(\xi)\; e'_j(\eta) \;+ \sum_{i=1}^{N}\sum_{j=1}^{N+1} \Big((\sigma_{\eta x})_{i,j} - (\sigma_{\eta x})_{i,j-1} \Big)\; e_i(\xi)\; e'_j(\eta)\;, \\
\frac{\partial \overline{\sigma_{\xi y}}}{\partial \xi} + \frac{\partial \overline{\sigma_{\eta y}}}{\partial \eta} &= \sum_{i=1}^{N+1}\sum_{j=1}^{N} \Big((\sigma_{\xi y})_{i,j} - (\sigma_{\xi y})_{i-1,j} \Big)\; e'_i(\xi)\; e_j(\eta) \;+ \sum_{i=1}^{N+1}\sum_{j=1}^{N} \Big((\sigma_{\eta y})_{i,j+1} - (\sigma_{\eta y})_{i,j} \Big)\; e'_i(\xi)\; e_j(\eta)\;,
\end{aligned}$$

including the boundary conditions $(\sigma_{\eta x})_{i,0}$ and $(\sigma_{\eta x})_{i,N+1}$ for the equation along x, and $(\sigma_{\xi y})_{0,j}$ and $(\sigma_{\xi y})_{N+1,j}$ for the equation along y. Thus, these equations ensure that the derivatives of the stress components in the ξ- and η- can be represented by the same bases.

The displacements act as the Lagrange multipliers for the conservation of linear momentum, as mentioned before. To make these equations completely topological, the bases for the corresponding Lagrange multipliers are chosen to be the dual of the expansions listed above. Thus,

$$\overline{u_x} = \sum_{i=1}^{N} \sum_{j=1}^{N+1} (u_x)_{ij}\ h_i'(\xi)\ h_j(\eta)\ ,$$
$$\overline{u_y} = \sum_{i=1}^{N+1} \sum_{j=1}^{N} (u_y)_{ij}\ h_i(\xi)\ h_j'(\eta)\ .$$

The rotation is expanded as

$$\overline{\omega} = \sum_{i=1}^{N} \sum_{j=1}^{N} (\omega)_{ij}\ h_i'(\xi)\ h_j'(\eta)\ .$$

The stress components are converted into the dual of the spectral bases for ω and then the equation for the conservation of angular momentum is written down.

With these spectral bases, the system can be written to find the unknown degrees of freedom as

$$\begin{bmatrix} \mathbb{M}_\sigma & \mathbb{E}_\sigma^T & \mathbb{R}^T \\ \mathbb{E}_\sigma & 0 & 0 \\ \mathbb{R}_\sigma & 0 & 0 \end{bmatrix} \begin{bmatrix} \boldsymbol{\sigma}^h \\ \mathbf{u}^h \\ \boldsymbol{\omega}^h \end{bmatrix} = \begin{bmatrix} -\mathbf{g}_\sigma^h \\ -\mathbf{f}^h - \mathbf{g}_u^h \\ \mathbf{0} \end{bmatrix} \tag{6.17}$$

In this representation, let

$$\boldsymbol{\sigma}^h = \begin{bmatrix} \sigma_{\xi x}^h & \sigma_{\eta x}^h & \sigma_{\xi y}^h & \sigma_{\eta y}^h \end{bmatrix}^T , \tag{6.18}$$

and

$$\mathbf{u}^h = \begin{bmatrix} u^h & v^h \end{bmatrix} , \tag{6.19}$$

making it easier to arrange the unknowns for the tensor and vector quantities. In addition, it should be easier to construct matrices if the quantities are arranged in this order.

$\mathbf{g}_\sigma^h$ indicates the array containing the normal displacements at the boundaries, while $\mathbf{g}_u^h$ indicates the shear stresses at the boundaries. The body force is included in the term $\mathbf{f}^h$.

The other terms in this system will be analysed in the following sections.

6.6. Incidence matrix

The conservation of linear momentum is designed to be topological in the computational (reference) domain. With this, the matrix that needs to be made should not involve any terms other than ± 1 or 0. Looking at how the divergence operator is expanded using spectral bases, as in Section 6.5, this is accomplished.

With the stress degree of freedoms arranged as (6.18), the matrix can be decomposed into two parts $(\mathbb{E}_\sigma)_x$ and $(\mathbb{E}_\sigma)_y$, written as

$$\mathbb{E}_\sigma = \begin{bmatrix} (\mathbb{E}_\sigma)_x & 0 \\ 0 & (\mathbb{E}_\sigma)_y \end{bmatrix}$$

This decomposes the conservation of linear momentum into two directions, $x-$ and $y-$. $\widetilde{u}^h$ and $\widetilde{v}^h$ act as the Lagrange multipliers to enforce the conservation of linear momentum in these directions respectively. Thus, $(\mathbb{E}_\sigma)_x$ is a linear operator on $[\sigma_{\xi x}^h \ \ \sigma_{\eta x}^h]$, while $(\mathbb{E}_\sigma)_y$ is a linear operator on $[\sigma_{\xi y}^h \ \ \sigma_{\eta y}^h]$.

Following the x-lexicographic arrangement for these degrees of freedom, the components of $\mathbb{E}_\sigma$ (for $N = 2$) are given below.

$$(\mathbb{E}_\sigma)_x = \begin{bmatrix} 1 & -1 & 0 & 0 & 0 & 0 & 0 & 0 & 0 & -1 & 0 & 0 & 0 \\ 0 & 1 & -1 & 0 & 0 & 0 & 0 & 0 & 0 & 0 & -1 & 0 & 0 \\ 0 & 0 & 0 & 1 & -1 & 0 & 0 & 0 & 0 & 1 & 0 & -1 & 0 \\ 0 & 0 & 0 & 0 & 1 & -1 & 0 & 0 & 0 & 0 & 1 & 0 & -1 \\ 0 & 0 & 0 & 0 & 0 & 0 & 1 & -1 & 0 & 0 & 0 & 1 & 0 \\ 0 & 0 & 0 & 0 & 0 & 0 & 0 & 1 & -1 & 0 & 0 & 0 & 1 \end{bmatrix}$$

$$(\mathbb{E}_\sigma)_y = \begin{bmatrix} -1 & 0 & 0 & 0 & 1 & 0 & 0 & -1 & 0 & 0 & 0 & 0 & 0 \\ 1 & -1 & 0 & 0 & 0 & 1 & 0 & 0 & -1 & 0 & 0 & 0 & 0 \\ 0 & 1 & 0 & 0 & 0 & 0 & 1 & 0 & 0 & -1 & 0 & 0 & 0 \\ 0 & 0 & -1 & 0 & 0 & 0 & 0 & 1 & 0 & 0 & -1 & 0 & 0 \\ 0 & 0 & 1 & -1 & 0 & 0 & 0 & 0 & 1 & 0 & 0 & -1 & 0 \\ 0 & 0 & 0 & 1 & 0 & 0 & 0 & 0 & 0 & 1 & 0 & 0 & -1 \end{bmatrix}$$

Note that the transpose of this matrix is also used to compute the components of the gradient, which is used in the constitutive laws to relate the displacements and the rotation with the stress components.

6.7. Mass matrix

The mass matrix is referred to the equations in this formulation where the stress components themselves act as the test functions. Specifically, this is one of the mass matrices used to enforce the constitutive law.

Because there are 4 stress components in the two-dimensional formulation, there are also 4 equations enforcing the constitutive relation. In general, the mass matrix can be written as $\left[(\widetilde{\boldsymbol{\sigma}}^h)^T \mathbb{M}_\sigma \boldsymbol{\sigma}^h\right]$. To make it easier to write it down, $\mathbb{M}_\sigma$ can be separated into 4 horizontal matrices, representing each of the constitutive equations, as

$$\mathbb{M}_\sigma = \begin{bmatrix} \mathbb{M}_1 \\ \mathbb{M}_2 \\ \mathbb{M}_3 \\ \mathbb{M}_4 \end{bmatrix}.$$

Let us look at how the different matrices are constructed.

6.7.1. Constitutive relation 1

This relation has $\widetilde{\sigma_{\xi x}}$ as the test function. Thus, looking at (6.7), the relation can be expanded as

$$\mathbb{M}_{11}\,\sigma^h_{\xi x} + \mathbb{M}_{12}\,\sigma^h_{\eta x} + \mathbb{M}_{13}\,\sigma^h_{\xi y} + \mathbb{M}_{14}\,\sigma^h_{\eta y},$$

which represents the integral

$$\int \widetilde{\sigma_{\xi x}}\,(C'_{11}\,\sigma_{\xi x} + C'_{12}\,\sigma_{\eta x} + C'_{13}\,\sigma_{\xi y} + C'_{14}\,\sigma_{\eta y})\,\mathrm{d}\xi \wedge \mathrm{d}\eta,$$

where

$$\begin{aligned} C'_{11} &= \frac{1}{\det \mathcal{J}} \left[\left(\frac{\partial x}{\partial \xi}\right)^2 \left(\frac{1}{E}\right) + \left(\frac{\partial y}{\partial \xi}\right)^2 \left(\frac{1+\nu}{E}\right) \right], \\ C'_{12} &= \frac{1}{\det \mathcal{J}} \left[\left(\frac{\partial x}{\partial \xi}\frac{\partial x}{\partial \eta}\right) \left(\frac{1}{E}\right) + \left(\frac{\partial y}{\partial \xi}\frac{\partial y}{\partial \eta}\right) \left(\frac{1+\nu}{E}\right) \right], \\ C'_{13} &= \frac{1}{\det \mathcal{J}} \left[\frac{\partial y}{\partial \xi}\frac{\partial x}{\partial \xi} \left(-\frac{\nu}{E}\right) \right], \\ C'_{14} &= \frac{1}{\det \mathcal{J}} \left[\frac{\partial x}{\partial \xi}\frac{\partial y}{\partial \eta} \left(-\frac{\nu}{E}\right) \right]. \end{aligned}$$

$\mathbb{M}_{11}$ represents the first term and the first integral. Writing down the bases for the components,

$$\int \widetilde{\sigma_{\xi x}}\,C'_{11}\,\sigma_{\xi x}\mathrm{d}\xi \wedge \mathrm{d}\eta = \int \sum_{i=1}^{N+1}\sum_{j=1}^{N+1}\sum_{k=1}^{N+1}\sum_{l=1}^{N+1} (\widetilde{\sigma_{\xi x}})_{kl} C'_{11}(\xi,\eta)(\sigma_{\xi x})_{ij} h_i(\xi)\; e'_j(\eta)\; h_k(\xi)\; e'_l(\eta)\; \mathrm{d}\xi \wedge \mathrm{d}\eta.$$

The integral can be simplified using the quadrature using the Gauss-Lobatto nodes. Thus, the terms for $\mathbb{M}_{11}$ can be written as

$$(\mathbb{M}_{11})_{ijkl} = \sum_{r=1}^{N_x}\sum_{s=1}^{N_x} C'_{11}\,(\xi_r,\eta_s)\,h_i(\xi_r)\; e'_j(\eta_s)\; h_k(\xi_r)\; e'_l(\eta_s)\,w_r\,w_s, \tag{6.20}$$

where w_r and w_s are the integration weights associated with the nodes at ξ_r and η_s using Gaussian quadrature, and N_x denotes the number of Gauss-Lobatto nodes used for quadrature.

Similarly,

$$(\mathbb{M}_{12})_{ijkl} = \sum_{r=1}^{N_x}\sum_{s=1}^{N_x} C'_{12}\,(\xi_r,\eta_s)\,e_i(\xi_r)\;h'_j(\eta_s)\;h_k(\xi_r)\;e'_l(\eta_s)\,w_r\,w_s, \tag{6.21}$$

$$(\mathbb{M}_{13})_{ijkl} = \sum_{r=1}^{N_x}\sum_{s=1}^{N_x} C'_{13}\,(\xi_r,\eta_s)\,h'_i(\xi_r)\;e_j(\eta_s)\;h_k(\xi_r)\;e'_l(\eta_s)\,w_r\,w_s, \tag{6.22}$$

$$(\mathbb{M}_{14})_{ijkl} = \sum_{r=1}^{N_x}\sum_{s=1}^{N_x} C'_{14}\,(\xi_r,\eta_s)\,e'_i(\xi_r)\;h_j(\eta_s)\;h_k(\xi_r)\;e'_l(\eta_s)\,w_r\,w_s. \tag{6.23}$$

Once these matrices are formed $\mathbb{M}_1 = [\mathbb{M}_{11}\;\;\mathbb{M}_{12}\;\;\mathbb{M}_{13}\;\;\mathbb{M}_{14}]$.

6.7.2. Constitutive relation 2

A similar method to the way the matrices are derived can be used to determine the matrices for the second constitutive relation, with the test function being $\widetilde{\sigma_{\eta x}}$. The expressions are given below.

$$(\mathbb{M}_{21})_{ijkl} = \sum_{r=1}^{N_x}\sum_{s=1}^{N_x} C'_{21}\,(\xi_r,\eta_s)\,h_i(\xi_r)\;e'_j(\eta_s)\;e_k(\xi_r)\;h'_l(\eta_s)\,w_r\,w_s, \tag{6.24}$$

$$(\mathbb{M}_{22})_{ijkl} = \sum_{r=1}^{N_x}\sum_{s=1}^{N_x} C'_{22}\,(\xi_r,\eta_s)\,e_i(\xi_r)\;h'_j(\eta_s)\;e_k(\xi_r)\;h'_l(\eta_s)\,w_r\,w_s, \tag{6.25}$$

$$(\mathbb{M}_{23})_{ijkl} = \sum_{r=1}^{N_x}\sum_{s=1}^{N_x} C'_{23}\,(\xi_r,\eta_s)\,h'_i(\xi_r)\;e_j(\eta_s)\;e_k(\xi_r)\;h'_l(\eta_s)\,w_r\,w_s, \tag{6.26}$$

$$(\mathbb{M}_{24})_{ijkl} = \sum_{r=1}^{N_x}\sum_{s=1}^{N_x} C'_{24}\,(\xi_r,\eta_s)\,e'_i(\xi_r)\;h_j(\eta_s)\;e_k(\xi_r)\;h'_l(\eta_s)\,w_r\,w_s. \tag{6.27}$$

where

$$\begin{aligned}
C'_{21} &= \frac{1}{\det\mathcal{J}}\left[\left(\frac{\partial x}{\partial\xi}\frac{\partial x}{\partial\eta}\right)\left(\frac{1}{E}\right) + \left(\frac{\partial y}{\partial\xi}\frac{\partial y}{\partial\eta}\right)\left(\frac{1+\nu}{E}\right)\right],\\
C'_{22} &= \frac{1}{\det\mathcal{J}}\left[\left(\frac{\partial x}{\partial\xi}\frac{\partial x}{\partial\xi}\right)\left(\frac{1}{E}\right) + \left(\frac{\partial y}{\partial\xi}\frac{\partial y}{\partial\xi}\right)\left(\frac{1+\nu}{E}\right)\right],\\
C'_{23} &= \frac{1}{\det\mathcal{J}}\left[\frac{\partial y}{\partial\xi}\frac{\partial x}{\partial\eta}\left(-\frac{\nu}{E}\right)\right],\\
C'_{24} &= \frac{1}{\det\mathcal{J}}\left[\frac{\partial x}{\partial\eta}\frac{\partial y}{\partial\eta}\left(-\frac{\nu}{E}\right)\right].
\end{aligned}$$

Then we get $\mathbb{M}_2 = [\mathbb{M}_{21}\;\;\mathbb{M}_{22}\;\;\mathbb{M}_{23}\;\;\mathbb{M}_{24}]$.

6.7.3. Constitutive relation 3

The third constitutive relation has $\widetilde{\sigma_{\xi y}}$ as the test function. The expressions are given below.

$$(\mathbb{M}_{31})_{ijkl} = \sum_{r=1}^{N_x}\sum_{s=1}^{N_x} C'_{31}\,(\xi_r,\eta_s)\,h_i(\xi_r)\;e'_j(\eta_s)\;h'_k(\xi_r)\;e_l(\eta_s)\,w_r\,w_s, \tag{6.28}$$

$$(\mathbb{M}_{32})_{ijkl} = \sum_{r=1}^{N_x}\sum_{s=1}^{N_x} C'_{32}\,(\xi_r,\eta_s)\,e_i(\xi_r)\;h'_j(\eta_s)\;h'_k(\xi_r)\;e_l(\eta_s)\,w_r\,w_s, \tag{6.29}$$

$$(\mathbb{M}_{33})_{ijkl} = \sum_{r=1}^{N_x}\sum_{s=1}^{N_x} C'_{33}\,(\xi_r,\eta_s)\,h'_i(\xi_r)\;e_j(\eta_s)\;h'_k(\xi_r)\;e_l(\eta_s)\,w_r\,w_s, \tag{6.30}$$

$$(\mathbb{M}_{34})_{ijkl} = \sum_{r=1}^{N_x}\sum_{s=1}^{N_x} C'_{34}\,(\xi_r,\eta_s)\,e'_i(\xi_r)\;h_j(\eta_s)\;h'_k(\xi_r)\;e_l(\eta_s)\,w_r\,w_s, \tag{6.31}$$

where

$$\begin{aligned}
C'_{31} &= \frac{1}{\det\mathcal{J}}\left[\frac{\partial y}{\partial\xi}\frac{\partial x}{\partial\xi}\left(-\frac{\nu}{E}\right)\right],\\
C'_{32} &= \frac{1}{\det\mathcal{J}}\left[\frac{\partial y}{\partial\xi}\frac{\partial x}{\partial\eta}\left(-\frac{\nu}{E}\right)\right],\\
C'_{33} &= \frac{1}{\det\mathcal{J}}\left[\left(\frac{\partial x}{\partial\xi}\frac{\partial x}{\partial\xi}\right)\left(\frac{1+\nu}{E}\right)+\left(\frac{\partial y}{\partial\xi}\frac{\partial y}{\partial\xi}\right)\left(\frac{1}{E}\right)\right],\\
C'_{34} &= \frac{1}{\det\mathcal{J}}\left[\left(\frac{\partial x}{\partial\xi}\frac{\partial x}{\partial\eta}\right)\left(\frac{1+\nu}{E}\right)+\left(\frac{\partial y}{\partial\xi}\frac{\partial y}{\partial\eta}\right)\left(\frac{1}{E}\right)\right].
\end{aligned}$$

Then we get $\mathbb{M}_3 = [\mathbb{M}_{31}\;\;\mathbb{M}_{32}\;\;\mathbb{M}_{33}\;\;\mathbb{M}_{34}]$.

6.7.4. Constitutive relation 4

The third constitutive relation has $\widetilde{\sigma_{\eta y}}$ as the test function. The expressions are given below.

$$(\mathbb{M}_{41})_{ijkl} = \sum_{r=1}^{N_x}\sum_{s=1}^{N_x} C'_{41}\,(\xi_r,\eta_s)\,h_i(\xi_r)\;e'_j(\eta_s)\;e'_k(\xi_r)\;h_l(\eta_s)\,w_r\,w_s, \tag{6.32}$$

$$(\mathbb{M}_{42})_{ijkl} = \sum_{r=1}^{N_x}\sum_{s=1}^{N_x} C'_{42}\,(\xi_r,\eta_s)\,e_i(\xi_r)\;h'_j(\eta_s)\;e'_k(\xi_r)\;h_l(\eta_s)\,w_r\,w_s, \tag{6.33}$$

$$(\mathbb{M}_{43})_{ijkl} = \sum_{r=1}^{N_x}\sum_{s=1}^{N_x} C'_{43}\,(\xi_r,\eta_s)\,h'_i(\xi_r)\;e_j(\eta_s)\;e'_k(\xi_r)\;h_l(\eta_s)\,w_r\,w_s, \tag{6.34}$$

$$(\mathbb{M}_{44})_{ijkl} = \sum_{r=1}^{N_x}\sum_{s=1}^{N_x} C'_{44}\,(\xi_r,\eta_s)\,e'_i(\xi_r)\;h_j(\eta_s)\;e'_k(\xi_r)\;h_l(\eta_s)\,w_r\,w_s, \tag{6.35}$$

where

$$\begin{aligned}
C'_{41} &= \frac{1}{\det\mathcal{J}}\left[\frac{\partial y}{\partial\eta}\frac{\partial x}{\partial\xi}\left(-\frac{\nu}{E}\right)\right],\\
C'_{42} &= \frac{1}{\det\mathcal{J}}\left[\frac{\partial y}{\partial\eta}\frac{\partial x}{\partial\eta}\left(-\frac{\nu}{E}\right)\right],\\
C'_{43} &= \frac{1}{\det\mathcal{J}}\left[\left(\frac{\partial x}{\partial\xi}\frac{\partial x}{\partial\eta}\right)\left(\frac{1+\nu}{E}\right)+\left(\frac{\partial y}{\partial\xi}\frac{\partial y}{\partial\eta}\right)\left(\frac{1}{E}\right)\right],\\
C'_{44} &= \frac{1}{\det\mathcal{J}}\left[\left(\frac{\partial x}{\partial\eta}\frac{\partial x}{\partial\eta}\right)\left(\frac{1+\nu}{E}\right)+\left(\frac{\partial y}{\partial\eta}\frac{\partial y}{\partial\eta}\right)\left(\frac{1}{E}\right)\right].
\end{aligned}$$

Then we get $\mathbb{M}_4 = [\mathbb{M}_{41}\;\;\mathbb{M}_{42}\;\;\mathbb{M}_{43}\;\;\mathbb{M}_{44}]$.
With these components, the mass matrix can be set up by vertically stacking $\mathbb{M}_1, \mathbb{M}_2, \mathbb{M}_3$ and $\mathbb{M}_4$ respectively.

6.8. Rotation matrix

The Rotation matrix enforces the weak conservation of angular momentum for the system. The idea is to understand and rewrite (6.16) for an element. This looks like

$$\widetilde{\boldsymbol{\omega}}^h\mathbb{R}_\sigma\boldsymbol{\sigma}^h = \widetilde{\boldsymbol{\omega}}^h\left(\mathbb{R}_1\sigma^h_{\xi x}+\mathbb{R}_2\sigma^h_{\eta x}+\mathbb{R}_3\sigma^h_{\xi y}+\mathbb{R}_4\sigma^h_{\eta y}\right),$$

where each $\mathbb{R}_i$ represents integration over the domain, such as

$$\int \widetilde{\omega} \left(-\frac{\partial y}{\partial \xi}\right) \sigma_{\xi x} \mathrm{d}\xi \wedge \mathrm{d}\eta = \int \sum_{i=1}^{N+1} \sum_{j=1}^{N+1} \sum_{k=1}^{N} \sum_{l=1}^{N} (\widetilde{\omega})_{kl} \left(-\frac{\partial y}{\partial \xi}\right) (\xi,\eta)(\sigma_{\xi x})_{ij} h_i(\xi)\, e'_j(\eta)\, h'_k(\xi)\, h'_l(\eta)\, \mathrm{d}\xi \wedge \mathrm{d}\eta.$$

On writing down these integrals for all the stress components, the rotation matrices are written down as

$$(\mathbb{R}_1)_{ijkl} = \sum_{r=1}^{N_x} \sum_{s=1}^{N_x} \left(-\frac{\partial y}{\partial \xi}\right) (\xi_r,\eta_s)\, h_i(\xi_r)\, e'_j(\eta_s)\, h'_k(\xi_r)\, h'_l(\eta_s)\, w_r\, w_s, \tag{6.36}$$

$$(\mathbb{R}_2)_{ijkl} = \sum_{r=1}^{N_x} \sum_{s=1}^{N_x} \left(-\frac{\partial y}{\partial \eta}\right) (\xi_r,\eta_s)\, e_i(\xi_r)\, h'_j(\eta_s)\, h'_k(\xi_r)\, h'_l(\eta_s)\, w_r\, w_s, \tag{6.37}$$

$$(\mathbb{R}_3)_{ijkl} = \sum_{r=1}^{N_x} \sum_{s=1}^{N_x} \left(\frac{\partial x}{\partial \xi}\right) (\xi_r,\eta_s)\, h'_i(\xi_r)\, e_j(\eta_s)\, h'_k(\xi_r)\, h'_l(\eta_s)\, w_r\, w_s, \tag{6.38}$$

$$(\mathbb{R}_4)_{ijkl} = \sum_{r=1}^{N_x} \sum_{s=1}^{N_x} \left(\frac{\partial x}{\partial \eta}\right) (\xi_r,\eta_s)\, e'_i(\xi_r)\, h_j(\eta_s)\, h'_k(\xi_r)\, h'_l(\eta_s)\, w_r\, w_s. \tag{6.39}$$

6.9. Boundary conditions

The boundary conditions can be enforced using a trick arising from the definition of the dual basis functions themselves. But care should be taken on which perspective you are using depending on which boundary condition you are finding the contributions of.

6.9.1. 'Normal' displacements for the Constitutive relation

The boundary condition for the constitutive relation with $\widetilde{\sigma_{\xi x}}$ shall be considered first. When looking at the reference domain, the displacement in the $x-$direction (i.e. in the *physical* coordinates) is prescribed on the left and right boundaries in the *reference* domain.

On the boundary, the prescribed $x-$displacement is expanded as

$$\int_{\partial\hat{\Omega}} u^{ex}\left(y(\xi,\eta)\right) \mathrm{d}\eta \approx \int_{\partial\hat{\Omega}} \sum_{l=1}^{N+1} (u_P)_l h_l\left(\eta\right) \mathrm{d}\eta,$$

where u_P is the prescribed displacement. Using the dual polynomials, this integral can be reformulated as

$$\int_{\partial\hat{\Omega}} \sum_{j=1}^{N+1} \sum_{l=1}^{N+1} (u_P)_l h_l(\eta) e'_j(\eta) \mathrm{d}\eta \approx \int_{\partial\hat{\Omega}} \sum_{j=1}^{N+1} u^{ex}(y(\xi,\eta)) e'_j(\eta) \mathrm{d}\eta = u_{a,j}.$$

where $a = 0$ or $a = N+1$ depending on whether it is the left or the right boundary.
Thus, the boundary condition becomes

$$\int_{\partial\hat{\Omega}} u_P \widetilde{\sigma_{\xi x}} n_\xi \mathrm{d}\Gamma = \int_{\partial\hat{\Omega}} \sum_{j=1}^{N+1} \sum_{l=1}^{N+1} (\widetilde{\sigma_{\xi x}})_{a,l}\, u^{ex}\left(y(\xi,\eta)\right) e'_j(\eta) \mathrm{d}\eta = \sum_{j=1}^{N+1} \sum_{l=1}^{N+1} (\widetilde{\sigma_{\xi x}})_{a,l}\, u_{a,j}. \tag{6.40}$$

In a similar manner, the $y-$displacement is prescribed to the constitutive relation with $\widetilde{\sigma_{\eta y}}$ on the bottom and top boundaries in the *reference* domain, as

$$\int_{\partial\hat{\Omega}} v_P \widetilde{\sigma_{\eta y}} n_\eta \mathrm{d}\Gamma = \int_{\partial\hat{\Omega}} \sum_{j=1}^{N+1} \sum_{l=1}^{N+1} (\widetilde{\sigma_{\eta y}})_{l,a}\, v^{ex}\left(x(\xi,\eta)\right) e'_j(\xi) \mathrm{d}\xi = \sum_{j=1}^{N+1} \sum_{l=1}^{N+1} (\widetilde{\sigma_{\eta y}})_{l,a}\, v_{j,a}, \tag{6.41}$$

where $a = 0$ and $a = N+1$ for the bottom and top boundaries respectively, and v_P indicates the prescribed displacement.

Do note that the prescribed displacements u_P and v_P are not actually the 'normal' displacements at the boundaries, as that would be the components of the displacement along the ξ- and η- directions respectively. This makes the formulation easier to apply these boundary conditions, as the displacement in the local coordinates need not be calculated. Instead, as long as the boundary points in the physical domain correspond to the edges of the boundary in the reference domain, the x- and y- displacements can be prescribed to the horizontal and vertical boundary points respectively.

Another important note is that the boundary conditions do not require the use of the basis functions, only requiring the degrees of freedom at the boundaries. This is another benefit of using this formulation.

6.9.2. 'Shear' stresses for conservation of linear momentum

Because the components of the stress tensor are expressed using two different coordinates for the normals and the component of the traction force, it is necessary to write down the components that need to be prescribed at the boundaries for this formulation.

Considering the conservation of linear momentum for the stresses along the x-direction (for which $\widetilde{u}$ is the test function), the stress component $\sigma_{\eta x}$ needs to be prescribed at the top and bottom boundaries in the (again) reference domain.

This stress component can be expanded as

$$\int_{\partial\hat{\Omega}} \sigma_{\eta x}^{ex}\left(x(\xi,\eta)\right) \mathrm{d}\xi \approx \int_{\partial\hat{\Omega}} \sum_{l=1}^{N} (\sigma_{\eta x})_P e_l(\xi) \mathrm{d}\xi,$$

where $(\sigma_{\eta x})_P$ is prescribed at the boundaries. Using dual polynomials, this can be modified as

$$\int_{\partial\hat{\Omega}} \sum_{j=1}^{N}\sum_{l=1}^{N} (\sigma_{\eta x})_P e_l(\xi) h_j'(\xi) \mathrm{d}\xi \approx \int_{\partial\hat{\Omega}} \sum_{j=1}^{N} \sigma_{\eta x}^{ex}\left(x(\xi,\eta)\right) h_j'(\xi) \mathrm{d}\xi = (\sigma_{\eta x})_{j,a},$$

where $a = 0$ and $a = N+1$ respectively for the bottom and top boundaries.

Thus, the boundary integral can be reformulated as

$$\int_{\partial\hat{\Omega}} \widetilde{u}\left(\sigma_{\eta x}\right)_P n_\eta \mathrm{d}\Gamma = \int_{\partial\hat{\Omega}} \sum_{j=1}^{N}\sum_{l=1}^{N} (\widetilde{u})_{l,a} \sigma_{\eta x}^{ex}\left(x(\xi,\eta)\right) h_j'(\xi) \mathrm{d}\xi = \sum_{j=1}^{N}\sum_{l=1}^{N} (\widetilde{u})_{l,a} (\sigma_{\eta x})_{j,a}. \tag{6.42}$$

Similarly, considering the conservation of linear momentum for the stresses along the y-direction (with $\widetilde{v}$ as the Lagrange multiplier), the stress component $\sigma_{\xi y}$ needs to be prescribed at the left and right boundaries. The integral can be simplified as

$$\int_{\partial\hat{\Omega}} \widetilde{v}\left(\sigma_{\xi y}\right)_P n_\xi \mathrm{d}\Gamma = \int_{\partial\hat{\Omega}} \sum_{j=1}^{N}\sum_{l=1}^{N} (\widetilde{v})_{a,l} \sigma_{\xi y}^{ex}\left(y(\xi,\eta)\right) h_j'(\eta) \mathrm{d}\eta = \sum_{j=1}^{N}\sum_{l=1}^{N} (\widetilde{v})_{a,l} (\sigma_{\xi y})_{a,j}, \tag{6.43}$$

where $(\sigma_{\xi y})_P$ is the prescribed shear stress at the boundary. An important observation with these is that (like the displacements) the tractions at the boundaries need not be resolved into their normal and tangential components. Instead, the boundaries only require that the tractions be defined in the x- or y-directions depending on which boundary is being observed. Like the displacements, this boundary condition does not require the use of basis functions. Using the degrees of freedom for this purpose is another benefit of using this formulation.

6.9.3. Contributions from the forcing function

The forcing function in both directions needs to have the same basis as the derivatives of the stresses, i.e.

$$\overline{f_x} = \sum_{i=1}^{N}\sum_{j=1}^{N+1} (f_x)_{i,j} e_i(\xi) e_j'(\eta),$$

$$\overline{f_y} = \sum_{i=1}^{N+1}\sum_{j=1}^{N} (f_y)_{i,j} e_i'(\xi) e_j(\eta).$$

Similar to the boundary conditions, the degrees of freedom for the body forces can be computed using the property of the dual basis functions.

$$
\begin{aligned}
(f_x)_{k,l} &= \int_{\hat{\Omega}} \sum_{i=1}^{N} \sum_{j=1}^{N+1} (f_x)_{i,j} e_i(\xi) e'_j(\eta) h'_k(\xi) h_l(\eta) \mathrm{d}\xi \wedge \mathrm{d}\eta \\
&= \int_{\hat{\Omega}} f_x^{ex}\left(x(\xi,\eta), y(\xi,\eta)\right) (\det \mathcal{J}) h'_k(\xi) h_l(\eta) \mathrm{d}\xi \wedge \mathrm{d}\eta.
\end{aligned}
$$

$$
\begin{aligned}
(f_y)_{k,l} &= \int_{\hat{\Omega}} \sum_{i=1}^{N+1} \sum_{j=1}^{N} (f_y)_{i,j} e'_i(\xi) e_j(\eta) h_k(\xi) h'_l(\eta) \mathrm{d}\xi \wedge \mathrm{d}\eta \\
&= \int_{\hat{\Omega}} f_y^{ex}\left(x(\xi,\eta), y(\xi,\eta)\right) (\det \mathcal{J}) h_k(\xi) h'_l(\eta) \mathrm{d}\xi \wedge \mathrm{d}\eta.
\end{aligned}
$$

Note that the $\det \mathcal{J}$ term enters the integral because of the change of integration volumes, from the physical domain to the reference domain.

6.10. Hybridized system

Like the formulation for the Poisson equation in Chapter 5, this formulation can also hybridized. The intent is that the physical domain is divided into various subdomains, with the formulation applied to each subdomain as if it were independent. And Lagrange multipliers at the boundaries of the elements enforce continuity between elements, with each subdomain allowed to have its own function map between the physical and reference domains.

Similar to the hybrid system in Chapter 5, the hybrid system will look like

$$
\begin{bmatrix} \mathbb{A} & \mathbb{B}^T \\ \mathbb{B} & 0 \end{bmatrix} \begin{bmatrix} \mathbf{x}^h \\ \boldsymbol{\lambda}^h \end{bmatrix} = \begin{bmatrix} \mathbf{f}^h \\ 0 \end{bmatrix} \tag{6.44}
$$

However, $\mathbb{A}$ will contain the diagonal blocks of mass, incidence and rotation matrices, with each block belonging to an element and the elements themselves arranged in x-lexicographic order.

Similar to the Poisson formulation, $\mathbb{B}$ contains the relations which enforce continuity to be the same at the element boundaries. The continuity relations with this formulation, at the *horizontal* boundaries, are

$$
\begin{aligned}
\widetilde{\sigma_{\xi x}} \,|_l &= \widetilde{\sigma_{\xi x}} \,|_r \,, \\
\widetilde{v} \,|_l &= \widetilde{v} \,|_r \,,
\end{aligned}
$$

where l and r denote the left and right boundaries respectively. At the *vertical* boundaries,

$$
\begin{aligned}
\widetilde{\sigma_{\eta y}} \,|_b &= \widetilde{\sigma_{\eta y}} \,|_t \,, \\
\widetilde{u} \,|_b &= \widetilde{u} \,|_t \,,
\end{aligned}
$$

where b and t indicate the bottom and top boundaries respectively. A sample hybridized domain with $K_x = K_y = 2$ and $N = 1$ is indicated in Figure 6.1, where the coupling and the Lagrange multipliers between them can be observed.

6.11. Results

This formulation is tested against a manufactured solution. Here, the displacements are assumed to be

$$
\begin{aligned}
u^{ex}(x,y) &= \sin(2\pi x)\sin(2\pi y), \\
v^{ex}(x,y) &= \sin(2\pi x)\sin(2\pi y).
\end{aligned}
$$

The exact rotation

$$
\omega^{ex}(x,y) = \frac{1}{2}\left(\frac{\partial v}{\partial x} - \frac{\partial u}{\partial y}\right) = \pi\left(\cos(2\pi x)\sin(2\pi y) - \sin(2\pi x)\cos(2\pi y)\right).
$$

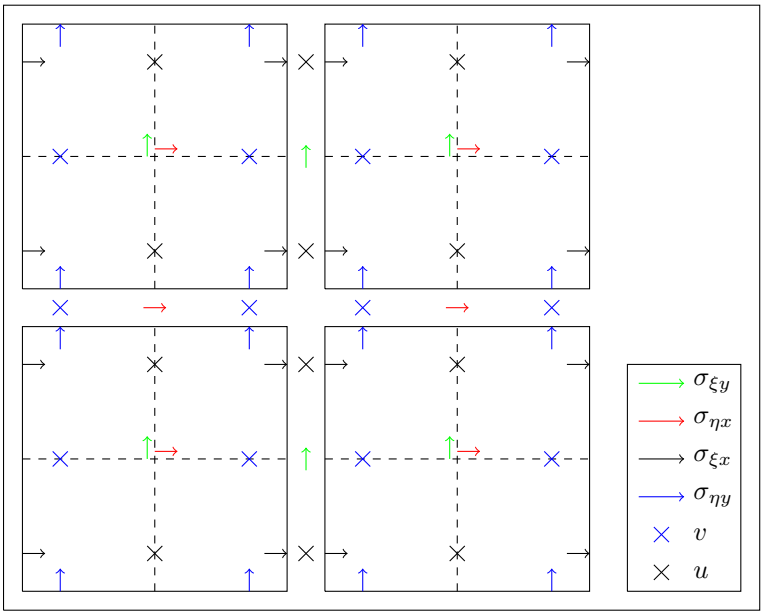

Figure 6.1: Degrees of freedom of quantities for the hybrid formulation on the reference domain with $K_x = K_y = 2$, $N = 1$

And the strains

$$\underline{\underline{\epsilon}}^{ex}(x,y) = 2\pi \begin{bmatrix} \cos(2\pi x)\sin(2\pi y) & \frac{1}{2}\left[\sin(2\pi x)\cos(2\pi y) + \cos(2\pi x)\sin(2\pi y)\right] \\ \frac{1}{2}\left[\sin(2\pi x)\cos(2\pi y) + \cos(2\pi x)\sin(2\pi y)\right] & \sin(2\pi x)\cos(2\pi y) \end{bmatrix}.$$

The stress components are equal to

$$\begin{aligned}
\sigma_{xx}^{ex}(x,y) &= \frac{2\pi E}{1-\nu^2}\left[\cos(2\pi x)\sin(2\pi y) + \nu\sin(2\pi x)\cos(2\pi y)\right], \\
\sigma_{yx}^{ex}(x,y) &= \frac{2\pi E}{2(1+\nu)}\left[\sin(2\pi x)\cos(2\pi y) + \cos(2\pi x)\sin(2\pi y)\right] = \sigma_{xy}^{ex}(x,y), \\
\sigma_{yy}^{ex}(x,y) &= \frac{2\pi E}{1-\nu^2}\left[\sin(2\pi x)\cos(2\pi y) + \nu\cos(2\pi x)\sin(2\pi y)\right].
\end{aligned}$$

In order to balance the forces generated by these stresses, there is a body force prescribed, which is given by

$$\begin{aligned}
f_x^{ex}(x,y) &= \frac{4\pi^2 E}{1-\nu^2}\left[\frac{1}{2}(2-\nu)\sin(2\pi x)\sin(2\pi y) - \frac{1}{2}(1+\nu)\cos(2\pi x)\cos(2\pi y)\right], \\
f_y^{ex}(x,y) &= \frac{4\pi^2 E}{1-\nu^2}\left[\frac{1}{2}(2-\nu)\sin(2\pi x)\sin(2\pi y) - \frac{1}{2}(1+\nu)\cos(2\pi x)\cos(2\pi y)\right].
\end{aligned}$$

6.11.1. Domain

The same trapezoidal domain as in the Poisson formulation, visualised in Figure 5.2 is used to test this formulation.

The points on this physical domain are mapped onto the points in the reference domain (Figure 4.2) using bilinear transfinite mapping. The Gauss-Lobatto points on the reference domain are then mapped onto the physical domain. When the domain is divided into several elements, the boundaries of the elements are first calculated using a bilinear transfinite mapping, and using these maps the Gauss-Lobatto points are mapped onto the physical domain. Note that the maps for each element can be different. These can be visualised in Figure 5.3.

On these domains, the displacement u^{ex} and the stress component $\sigma_{\xi y}^{ex}$ are prescribed on the left and right boundary, and the displacement v^{ex} and $\sigma_{\eta x}^{ex}$ is prescribed at the bottom and top boundary.

6.11.2. Observations and Conclusions

From Figure 6.2 and Figure 6.3, we can observe that the numerical solutions are consistent with how the exact manufactured solution looks like. In this discretisation, the continuity of u in the vertical direction and v in the horizontal direction is clearly seen especially at low resolutions. One can also observe how u has a higher resolution in the η-direction, while v has a higher resolution in the ξ-direction, due to how the spectral bases functions are defined for both these quantities. Even Figure 6.8 are as expected, however, there is no continuity between elements observed, which is seen clearly for $K_x = K_y = 8$ and $N = 1$.

One can observe consistent numerical solutions for the Cauchy stress components σ_{xx}, σ_{yy}, σ_{yx} and σ_{xy} when compared to the exact solution in Figure 6.4, Figure 6.5, Figure 6.7 and Figure 6.6 respectively. However, the continuity of these quantities between elements cannot be established as easily as it was for displacements. This is because continuity between the non-orthogonal elements is established using the reference domain components, of which $\sigma_{\xi x}$ and $\sigma_{\eta y}$ are better resolved and continuous between elements while $\sigma_{\xi y}$ and $\sigma_{\eta x}$ have a comparatively lower resolution without enforcement of continuity between elements. As a general comment, it can be said that the resolution of the Cauchy stress components is somewhere in between that of $\mathcal{P}^{(N+1,N+1)}$ (which is the resolution of $\sigma_{\xi x}$, $\sigma_{\eta y}$) and $\mathcal{P}^{(N,N)}$ (which is the resolution of $\sigma_{\xi y}$, $\sigma_{\eta x}$).

However, this complication means that the equation to enforce the symmetry of the Cauchy stress tensor in this formulation involves contributions from all 4 components, which also include components of the Jacobian, which vary continuously throughout the element. This means that while we can replicate that the error in the conservation of linear momentum ϵ_{lin} is seen to be pointwise exact (see Figure 6.9a, Figure 6.9c and Figure 6.9e) like in [23], the symmetry of the Cauchy stress tensor, which was pointwise exact in [23], is only weakly enforced as can be seen in Figure 6.9b, Figure 6.9d and Figure 6.9f. The reason is probably due to the different resolutions for all the stress components within an element as mentioned before.

The weak enforcement of symmetry of the Cauchy stress tensor can be seen in Figure 6.13, where optimal convergence is observed for the error in symmetry of the stress tensor on increasing the number of elements. A similar optimal convergence trend is observed for other physical quantities too, while the conservation of linear momentum is seen to be pointwise with the L_∞ error being of the order of 10^{-10}. An exponential convergence trend (as desired) is observed in Figure 6.14, for all physical quantities as well as the error in the symmetry of the Cauchy stress tensor. The error in linear momentum is again seen to be of very low order.

An important observation made is that there are no spurious kinematic modes appearing anywhere. This formulation helps avoid these kinematic modes, and convergence results are proof of this.

Further results in Section B.2 are in line with the observations made here, even though that was conducted on a different domain.

6.12. Summary

In this section, a new formulation was tested to construct a hybridized formulation to simultaneously conserve linear momentum, and angular momentum exactly regardless of the number of elements the domain is subdivided into, and the polynomial degree of spectral bases used for quadrature within the element. The idea was to represent the stresses in the form of a covector-valued pseudo-form, with the form part being transformed into its corresponding counterpart in the reference domain. The displacements are consecutively written as vector-valued 0-forms, such that the covector- and vector-valued parts of these quantities nullify each other. With this in mind, a hybrid formulation was constructed in a way that the total energy written down in the physical domain remains conserved, and the conservation of linear momentum remains topological. However, this attempt did not establish a strong conservation of angular momentum, with the Cauchy stress tensor being only weakly symmetric. However, convergence is seen for other quantities, including the symmetry of the Cauchy stress tensor. No indication of spurious kinematic modes is seen.

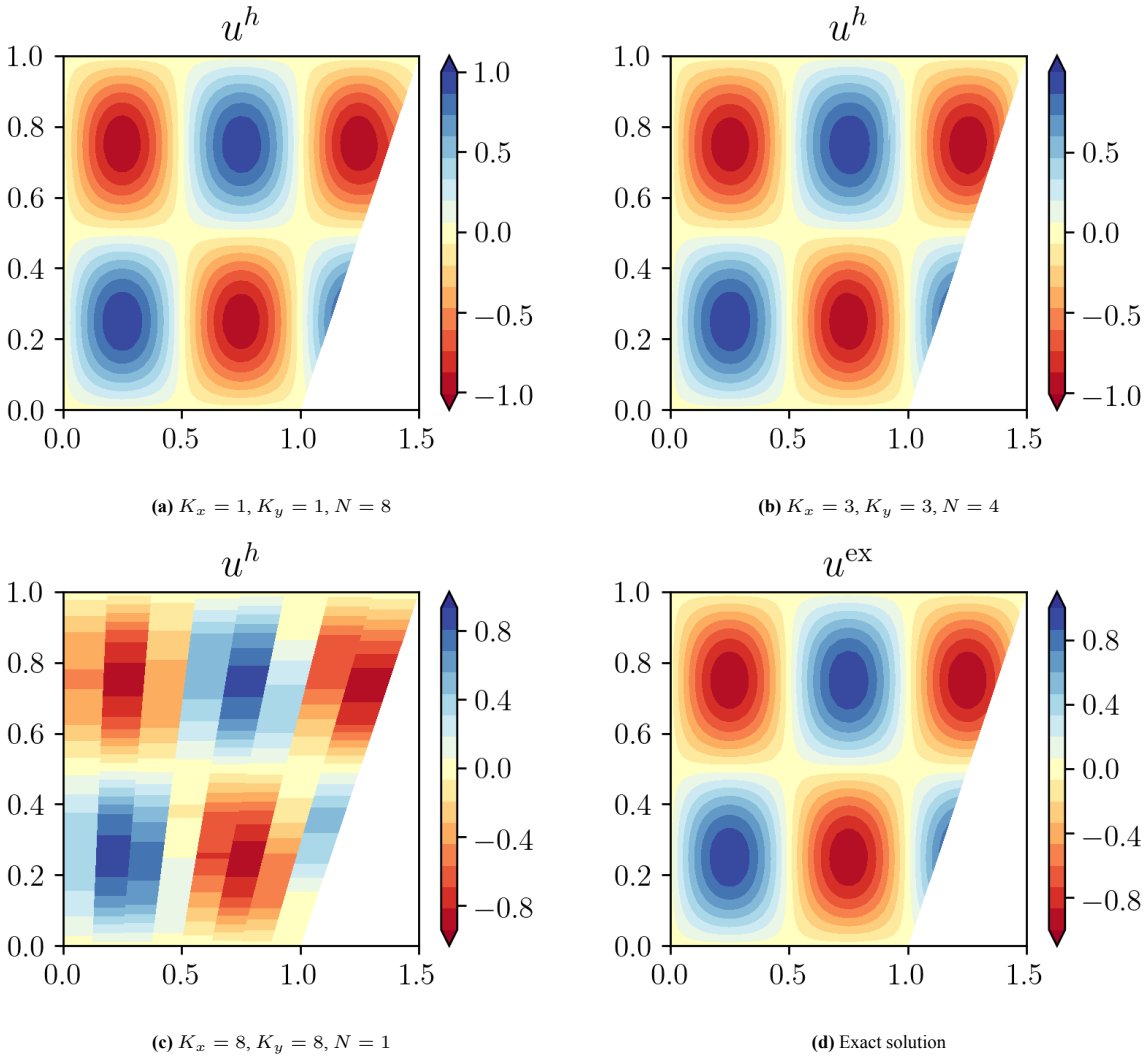

(a) $K_x = 1, K_y = 1, N = 8$

(b) $K_x = 3, K_y = 3, N = 4$

(c) $K_x = 8, K_y = 8, N = 1$

(d) Exact solution

Figure 6.2: Results for u^h in the physical domain

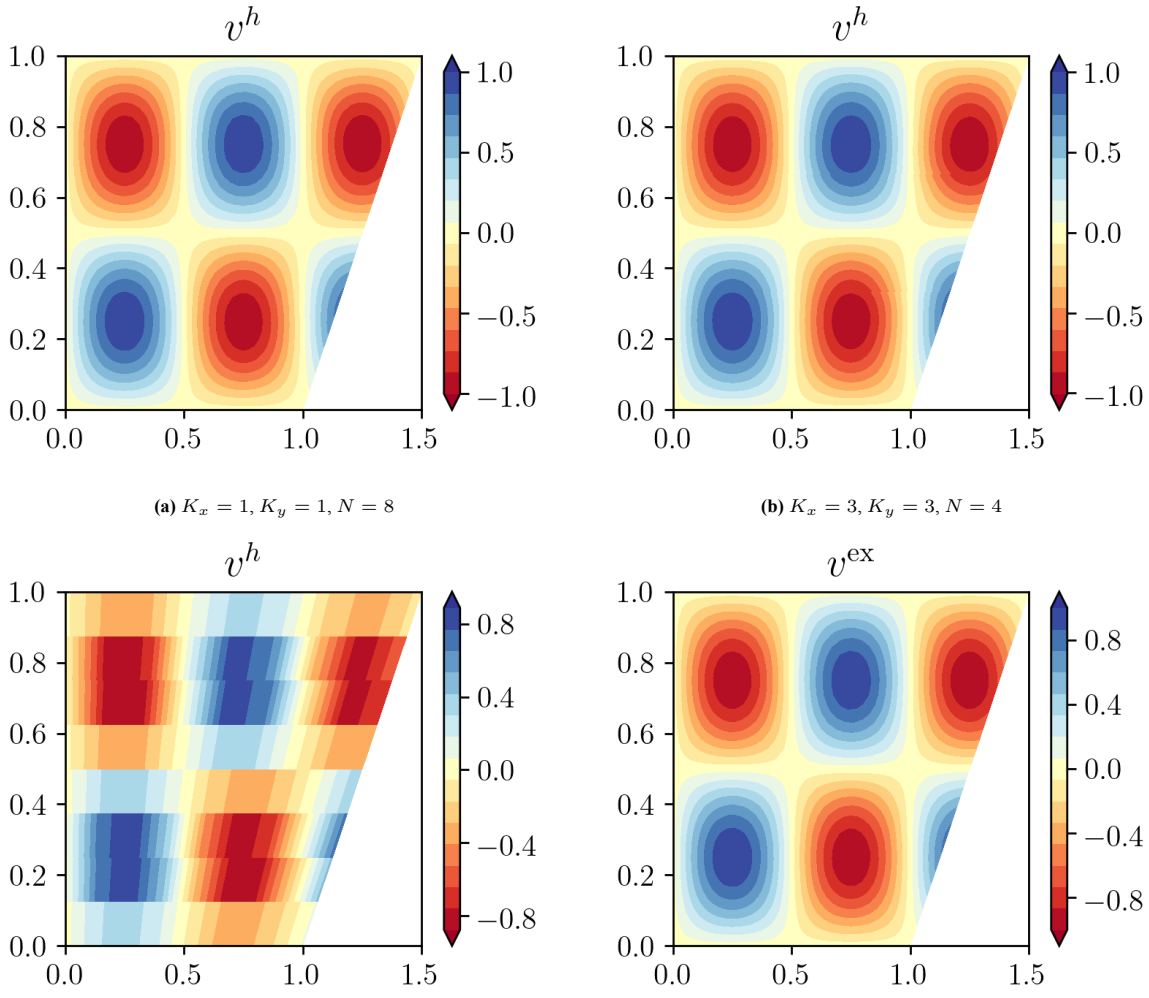

(a) $K_x = 1, K_y = 1, N = 8$

(b) $K_x = 3, K_y = 3, N = 4$

(c) $K_x = 8, K_y = 8, N = 1$

(d) Exact solution

Figure 6.3: Results for v^h in the physical domain

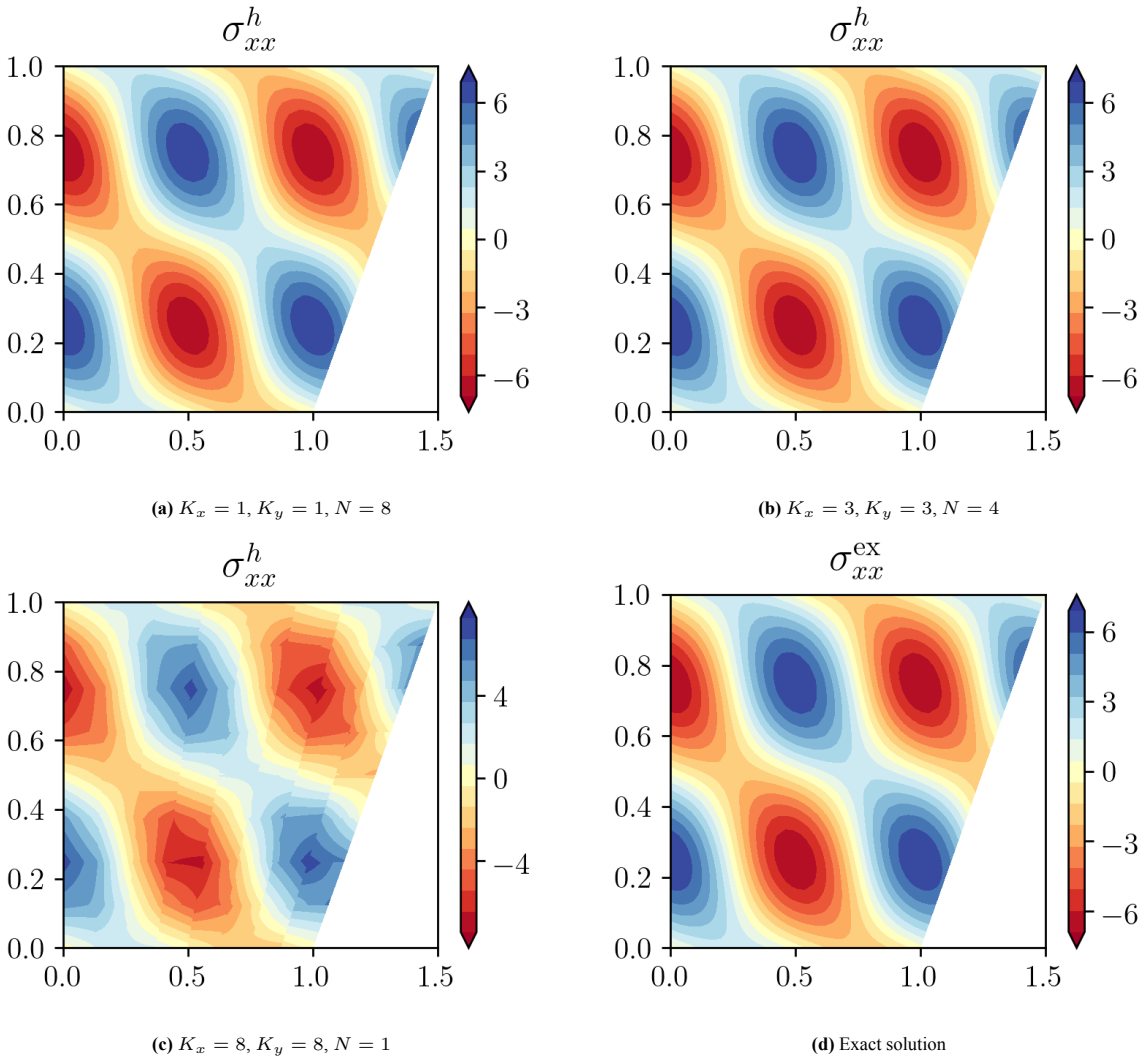

(a) $K_x = 1, K_y = 1, N = 8$

(b) $K_x = 3, K_y = 3, N = 4$

(c) $K_x = 8, K_y = 8, N = 1$

(d) Exact solution

Figure 6.4: Results for σ^h_{xx} in the physical domain

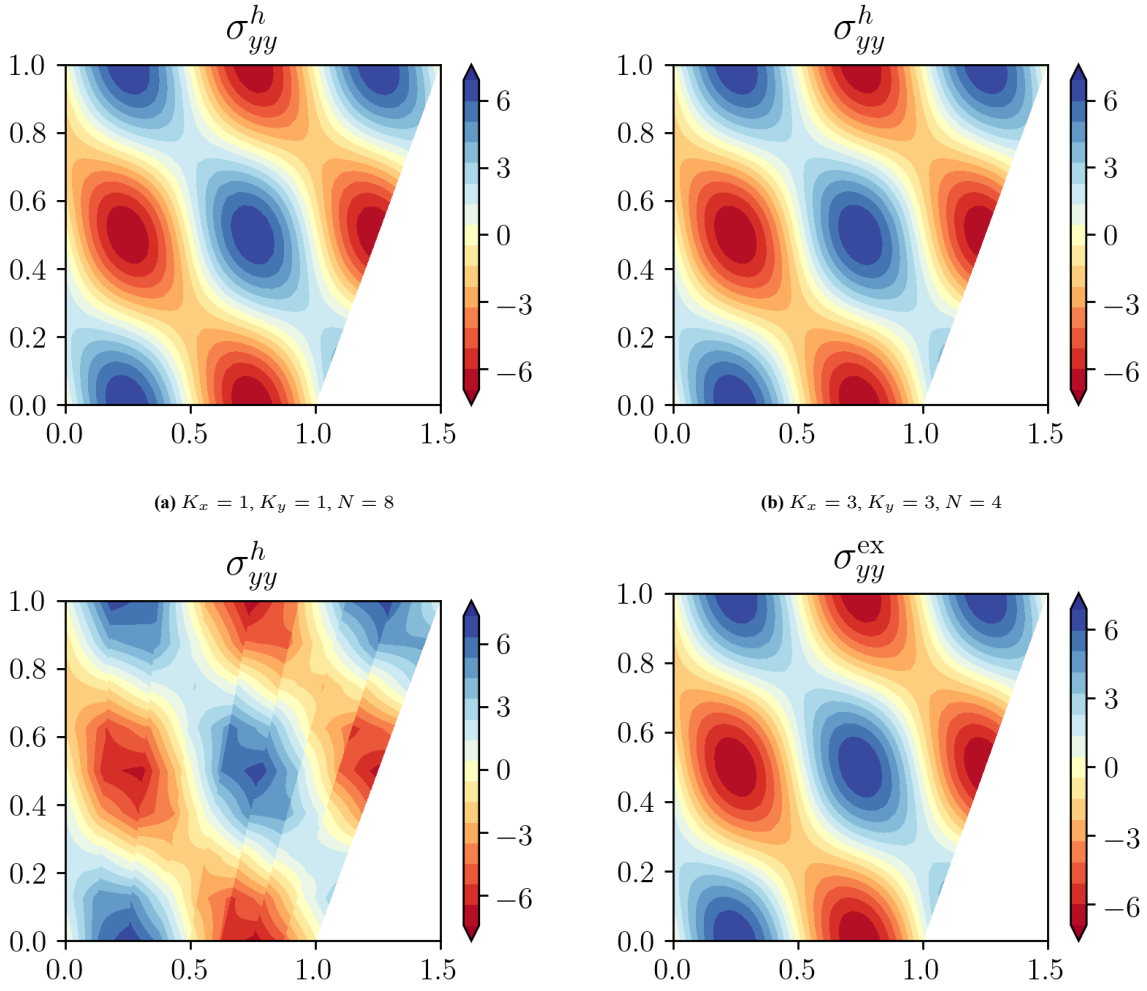

(a) $K_x = 1, K_y = 1, N = 8$

(b) $K_x = 3, K_y = 3, N = 4$

(c) $K_x = 8, K_y = 8, N = 1$

(d) Exact solution

Figure 6.5: Results for σ^h_{yy} in the physical domain

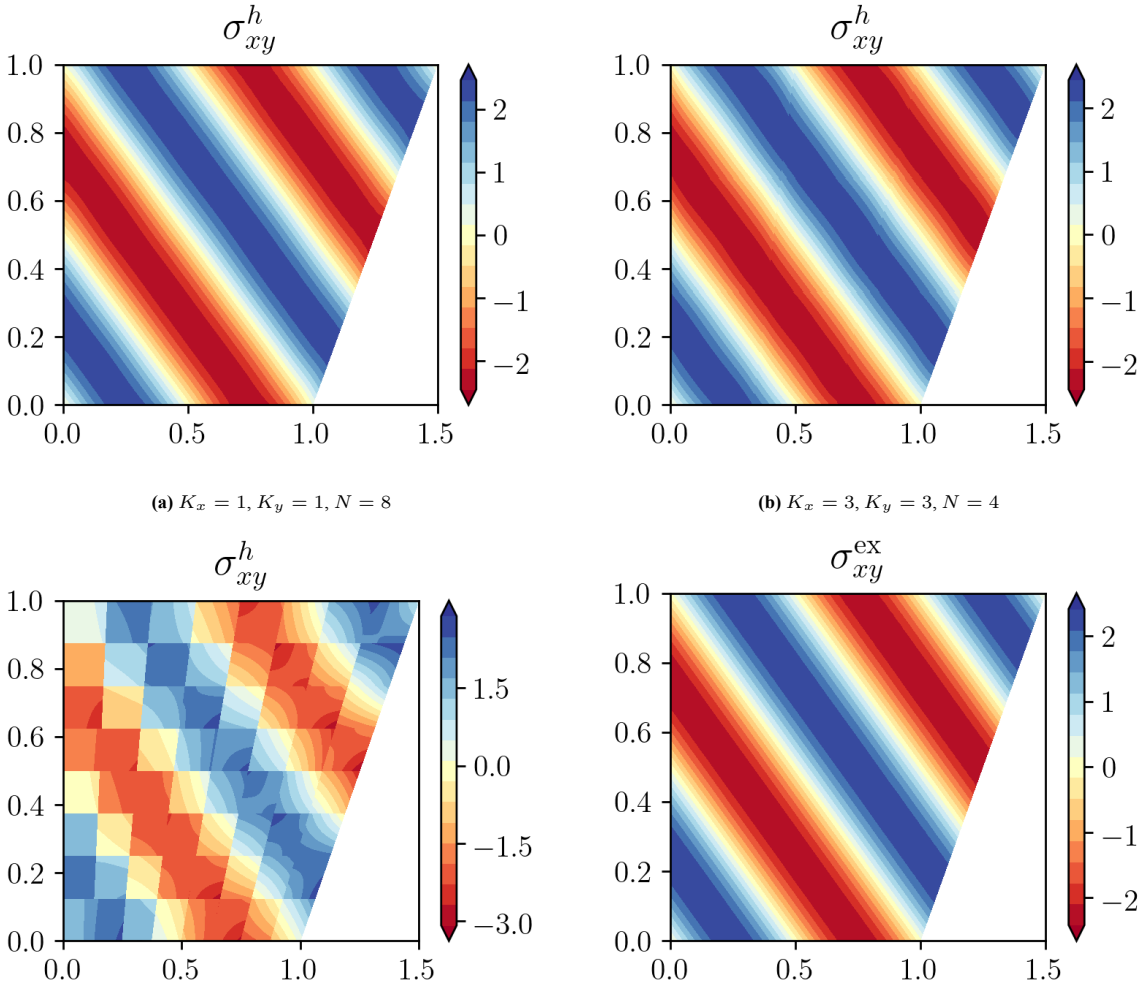

(a) $K_x = 1, K_y = 1, N = 8$

(b) $K_x = 3, K_y = 3, N = 4$

(c) $K_x = 8, K_y = 8, N = 1$

(d) Exact solution

Figure 6.6: Results for σ^h_{xy} in the physical domain

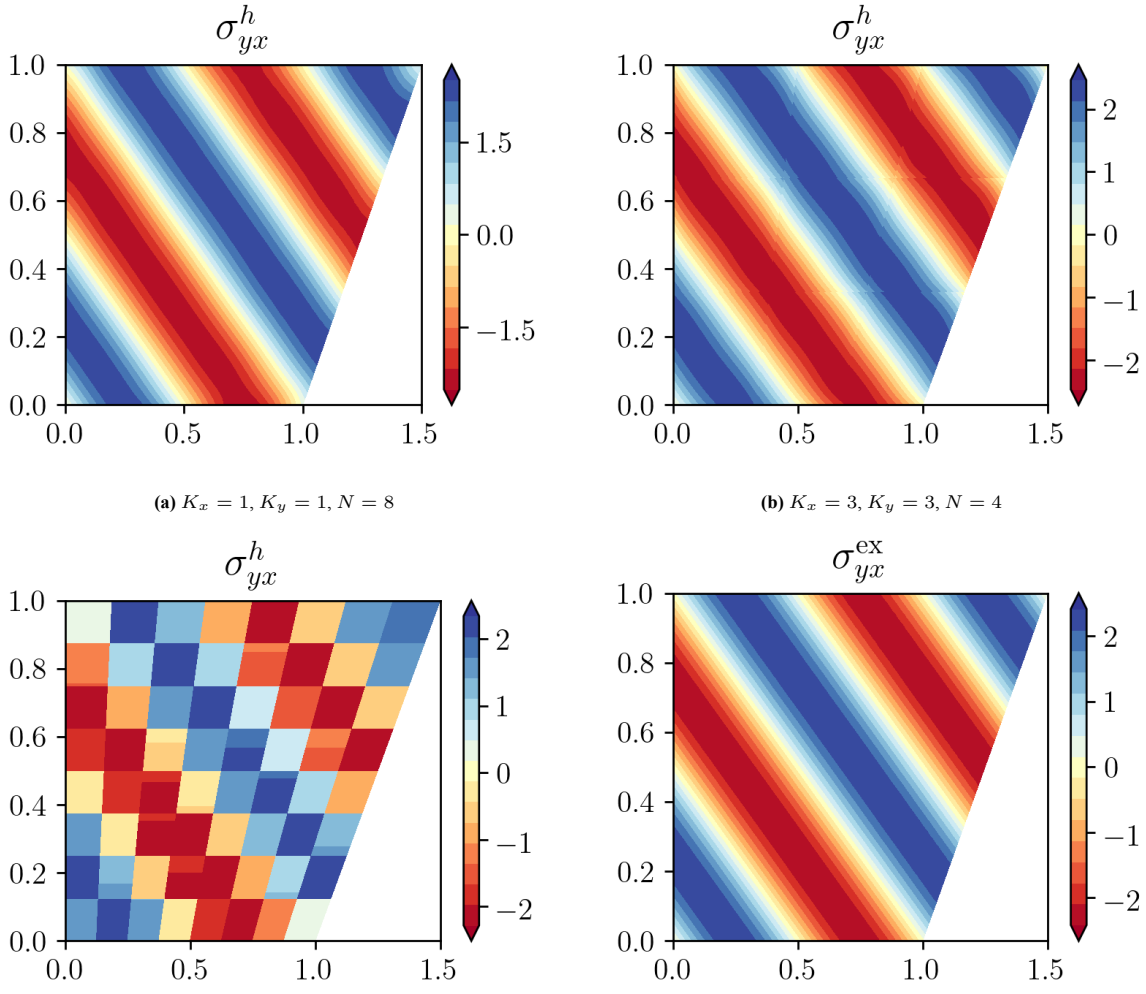

(a) $K_x = 1, K_y = 1, N = 8$

(b) $K_x = 3, K_y = 3, N = 4$

(c) $K_x = 8, K_y = 8, N = 1$

(d) Exact solution

Figure 6.7: Results for σ^h_{yx} in the physical domain

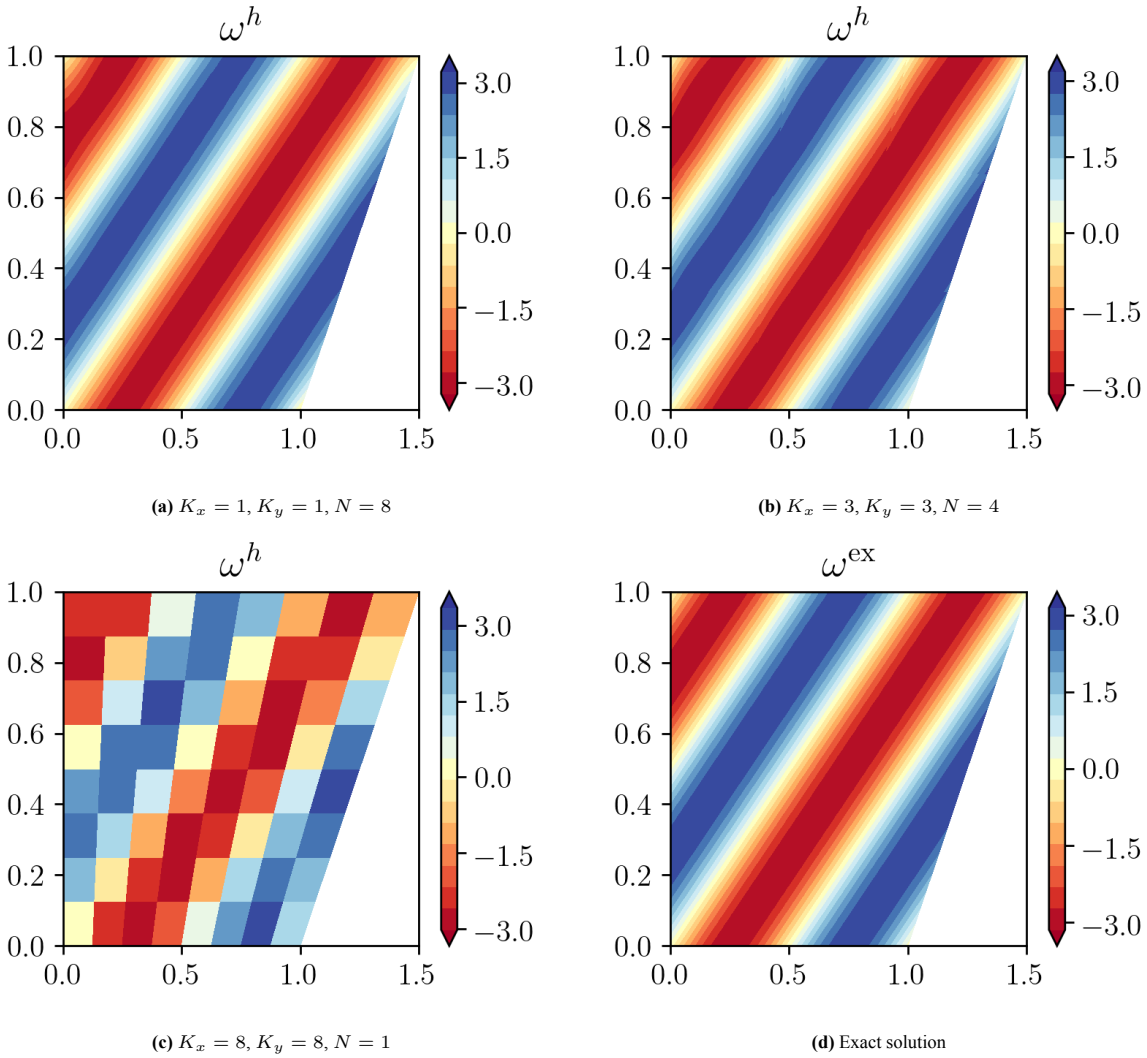

(a) $K_x = 1, K_y = 1, N = 8$

(b) $K_x = 3, K_y = 3, N = 4$

(c) $K_x = 8, K_y = 8, N = 1$

(d) Exact solution

Figure 6.8: Results for ω^h in the physical domain

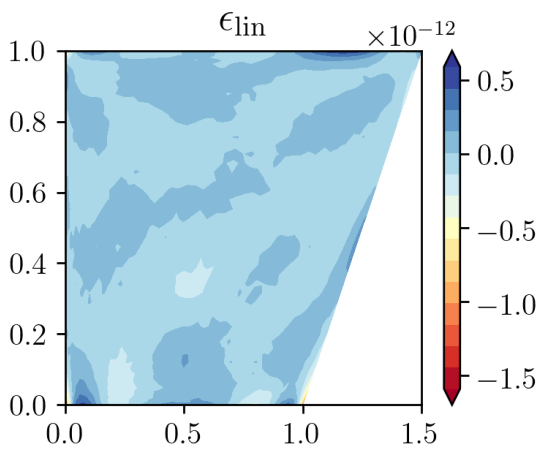

(a) Error in conservation of linear momentum for $K_x = 1$, $K_y = 1$, $N = 8$

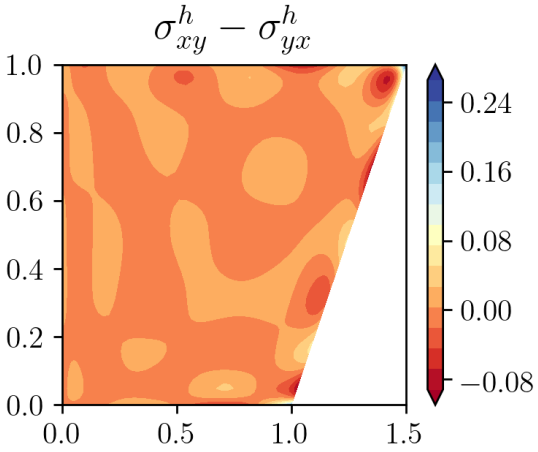

(b) Error in symmetry of stress tensor for $K_x = 1$, $K_y = 1$, $N = 8$

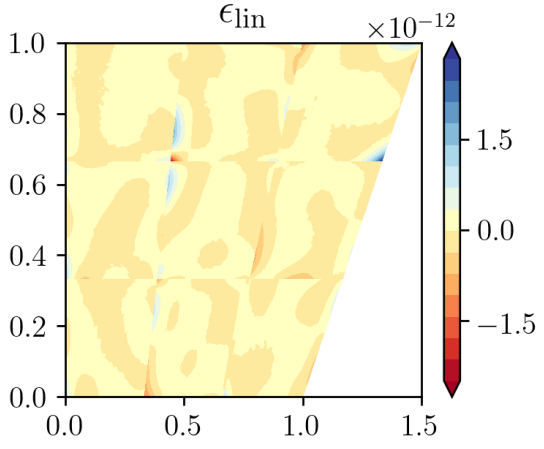

(c) Error in conservation of linear momentum for $K_x = 3$, $K_y = 3$, $N = 4$

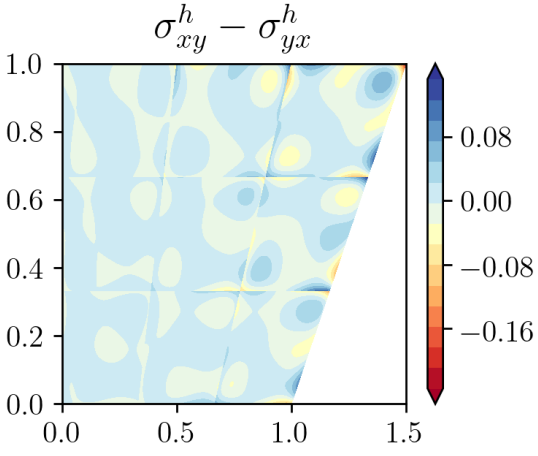

(d) Error in symmetry of stress tensor for $K_x = 3$, $K_y = 3$, $N = 4$

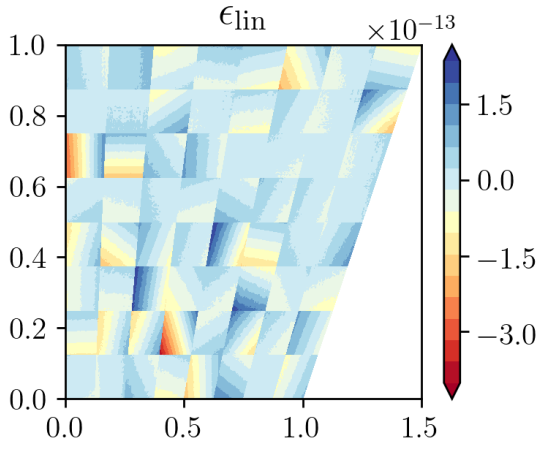

(e) Error in conservation of linear momentum for $K_x = 8$, $K_y = 8$, $N = 1$

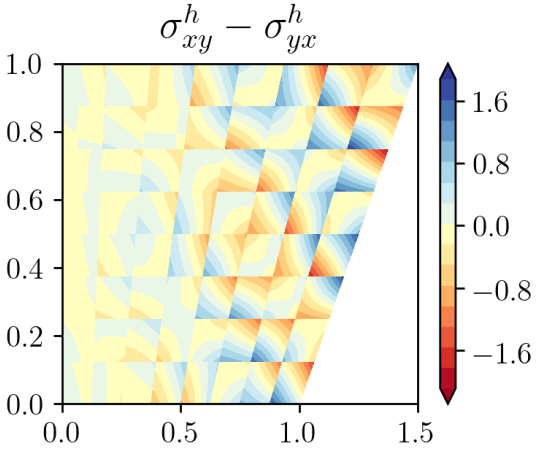

(f) Error in symmetry of stress tensor for $K_x = 8$, $K_y = 8$, $N = 1$

Figure 6.9: Results for errors in conservation of linear momentum and angular momentum

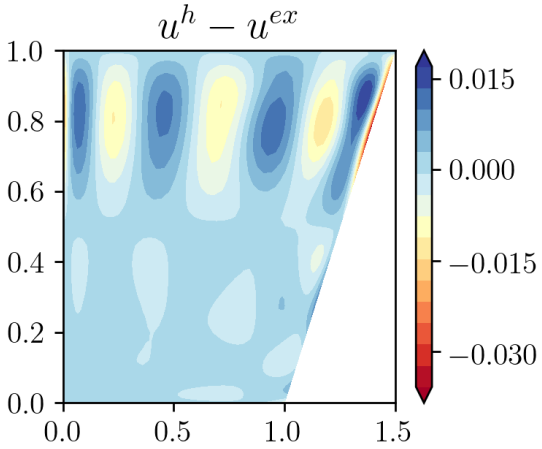

(a) $u_x^h - u_x^{ex}$ for $K_x = 1, K_y = 1, N = 8$

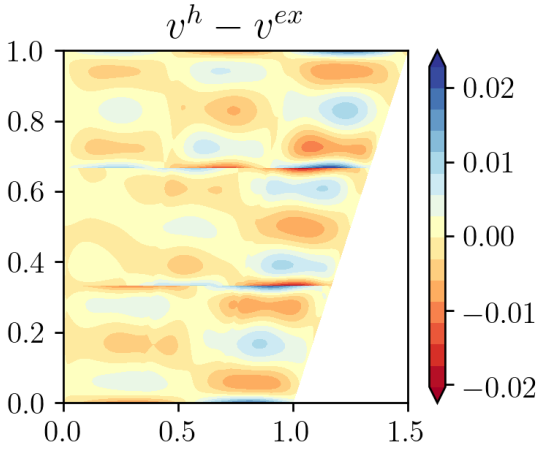

(b) $u_y^h - u_y^{ex}$ for $K_x = 1, K_y = 1, N = 8$

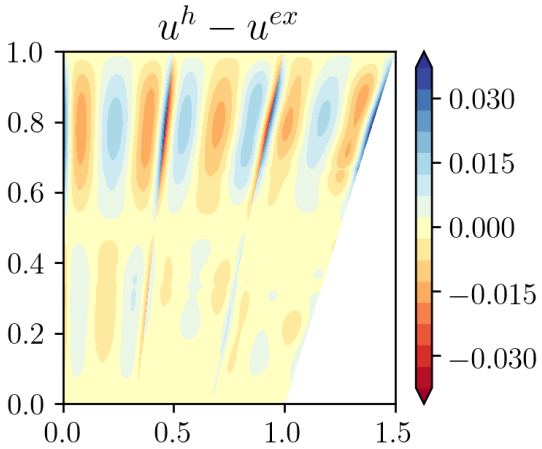

(c) $u_x^h - u_x^{ex}$ for $K_x = 3, K_y = 3, N = 4$

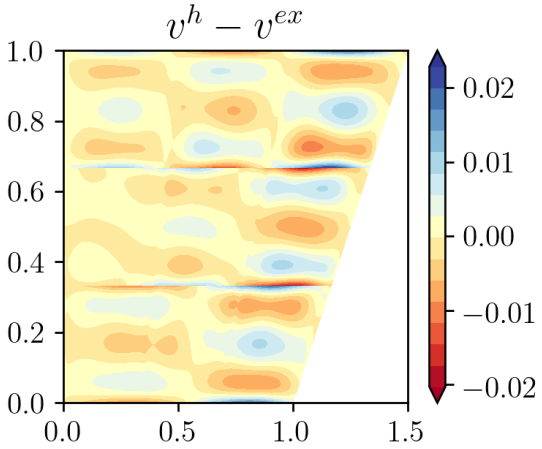

(d) $u_y^h - u_y^{ex}$ for $K_x = 3, K_y = 3, N = 4$

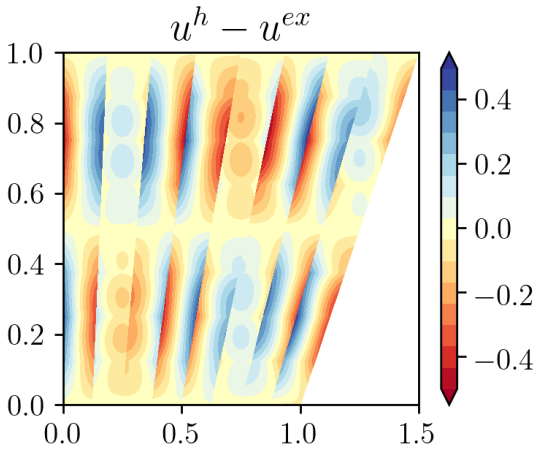

(e) $u_x^h - u_x^{ex}$ for $K_x = 8, K_y = 8, N = 1$

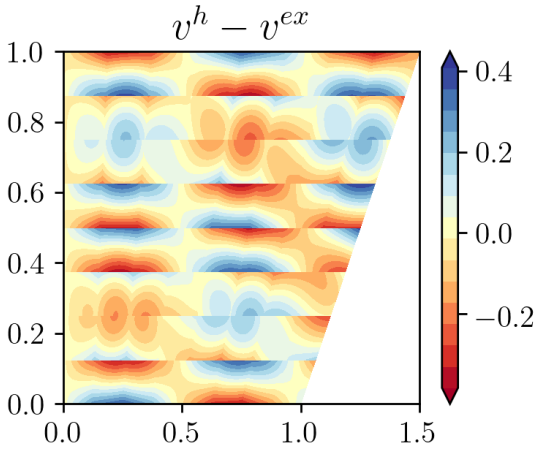

(f) $u_y^h - u_y^{ex}$ for $K_x = 8, K_y = 8, N = 1$

Figure 6.10: Results for errors in u_x^h and u_y^h from the exact solutions

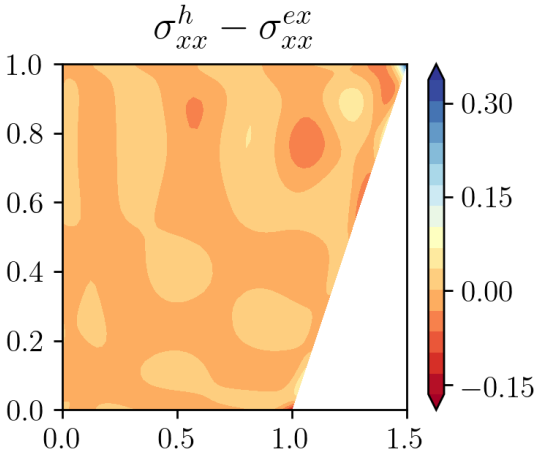

(a) $\sigma^h_{xx} - \sigma^{ex}_{xx}$ for $K_x = 1, K_y = 1, N = 8$

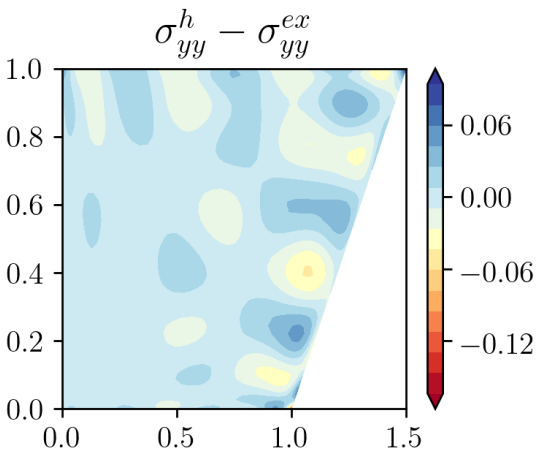

(b) $\sigma^h_{yy} - \sigma^{ex}_{yy}$ for $K_x = 1, K_y = 1, N = 8$

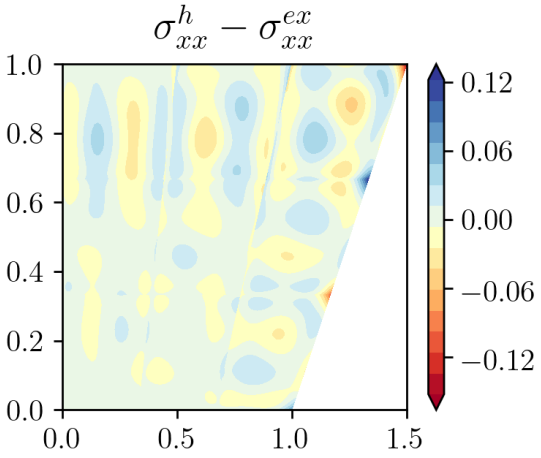

(c) $\sigma^h_{xx} - \sigma^{ex}_{xx}$ for $K_x = 3, K_y = 3, N = 4$

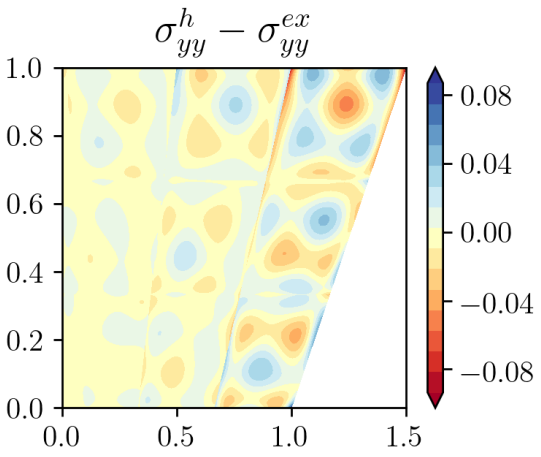

(d) $\sigma^h_{yy} - \sigma^{ex}_{yy}$ for $K_x = 3, K_y = 3, N = 4$

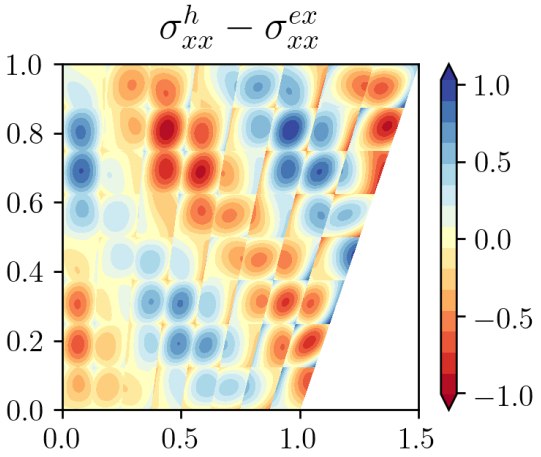

(e) $\sigma^h_{xx} - \sigma^{ex}_{xx}$ for $K_x = 8, K_y = 8, N = 1$

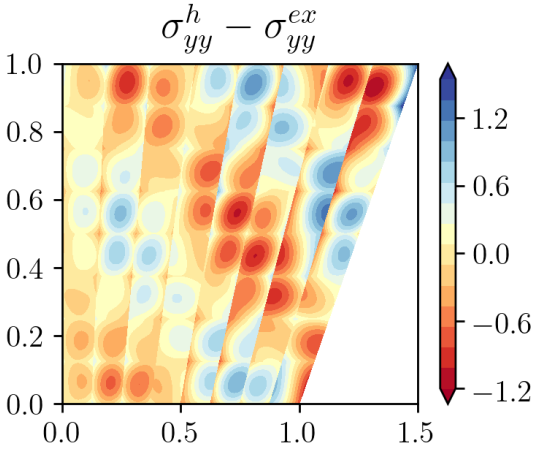

(f) $\sigma^h_{yy} - \sigma^{ex}_{yy}$ for $K_x = 8, K_y = 8, N = 1$

Figure 6.11: Results for errors in σ^h_{xx} and σ^h_{yy} from the exact solutions

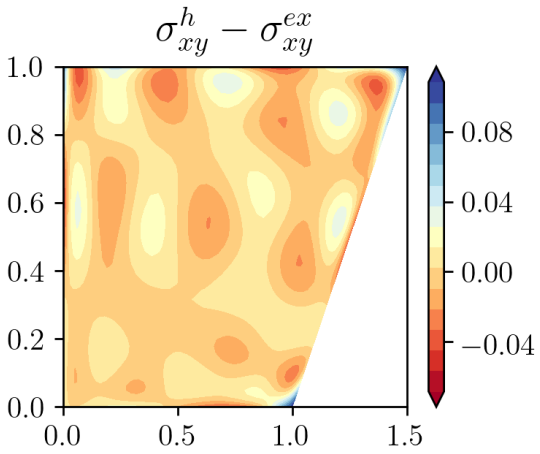

(a) $\sigma^h_{xy} - \sigma^{ex}_{xy}$ for $K_x = 1, K_y = 1, N = 8$

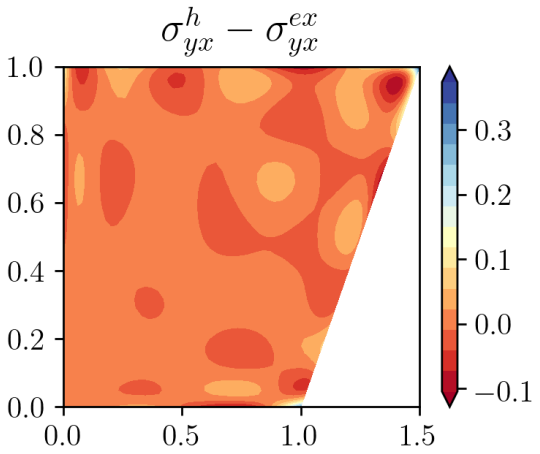

(b) $\sigma^h_{yx} - \sigma^{ex}_{yx}$ for $K_x = 1, K_y = 1, N = 8$

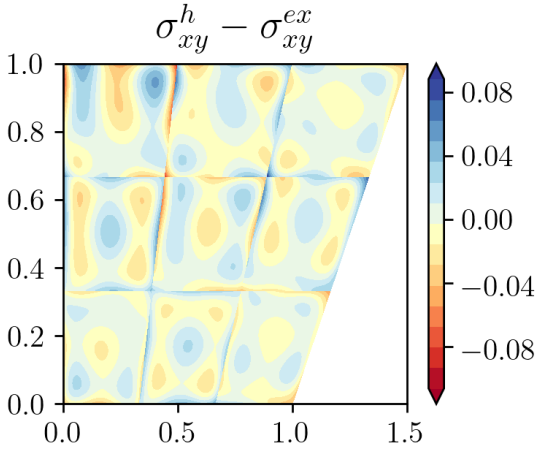

(c) $\sigma^h_{xy} - \sigma^{ex}_{xy}$ for $K_x = 3, K_y = 3, N = 4$

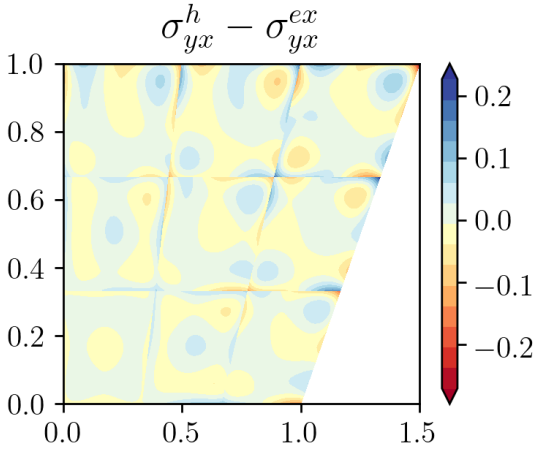

(d) $\sigma^h_{yx} - \sigma^{ex}_{yx}$ for $K_x = 3, K_y = 3, N = 4$

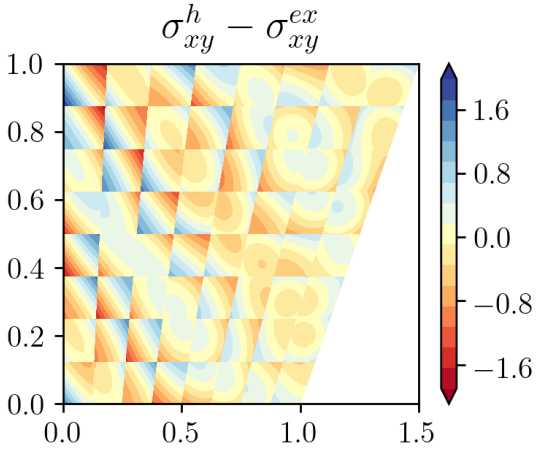

(e) $\sigma^h_{xy} - \sigma^{ex}_{xy}$ for $K_x = 8, K_y = 8, N = 1$

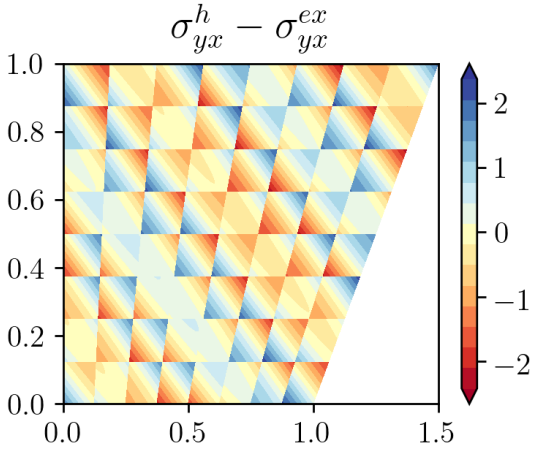

(f) $\sigma^h_{yx} - \sigma^{ex}_{yx}$ for $K_x = 8, K_y = 8, N = 1$

Figure 6.12: Results for errors in σ^h_{xy} and σ^h_{yx} from the exact solutions

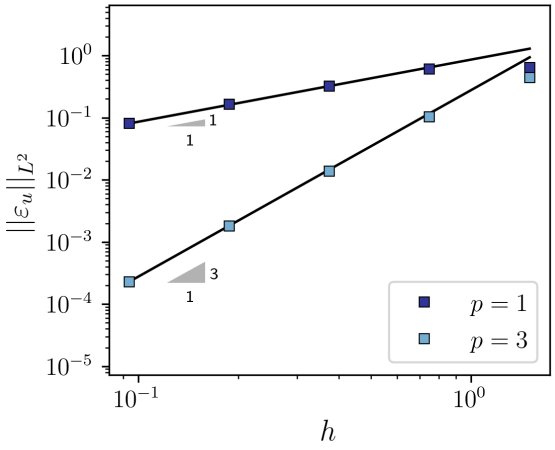

(a) Convergence with mesh width of L^2 error for u^h

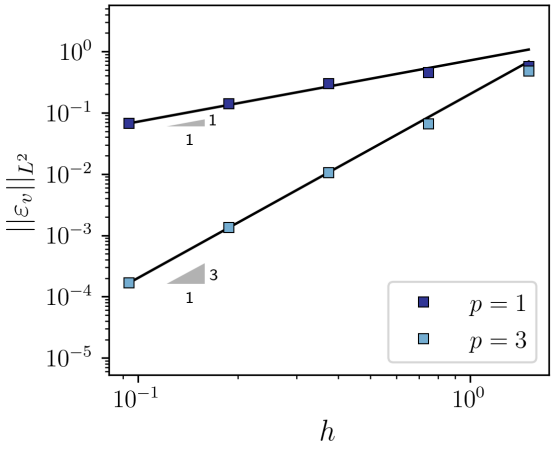

(b) Convergence with mesh width of L^2 error for v^h

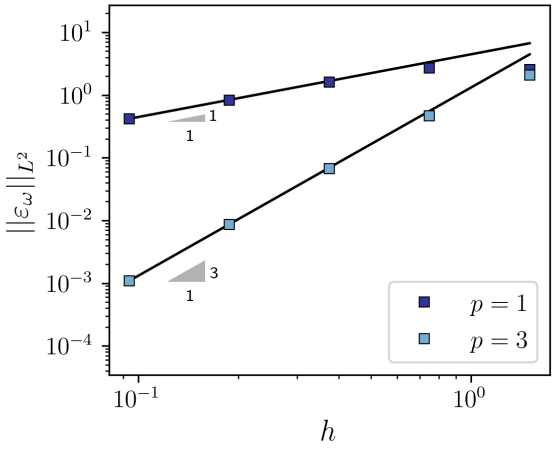

(c) Convergence with mesh width of L^2 error for ω^h

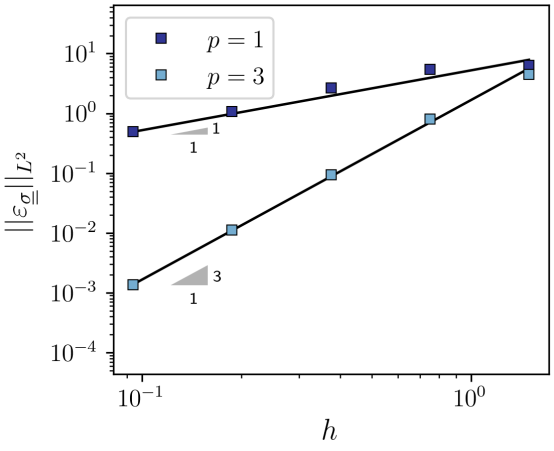

(d) Convergence with mesh width of L^2 error for $\underline{\underline{\boldsymbol{\sigma}}}^h$

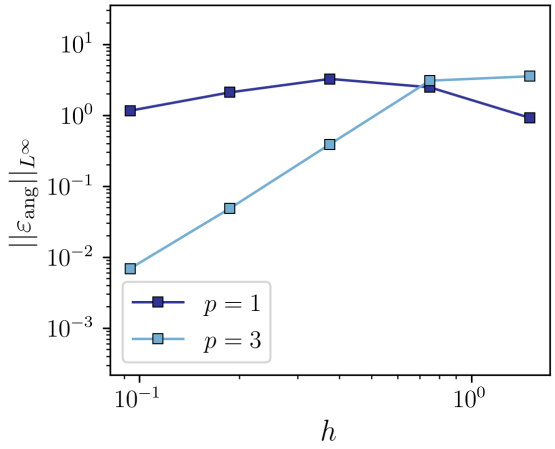

(e) Convergence with mesh width of L^∞ error for conservation of angular momentum

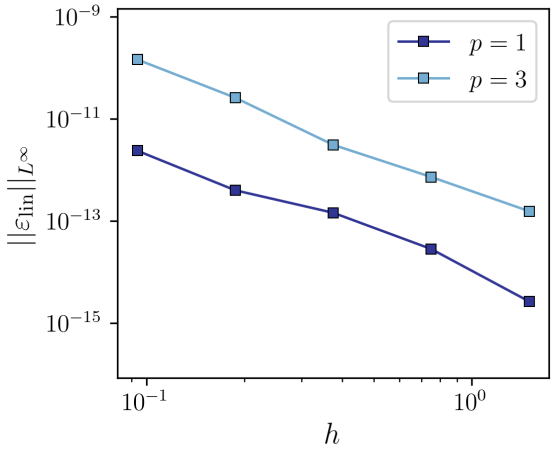

(f) Convergence with mesh width of L^∞ error for conservation of linear momentum

Figure 6.13: Results from the h-convergence study

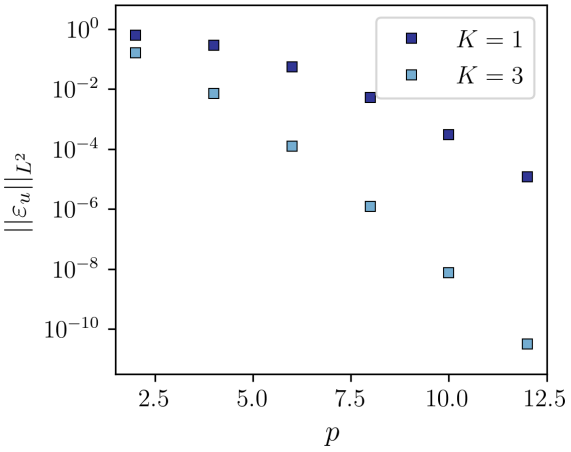

(a) L^2 error for u^h

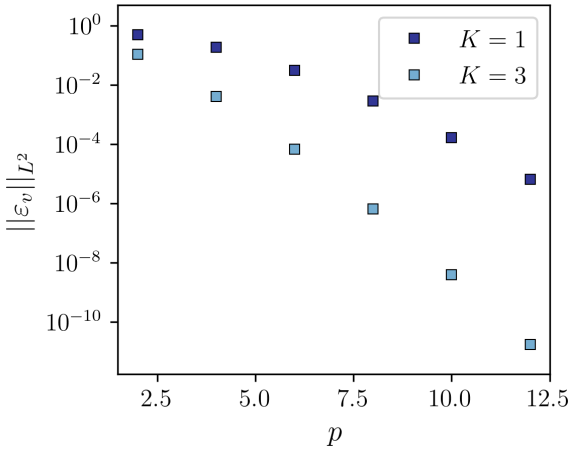

(b) L^2 error for v^h

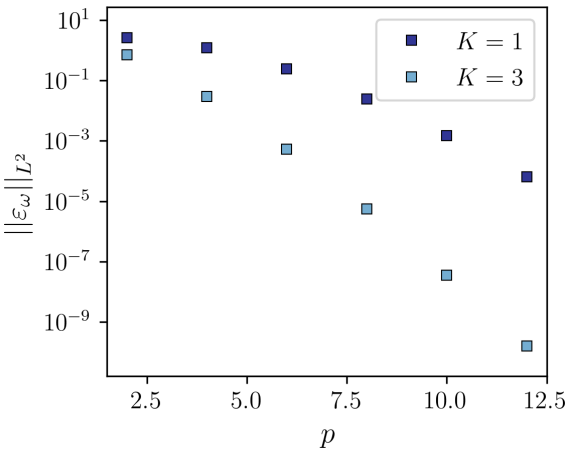

(c) L^2 error for ω^h

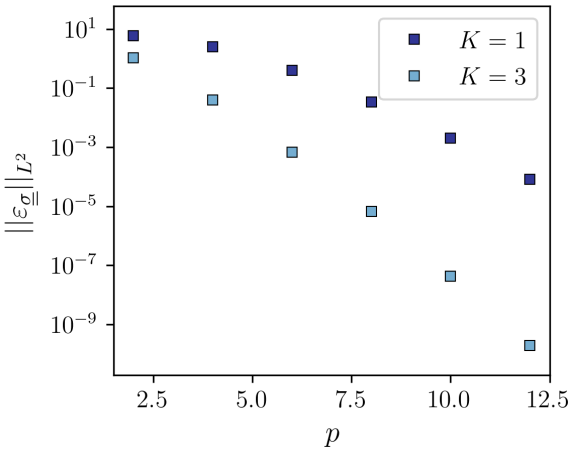

(d) L^2 error for $\underline{\underline{\boldsymbol{\sigma}}}^h$

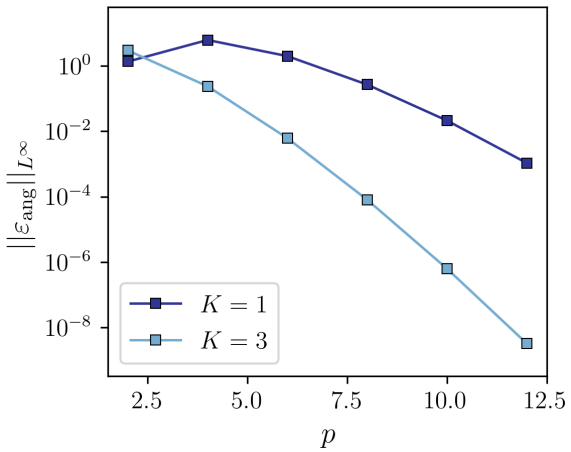

(e) L^∞ error in conservation of angular momentum

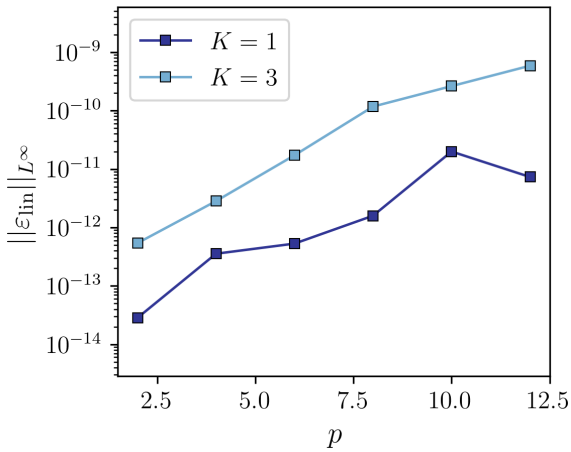

(f) L^∞ error in conservation of linear momentum

Figure 6.14: Results from the polynomial convergence study

7

Dual Lagrangian formulation

With the current formulation not helping conserve angular momentum in a strong sense, an alternative formulation was devised where the transformed shear stresses would have more degrees of freedom per element than the transformed normal stresses. In this way, the higher resolution of the shear stresses should play a bigger role in the equation for equating the Cauchy shear stresses. This will hopefully produce a formulation that conserves angular momentum within the element up to machine precision.

7.1. Problem formulation

With the goal of having a higher resolution for the shear components, the formulation was changed to prescribe the tangential displacements and the normal stress components at the boundaries. This enables the shear stress components to be on the primal mesh, resulting in a higher resolution. This is also why this formulation can be seen as dual to the one written in Chapter 6.

This dual theoretical formulation can be written as

$$\mathcal{L}\Big(\underline{\underline{\boldsymbol{\sigma}}}, \mathbf{u}, \boldsymbol{\omega}, \underline{\underline{\mathbf{C}}}\Big) = \begin{array}{l} \int_{\hat{\Omega}} \boldsymbol{\omega}\Big(\sigma_{\xi y}\frac{\partial \eta}{\partial y} - \sigma_{\eta y}\frac{\partial \xi}{\partial y} - \sigma_{\eta x}\frac{\partial \xi}{\partial x} + \sigma_{\xi x}\frac{\partial \eta}{\partial x}\Big)\mathrm{d}\hat{\Omega} \\ + \int_{\hat{\Omega}} \Big(\big(-\frac{\partial u}{\partial \xi}\sigma_{\xi x} + u\frac{\partial \sigma_{\eta x}}{\partial \eta} + v\frac{\partial \sigma_{\xi y}}{\partial \xi} - \frac{\partial v}{\partial \eta}\sigma_{\eta y}\big)\frac{1}{\det \mathcal{J}} + u\, f_x + v\, f_y\Big)\mathrm{d}\hat{\Omega} \\ + \int_{\hat{\Omega}} \Big(\frac{1}{2}\underline{\underline{\boldsymbol{\sigma}}}^T\big(\mathbf{F}^T\underline{\underline{\mathbf{C}}}\mathbf{F}\big)\underline{\underline{\boldsymbol{\sigma}}}\Big)\mathrm{d}\hat{\Omega} \\ - \oint_{\partial\hat{\Omega}} \big(u_P\sigma_{\eta x}n_\eta + v_P\sigma_{\xi y}n_\xi\big)\frac{1}{\det \mathcal{J}}\mathrm{d}\Gamma \\ + \oint_{\partial\hat{\Omega}} \big(u(\sigma_{\xi x})_P n_\xi + v(\sigma_{\eta y})_P n_\eta\big)\frac{1}{\det \mathcal{J}}\mathrm{d}\Gamma \end{array} \tag{7.1}$$

where $\mathbf{F}$ denotes the transformation tensor for the components of the Cauchy stress into the reference stresses as mentioned previously. Thus,

$$\begin{bmatrix} \sigma_{xx} \\ \sigma_{yx} \\ \sigma_{xy} \\ \sigma_{yy} \end{bmatrix} = \mathbf{F}\begin{bmatrix} \sigma_{\xi x} \\ \sigma_{\eta x} \\ \sigma_{\xi y} \\ \sigma_{\eta y} \end{bmatrix} = \frac{1}{\det \mathcal{J}}\begin{bmatrix} \frac{\partial x}{\partial \xi} & \frac{\partial x}{\partial \eta} & 0 & 0 \\ \frac{\partial y}{\partial \xi} & \frac{\partial y}{\partial \eta} & 0 & 0 \\ 0 & 0 & \frac{\partial x}{\partial \xi} & \frac{\partial x}{\partial \eta} \\ 0 & 0 & \frac{\partial y}{\partial \xi} & \frac{\partial y}{\partial \eta} \end{bmatrix}\begin{bmatrix} \sigma_{\xi x} \\ \sigma_{\eta x} \\ \sigma_{\xi y} \\ \sigma_{\eta y} \end{bmatrix}$$

.

7.1.1. Constitutional Law

On taking the variational derivative of the functional with respect to $\underline{\underline{\boldsymbol{\sigma}}}$ and equating it to zero, the functional reduces to

$$\begin{array}{l} \int_{\hat{\Omega}} \Big(\boldsymbol{\omega}\Big(\widetilde{\sigma_{\xi y}}\frac{\partial \eta}{\partial y} - \widetilde{\sigma_{\eta y}}\frac{\partial \xi}{\partial y} - \widetilde{\sigma_{\eta x}}\frac{\partial \xi}{\partial x} + \widetilde{\sigma_{\xi x}}\frac{\partial \eta}{\partial x}\Big)\mathrm{d}\hat{\Omega} \\ + \int_{\hat{\Omega}} \Big(\big(-\frac{\partial u}{\partial \xi}\widetilde{\sigma_{\xi x}} + u\frac{\partial \widetilde{\sigma_{\eta x}}}{\partial \eta} + v\frac{\partial \widetilde{\sigma_{\xi y}}}{\partial \xi} - \frac{\partial v}{\partial \eta}\widetilde{\sigma_{\eta y}}\big)\frac{1}{\det \mathcal{J}}\Big)\mathrm{d}\hat{\Omega} \quad = B_\sigma. \\ + \int_{\hat{\Omega}} \underline{\underline{\widetilde{\boldsymbol{\sigma}}}}^T(\mathbf{F}^T\underline{\underline{\mathbf{C}}}\mathbf{F})\underline{\underline{\boldsymbol{\sigma}}}\Big)\mathrm{d}\hat{\Omega} \end{array} \tag{7.2}$$

This results in the constitutive laws as derived in Section 6.3.1, which can be verified by using integration by parts as,

$$\begin{aligned}&\int_{\hat{\Omega}} \Big(\boldsymbol{\omega}(\det \mathcal{J})\Big(\widetilde{\sigma_{\xi y}}\frac{\partial \eta}{\partial y} - \widetilde{\sigma_{\eta y}}\frac{\partial \xi}{\partial y} - \widetilde{\sigma_{\eta x}}\frac{\partial \xi}{\partial x} + \widetilde{\sigma_{\xi x}}\frac{\partial \eta}{\partial x}\Big)\mathrm{d}\hat{\Omega}\\ &+ \int_{\hat{\Omega}} \Big(\big(-\tfrac{\partial u}{\partial \xi}\widetilde{\sigma_{\xi x}} - \tfrac{\partial u}{\partial \eta}\widetilde{\sigma_{\eta x}} - \tfrac{\partial v}{\partial \xi}\widetilde{\sigma_{\xi y}} - \tfrac{\partial v}{\partial \eta}\widetilde{\sigma_{\eta y}}\big)\Big)\mathrm{d}\hat{\Omega} \qquad = 0,\\ &+ \int_{\hat{\Omega}} \underline{\underline{\widetilde{\boldsymbol{\sigma}}}}^T\big((\det \mathcal{J})\mathbf{F}^T\underline{\underline{\mathbf{C}}}\mathbf{F}\big)\underline{\underline{\boldsymbol{\sigma}}}\Big)\mathrm{d}\hat{\Omega}\end{aligned}$$

Important consideration is that

$$\mathcal{B}_\sigma = \oint_{\partial\hat{\Omega}} \big(u_P\widetilde{\sigma_{\eta x}}n_\eta + v_P\widetilde{\sigma_{\xi y}}n_\xi\big)\mathrm{d}\Gamma, \tag{7.3}$$

which makes sure that the correct constitutive relation is solved, using the values of the displacement at the tangential boundaries.

As mentioned before, an important distinction from the formulation in chapter 6 is that in this formulation, the tangential displacement is prescribed, while in chapter 6 the normal displacements are prescribed.

7.1.2. Conservation of linear momentum

On taking the variational derivative of the functional with respect to **u** and equating it to zero, the functional reduces to

$$\int_{\hat{\Omega}} \Big(\big(-\frac{\partial \widetilde{u}}{\partial \xi}\sigma_{\xi x} + \widetilde{u}\frac{\partial \sigma_{\eta x}}{\partial \eta} + \widetilde{v}\frac{\partial \sigma_{\xi y}}{\partial \xi} - \frac{\partial \widetilde{v}}{\partial \eta}\sigma_{\eta y}\big)\frac{1}{\det \mathcal{J}} + \widetilde{u}\,f_x + \widetilde{v}\,f_y\Big)\mathrm{d}\hat{\Omega} = -B_{\mathbf{u}}, \tag{7.4}$$

where

$$B_{\mathbf{u}} = \oint_{\partial\hat{\Omega}} \big(\widetilde{u}(\sigma_{\xi x})_P n_\xi + \widetilde{v}(\sigma_{\eta y})_P n_\eta\big)\mathrm{d}\Gamma. \tag{7.5}$$

With an arbitrary $\widetilde{u}$ and $\widetilde{v}$ and assuming this holds for any arbitrary domain, this equation is the same as the one derived for the conservation of linear momentum in subsection 6.3.2. It can be verified by including the boundary terms using integration by parts. This means that the linear momentum will be conserved point-wise.

Again there is a distinction made between the boundary conditions for this formulation from the one in Chapter 6, with the normal stresses being prescribed instead of the shear stresses in Chapter 6.

7.1.3. Conservation of angular momentum

On taking the variational derivative of the functional with respect to $\boldsymbol{\omega}$ and equating it to zero, the functional reduces to

$$\int_{\hat{\Omega}} \widetilde{\boldsymbol{\omega}}\Big(\sigma_{\xi y}\frac{\partial \eta}{\partial y} - \sigma_{\eta y}\frac{\partial \xi}{\partial y} - \sigma_{\eta x}\frac{\partial \xi}{\partial x} + \sigma_{\xi x}\frac{\partial \eta}{\partial x}\Big)\mathrm{d}\hat{\Omega} = 0. \tag{7.6}$$

With an arbitrary $\widetilde{\boldsymbol{\omega}}$ and assuming this holds for any arbitrary domain, means that the symmetry of the Cauchy stress tensor is enforced. This means that the angular momentum is conserved.

This is the same equation that is solved for the symmetry of the Cauchy tensor in Chapter 6. However, the key difference is that in this formulation the shear stress is not used to ensure continuity of components of displacement between elements, as was in Chapter 6. The normal stresses are tasked with that job here, meaning that the shear stresses can be better resolved within the element. The intention is that this will conserve angular momentum exactly in this formulation, compared to the previous one.

7.2. Spectral bases

In this section, the expansion of the quantities in the reference domain are shown. The overhead bar indicates that they are reconstructed (using the spectral bases functions).

$$\overline{\sigma_{\xi x}} = \sum_{i=1}^{N}\sum_{j=1}^{N}(\sigma_{\xi x})_{ij}\ h'_i(\xi)\ e_j(\eta)\ ,$$
$$\overline{\sigma_{\eta x}} = \sum_{i=1}^{N+1}\sum_{j=1}^{N+1}(\sigma_{\eta x})_{ij}\ e'_i(\xi)\ h_j(\eta)\ ,$$
$$\overline{\sigma_{\xi y}} = \sum_{i=1}^{N+1}\sum_{j=1}^{N+1}(\sigma_{\xi y})_{ij}\ h_i(\xi)\ e'_j(\eta)\ ,$$
$$\overline{\sigma_{\eta y}} = \sum_{i=1}^{N}\sum_{j=1}^{N}(\sigma_{\eta y})_{ij}\ e_i(\xi)\ h'_j(\eta)\ .$$

Do note that these expansions are dual to the ones used in Chapter 6.

Using these bases, if we write the conservation of linear momentum in the reference domain, we get

$$\frac{\partial\overline{\sigma_{\xi x}}}{\partial\xi} + \frac{\partial\overline{\sigma_{\eta x}}}{\partial\eta} = \sum_{i=1}^{N+1}\sum_{j=1}^{N}\Big((\sigma_{\xi x})_{i,j} - (\sigma_{\xi x})_{i-1,j}\Big)\ e'_i(\xi)\ e_j(\eta)\ + \sum_{i=1}^{N+1}\sum_{j=1}^{N}\Big((\sigma_{\eta x})_{i,j+1} - (\sigma_{\eta x})_{i,j}\Big)\ e'_i(\xi)\ e_j(\eta)\ ,$$
$$\frac{\partial\overline{\sigma_{\xi y}}}{\partial\xi} + \frac{\partial\overline{\sigma_{\eta y}}}{\partial\eta} = \sum_{i=1}^{N}\sum_{j=1}^{N+1}\Big((\sigma_{\xi y})_{i+1,j} - (\sigma_{\xi y})_{i,j}\Big)\ e_i(\xi)\ e'_j(\eta)\ + \sum_{i=1}^{N}\sum_{j=1}^{N+1}\Big((\sigma_{\eta y})_{i,j} - (\sigma_{\eta y})_{i,j-1}\Big)\ e_i(\xi)\ e'_j(\eta)\ ,$$

including the boundary conditions $(\sigma_{\xi x})_{i,0}$ and $(\sigma_{\xi x})_{i,N+1}$ for the equation along x, and $(\sigma_{\eta y})_{0,j}$ and $(\sigma_{\eta y})_{N+1,j}$ for the equation along y. Thus, these equations ensure that the derivatives of the stress components in the ξ- and η- can be represented by the same bases.

The components of displacement act as the Lagrange multipliers for the conservation of linear momentum, as mentioned before. To make these equations completely topological, the bases for the corresponding Lagrange multipliers are chosen to be the dual of the expansions listed above. Thus,

$$\overline{u_x} = \sum_{i=1}^{N+1}\sum_{j=1}^{N}(u_x)_{ij}\ h_i(\xi)\ h'_j(\eta)\ ,$$
$$\overline{u_y} = \sum_{i=1}^{N}\sum_{j=1}^{N+1}(u_y)_{ij}\ h'_i(\xi)\ h_j(\eta)\ .$$

Again, we can observe that these expansions for the displacement are dual to the ones used in Chapter 6. The rotation is also expanded as

$$\overline{\omega} = \sum_{i=1}^{N}\sum_{j=1}^{N}(\omega)_{ij}\ h_i(\xi)\ h_j(\eta)\ .$$

to ensure that the rotation has the same number of degrees of freedom as $\sigma_{\eta x}$ and $\sigma_{\xi y}$, which also means that this representation is dual to the one seen in Chapter 6. Similar to Chapter 6, the stress components are converted into a dual of the spectral bases for ω and then the equation for the conservation of angular momentum is written down.

With these spectral bases, the system can be written to find the unknown degrees of freedom as

$$\begin{bmatrix} \mathbb{M}_\sigma & \mathbb{E}_\sigma^T & \mathbb{R}^T \\ \mathbb{E}_\sigma & 0 & 0 \\ \mathbb{R}_\sigma & 0 & 0 \end{bmatrix} \begin{bmatrix} \boldsymbol{\sigma}^h \\ \mathbf{u}^h \\ \boldsymbol{\omega}^h \end{bmatrix} = \begin{bmatrix} -\mathbf{g}_\sigma^h \\ -\mathbf{f}^h - \mathbf{g}_u^h \\ \mathbf{0} \end{bmatrix}. \tag{7.7}$$

In this representation, let

$$\boldsymbol{\sigma}^h = \begin{bmatrix} \sigma_{\xi x}^h & \sigma_{\eta x}^h & \sigma_{\xi y}^h & \sigma_{\eta y}^h \end{bmatrix}^T, \tag{7.8}$$

$$\mathbf{u}^h = \begin{bmatrix} u^h & v^h \end{bmatrix}. \tag{7.9}$$

Making it easier to arrange the unknowns for the tensor and vector quantities. In addition, it should be easier for the construction of the matrices.

The other terms in this system will be analysed in the following sections.

7.3. Incidence matrix

The conservation of linear momentum is designed to be topological in the computational (reference) domain. With this, the matrix that needs to be made should not involve any terms other than ± 1 or 0, as is evident from how the divergence of stress is written down using spectral bases, mentioned in Section 7.2.

With the stress degree of freedoms arranged as (7.8), the matrix can be decomposed into two parts $(\mathbb{E}_\sigma)_x$ and $(\mathbb{E}_\sigma)_y$, written as

$$\mathbb{E}_\sigma = \begin{bmatrix} (\mathbb{E}_\sigma)_x & 0 \\ 0 & (\mathbb{E}_\sigma)_y \end{bmatrix}.$$

This decomposes the conservation of linear momentum into two directions, $x-$ and $y-$. $\widetilde{u}^h$ and $\widetilde{v}^h$ act as the Lagrange multipliers to enforce the conservation of linear momentum in these directions respectively. Thus, $(\mathbb{E}_\sigma)_x$ is a linear operator on $[\sigma_{\xi x}^h \;\; \sigma_{\eta x}^h]$, while $(\mathbb{E}_\sigma)_y$ is a linear operator on $[\sigma_{\xi y}^h \;\; \sigma_{\eta y}^h]$.

Following the x-lexicographic arrangement for these degrees of freedom, the components of $\mathbb{E}_\sigma$ (for $N = 2$) are given below.

$$(\mathbb{E}_\sigma)_x = \begin{bmatrix} -1 & 0 & 0 & 0 & 1 & 0 & 0 & -1 & 0 & 0 & 0 & 0 & 0 \\ 1 & -1 & 0 & 0 & 0 & 1 & 0 & 0 & -1 & 0 & 0 & 0 & 0 \\ 0 & 1 & 0 & 0 & 0 & 0 & 1 & 0 & 0 & -1 & 0 & 0 & 0 \\ 0 & 0 & -1 & 0 & 0 & 0 & 0 & 1 & 0 & 0 & -1 & 0 & 0 \\ 0 & 0 & 1 & -1 & 0 & 0 & 0 & 0 & 1 & 0 & 0 & -1 & 0 \\ 0 & 0 & 0 & 1 & 0 & 0 & 0 & 0 & 0 & 1 & 0 & 0 & -1 \end{bmatrix}$$

$$(\mathbb{E}_\sigma)_y = \begin{bmatrix} 1 & -1 & 0 & 0 & 0 & 0 & 0 & 0 & 0 & -1 & 0 & 0 & 0 \\ 0 & 1 & -1 & 0 & 0 & 0 & 0 & 0 & 0 & 0 & -1 & 0 & 0 \\ 0 & 0 & 0 & 1 & -1 & 0 & 0 & 0 & 0 & 1 & 0 & -1 & 0 \\ 0 & 0 & 0 & 0 & 1 & -1 & 0 & 0 & 0 & 0 & 1 & 0 & -1 \\ 0 & 0 & 0 & 0 & 0 & 0 & 1 & -1 & 0 & 0 & 0 & 1 & 0 \\ 0 & 0 & 0 & 0 & 0 & 0 & 0 & 1 & -1 & 0 & 0 & 0 & 1 \end{bmatrix}$$

Note that the transpose of this matrix should give the matrix which will be used to calculate the gradient, which is used in the constitutive law. Also note that the parts for the two directions $x-$ and $y-$ are switched from the original formulation in this one.

7.4. Mass matrix

Similar to the previous formulation, here the mass matrix can be separated into 4 horizontal matrices, representing each of the constitutive equations.

$$\mathbb{M}_\sigma = \begin{bmatrix} \mathbb{M}_1 \\ \mathbb{M}_2 \\ \mathbb{M}_3 \\ \mathbb{M}_4 \end{bmatrix}$$

Let us look at how the different components are written down as

7.4.1. Constitutive relation 1

The matrices for this constitutive relation (with $\sigma_{\xi x}$ as the test function) can be written as

$$(\mathbb{M}_{11})_{ijkl} = \sum_{r=1}^{N_x}\sum_{s=1}^{N_x} C'_{11}\,(\xi_r,\eta_s)\,h'_i(\xi_r)\;e_j(\eta_s)\;h'_k(\xi_r)\;e_l(\eta_s)\,w_r\,w_s, \tag{7.10}$$

where w_r and w_s are the integration weights associated with the nodes at ξ_r and η_s using Gaussian quadrature, and N_x denotes the number of Gauss-Lobatto nodes used for quadrature.

Similarly,

$$(\mathbb{M}_{12})_{ijkl} = \sum_{r=1}^{N_x}\sum_{s=1}^{N_x} C'_{12}\,(\xi_r,\eta_s)\,e'_i(\xi_r)\;h_j(\eta_s)\;h'_k(\xi_r)\;e_l(\eta_s)\,w_r\,w_s, \tag{7.11}$$

$$(\mathbb{M}_{13})_{ijkl} = \sum_{r=1}^{N_x}\sum_{s=1}^{N_x} C'_{13}\,(\xi_r,\eta_s)\,h_i(\xi_r)\;e'_j(\eta_s)\;h'_k(\xi_r)\;e_l(\eta_s)\,w_r\,w_s, \tag{7.12}$$

$$(\mathbb{M}_{14})_{ijkl} = \sum_{r=1}^{N_x}\sum_{s=1}^{N_x} C'_{14}\,(\xi_r,\eta_s)\,e_i(\xi_r)\;h'_j(\eta_s)\;h'_k(\xi_r)\;e_l(\eta_s)\,w_r\,w_s, \tag{7.13}$$

Note that the coefficients C'_{11}, C'_{12}, C'_{13}, C'_{14} are the same ones used in the previous formulation, written in (6.7).

Once these matrices are formed $\mathbb{M}_1 = [\mathbb{M}_{11}\;\;\mathbb{M}_{12}\;\;\mathbb{M}_{13}\;\;\mathbb{M}_{14}]$

7.4.2. Constitutive relation 2

The matrices for this constitutive relation (with $\sigma_{\eta x}$ as the test function) can be written as

$$(\mathbb{M}_{21})_{ijkl} = \sum_{r=1}^{N_x}\sum_{s=1}^{N_x} C'_{21}\,(\xi_r,\eta_s)\,h'_i(\xi_r)\;e_j(\eta_s)\;e'_k(\xi_r)\;h_l(\eta_s)\,w_r\,w_s, \tag{7.14}$$

$$(\mathbb{M}_{22})_{ijkl} = \sum_{r=1}^{N_x}\sum_{s=1}^{N_x} C'_{22}\,(\xi_r,\eta_s)\,e'_i(\xi_r)\;h_j(\eta_s)\;e'_k(\xi_r)\;h_l(\eta_s)\,w_r\,w_s, \tag{7.15}$$

$$(\mathbb{M}_{23})_{ijkl} = \sum_{r=1}^{N_x}\sum_{s=1}^{N_x} C'_{23}\,(\xi_r,\eta_s)\,h_i(\xi_r)\;e'_j(\eta_s)\;e'_k(\xi_r)\;h_l(\eta_s)\,w_r\,w_s, \tag{7.16}$$

$$(\mathbb{M}_{24})_{ijkl} = \sum_{r=1}^{N_x}\sum_{s=1}^{N_x} C'_{24}\,(\xi_r,\eta_s)\,e_i(\xi_r)\;h'_j(\eta_s)\;e'_k(\xi_r)\;h_l(\eta_s)\,w_r\,w_s, \tag{7.17}$$

where the coefficients C'_{21}, C'_{22}, C'_{23}, C'_{24} are the same ones used in the previous formulation, written in (6.8).

Then we get $\mathbb{M}_2 = [\mathbb{M}_{21}\;\;\mathbb{M}_{22}\;\;\mathbb{M}_{23}\;\;\mathbb{M}_{24}]$

7.4.3. Constitutive relation 3

The third constitutive relation has $\widetilde{\sigma_{\xi y}}$ as the test function. The expressions are given below.

$$(\mathbb{M}_{31})_{ijkl} = \sum_{r=1}^{N_x}\sum_{s=1}^{N_x} C'_{31}\,(\xi_r,\eta_s)\,h'_i(\xi_r)\;e_j(\eta_s)\;h_k(\xi_r)\;e'_l(\eta_s)\,w_r\,w_s, \tag{7.18}$$

$$(\mathbb{M}_{32})_{ijkl} = \sum_{r=1}^{N_x}\sum_{s=1}^{N_x} C'_{32}\,(\xi_r,\eta_s)\,e'_i(\xi_r)\;h_j(\eta_s)\;h_k(\xi_r)\;e'_l(\eta_s)\,w_r\,w_s, \tag{7.19}$$

$$(\mathbb{M}_{33})_{ijkl} = \sum_{r=1}^{N_x}\sum_{s=1}^{N_x} C'_{33}\,(\xi_r,\eta_s)\,h_i(\xi_r)\;e'_j(\eta_s)\;h_k(\xi_r)\;e'_l(\eta_s)\,w_r\,w_s, \tag{7.20}$$

$$(\mathbb{M}_{34})_{ijkl} = \sum_{r=1}^{N_x}\sum_{s=1}^{N_x} C'_{34}\,(\xi_r,\eta_s)\,e_i(\xi_r)\;h'_j(\eta_s)\;h_k(\xi_r)\;e'_l(\eta_s)\,w_r\,w_s, \tag{7.21}$$

where the coefficients C'_{31}, C'_{32}, C'_{33}, C'_{34} are the same ones used in the previous formulation, written in (6.9).

Then we get $\mathbb{M}_3 = [\mathbb{M}_{31}\;\;\mathbb{M}_{32}\;\;\mathbb{M}_{33}\;\;\mathbb{M}_{34}]$

7.4.4. Constitutive relation 4

The third constitutive relation has $\widetilde{\sigma_{\eta y}}$ as the test function. The expressions are given below.

$$(\mathbb{M}_{41})_{ijkl} = \sum_{r=1}^{N_x}\sum_{s=1}^{N_x} C'_{41}\,(\xi_r,\eta_s)\,h'_i(\xi_r)\;e_j(\eta_s)\;e_k(\xi_r)\;h'_l(\eta_s)\,w_r\,w_s, \tag{7.22}$$

$$(\mathbb{M}_{42})_{ijkl} = \sum_{r=1}^{N_x}\sum_{s=1}^{N_x} C'_{42}\,(\xi_r,\eta_s)\,e'_i(\xi_r)\;h_j(\eta_s)\;e_k(\xi_r)\;h'_l(\eta_s)\,w_r\,w_s, \tag{7.23}$$

$$(\mathbb{M}_{43})_{ijkl} = \sum_{r=1}^{N_x}\sum_{s=1}^{N_x} C'_{43}\,(\xi_r,\eta_s)\,h_i(\xi_r)\;e'_j(\eta_s)\;e_k(\xi_r)\;h'_l(\eta_s)\,w_r\,w_s, \tag{7.24}$$

$$(\mathbb{M}_{44})_{ijkl} = \sum_{r=1}^{N_x}\sum_{s=1}^{N_x} C'_{44}\,(\xi_r,\eta_s)\,e_i(\xi_r)\;h'_j(\eta_s)\;e_k(\xi_r)\;h'_l(\eta_s)\,w_r\,w_s, \tag{7.25}$$

where the coefficients C'_{41}, C'_{42}, C'_{43}, C'_{44} are the same ones used in the previous formulation, written in Equation 6.10.

Then we get $\mathbb{M}_4 = [\mathbb{M}_{41}\ \ \mathbb{M}_{42}\ \ \mathbb{M}_{43}\ \ \mathbb{M}_{44}]$

With these components, the mass matrix can be set up by vertically stacking $\mathbb{M}_1, \mathbb{M}_2, \mathbb{M}_3$ and $\mathbb{M}_4$ respectively.

7.5. Rotation matrix

The Rotation matrix enforces the weak conservation of angular momentum for the system. The idea is to understand and rewrite (7.6) for an element, and integrate each component over the domain, as done in the previous formulation.

On writing down these integrals for all the stress components, the rotation matrices are written down as

$$(\mathbb{R}_1)_{ijkl} = \sum_{r=1}^{N_x}\sum_{s=1}^{N_x}\left(-\frac{\partial y}{\partial \xi}\right)(\xi_r,\eta_s)\,h'_i(\xi_r)\;e_j(\eta_s)\;h_k(\xi_r)\;h_l(\eta_s)\,w_r\,w_s, \tag{7.26}$$

$$(\mathbb{R}_2)_{ijkl} = \sum_{r=1}^{N_x}\sum_{s=1}^{N_x}\left(-\frac{\partial y}{\partial \eta}\right)(\xi_r,\eta_s)\,e'_i(\xi_r)\;h_j(\eta_s)\;h_k(\xi_r)\;h_l(\eta_s)\,w_r\,w_s, \tag{7.27}$$

$$(\mathbb{R}_3)_{ijkl} = \sum_{r=1}^{N_x}\sum_{s=1}^{N_x}\left(\frac{\partial x}{\partial \xi}\right)(\xi_r,\eta_s)\,h_i(\xi_r)\;e'_j(\eta_s)\;h_k(\xi_r)\;h_l(\eta_s)\,w_r\,w_s, \tag{7.28}$$

$$(\mathbb{R}_4)_{ijkl} = \sum_{r=1}^{N_x}\sum_{s=1}^{N_x}\left(\frac{\partial x}{\partial \eta}\right)(\xi_r,\eta_s)\,e_i(\xi_r)\;h'_j(\eta_s)\;h_k(\xi_r)\;h_l(\eta_s)\,w_r\,w_s. \tag{7.29}$$

Note that the coefficients are the same ones used in the previous formulation, however, the matrices themselves have a different basis owing to the different spectral bases used for both the stress components and the test function $\widetilde{\omega}$.

7.6. Boundary conditions

As before, the boundary conditions can be enforced using a trick arising from the definition of the dual basis functions themselves. But care should be taken on which perspective you are using depending on which boundary condition you are finding the contributions of. Unlike in the previous formulation, where the 'normal' displacements and the 'shear' stresses are prescribed, in this formulation the 'shear' displacements and the 'normal' stresses are prescribed.

7.6.1. 'Shear' displacements for the Constitutive relation

The boundary condition for the constitutive relation with $\widetilde{\sigma_{\eta x}}$ shall be considered first. When looking at the reference domain, the displacement in the $x-$direction (i.e. in the *physical* coordinates) is prescribed on the top and bottom boundaries in the *reference* domain.

On the boundary, the prescribed $x-$displacement is expanded as

$$\int_{\partial\hat{\Omega}} u^{ex}\left(x(\xi,\eta)\right)\mathrm{d}\xi \approx \int_{\partial\hat{\Omega}} \sum_{l=1}^{N+1} (u_P)_l h_l\left(\xi\right)\mathrm{d}\xi,$$

where u_P indicates the prescribed horizontal displacement. Using the dual polynomials, this integral can be reformulated as

$$\int_{\partial\hat{\Omega}} \sum_{i=1}^{N+1}\sum_{l=1}^{N+1} (u_P)_l h_l(\xi) e_i'(\xi)\mathrm{d}\xi \approx \int_{\partial\hat{\Omega}} \sum_{j=1}^{N+1} u^{ex}(x(\xi,\eta)) e_i'(\xi)\mathrm{d}\xi = u_{i,a},$$

where $a = 0$ or $a = N+1$ depending on whether it is the bottom or the top boundary.

Thus, the boundary condition becomes

$$\int_{\partial\hat{\Omega}} u_P \widetilde{\sigma_{\eta x}} n_\eta \mathrm{d}\Gamma = \int_{\partial\hat{\Omega}} \sum_{i=1}^{N+1}\sum_{l=1}^{N+1} \left(\widetilde{\sigma_{\eta x}}\right)_{l,a} u^{ex}\left(x(\xi,\eta)\right) e_j'(\xi)\mathrm{d}\xi = \sum_{i=1}^{N+1}\sum_{l=1}^{N+1} \left(\widetilde{\sigma_{\eta x}}\right)_{l,a} u_{i,a} \tag{7.30}$$

In a similar manner, the y-displacement is prescribed to the constitutive relation with $\widetilde{\sigma_{\xi y}}$ on the left and right boundaries in the *reference* domain, as

$$\int_{\partial\hat{\Omega}} v_P \widetilde{\sigma_{\xi y}} n_\xi \mathrm{d}\Gamma = \int_{\partial\hat{\Omega}} \sum_{j=1}^{N+1}\sum_{l=1}^{N+1} \left(\widetilde{\sigma_{\xi y}}\right)_{a,l} v^{ex}\left(y(\xi,\eta)\right) e_j'(\eta)\mathrm{d}\eta = \sum_{j=1}^{N+1}\sum_{l=1}^{N+1} \left(\widetilde{\sigma_{\eta y}}\right)_{a,l} v_{a,j} \tag{7.31}$$

where $a = 0$ and $a = N+1$ for the left and right boundaries, respectively.

Do note that the prescribed displacements u_P and v_P are not actually the 'shear' displacements at the boundaries, as that would be the component of the displacement along the ξ- and η- directions respectively. This makes the formulation easier to apply these boundary conditions, as the displacement in the local coordinates need not be calculated. Instead, as long as the boundary points in the physical domain correspond to the edges of the boundary in the reference domain, the x- and y- displacements can be prescribed to the horizontal and vertical boundary points respectively. Similar to the previous formulation, only the degrees of freedom are enough to prescribe these boundary conditions.

7.6.2. 'Normal' stresses for conservation of linear momentum

Because the components of the stress tensor are expressed using two different coordinate systems for the normals and the component of the traction force, it is necessary to write down the components that need to be prescribed at the boundaries for this formulation.

Considering the conservation of linear momentum for the stresses along the x-direction (for which $\widetilde{u}$ is the Lagrange multiplier), the stress component $\sigma_{\xi x}$ needs to be prescribed at the left and right boundaries in the reference domain.

This stress component can be expanded as

$$\int_{\partial\hat{\Omega}} \sigma_{\xi x}^{ex}\left(y(\xi,\eta)\right)\mathrm{d}\eta \approx \int_{\partial\hat{\Omega}} \sum_{l=1}^{N} (\sigma_{\xi x})_P e_l(\eta)\mathrm{d}\eta$$

Using dual polynomials, this can be modified as

$$\int_{\partial\hat{\Omega}} \sum_{j=1}^{N}\sum_{l=1}^{N} (\sigma_{\xi x})_P e_l(\eta) h_j'(\eta)\mathrm{d}\eta \approx \int_{\partial\hat{\Omega}} \sum_{j=1}^{N} \sigma_{\xi x}^{ex}\left(y(\xi,\eta)\right) h_j'(\eta)\mathrm{d}\eta = (\sigma_{\eta x})_{a,j}$$

where $a = 0$ and $a = N+1$ respectively for the left and right boundaries.

Thus, the boundary integral can be reformulated as

$$\int_{\partial\hat{\Omega}} \widetilde{u}\,(\sigma_{\xi x})_P\, n_\xi \mathrm{d}\Gamma = \int_{\partial\hat{\Omega}} \sum_{j=1}^{N}\sum_{l=1}^{N} (\widetilde{u})_{a,l}\sigma^{ex}_{\xi x}\left(y(\xi,\eta)\right) h'_j(\eta)\mathrm{d}\eta = \sum_{j=1}^{N}\sum_{l=1}^{N} (\widetilde{u})_{a,l}(\sigma_{\xi x})_{a,j} \tag{7.32}$$

Similarly, considering the conservation of linear momentum for the stresses along the $y-$direction (with $\widetilde{v}$ as the Lagrange multiplier), the stress component $\sigma_{\eta y}$ needs to be prescribed at the bottom and top boundaries. The integral can be simplified as

$$\int_{\partial\hat{\Omega}} \widetilde{v}\,(\sigma_{\eta y})_P\, n_\eta \mathrm{d}\Gamma = \int_{\partial\hat{\Omega}} \sum_{i=1}^{N}\sum_{l=1}^{N} (\widetilde{v})_{l,a}\sigma^{ex}_{\eta y}\left(x(\xi,\eta)\right) h'_j(\xi)\mathrm{d}\xi = \sum_{i=1}^{N}\sum_{l=1}^{N} (\widetilde{v})_{l,a}(\sigma_{\eta y})_{i,a} \tag{7.33}$$

An important observation with these is that (like the displacements) the tractions at the boundaries need not be resolved into their normal and tangential components at the boundaries. Instead, the boundaries only require that the tractions be defined in the x- or y- directions depending on which boundary is being observed. As in Chapter 6 only the degrees of freedom are required to prescribe these boundary conditions.

7.7. Contributions from the forcing function

The forcing function in both directions needs to have the same basis as the derivatives of the stresses, i.e.

$$\overline{f_x} = \sum_{i=1}^{N+1}\sum_{j=1}^{N} (f_x)_{i,j} e'_i(\xi) e_j(\eta)$$

$$\overline{f_y} = \sum_{i=1}^{N}\sum_{j=1}^{N+1} (f_y)_{i,j} e_i(\xi) e'_j(\eta)$$

Similar to the boundary conditions, the degrees of freedom for the body forces can be computed using the property of dual basis functions.

$$\begin{aligned}(f_x)_{k,l} &= \int_{\hat{\Omega}} \sum_{i=1}^{N+1}\sum_{j=1}^{N} (f_x)_{i,j} e'_i(\xi) e_j(\eta) h_k(\xi) h'_l(\eta)\mathrm{d}\xi\wedge\mathrm{d}\eta \\ &= \int_{\hat{\Omega}} f_x^{ex}\left(x(\xi,\eta), y(\xi,\eta)\right)(\det\mathcal{J}) h_k(\xi) h'_l(\eta)\mathrm{d}\xi\wedge\mathrm{d}\eta\end{aligned}$$

$$\begin{aligned}(f_y)_{k,l} &= \int_{\hat{\Omega}} \sum_{i=1}^{N}\sum_{j=1}^{N+1} (f_y)_{i,j} e_i(\xi) e'_j(\eta) h'_k(\xi) h_l(\eta)\mathrm{d}\xi\wedge\mathrm{d}\eta \\ &= \int_{\hat{\Omega}} f_y^{ex}\left(x(\xi,\eta), y(\xi,\eta)\right)(\det\mathcal{J}) h'_k(\xi) h_l(\eta)\mathrm{d}\xi\wedge\mathrm{d}\eta\end{aligned}$$

Note that the $\det\mathcal{J}$ term enters the integral because of the change of integration volumes, from the physical domain to the reference domain, exactly like the previous formulation.

7.8. Hybridized system

Just like the formulation in Chapter 6, it is possible to hybridize the physical domain with this one. This makes the method attractive when looking at it from a computational perspective.

The idea is very similar to the one used in the original formulation. In order to not overdefine the problem, the Lagrange multipliers are used to constrain quantities neighbouring elements to be the same. This will result in a system matrix of the form

$$\begin{bmatrix} \mathbb{A} & \mathbb{B}^T \\ \mathbb{B} & 0 \end{bmatrix} \begin{bmatrix} \mathbf{x}^h \\ \boldsymbol{\lambda}^h \end{bmatrix} = \begin{bmatrix} \mathbf{f}^h \\ 0 \end{bmatrix} \tag{7.34}$$

The matrix $\mathbb{A}$ contains element stiffness matrices, arranged in (again) x-lexicographic order. This enables it to be ordered in a block-diagonal matrix, with the stiffness matrix for each element having contributions from the mass, incidence and rotation matrices for each element.

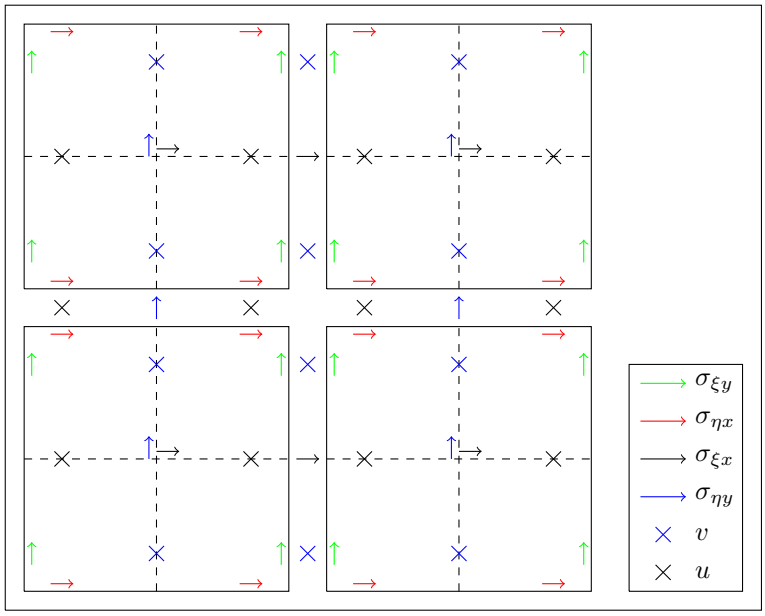

Figure 7.1: Degrees of freedom of quantities for the hybrid formulation on the reference domain with $K_x = K_y = 2$, $N = 1$

$\mathbb{B}$ contains the relations which enforce the required continuity at the element boundaries, as long as it is also not a boundary of the physical domain. With this formulation, the relations used at the *horizontal* boundaries are

$$\widetilde{\sigma_{\xi y}}|_l = \widetilde{\sigma_{\xi y}}|_r \,,$$
$$\widetilde{u}|_l = \widetilde{u}|_r \,,$$

where l and r denote the left and right boundaries respectively. At the *vertical* boundaries,

$$\widetilde{\sigma_{\eta x}}|_b = \widetilde{\sigma_{\eta x}}|_t \,,$$
$$\widetilde{v}|_b = \widetilde{v}|_t \,,$$

where b and t denote the bottom and top boundaries respectively. These relations differ from the ones in Chapter 6 in that these enforce continuity between the shear stresses at the element boundaries, and displacements at normal boundaries instead of tangential boundaries. The differences can be clearly visualised in Figure 7.1.

7.9. Results

This formulation is tested against a manufactured solution. A different manufactured solution is used from Chapter 6, such that the resulting Cauchy shear stress components are zero. Here, the displacements are assumed to be

$$u^{ex}(x,y) = \cos(2\pi x)\cos(2\pi y),$$
$$v^{ex}(x,y) = \sin(2\pi x)\sin(2\pi y).$$

The exact rotation

$$\omega^{ex}(x,y) = \frac{1}{2}\left(\frac{\partial v}{\partial x} - \frac{\partial u}{\partial y}\right) = 2\pi\left(\cos(2\pi x)\sin(2\pi y)\right).$$

And the strains

$$\underline{\underline{\epsilon}}^{ex}(x,y) = 2\pi \begin{bmatrix} -\sin(2\pi x)\cos(2\pi y) & 0 \\ 0 & \sin(2\pi x)\cos(2\pi y) \end{bmatrix},$$

The stress components are equal to

$$\begin{aligned}\sigma_{xx}^{ex}(x,y) &= -\frac{2\pi E}{1+\nu}\left[\sin(2\pi x)\cos(2\pi y)\right],\\ \sigma_{yx}^{ex}(x,y) = \sigma_{xy}^{ex}(x,y) &= 0,\\ \sigma_{yy}^{ex}(x,y) &= \frac{2\pi E}{1+\nu}\left[\sin(2\pi x)\cos(2\pi y)\right].\end{aligned}$$

In order to balance the forces generated by these stresses, there is a body force prescribed, which is given by

$$\begin{aligned}f_x^{ex}(x,y) &= -\frac{4\pi^2 E}{1+\nu}\left[\cos(2\pi x)\cos(2\pi y)\right],\\ f_y^{ex}(x,y) &= -\frac{4\pi^2 E}{1+\nu}\left[\sin(2\pi x)\sin(2\pi y)\right].\end{aligned}$$

7.9.1. Domain

The domain is the same as the one in the original formulation (Figure 5.2) with the mesh and the elements generated in the same way as in the original formulation (Figure 5.3). On these domains, the displacement v^{ex} and the stress component $\sigma_{\xi x}^{ex}$ are prescribed on the left and right boundary, and the displacement u^{ex} and $\sigma_{\eta y}^{ex}$ is prescribed on the bottom and top boundary.

7.9.2. Observations and Conclusions

For both u and v displacements, the results are consistent with the manufactured solution apart from when $N = 1$, as seen in Figure 7.2 and Figure 7.3. For $N = 1$, the displacements are overestimated. However, continuity is seen for all discretizations, in the horizontal direction for u and in the vertical direction for v.

The reason for this overestimation can be seen in Figure 7.7, where fro $N = 1$ there is a singularity observed at the corners of the element. One probable cause for this discontinuity is the definition of ω at the primal boundaries at the element, which may cause it to be overdefined at the boundaries. However, apart from $N = 1$, there is decent consistency in results for ω, when compared with the manufactured exact solution.

Again, for both the normal stresses σ_{xx} and σ_{yy} there is a problem when $N = 1$. However, the results in Figure 7.4 and Figure 7.5 show that for other polynomial degrees and discretization, there is a good correlation with the exact solution. There is a similar observation for the shear stress components σ_{xy} and σ_{yx}, shown in Figure 7.6. The exact solution for these components is zero all through the domain, which is close to the numerical results obtained, apart from when $N = 1$. However, even with higher resolution for the shear stresses, it is seen in Figure 7.8 that the symmetry of the Cauchy shear stresses is not strongly enforced. The value of the error seen with this formulation is lesser than the ones seen in Figure 6.9, probably owing to the higher resolution used for the shear stresses.

The results shown in Figure 7.9 and Figure 7.10 show that there is optimal convergence observed on increasing the number of elements, and spectral convergence on increasing the polynomial degree respectively, for all cases except when $N = 1$. For $N = 1$, divergence in results of quantity is seen, with almost a constant value of error when looking at the value of the error in symmetry of the Cauchy shear stresses. The observed singularity at the corners of the element is probably the cause for this error. For higher polynomial degrees the results look optimal. But again, one should notice that the symmetry of the Cauchy stress tensor is only weakly imposed.

For a polynomial degree greater than 1, no spurious kinematic modes are observed. And similar results for an alternate skewed domain are seen, with them listed in section B.3.

7.10. Summary

In this section, a modified formulation was tested to construct a hybridized formulation to simultaneously conserve linear momentum, and angular momentum exactly regardless of the number of elements the domain is subdivided into, and the polynomial degree of spectral bases used for quadrature within the element. The idea was to modify the previous formulation, such that the Cauchy shear stresses can be represented with a higher number of degrees of freedom, which would ideally eliminate the error in the symmetry of the Cauchy shear stress thus resulting in exact angular momentum conservation in the discrete scenario. However, while the error did reduce, it could not be eliminated with this change. In addition, because the shear displacements and the normal stresses are being

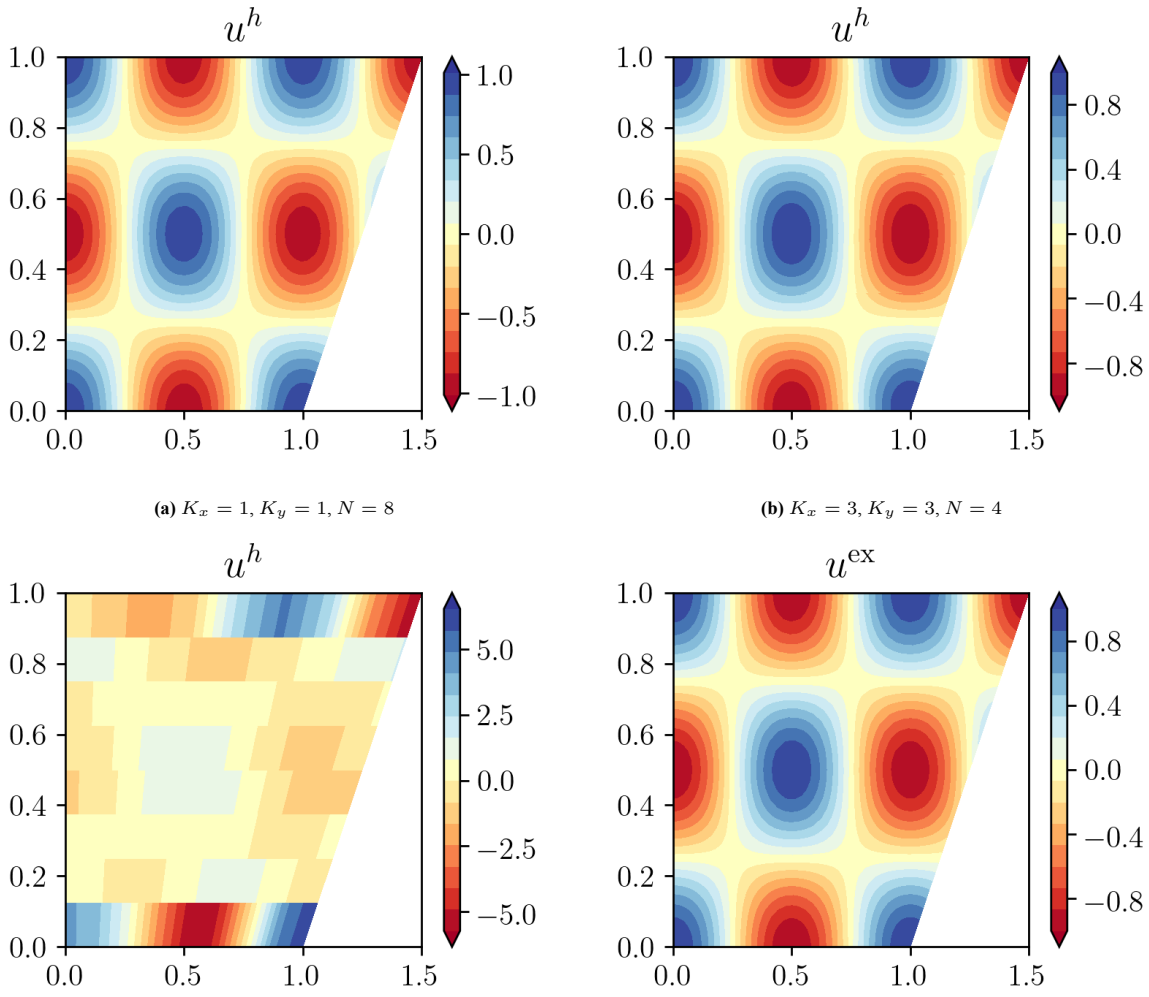

(a) $K_x = 1, K_y = 1, N = 8$

(b) $K_x = 3, K_y = 3, N = 4$

(c) $K_x = 8, K_y = 8, N = 1$

(d) Exact solution

Figure 7.2: Results for u^h in the physical domain

prescribed to the formulation instead of the normal displacements and the shear stresses respectively, there are singular modes seen for $N = 1$, with suboptimal convergence. However, this is eliminated by further refining the polynomial degree.

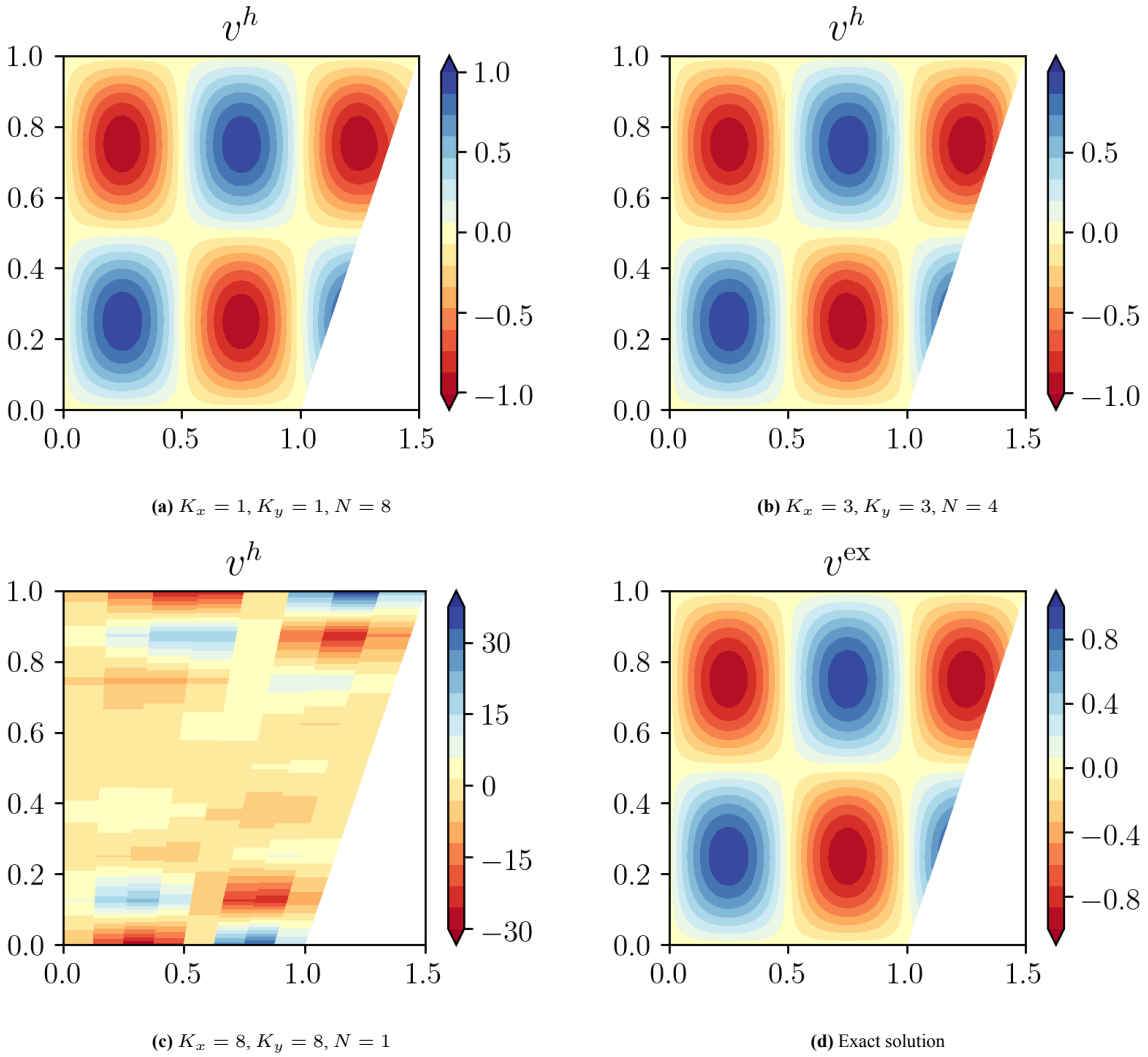

(a) $K_x = 1, K_y = 1, N = 8$

(b) $K_x = 3, K_y = 3, N = 4$

(c) $K_x = 8, K_y = 8, N = 1$

(d) Exact solution

Figure 7.3: Results for v^h in the physical domain

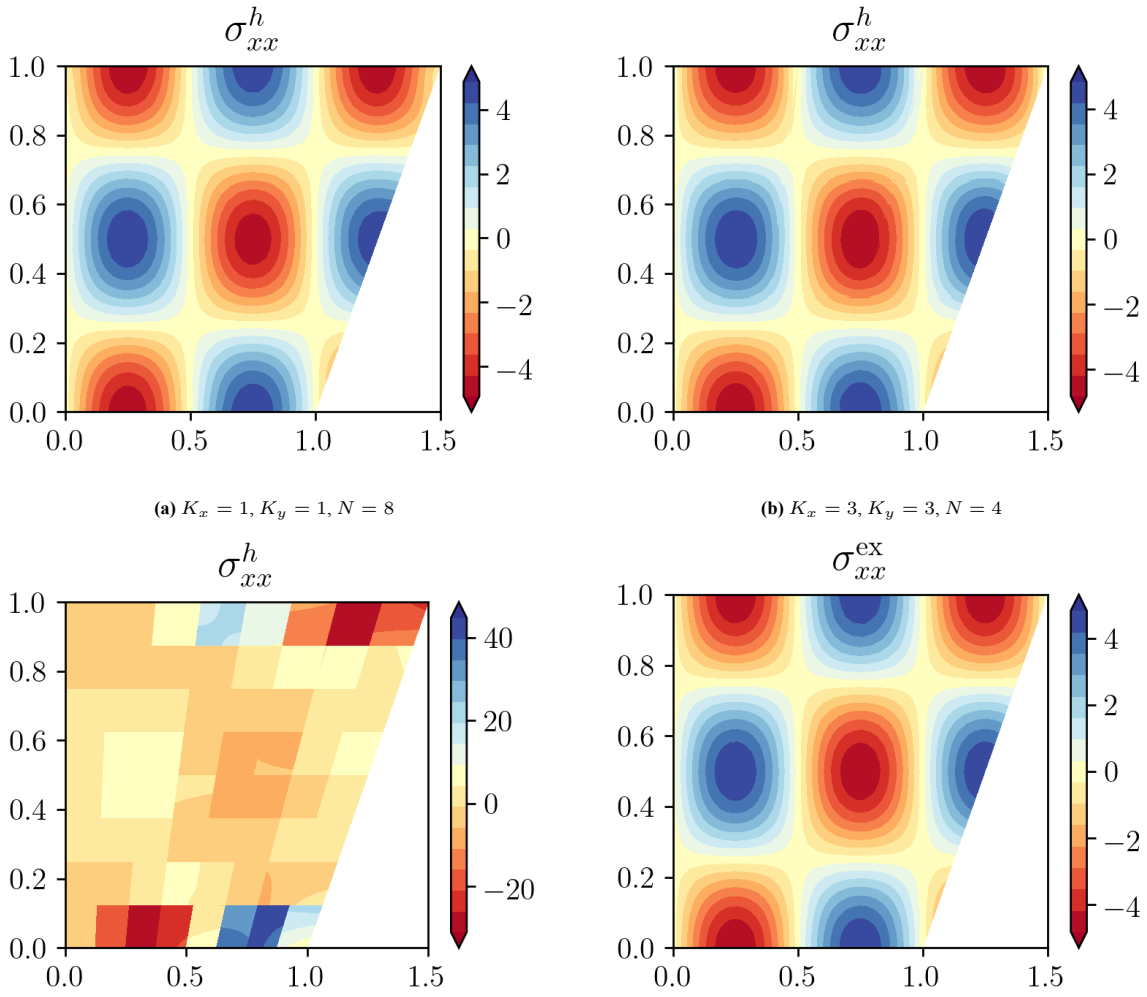

(a) $K_x = 1, K_y = 1, N = 8$

(b) $K_x = 3, K_y = 3, N = 4$

(c) $K_x = 8, K_y = 8, N = 1$

(d) Exact solution

Figure 7.4: Results for σ^h_{xx} in the physical domain

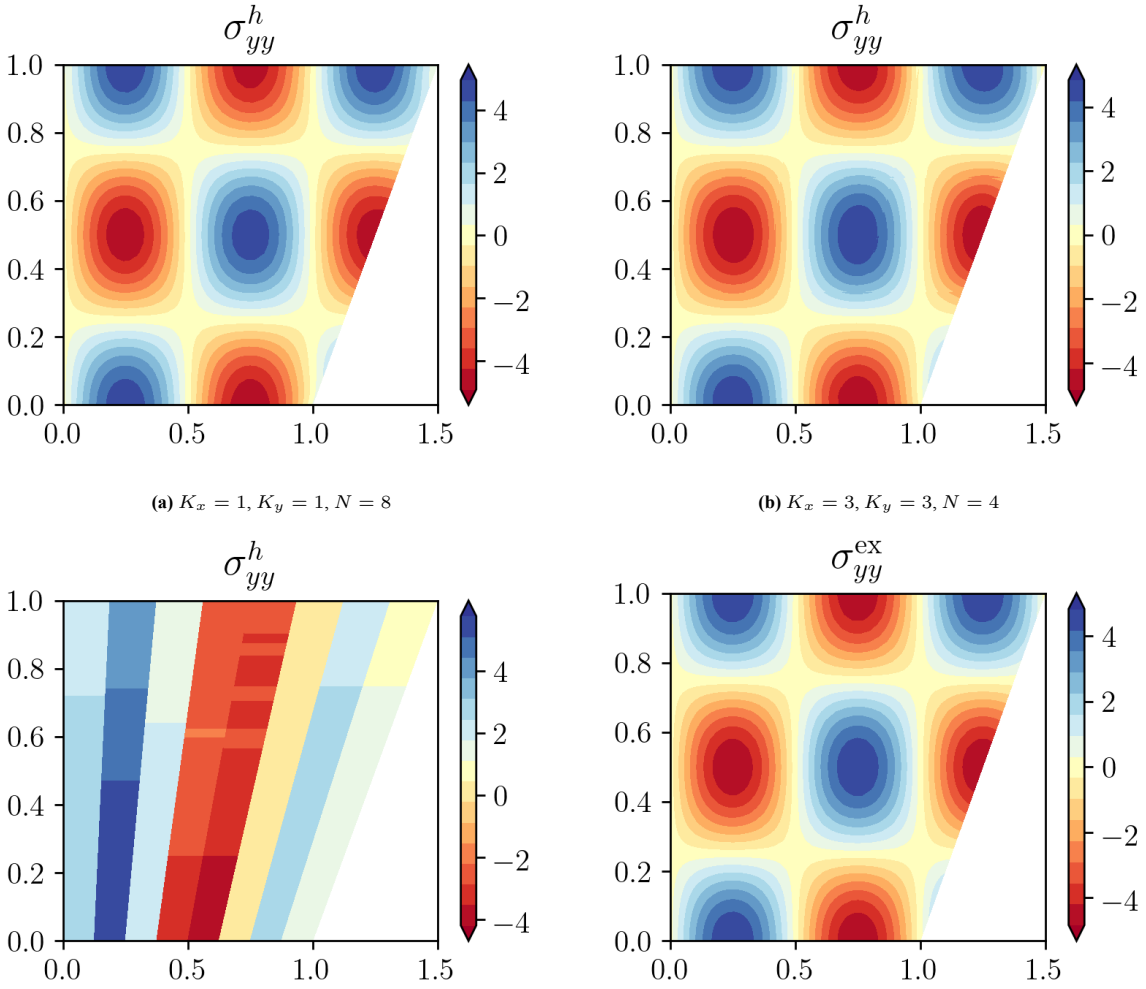

(a) $K_x = 1, K_y = 1, N = 8$

(b) $K_x = 3, K_y = 3, N = 4$

(c) $K_x = 8, K_y = 8, N = 1$

(d) Exact solution

Figure 7.5: Results for σ^h_{yy} in the physical domain

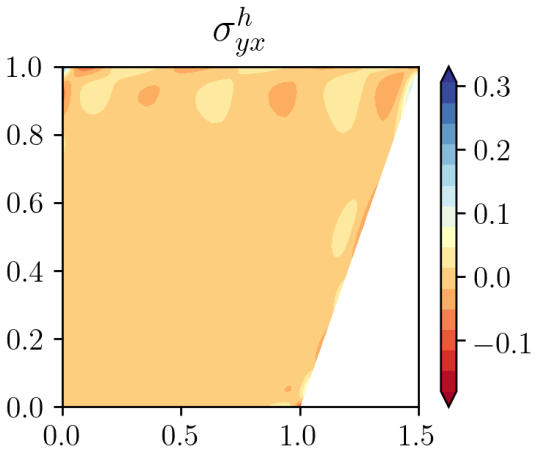

(a) σ^h_{yx} for $K_x = 1, K_y = 1, N = 8$

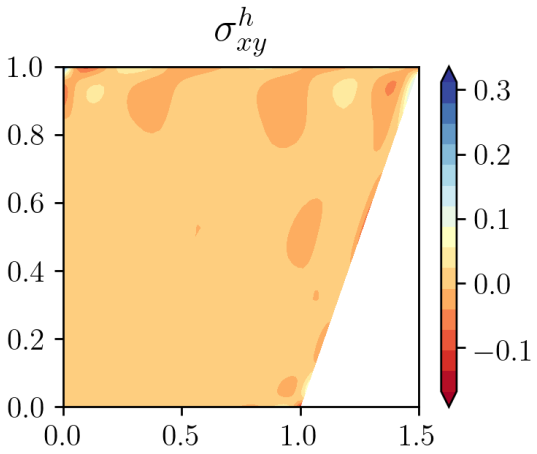

(b) σ^h_{xy} for $K_x = 1, K_y = 1, N = 8$

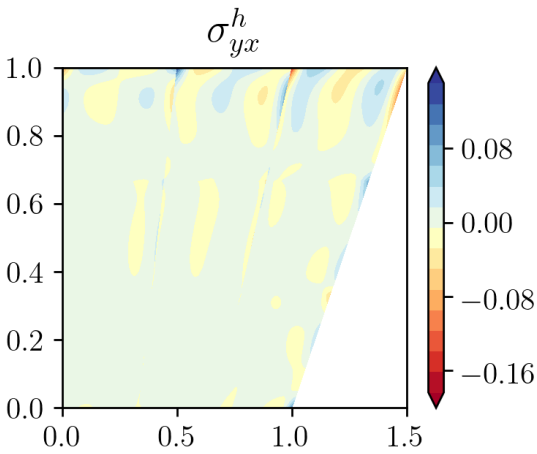

(c) σ^h_{yx} for $K_x = 3, K_y = 3, N = 4$

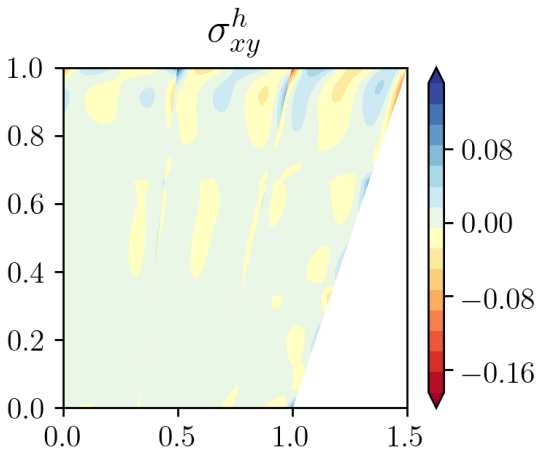

(d) σ^h_{xy} for $K_x = 3, K_y = 3, N = 4$

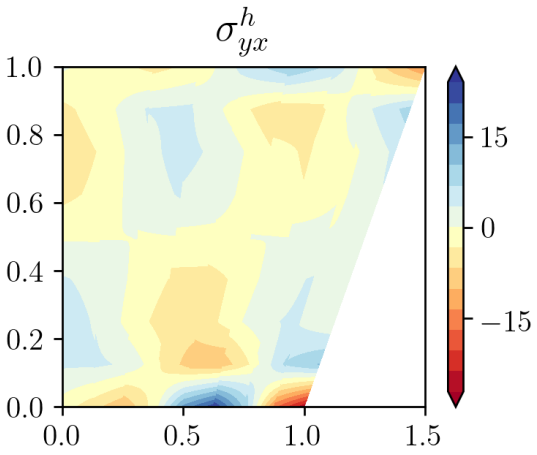

(e) σ^h_{yx} for $K_x = 8, K_y = 8, N = 1$

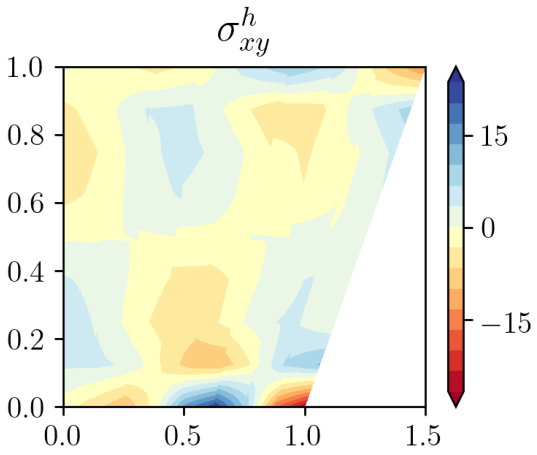

(f) σ^h_{xy} for $K_x = 8, K_y = 8, N = 1$

Figure 7.6: Results for σ^h_{yx} and σ^h_{xy} in the physical domain

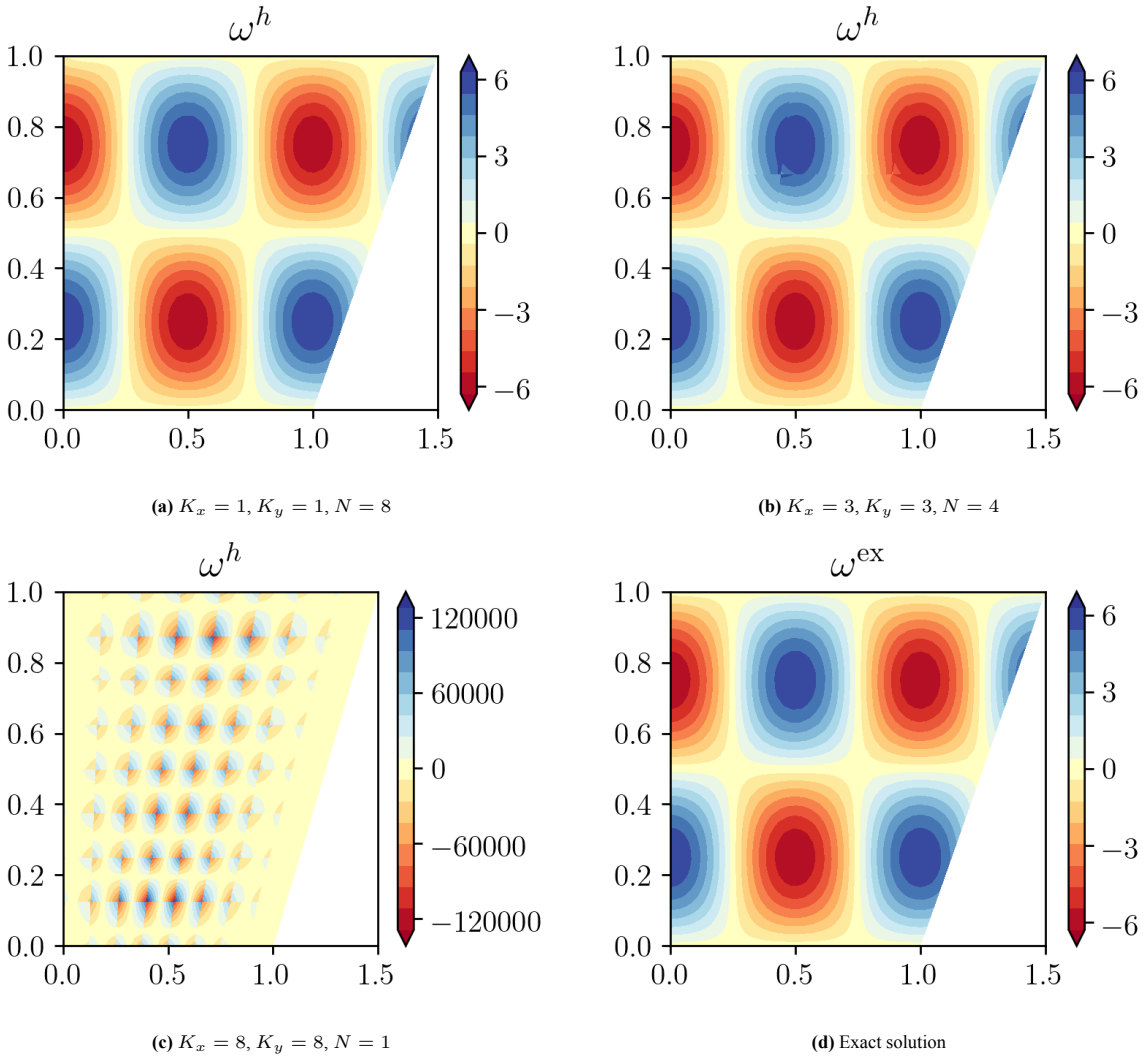

(a) $K_x = 1, K_y = 1, N = 8$

(b) $K_x = 3, K_y = 3, N = 4$

(c) $K_x = 8, K_y = 8, N = 1$

(d) Exact solution

Figure 7.7: Results for ω^h in the physical domain

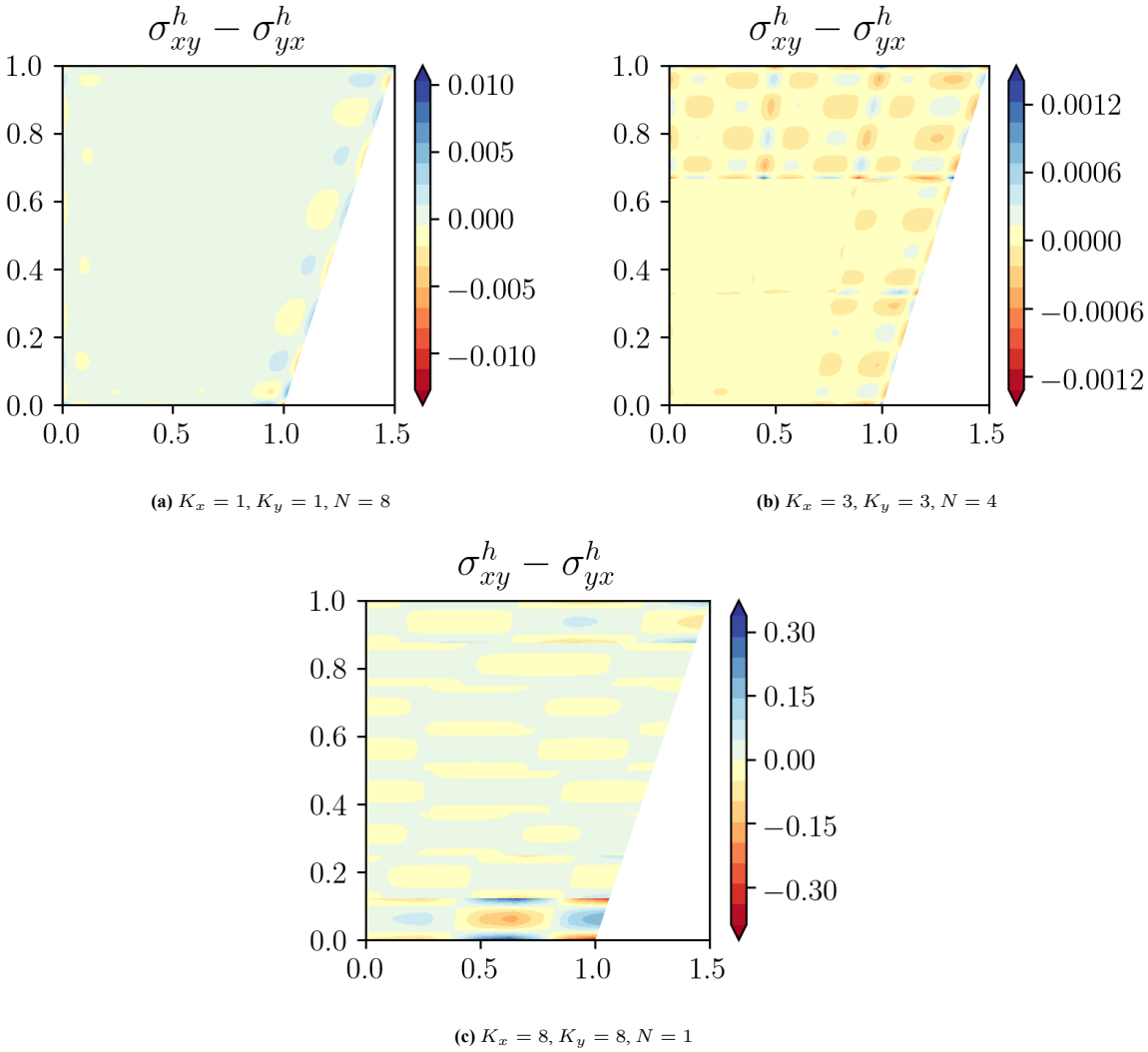

(a) $K_x = 1, K_y = 1, N = 8$

(b) $K_x = 3, K_y = 3, N = 4$

(c) $K_x = 8, K_y = 8, N = 1$

Figure 7.8: Error in the symmetry of the Cauchy stress tensor

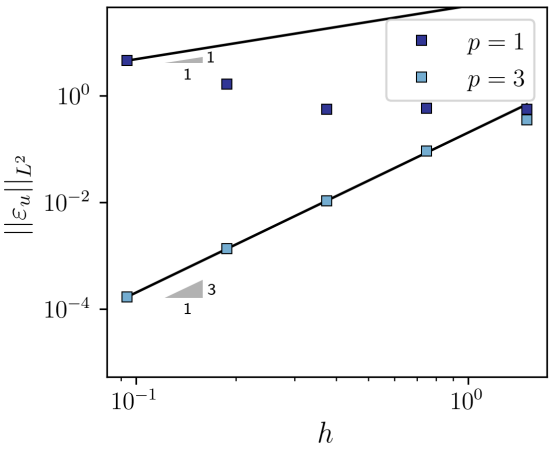

(a) Convergence with mesh width of L^2 error for u^h

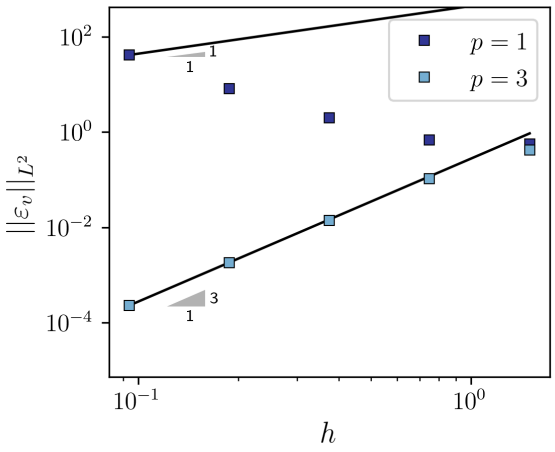

(b) Convergence with mesh width of L^2 error for v^h

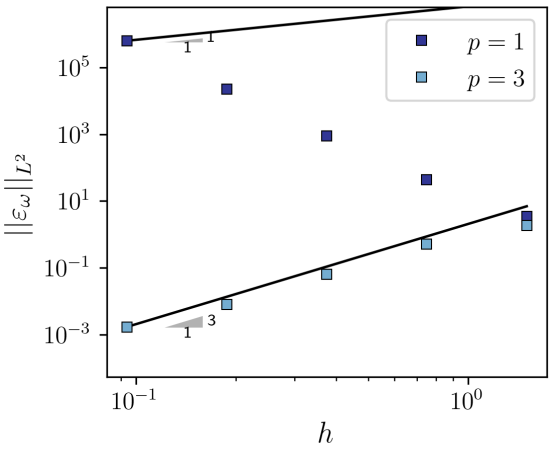

(c) Convergence with mesh width of L^2 error for ω^h

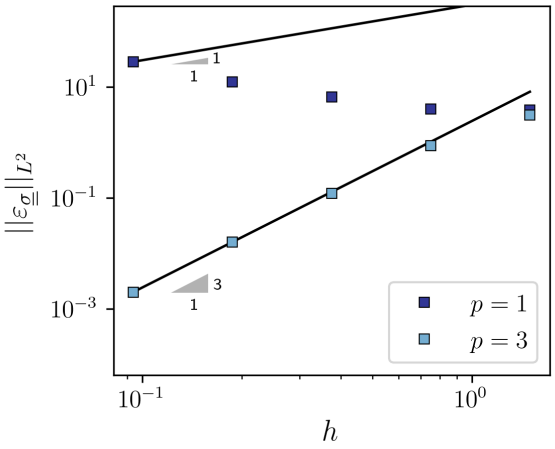

(d) Convergence with mesh width of L^2 error for $\underline{\underline{\boldsymbol{\sigma}}}^h$

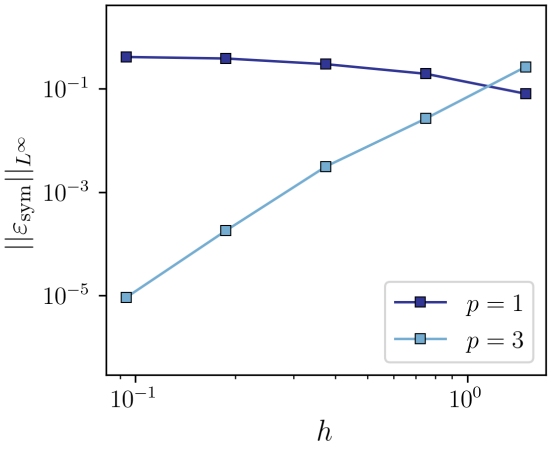

(e) Convergence with mesh width of L^∞ error for conservation of angular momentum

Figure 7.9: Results from the h-convergence study

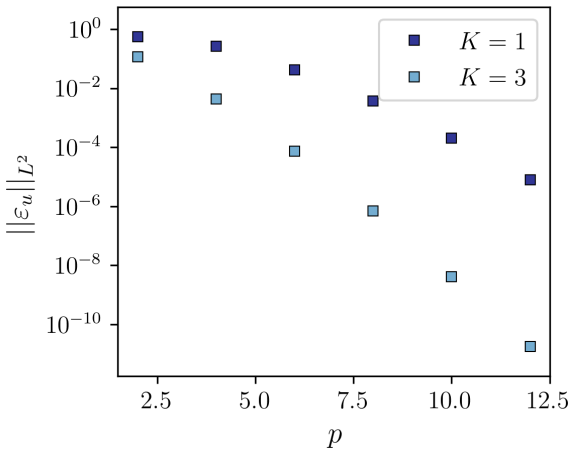

(a) L^2 error for u^h

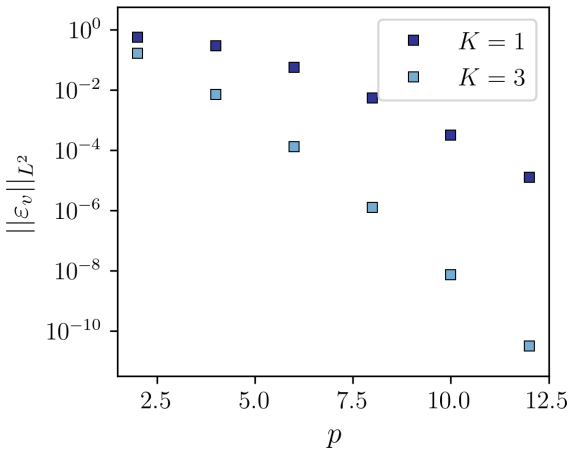

(b) L^2 error for v^h

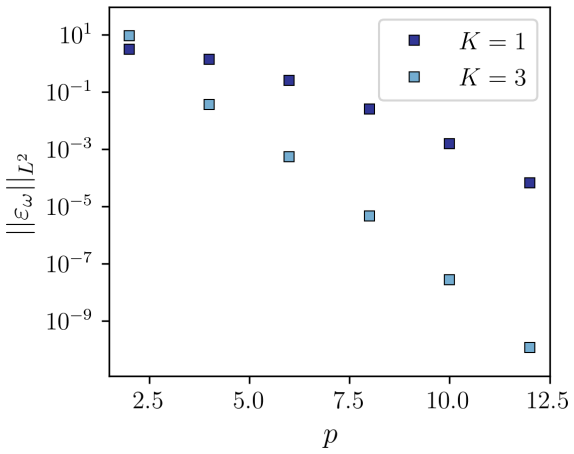

(c) L^2 error for ω^h

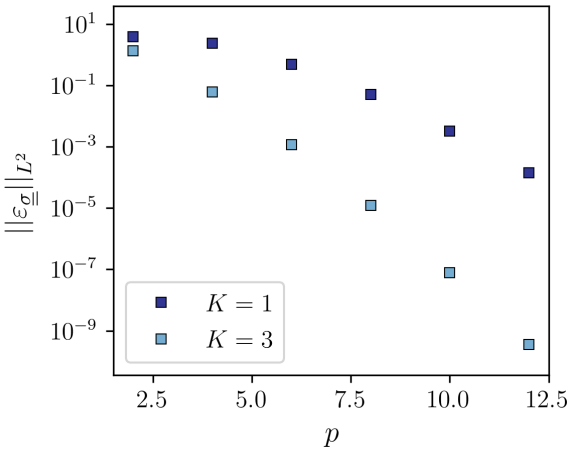

(d) L^2 error for $\underline{\underline{\boldsymbol{\sigma}}}^h$

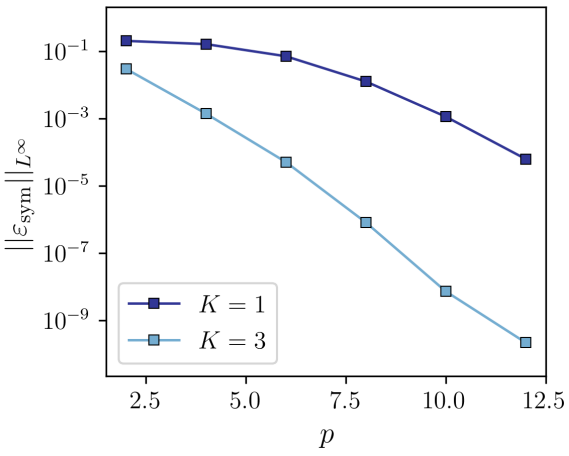

(e) L^∞ error in conservation of angular momentum

Figure 7.10: Results from the polynomial convergence study

8

Complete Transformation

So far, the linear elasticity formulations contain the value parts in the physical domain, while the form part is transformed into the reference domain. With the symmetry of the Cauchy stress tensor was not achieved even when the 'shear' components were given more degrees of freedom, other avenues were looked at to conserve angular momentum. The next simple idea would be to change the formulation of stress components, such that both the value and the form parts will be in the same coordinate system. This means that symmetry can again be enforced.

Here, a trial of the method in which both the vector- and covector-values, as well as the forms are in the reference domain is considered. In this way, the nature of the computational domain is used effectively and calculations with the forms are carried out easily. With this, the stress tensor can also be refined accurately and the assumption is that symmetry of the stress tensor can be exact because both the value and the form parts are in the same coordinate system.

8.1. Components in the reference domain

In this section, we will deal with how the components of the quantities are represented in the reference domain. This will help to map the quantities into the reference domain and back, as well as apply the boundary conditions to the problem.

8.1.1. Reference domain

In this scenario, the reference domain is chosen to be $\left[-1,1\right] \times \left[-1,1\right]$ 2-dimensional square, with the independent dimensions being ξ and η, as shown in Figure 4.2.

This is ideal because the Gauss-Lobatto points which are used to construct the spectral bases lie in this domain.

8.1.2. Stress

The stress is described as a vector-valued 1-form. In the physical domain, it is represented as

$$\underline{\underline{\boldsymbol{\sigma}}} = \frac{\partial}{\partial x} \otimes \left(\sigma_{xx}\mathrm{d}y - \sigma_{yx}\mathrm{d}x\right) + \frac{\partial}{\partial y} \otimes \left(\sigma_{xy}\mathrm{d}y - \sigma_{yy}\mathrm{d}x\right). \tag{8.1}$$

When fully transformed into the reference domain, this would look like

$$\underline{\underline{\boldsymbol{\sigma}}} = \frac{\partial}{\partial \xi} \otimes \left(\sigma_{\xi\xi}\mathrm{d}\eta - \sigma_{\eta\xi}\mathrm{d}\xi\right) + \frac{\partial}{\partial \eta} \otimes \left(\sigma_{\xi\eta}\mathrm{d}\eta - \sigma_{\eta\eta}\mathrm{d}\xi\right). \tag{8.2}$$

One of the several distinctions from previous formulations is that this formulation considers the stress to be a vector-valued form, while previous formulations considered the stress to be a covector-valued form.

Assuming that the x and y as functions of (ξ, η) are known, the stress components can be converted between the two domains as

$$\sigma_{xx} = \frac{1}{\det \mathcal{J}} \left[\left(\frac{\partial x}{\partial \xi} \frac{\partial x}{\partial \xi} \right) \sigma_{\xi\xi} + \left(\frac{\partial x}{\partial \eta} \frac{\partial x}{\partial \xi} \right) \sigma_{\eta\xi} + \left(\frac{\partial x}{\partial \xi} \frac{\partial x}{\partial \eta} \right) \sigma_{\xi\eta} + \left(\frac{\partial x}{\partial \eta} \frac{\partial x}{\partial \eta} \right) \sigma_{\eta\eta} \right],$$
$$\sigma_{yx} = \frac{1}{\det \mathcal{J}} \left[\left(\frac{\partial y}{\partial \xi} \frac{\partial x}{\partial \xi} \right) \sigma_{\xi\xi} + \left(\frac{\partial y}{\partial \eta} \frac{\partial x}{\partial \xi} \right) \sigma_{\eta\xi} + \left(\frac{\partial y}{\partial \xi} \frac{\partial x}{\partial \eta} \right) \sigma_{\xi\eta} + \left(\frac{\partial y}{\partial \eta} \frac{\partial x}{\partial \eta} \right) \sigma_{\eta\eta} \right],$$
$$\sigma_{xy} = \frac{1}{\det \mathcal{J}} \left[\left(\frac{\partial x}{\partial \xi} \frac{\partial y}{\partial \xi} \right) \sigma_{\xi\xi} + \left(\frac{\partial x}{\partial \eta} \frac{\partial y}{\partial \xi} \right) \sigma_{\eta\xi} + \left(\frac{\partial x}{\partial \xi} \frac{\partial y}{\partial \eta} \right) \sigma_{\xi\eta} + \left(\frac{\partial x}{\partial \eta} \frac{\partial y}{\partial \eta} \right) \sigma_{\eta\eta} \right],$$
$$\sigma_{yy} = \frac{1}{\det \mathcal{J}} \left[\left(\frac{\partial y}{\partial \xi} \frac{\partial y}{\partial \xi} \right) \sigma_{\xi\xi} + \left(\frac{\partial y}{\partial \eta} \frac{\partial y}{\partial \xi} \right) \sigma_{\eta\xi} + \left(\frac{\partial y}{\partial \xi} \frac{\partial y}{\partial \eta} \right) \sigma_{\xi\eta} + \left(\frac{\partial y}{\partial \eta} \frac{\partial y}{\partial \eta} \right) \sigma_{\eta\eta} \right],$$

and

$$\sigma_{\xi\xi} = \frac{1}{\det \mathcal{J}} \left[\left(\frac{\partial y}{\partial \eta} \frac{\partial y}{\partial \eta} \right) \sigma_{xx} + \left(-\frac{\partial y}{\partial \eta} \frac{\partial x}{\partial \eta} \right) \sigma_{yx} + \left(-\frac{\partial x}{\partial \eta} \frac{\partial y}{\partial \eta} \right) \sigma_{xy} + \left(\frac{\partial x}{\partial \eta} \frac{\partial x}{\partial \eta} \right) \sigma_{yy} \right],$$
$$\sigma_{\eta\xi} = \frac{1}{\det \mathcal{J}} \left[\left(-\frac{\partial y}{\partial \eta} \frac{\partial y}{\partial \xi} \right) \sigma_{xx} + \left(\frac{\partial y}{\partial \eta} \frac{\partial x}{\partial \xi} \right) \sigma_{yx} + \left(\frac{\partial x}{\partial \eta} \frac{\partial y}{\partial \xi} \right) \sigma_{xy} + \left(-\frac{\partial x}{\partial \eta} \frac{\partial x}{\partial \xi} \right) \sigma_{yy} \right],$$
$$\sigma_{\xi\eta} = \frac{1}{\det \mathcal{J}} \left[\left(-\frac{\partial y}{\partial \xi} \frac{\partial y}{\partial \eta} \right) \sigma_{xx} + \left(\frac{\partial y}{\partial \xi} \frac{\partial x}{\partial \eta} \right) \sigma_{yx} + \left(\frac{\partial x}{\partial \xi} \frac{\partial y}{\partial \eta} \right) \sigma_{xy} + \left(-\frac{\partial x}{\partial \xi} \frac{\partial x}{\partial \eta} \right) \sigma_{yy} \right],$$
$$\sigma_{\eta\eta} = \frac{1}{\det \mathcal{J}} \left[\left(\frac{\partial y}{\partial \xi} \frac{\partial y}{\partial \xi} \right) \sigma_{xx} + \left(-\frac{\partial y}{\partial \xi} \frac{\partial x}{\partial \xi} \right) \sigma_{yx} + \left(-\frac{\partial x}{\partial \xi} \frac{\partial y}{\partial \xi} \right) \sigma_{xy} + \left(\frac{\partial x}{\partial \xi} \frac{\partial x}{\partial \xi} \right) \sigma_{yy} \right],$$

where $\det \mathcal{J} = \frac{\partial x}{\partial \xi} \frac{\partial y}{\partial \eta} - \frac{\partial x}{\partial \eta} \frac{\partial y}{\partial \xi}$.

Apart from this, the stresses in the reference domain can be related to the Lagrangian stresses (used in the formulations in chapter 6 and chapter 7), which are represented with the vector-value in the physical domain while the form part is transformed into the reference domain given by

$$\underline{\underline{\boldsymbol{\sigma}}} = \frac{\partial}{\partial x} \otimes \left(\sigma_{\xi x} \mathrm{d}\eta - \sigma_{\eta x} \mathrm{d}\xi \right) + \frac{\partial}{\partial y} \otimes \left(\sigma_{\xi y} \mathrm{d}\eta - \sigma_{\eta y} \mathrm{d}\xi \right),$$

as

$$\sigma_{\xi\xi} = \frac{1}{\det \mathcal{J}} \left[\sigma_{\xi x} \frac{\partial y}{\partial \eta} - \sigma_{\xi y} \frac{\partial x}{\partial \eta} \right], \qquad \sigma_{\xi\eta} = \frac{1}{\det \mathcal{J}} \left[-\sigma_{\xi x} \frac{\partial y}{\partial \xi} + \sigma_{\xi y} \frac{\partial x}{\partial \xi} \right],$$
$$\sigma_{\eta\xi} = \frac{1}{\det \mathcal{J}} \left[\sigma_{\eta x} \frac{\partial y}{\partial \eta} - \sigma_{\eta y} \frac{\partial x}{\partial \eta} \right], \qquad \sigma_{\eta\eta} = \frac{1}{\det \mathcal{J}} \left[-\sigma_{\eta x} \frac{\partial y}{\partial \xi} + \sigma_{\eta y} \frac{\partial x}{\partial \xi} \right],$$

and

$$\sigma_{\xi x} = \sigma_{\xi\xi} \frac{\partial x}{\partial \xi} + \sigma_{\xi\eta} \frac{\partial x}{\partial \eta}, \qquad \sigma_{\xi y} = \sigma_{\xi\xi} \frac{\partial y}{\partial \xi} + \sigma_{\xi\eta} \frac{\partial y}{\partial \eta},$$
$$\sigma_{\eta x} = \sigma_{\eta\xi} \frac{\partial x}{\partial \xi} + \sigma_{\eta\eta} \frac{\partial x}{\partial \eta}, \qquad \sigma_{\eta y} = \sigma_{\eta\xi} \frac{\partial y}{\partial \xi} + \sigma_{\eta\eta} \frac{\partial y}{\partial \eta}.$$

With this transformation, the equation written down using the Lagrangian formulation can be used to derive the equations for when the stresses are determined in the reference domain, as will be done in subsection 8.2.2.

Do notice that the stresses are actually written as vector-valued forms instead of covector-valued forms, as in previous formulations. This is because to transform the Lagrangian stresses to the stresses in the reference domain, only the components of the inverse Jacobian are required (i.e. $\frac{\partial \xi}{\partial x}, \frac{\partial \xi}{\partial y}, \frac{\partial \eta}{\partial x}, \frac{\partial \eta}{\partial y}$) if stress is written as a vector-valued form. These components are invariant in the reference domain, that is the derivatives of these components with respect to ξ or η is zero, assuming that these functions are smooth. This will help when writing down the divergence of stress when using the reference stresses.

8.1.3. Displacement

The displacement is described as a covector-valued 0-form. In the physical domain, it looks like

$$\mathbf{u} = \mathrm{d}x \otimes u_x + \mathrm{d}y \otimes u_y, \tag{8.3}$$

while in the reference domain, it will look like

$$\mathbf{u} = \mathrm{d}\xi \otimes u_\xi + \mathrm{d}\eta \otimes u_\eta. \tag{8.4}$$

The reason to use the covector-valued form for the displacement instead of the vector-valued form like in previous formulations for displacement, is to accompany the change to vector-valued forms for the stress components.

The components can be converted between them as

$$\begin{aligned} u_x &= u_\xi \frac{\partial \xi}{\partial x} + u_\eta \frac{\partial \eta}{\partial x}, \\ u_y &= u_\xi \frac{\partial \xi}{\partial y} + u_\eta \frac{\partial \eta}{\partial y}, \end{aligned}$$

and

$$\begin{aligned} u_\xi &= u_x \frac{\partial x}{\partial \xi} + u_y \frac{\partial y}{\partial \xi}, \\ u_\eta &= u_x \frac{\partial x}{\partial \eta} + u_y \frac{\partial y}{\partial \eta}. \end{aligned}$$

Note that the displacement is covector-valued, instead of being vector-valued as in previous formulations. This is just a consequence of writing stress components as vector-valued forms instead of covector-valued forms. With displacements having a covector value, the value part is again nullified because there is a duality pairing between components of displacement and components of stresses.

8.1.4. Rotation

The rotation is defined as the antisymmetric part of the displacement gradient (of the displacement in the physical domain). Thus, it is a second-order tensor. It is described as a scalar-valued 0-form. Which means that it remains the same irrespective of the domain.

$$\boldsymbol{\omega} = \omega \begin{bmatrix} 0 & 1 \\ -1 & 1 \end{bmatrix} \tag{8.5}$$

8.1.5. Body force

The body force/ forcing function is described as a vector-valued 2-form. In the physical domain, this can be written as

$$\mathbf{f} = \frac{\partial}{\partial x} \otimes f_x \mathrm{d}x\mathrm{d}y + \frac{\partial}{\partial y} \otimes f_y \mathrm{d}x\mathrm{d}y, \tag{8.6}$$

while in the reference domain

$$\mathbf{f} = \frac{\partial}{\partial \xi} \otimes f_\xi \mathrm{d}\xi\mathrm{d}\eta + \frac{\partial}{\partial \eta} \otimes f_\eta \mathrm{d}\xi\mathrm{d}\eta. \tag{8.7}$$

Thus, we can convert between the two domains as

$$\begin{aligned} f_x &= \frac{1}{\det \mathcal{J}} \left[f_\xi \frac{\partial x}{\partial \xi} + f_\eta \frac{\partial x}{\partial \eta} \right] \\ f_y &= \frac{1}{\det \mathcal{J}} \left[f_\xi \frac{\partial y}{\partial \xi} + f_\eta \frac{\partial y}{\partial \eta} \right], \end{aligned}$$

and

$$\begin{aligned} f_\xi &= f_x \frac{\partial y}{\partial \eta} - f_y \frac{\partial x}{\partial \eta} \\ f_\eta &= -f_x \frac{\partial y}{\partial \xi} + f_y \frac{\partial x}{\partial \xi}. \end{aligned}$$

8.2. Equations in the reference domain

The aim of this section is to translate the equations which were already derived in the physical/cartesian domain into the reference domain. By doing this, the result should be such that the solution obtained in the reference domain should be analogous to how the solution would be obtained had the equations been solved in the physical domain itself.

8.2.1. Constitutive law

For isotropic linear elastic materials, the compliance tensor can be described using only the elastic modulus E and the Poisson's ratio ν. This means that the constitutive relations can be written as

$$\begin{aligned} C_{11}\sigma_{xx} + C_{14}\sigma_{yy} &= \frac{\partial u_x}{\partial x} \\ C_{22}\sigma_{yx} &= \frac{\partial u_x}{\partial y} + \omega \\ C_{33}\sigma_{xy} &= \frac{\partial u_y}{\partial x} - \omega \\ C_{44}\sigma_{yy} + C_{41}\sigma_{xx} &= \frac{\partial u_y}{\partial y}, \end{aligned}$$

where

$$\begin{aligned} C_{11} = C_{44} &= \frac{1}{E} \\ C_{22} = C_{33} &= \frac{(1+\nu)}{E} \\ C_{14} = C_{41} &= -\frac{\nu}{E} \end{aligned}$$

with ν being the Poisson's ratio, and E being the Young's modulus of the material.

In order to make it easier to rewrite the components, the stress tensor will be written in a vector format $\boldsymbol{\sigma}^h_{x,y} = \begin{bmatrix}\sigma^h_{xx} & \sigma^h_{yx} & \sigma^h_{xy} & \sigma^h_{yy}\end{bmatrix}^T$, while in the reference domain, it would look like $\boldsymbol{\sigma}^h_{\xi,\eta} = \begin{bmatrix}\sigma^h_{\xi\xi} & \sigma^h_{\eta\xi} & \sigma^h_{\xi\eta} & \sigma^h_{\eta\eta}\end{bmatrix}^T$

The linear operator to convert the physical stresses into their reference domain counterparts can be written as

$$\begin{bmatrix} \sigma_{xx} \\ \sigma_{yx} \\ \sigma_{xy} \\ \sigma_{yy} \end{bmatrix} = F_\sigma \begin{bmatrix} \sigma_{\xi\xi} \\ \sigma_{\eta\xi} \\ \sigma_{\xi\eta} \\ \sigma_{\eta\eta} \end{bmatrix}, \tag{8.8}$$

where

$$F_\sigma = \begin{bmatrix} \frac{\partial \eta}{\partial y} & -\frac{\partial \xi}{\partial y} & 0 & 0 \\ -\frac{\partial \eta}{\partial x} & \frac{\partial \xi}{\partial x} & 0 & 0 \\ 0 & 0 & \frac{\partial \eta}{\partial y} & -\frac{\partial \xi}{\partial y} \\ 0 & 0 & -\frac{\partial \eta}{\partial x} & \frac{\partial \xi}{\partial x} \end{bmatrix} \begin{bmatrix} \frac{\partial x}{\partial \xi} & 0 & \frac{\partial x}{\partial \eta} & 0 \\ 0 & \frac{\partial x}{\partial \xi} & 0 & \frac{\partial x}{\partial \eta} \\ \frac{\partial y}{\partial \xi} & 0 & \frac{\partial y}{\partial \eta} & 0 \\ 0 & \frac{\partial y}{\partial \xi} & 0 & \frac{\partial y}{\partial \eta} \end{bmatrix}.$$

To convert this in the reference domain, we need to rewrite the stress components in the physical domain into their respective counterparts in the reference domain. In addition, the derivatives can be rewritten as

$$\begin{aligned} \frac{\partial}{\partial x} &= \frac{\partial \xi}{\partial x}\frac{\partial}{\partial \xi} + \frac{\partial \eta}{\partial x}\frac{\partial}{\partial \eta} \\ \frac{\partial}{\partial y} &= \frac{\partial \xi}{\partial y}\frac{\partial}{\partial \xi} + \frac{\partial \eta}{\partial y}\frac{\partial}{\partial \eta}. \end{aligned}$$

Thus, if the components of the gradient of displacement in the physical domain are written as a vector $\nabla_{x,y} u = \begin{bmatrix}\frac{\partial u_x}{\partial x} & \frac{\partial u_x}{\partial y} & \frac{\partial u_y}{\partial x} & \frac{\partial u_y}{\partial y}\end{bmatrix}^T$, while its counterpart in the reference domain is $\nabla_{\xi,\eta} u = \begin{bmatrix}\frac{\partial u_\xi}{\partial \xi} & \frac{\partial u_\xi}{\partial \eta} & \frac{\partial u_\eta}{\partial \xi} & \frac{\partial u_\eta}{\partial \eta}\end{bmatrix}^T$, then they can be related as

$$\begin{bmatrix} \frac{\partial u_x}{\partial x} \\ \frac{\partial u_x}{\partial y} \\ \frac{\partial u_y}{\partial x} \\ \frac{\partial u_y}{\partial y} \end{bmatrix} = F_u \begin{bmatrix} \frac{\partial u_\xi}{\partial \xi} \\ \frac{\partial u_\xi}{\partial \eta} \\ \frac{\partial u_\eta}{\partial \xi} \\ \frac{\partial u_\eta}{\partial \eta} \end{bmatrix}, \tag{8.9}$$

where

$$F_u = \begin{bmatrix} \frac{\partial \xi}{\partial x} & \frac{\partial \eta}{\partial x} & 0 & 0 \\ \frac{\partial \xi}{\partial y} & \frac{\partial \eta}{\partial y} & 0 & 0 \\ 0 & 0 & \frac{\partial \xi}{\partial x} & \frac{\partial \eta}{\partial x} \\ 0 & 0 & \frac{\partial \xi}{\partial y} & \frac{\partial \eta}{\partial y} \end{bmatrix} \begin{bmatrix} \frac{\partial \xi}{\partial x} & 0 & \frac{\partial \eta}{\partial x} & 0 \\ 0 & \frac{\partial \xi}{\partial x} & 0 & \frac{\partial \eta}{\partial x} \\ \frac{\partial \xi}{\partial y} & 0 & \frac{\partial \eta}{\partial y} & 0 \\ 0 & \frac{\partial \xi}{\partial y} & 0 & \frac{\partial \eta}{\partial y} \end{bmatrix}.$$

Now, rewriting the constitutive equation in terms of $\boldsymbol{\sigma}^h_{\xi,\eta}$ and $\nabla_{\xi,\eta} u$, we have

$$[\boldsymbol{C}] \left[F_\sigma \boldsymbol{\sigma}^h_{\xi,\eta}\right] = [F_u \nabla_{\xi,\eta} u] + \begin{bmatrix} 0 \\ \omega \\ -\omega \\ 0 \end{bmatrix}.$$

This means that the relation can be rewritten by taking the linear operator F_u^{-1} over the equation as

$$[\boldsymbol{C'}] \left[\boldsymbol{\sigma}^h_{\xi,\eta}\right] = [\nabla_{\xi,\eta} u] + (\det \mathcal{J}) [\mathbf{R}] \left[\boldsymbol{\omega}^h\right]. \tag{8.10}$$

Here,

$$[\mathbf{R}] = \begin{bmatrix} 0 \\ 1 \\ -1 \\ 0 \end{bmatrix},$$

and

$$[\boldsymbol{C'}] = \begin{bmatrix} C'_{11} & C'_{12} & C'_{13} & C'_{14} \\ C'_{21} & C'_{22} & C'_{23} & C'_{24} \\ C'_{31} & C'_{32} & C'_{33} & C'_{34} \\ C'_{41} & C'_{42} & C'_{43} & C'_{44} \end{bmatrix},$$

where

$$
\begin{aligned}
C'_{11} &= \left(\frac{\partial x}{\partial \xi}\right)^2 \left[C_{11}\left(\frac{\partial \eta}{\partial y}\frac{\partial x}{\partial \xi}\right) + C_{14}\left(-\frac{\partial \eta}{\partial x}\frac{\partial y}{\partial \xi}\right)\right] + \left(\frac{\partial x}{\partial \xi}\frac{\partial y}{\partial \xi}\right)\left[C_{22}\left(-\frac{\partial \eta}{\partial x}\frac{\partial x}{\partial \xi}\right) + C_{33}\left(\frac{\partial \eta}{\partial y}\frac{\partial y}{\partial \xi}\right)\right] \\
&\quad + \left(\frac{\partial y}{\partial \xi}\right)^2 \left[C_{41}\left(\frac{\partial \eta}{\partial y}\frac{\partial x}{\partial \xi}\right) + C_{44}\left(-\frac{\partial \eta}{\partial x}\frac{\partial y}{\partial \xi}\right)\right], \\
C'_{12} &= \left(\frac{\partial x}{\partial \xi}\right)^2 \left[C_{11}\left(-\frac{\partial \xi}{\partial y}\frac{\partial x}{\partial \xi}\right) + C_{14}\left(\frac{\partial \xi}{\partial x}\frac{\partial y}{\partial \xi}\right)\right] + \left(\frac{\partial x}{\partial \xi}\frac{\partial y}{\partial \xi}\right)\left[C_{22}\left(\frac{\partial \xi}{\partial x}\frac{\partial x}{\partial \xi}\right) + C_{33}\left(-\frac{\partial \xi}{\partial y}\frac{\partial y}{\partial \xi}\right)\right] \\
&\quad + \left(\frac{\partial y}{\partial \xi}\right)^2 \left[C_{41}\left(-\frac{\partial \xi}{\partial y}\frac{\partial x}{\partial \xi}\right) + C_{44}\left(\frac{\partial \xi}{\partial x}\frac{\partial y}{\partial \xi}\right)\right], \\
C'_{13} &= \left(\frac{\partial x}{\partial \xi}\right)^2 \left[C_{11}\left(\frac{\partial \eta}{\partial y}\frac{\partial x}{\partial \eta}\right) + C_{14}\left(-\frac{\partial \eta}{\partial x}\frac{\partial y}{\partial \eta}\right)\right] + \left(\frac{\partial x}{\partial \xi}\frac{\partial y}{\partial \xi}\right)\left[C_{22}\left(-\frac{\partial \eta}{\partial x}\frac{\partial x}{\partial \eta}\right) + C_{33}\left(-\frac{\partial \xi}{\partial y}\frac{\partial y}{\partial \eta}\right)\right] \\
&\quad + \left(\frac{\partial y}{\partial \xi}\right)^2 \left[C_{41}\left(\frac{\partial \eta}{\partial y}\frac{\partial x}{\partial \eta}\right) + C_{44}\left(-\frac{\partial \eta}{\partial x}\frac{\partial y}{\partial \eta}\right)\right], \\
C'_{14} &= \left(\frac{\partial x}{\partial \xi}\right)^2 \left[C_{11}\left(-\frac{\partial \xi}{\partial y}\frac{\partial x}{\partial \eta}\right) + C_{14}\left(\frac{\partial \xi}{\partial x}\frac{\partial y}{\partial \eta}\right)\right] + \left(\frac{\partial x}{\partial \xi}\frac{\partial y}{\partial \xi}\right)\left[C_{22}\left(\frac{\partial \xi}{\partial x}\frac{\partial x}{\partial \eta}\right) + C_{33}\left(-\frac{\partial \xi}{\partial y}\frac{\partial y}{\partial \eta}\right)\right] \\
&\quad + \left(\frac{\partial y}{\partial \xi}\right)^2 \left[C_{41}\left(-\frac{\partial \xi}{\partial y}\frac{\partial x}{\partial \eta}\right) + C_{44}\left(\frac{\partial \xi}{\partial x}\frac{\partial y}{\partial \eta}\right)\right], \\
C'_{21} &= \left(\frac{\partial x}{\partial \xi}\frac{\partial x}{\partial \eta}\right)\left[C_{11}\left(\frac{\partial \eta}{\partial y}\frac{\partial x}{\partial \xi}\right) + C_{14}\left(-\frac{\partial \eta}{\partial x}\frac{\partial y}{\partial \xi}\right)\right] + \left(\frac{\partial x}{\partial \xi}\frac{\partial y}{\partial \eta}\right)\left[-C_{22}\frac{\partial \eta}{\partial x}\frac{\partial x}{\partial \xi}\right] \\
&\quad + \left(\frac{\partial y}{\partial \xi}\frac{\partial x}{\partial \eta}\right)\left[C_{33}\frac{\partial \eta}{\partial y}\frac{\partial y}{\partial \xi}\right] + \left(\frac{\partial y}{\partial \xi}\frac{\partial y}{\partial \eta}\right)\left[C_{41}\left(\frac{\partial \eta}{\partial y}\frac{\partial x}{\partial \xi}\right) + C_{44}\left(-\frac{\partial \eta}{\partial x}\frac{\partial y}{\partial \xi}\right)\right], \\
C'_{22} &= \left(\frac{\partial x}{\partial \xi}\frac{\partial x}{\partial \eta}\right)\left[C_{11}\left(-\frac{\partial \xi}{\partial y}\frac{\partial x}{\partial \xi}\right) + C_{14}\left(\frac{\partial \xi}{\partial x}\frac{\partial y}{\partial \xi}\right)\right] + \left(\frac{\partial x}{\partial \xi}\frac{\partial y}{\partial \eta}\right)\left[C_{22}\left(\frac{\partial \xi}{\partial x}\frac{\partial x}{\partial \xi}\right)\right] \\
&\quad + \left(\frac{\partial y}{\partial \xi}\frac{\partial x}{\partial \eta}\right)\left[-C_{33}\frac{\partial \xi}{\partial y}\frac{\partial y}{\partial \xi}\right] + \left(\frac{\partial y}{\partial \xi}\frac{\partial y}{\partial \eta}\right)\left[C_{41}\left(-\frac{\partial \xi}{\partial y}\frac{\partial x}{\partial \xi}\right) + C_{44}\left(\frac{\partial \xi}{\partial x}\frac{\partial y}{\partial \xi}\right)\right], \\
C'_{23} &= \left(\frac{\partial x}{\partial \xi}\frac{\partial x}{\partial \eta}\right)\left[C_{11}\left(\frac{\partial \eta}{\partial y}\frac{\partial x}{\partial \eta}\right) + C_{14}\left(-\frac{\partial \eta}{\partial x}\frac{\partial y}{\partial \eta}\right)\right] + \left(\frac{\partial x}{\partial \xi}\frac{\partial y}{\partial \eta}\right)\left[C_{22}\left(-\frac{\partial \eta}{\partial x}\frac{\partial x}{\partial \eta}\right)\right] \\
&\quad + \left(\frac{\partial y}{\partial \xi}\frac{\partial x}{\partial \eta}\right)\left[C_{33}\left(-\frac{\partial \xi}{\partial y}\frac{\partial y}{\partial \eta}\right)\right] + \left(\frac{\partial y}{\partial \xi}\frac{\partial y}{\partial \eta}\right)\left[C_{41}\left(\frac{\partial \eta}{\partial y}\frac{\partial x}{\partial \eta}\right) + C_{44}\left(-\frac{\partial \eta}{\partial x}\frac{\partial y}{\partial \eta}\right)\right], \\
C'_{24} &= \left(\frac{\partial x}{\partial \xi}\frac{\partial x}{\partial \eta}\right)\left[C_{11}\left(-\frac{\partial \xi}{\partial y}\frac{\partial x}{\partial \eta}\right) + C_{14}\left(\frac{\partial \xi}{\partial x}\frac{\partial y}{\partial \eta}\right)\right] + \left(\frac{\partial x}{\partial \xi}\frac{\partial y}{\partial \eta}\right)\left[C_{22}\left(\frac{\partial \xi}{\partial x}\frac{\partial x}{\partial \eta}\right)\right] \\
&\quad + \left(\frac{\partial y}{\partial \xi}\frac{\partial x}{\partial \eta}\right)\left[C_{33}\left(-\frac{\partial \xi}{\partial y}\frac{\partial y}{\partial \eta}\right)\right] + \left(\frac{\partial y}{\partial \xi}\right)^2\left[C_{41}\left(-\frac{\partial \xi}{\partial y}\frac{\partial x}{\partial \eta}\right) + C_{44}\left(\frac{\partial \xi}{\partial x}\frac{\partial y}{\partial \eta}\right)\right], \\
C'_{31} &= \left(\frac{\partial x}{\partial \xi}\frac{\partial x}{\partial \eta}\right)\left[C_{11}\left(\frac{\partial \eta}{\partial y}\frac{\partial x}{\partial \xi}\right) + C_{14}\left(-\frac{\partial \eta}{\partial x}\frac{\partial y}{\partial \xi}\right)\right] + \left(\frac{\partial x}{\partial \eta}\frac{\partial y}{\partial \xi}\right)\left[-C_{22}\frac{\partial \eta}{\partial x}\frac{\partial x}{\partial \xi}\right] \\
&\quad + \left(\frac{\partial y}{\partial \eta}\frac{\partial x}{\partial \xi}\right)\left[C_{33}\frac{\partial \eta}{\partial y}\frac{\partial y}{\partial \xi}\right] + \left(\frac{\partial y}{\partial \xi}\frac{\partial y}{\partial \eta}\right)\left[C_{41}\left(\frac{\partial \eta}{\partial y}\frac{\partial x}{\partial \xi}\right) + C_{44}\left(-\frac{\partial \eta}{\partial x}\frac{\partial y}{\partial \xi}\right)\right], \\
C'_{32} &= \left(\frac{\partial x}{\partial \xi}\frac{\partial x}{\partial \eta}\right)\left[C_{11}\left(-\frac{\partial \xi}{\partial y}\frac{\partial x}{\partial \xi}\right) + C_{14}\left(\frac{\partial \xi}{\partial x}\frac{\partial y}{\partial \xi}\right)\right] + \left(\frac{\partial x}{\partial \eta}\frac{\partial y}{\partial \xi}\right)\left[C_{22}\left(\frac{\partial \xi}{\partial x}\frac{\partial x}{\partial \xi}\right)\right] \\
&\quad + \left(\frac{\partial y}{\partial \eta}\frac{\partial x}{\partial \xi}\right)\left[-C_{33}\frac{\partial \xi}{\partial y}\frac{\partial y}{\partial \xi}\right] + \left(\frac{\partial y}{\partial \xi}\frac{\partial y}{\partial \eta}\right)\left[C_{41}\left(-\frac{\partial \xi}{\partial y}\frac{\partial x}{\partial \xi}\right) + C_{44}\left(\frac{\partial \xi}{\partial x}\frac{\partial y}{\partial \xi}\right)\right]
\end{aligned}
$$

,

$$
\begin{aligned}
C'_{33} &= \left(\frac{\partial x}{\partial \xi}\frac{\partial x}{\partial \eta}\right)\left[C_{11}\left(\frac{\partial \eta}{\partial y}\frac{\partial x}{\partial \eta}\right)+C_{14}\left(-\frac{\partial \eta}{\partial x}\frac{\partial y}{\partial \eta}\right)\right]+\left(\frac{\partial x}{\partial \eta}\frac{\partial y}{\partial \xi}\right)\left[C_{22}\left(-\frac{\partial \eta}{\partial x}\frac{\partial x}{\partial \eta}\right)\right]\\
&+\left(\frac{\partial y}{\partial \eta}\frac{\partial x}{\partial \xi}\right)\left[C_{33}\left(-\frac{\partial \xi}{\partial y}\frac{\partial y}{\partial \eta}\right)\right]+\left(\frac{\partial y}{\partial \xi}\frac{\partial y}{\partial \eta}\right)\left[C_{41}\left(\frac{\partial \eta}{\partial y}\frac{\partial x}{\partial \eta}\right)+C_{44}\left(-\frac{\partial \eta}{\partial x}\frac{\partial y}{\partial \eta}\right)\right],\\
C'_{34} &= \left(\frac{\partial x}{\partial \xi}\frac{\partial x}{\partial \eta}\right)\left[C_{11}\left(-\frac{\partial \xi}{\partial y}\frac{\partial x}{\partial \eta}\right)+C_{14}\left(\frac{\partial \xi}{\partial x}\frac{\partial y}{\partial \eta}\right)\right]+\left(\frac{\partial x}{\partial \eta}\frac{\partial y}{\partial \xi}\right)\left[C_{22}\left(\frac{\partial \xi}{\partial x}\frac{\partial x}{\partial \eta}\right)\right]\\
&+\left(\frac{\partial y}{\partial \eta}\frac{\partial x}{\partial \xi}\right)\left[C_{33}\left(-\frac{\partial \xi}{\partial y}\frac{\partial y}{\partial \eta}\right)\right]+\left(\frac{\partial y}{\partial \xi}\right)^2\left[C_{41}\left(-\frac{\partial \xi}{\partial y}\frac{\partial x}{\partial \eta}\right)+C_{44}\left(\frac{\partial \xi}{\partial x}\frac{\partial y}{\partial \eta}\right)\right],\\
C'_{41} &= \left(\frac{\partial x}{\partial \eta}\right)^2\left[C_{11}\left(\frac{\partial \eta}{\partial y}\frac{\partial x}{\partial \xi}\right)+C_{14}\left(-\frac{\partial \eta}{\partial x}\frac{\partial y}{\partial \xi}\right)\right]+\left(\frac{\partial x}{\partial \eta}\frac{\partial y}{\partial \eta}\right)\left[C_{22}\left(-\frac{\partial \eta}{\partial x}\frac{\partial x}{\partial \xi}\right)+C_{33}\left(\frac{\partial \eta}{\partial y}\frac{\partial y}{\partial \xi}\right)\right]\\
&+\left(\frac{\partial y}{\partial \eta}\right)^2\left[C_{41}\left(\frac{\partial \eta}{\partial y}\frac{\partial x}{\partial \xi}\right)+C_{44}\left(-\frac{\partial \eta}{\partial x}\frac{\partial y}{\partial \xi}\right)\right],\\
C'_{42} &= \left(\frac{\partial x}{\partial \eta}\right)^2\left[C_{11}\left(-\frac{\partial \xi}{\partial y}\frac{\partial x}{\partial \xi}\right)+C_{14}\left(\frac{\partial \xi}{\partial x}\frac{\partial y}{\partial \xi}\right)\right]+\left(\frac{\partial x}{\partial \eta}\frac{\partial y}{\partial \eta}\right)\left[C_{22}\left(\frac{\partial \xi}{\partial x}\frac{\partial x}{\partial \xi}\right)+C_{33}\left(-\frac{\partial \xi}{\partial y}\frac{\partial y}{\partial \xi}\right)\right]\\
&+\left(\frac{\partial y}{\partial \eta}\right)^2\left[C_{41}\left(-\frac{\partial \xi}{\partial y}\frac{\partial x}{\partial \xi}\right)+C_{44}\left(\frac{\partial \xi}{\partial x}\frac{\partial y}{\partial \xi}\right)\right],\\
C'_{43} &= \left(\frac{\partial x}{\partial \eta}\right)^2\left[C_{11}\left(\frac{\partial \eta}{\partial y}\frac{\partial x}{\partial \eta}\right)+C_{14}\left(-\frac{\partial \eta}{\partial x}\frac{\partial y}{\partial \eta}\right)\right]+\left(\frac{\partial x}{\partial \eta}\frac{\partial y}{\partial \eta}\right)\left[C_{22}\left(-\frac{\partial \eta}{\partial x}\frac{\partial x}{\partial \eta}\right)+C_{33}\left(-\frac{\partial \xi}{\partial y}\frac{\partial y}{\partial \eta}\right)\right]\\
&+\left(\frac{\partial y}{\partial \eta}\right)^2\left[C_{41}\left(\frac{\partial \eta}{\partial y}\frac{\partial x}{\partial \eta}\right)+C_{44}\left(-\frac{\partial \eta}{\partial x}\frac{\partial y}{\partial \eta}\right)\right],\\
C'_{44} &= \left(\frac{\partial x}{\partial \eta}\right)^2\left[C_{11}\left(-\frac{\partial \xi}{\partial y}\frac{\partial x}{\partial \eta}\right)+C_{14}\left(\frac{\partial \xi}{\partial x}\frac{\partial y}{\partial \eta}\right)\right]+\left(\frac{\partial x}{\partial \eta}\frac{\partial y}{\partial \eta}\right)\left[C_{22}\left(\frac{\partial \xi}{\partial x}\frac{\partial x}{\partial \eta}\right)+C_{33}\left(-\frac{\partial \xi}{\partial y}\frac{\partial y}{\partial \eta}\right)\right]\\
&+\left(\frac{\partial y}{\partial \eta}\right)^2\left[C_{41}\left(-\frac{\partial \xi}{\partial y}\frac{\partial x}{\partial \eta}\right)+C_{44}\left(\frac{\partial \xi}{\partial x}\frac{\partial y}{\partial \eta}\right)\right].
\end{aligned}
$$

and

$$
\begin{bmatrix} \frac{\partial \xi}{\partial x} & \frac{\partial \xi}{\partial y} \\ \frac{\partial \eta}{\partial x} & \frac{\partial \eta}{\partial y} \end{bmatrix} = \begin{bmatrix} \frac{\partial x}{\partial \xi} & \frac{\partial x}{\partial \eta} \\ \frac{\partial y}{\partial \xi} & \frac{\partial y}{\partial \eta} \end{bmatrix}^{-1} = \frac{1}{\det \mathcal{J}} \begin{bmatrix} \frac{\partial y}{\partial \eta} & -\frac{\partial x}{\partial \eta} \\ -\frac{\partial y}{\partial \xi} & \frac{\partial x}{\partial \xi} \end{bmatrix}.
$$

These equations can be used for assigning values to the matrices associated with the stress mass matrix, and the mass matrix corresponding to the rotation tensor.

8.2.2. Conservation of linear momentum

With the Lagrangian stresses, the conservation of linear momentum can be written down as

$$
\begin{aligned}
\frac{\partial \sigma_{\xi x}}{\partial \xi}+\frac{\partial \sigma_{\eta x}}{\partial \eta}+(f_x \det \mathcal{J}) &= 0\\
\frac{\partial \sigma_{\xi y}}{\partial \xi}+\frac{\partial \sigma_{\eta y}}{\partial \eta}+(f_y \det \mathcal{J}) &= 0
\end{aligned}
$$

Therefore,

$$
\begin{aligned}
\left(\frac{\partial \sigma_{\xi x}}{\partial \xi}\frac{\partial \xi}{\partial x}+\frac{\partial \sigma_{\xi y}}{\partial \xi}\frac{\partial \xi}{\partial y}\right)+\left(\frac{\partial \sigma_{\eta x}}{\partial \eta}\frac{\partial \xi}{\partial x}+\frac{\partial \sigma_{\eta y}}{\partial \eta}\frac{\partial \xi}{\partial y}\right)+\det \mathcal{J}\left(f_x\frac{\partial \xi}{\partial x}+f_y\frac{\partial \xi}{\partial y}\right) &= 0\\
\left(\frac{\partial \sigma_{\xi x}}{\partial \xi}\frac{\partial \eta}{\partial x}+\frac{\partial \sigma_{\xi y}}{\partial \xi}\frac{\partial \eta}{\partial y}\right)+\left(\frac{\partial \sigma_{\eta x}}{\partial \eta}\frac{\partial \eta}{\partial x}+\frac{\partial \sigma_{\eta y}}{\partial \eta}\frac{\partial \eta}{\partial y}\right)+\det \mathcal{J}\left(f_x\frac{\partial \xi}{\partial x}+f_y\frac{\partial \xi}{\partial y}\right) &= 0
\end{aligned}
$$

Since the components of the inverse Jacobian $\frac{\partial \xi}{\partial x}, \frac{\partial \xi}{\partial y}, \frac{\partial \eta}{\partial x}, \frac{\partial \eta}{\partial y}$ are invariant under ξ or η, these components can be taken under the differential. Then, these equations can be rewritten in terms of the reference stresses as

$$\frac{\partial \sigma_{\xi\xi}}{\partial \xi} + \frac{\partial \sigma_{\eta\xi}}{\partial \eta} + f_\xi = 0 \tag{8.11}$$

$$\frac{\partial \sigma_{\xi\eta}}{\partial \xi} + \frac{\partial \sigma_{\eta\eta}}{\partial \eta} + f_\eta = 0 \tag{8.12}$$

This is also why stress is written as a vector-valued quantity. If it was written as a covector-valued quantity, you would need to multiply the equations with components of Jacobian, which may not be invariant under ξ and η, unlike the components of the inverse Jacobian.

8.3. Theoretical formulation

By converting the stresses and displacements to their respective components in the reference domain, the idea is to solve these equations completely in the reference domain.

For this, the theoretical formulation (in the reference domain) can be written as

$$\mathcal{L}\Big(\underline{\underline{\boldsymbol{\sigma}}}, \mathbf{u}, \boldsymbol{\omega}, \underline{\underline{\mathbf{C}'}}\Big) = \begin{array}{l} \int_{\hat{\Omega}} \boldsymbol{\omega} \det J \Big(\sigma_{\xi\eta} - \sigma_{\eta\xi}\Big) \mathrm{d}\hat{\Omega} \\ + \int_{\hat{\Omega}} \Big(\big(u_\xi \frac{\partial \sigma_{\xi\xi}}{\partial \xi} - \frac{\partial u_\xi}{\partial \eta}\sigma_{\eta\xi} - \frac{\partial u_\eta}{\partial \xi}\sigma_{\xi\eta} + u_\eta \frac{\partial \sigma_{\eta\eta}}{\partial \eta}\big) + u_\xi f_\xi + u_\eta f_\eta \Big) \mathrm{d}\hat{\Omega} \\ + \int_{\hat{\Omega}} \Big(\frac{1}{2} \underline{\underline{\boldsymbol{\sigma}}}^T (\underline{\underline{\mathbf{C}'}}) \underline{\underline{\boldsymbol{\sigma}}} \Big) \mathrm{d}\hat{\Omega} \\ - \oint_{\partial\hat{\Omega}} \big((u_\xi)_P \sigma_{\xi\xi} n_\xi + (u_\eta)_P \sigma_{\eta\eta} n_\eta \big) \mathrm{d}\Gamma \\ + \oint_{\partial\hat{\Omega}} \big(u_\xi (\sigma_{\eta\xi})_P n_\eta + u_\eta (\sigma_{\xi\eta})_P n_\xi \big) \mathrm{d}\Gamma \end{array}, \tag{8.13}$$

where components of $\underline{\underline{\mathbf{C}'}}$ are listed previously.

8.3.1. Constitutional Law

On taking the variational derivative of the functional with respect to $\underline{\underline{\boldsymbol{\sigma}}}$ and equating it to 0, the functional reduces to

$$\begin{array}{l} \int_{\hat{\Omega}} \Big(\boldsymbol{\omega} (\det \mathcal{J}) \Big(\widetilde{\sigma_{\xi\eta}} - \widetilde{\sigma_{\eta\xi}} \Big) \mathrm{d}\hat{\Omega} \\ + \int_{\hat{\Omega}} \Big(u_\xi \frac{\partial \widetilde{\sigma_{\xi\xi}}}{\partial \xi} - \frac{\partial u_\xi}{\partial \eta}\widetilde{\sigma_{\eta\xi}} - \frac{\partial u_\eta}{\partial \xi}\widetilde{\sigma_{\xi\eta}} + u_\eta \frac{\partial \widetilde{\sigma_{\eta\eta}}}{\partial \eta} \Big) \mathrm{d}\hat{\Omega} \quad = B_\sigma, \\ + \int_{\hat{\Omega}} \underline{\underline{\widetilde{\boldsymbol{\sigma}}}}^T (\underline{\underline{\mathbf{C}'}}) \underline{\underline{\boldsymbol{\sigma}}} \Big) \mathrm{d}\hat{\Omega} \end{array} \tag{8.14}$$

which is the equation that is solved in the formulation.

Using integration by parts, it can be seen that

$$\begin{array}{l} \int_{\hat{\Omega}} \Big(\boldsymbol{\omega} (\det \mathcal{J}) \Big(\widetilde{\sigma_{\xi\eta}} - \widetilde{\sigma_{\eta\xi}} \Big) \mathrm{d}\hat{\Omega} \\ + \int_{\hat{\Omega}} \Big(- \frac{\partial u_\xi}{\partial \xi}\widetilde{\sigma_{\xi\xi}} - \frac{\partial u_\xi}{\partial \eta}\widetilde{\sigma_{\eta\xi}} - \frac{\partial u_\eta}{\partial \xi}\widetilde{\sigma_{\xi\eta}} - \frac{\partial u_\eta}{\partial \eta}\widetilde{\sigma_{\eta\eta}} \Big) \mathrm{d}\hat{\Omega} \quad = 0. \\ + \int_{\hat{\Omega}} \underline{\underline{\widetilde{\boldsymbol{\sigma}}}}^T (\underline{\underline{\mathbf{C}'}}) \underline{\underline{\boldsymbol{\sigma}}} \Big) \mathrm{d}\hat{\Omega} \end{array}$$

Assuming that this holds for any arbitrary value of $\underline{\underline{\widetilde{\boldsymbol{\sigma}}}}$, this will give the constitutive law derived previously.

An important consideration is that

$$\mathcal{B}_\sigma = \oint_{\partial\hat{\Omega}} \big((u_\xi)_P \widetilde{\sigma_{\xi\xi}} n_\xi + (u_\eta)_P \widetilde{\sigma_{\eta\eta}} n_\eta \big) \mathrm{d}\Gamma, \tag{8.15}$$

which makes sure that the correct constitutive relation is solved, using the values of the displacement at the normal boundaries.

8.3.2. Conservation of linear momentum

On taking the variational derivative of the functional with respect to $\mathbf{u}$ and equating it to zero, the functional reduces to

$$\int_{\hat{\Omega}} \Big(u_\xi \frac{\partial \sigma_{\xi\xi}}{\partial \xi} - \frac{\partial u_\xi}{\partial \eta}\sigma_{\eta\xi} - \frac{\partial u_\eta}{\partial \xi}\sigma_{\xi\eta} + u_\eta \frac{\partial \sigma_{\eta\eta}}{\partial \eta} + u_\xi f_\xi + u_\eta f_\eta \Big) \mathrm{d}\Omega = -B_{\mathbf{u}}, \tag{8.16}$$

where

$$B_{\mathbf{u}} = \oint_{\partial\hat{\Omega}} \left(\widetilde{u_\xi}(\sigma_{\eta\xi})_P n_\eta + \widetilde{u_\eta}(\sigma_{\xi\eta})_P n_\xi\right) \mathrm{d}\Gamma. \tag{8.17}$$

With an arbitrary $\widetilde{u_\xi}$ and $\widetilde{u_\eta}$ and assuming this holds for any arbitrary domain, it can be shown (using integration by parts) that these equations satisfy the equilibrium of forces, and thus the conservation of linear momentum.

8.3.3. Conservation of angular momentum

On taking the variational derivative of the functional with respect to $\boldsymbol{\omega}$ and equating it to zero, the functional reduces to

$$\int_{\hat{\Omega}} \widetilde{\boldsymbol{\omega}} \det \mathcal{J} \Big(\sigma_{\xi\eta} - \sigma_{\eta\xi}\Big) \mathrm{d}\Omega = 0. \tag{8.18}$$

This equation looks easier than its counterparts in Chapter 6 and Chapter 7. With an arbitrary $\widetilde{\boldsymbol{\omega}}$ and assuming this holds for any arbitrary domain, that means that angular momentum must be conserved, assuming that linear momentum is also conserved exactly.

8.4. Spectral bases

In this section, the expansion of the quantities in the reference domain is shown. The fully transformed stress components are the ones which are reduced onto the reference domain here, not the Lagrangian stresses as in previous formulations where the value part remains in the physical domain. The reason for this is to ensure that the fluxes at the boundaries of the element are exact, which happens only when the displacements are converted to the reference domain. When the value part of the displacements is converted to their reference counterparts in this way, the value part of the stress components also needs to be in their reference domain counterparts so that the inner duality pairing between the stress components and displacements can be made.

With this in mind, the stress components (fully-transformed) are written down as

$$\begin{aligned}
\overline{\sigma_{\xi\xi}} &= \sum_{i=1}^{N+1}\sum_{j=1}^{N+1} (\sigma_{\xi\xi})_{ij}\ h_i(\xi)\ e'_j(\eta) \\
\overline{\sigma_{\eta\xi}} &= \sum_{i=1}^{N}\sum_{j=1}^{N} (\sigma_{\eta\xi})_{ij}\ e_i(\xi)\ h'_j(\eta) \\
\overline{\sigma_{\xi\eta}} &= \sum_{i=1}^{N}\sum_{j=1}^{N} (\sigma_{\xi\eta})_{ij}\ h'_i(\xi)\ e_j(\eta) \\
\overline{\sigma_{\eta\eta}} &= \sum_{i=1}^{N+1}\sum_{j=1}^{N+1} (\sigma_{\eta\eta})_{ij}\ e'_i(\xi)\ h_j(\eta)
\end{aligned}$$

.

Note that these expansions are similar to the expansions used for the Lagrangian stresses used in Chapter 6.

For the conservation of linear momentum, the derivative of the normal stresses can be written as

$$\begin{aligned}
\widetilde{u_\xi}\frac{\partial\overline{\sigma_{\xi\xi}}}{\partial\xi} &= \widetilde{u_\xi}\left[\sum_{i=1}^{N}\sum_{j=1}^{N+1}\Big((\sigma_{\xi\xi})_{i+1,j} - (\sigma_{\xi\xi})_{i,j}\Big)\ e_i(\xi)\ e'_j(\eta)\right] \\
\widetilde{u_\eta}\frac{\partial\overline{\sigma_{\eta\eta}}}{\partial\eta} &= \widetilde{u_\eta}\left[\sum_{i=1}^{N+1}\sum_{j=1}^{N}\Big((\sigma_{\eta\eta})_{i,j+1} - (\sigma_{\eta\eta})_{i,j}\Big)\ e'_i(\xi)\ e_j(\eta)\right],
\end{aligned}$$

In order to make these relations topological, u_ξ and u_η have to dual to the expansions of $\frac{\partial\overline{\sigma_{\xi\xi}}}{\partial\xi}$ and $\frac{\partial\overline{\sigma_{\eta\eta}}}{\partial\eta}$ respectively. Thus,

$$\overline{u_\xi} = \sum_{i=1}^{N}\sum_{j=1}^{N+1}(u_\xi)_{ij}\ h_i'(\xi)\ h_j(\eta)$$
$$\overline{u_\eta} = \sum_{i=1}^{N+1}\sum_{j=1}^{N}(u_\eta)_{ij}\ h_i(\xi)\ h_j'(\eta)\ .$$

With these spectral bases for u_ξ and u_η, the other terms in the conservation of linear momentum $\frac{\partial u_\xi}{\partial \eta}\sigma_{\eta\xi}$ and $\frac{\partial u_\eta}{\partial \xi}\sigma_{\xi\eta}$ are also topological. This makes conservation of linear momentum topological.

The rotation is expanded as

$$\overline{\omega} = \sum_{i=1}^{N}\sum_{j=1}^{N}(\omega)_{ij}\ h_i'(\xi)\ h_j'(\eta)\ .$$

The stress components are converted into the dual of the spectral bases for ω and then the equation for the conservation of angular momentum is written down.

With these spectral bases, the system can be written to find the unknown degrees of freedom as

$$\begin{bmatrix} \mathbb{M}_\sigma & \mathbb{E}_\sigma^T & \mathbb{R}^T \\ \mathbb{E}_\sigma & 0 & 0 \\ \mathbb{R}_\sigma & 0 & 0 \end{bmatrix} \begin{bmatrix} \boldsymbol{\sigma}^h \\ \mathbf{u}^h \\ \boldsymbol{\omega}^h \end{bmatrix} = \begin{bmatrix} -\mathbf{g}_\sigma^h \\ -\mathbf{f}^h - \mathbf{g}_u^h \\ \mathbf{0} \end{bmatrix} \tag{8.19}$$

In this representation, let

$$\boldsymbol{\sigma}^h = \begin{bmatrix}\sigma_{\xi\xi}^h & \sigma_{\eta\xi}^h & \sigma_{\xi\eta}^h & \sigma_{\eta\eta}^h\end{bmatrix}^T, \tag{8.20}$$
$$\mathbf{u}^h = \begin{bmatrix}u_\xi^h & u_\eta^h\end{bmatrix}, \tag{8.21}$$

Making it easier to arrange the unknowns for the tensor and vector quantities. In addition, it should be easier to construct matrices if the quantities are arranged in this order.

The other terms in this system will be analysed in the following sections.

8.5. Incidence matrix

The conservation of linear momentum is designed to be topological in the computational (reference) domain. With this, the incidence matrix that needs to be made should not involve any terms other than ± 1 or 0.

With the stress degrees of freedom arranged as Equation 8.20, the matrix can be decomposed into two parts $(\mathbb{E}_\sigma)_\xi$ and $(\mathbb{E}_\sigma)_\eta$, written as

$$\mathbb{E}_\sigma = \begin{bmatrix} (\mathbb{E}_\sigma)_\xi & 0 \\ 0 & (\mathbb{E}_\sigma)_\eta \end{bmatrix}.$$

This decomposes the conservation of linear momentum into two directions, $\xi-$ and $\eta-$. $\widetilde{u_\xi}^h$ and $\widetilde{u_\eta}^h$ act as the Lagrange multipliers to enforce the equilibrium of forces in these directions respectively. Thus, $(\mathbb{E}_\sigma)_\xi$ is a linear operator on $[\sigma_{\xi\xi}^h \ \ \sigma_{\eta\xi}^h]$, while $(\mathbb{E}_\sigma)_\eta$ is a linear operator on $[\sigma_{\xi\eta}^h \ \ \sigma_{\eta\eta}^h]$.

Following the x-lexicographic arrangement for these degrees of freedom, the components of $\mathbb{E}_\sigma$ (for $N = 2$) are given below.

$$(\mathbb{E}_\sigma)_\xi = \begin{bmatrix} 1 & -1 & 0 & 0 & 0 & 0 & 0 & 0 & 0 & -1 & 0 & 0 & 0 \\ 0 & 1 & -1 & 0 & 0 & 0 & 0 & 0 & 0 & 0 & -1 & 0 & 0 \\ 0 & 0 & 0 & 1 & -1 & 0 & 0 & 0 & 0 & 1 & 0 & -1 & 0 \\ 0 & 0 & 0 & 0 & 1 & -1 & 0 & 0 & 0 & 0 & 1 & 0 & -1 \\ 0 & 0 & 0 & 0 & 0 & 0 & 1 & -1 & 0 & 0 & 0 & 1 & 0 \\ 0 & 0 & 0 & 0 & 0 & 0 & 0 & 1 & -1 & 0 & 0 & 0 & 1 \end{bmatrix}.$$

$$(\mathbb{E}_\sigma)_\eta = \begin{bmatrix} -1 & 0 & 0 & 0 & 1 & 0 & 0 & -1 & 0 & 0 & 0 & 0 & 0 \\ 1 & -1 & 0 & 0 & 0 & 1 & 0 & 0 & -1 & 0 & 0 & 0 & 0 \\ 0 & 1 & 0 & 0 & 0 & 0 & 1 & 0 & 0 & -1 & 0 & 0 & 0 \\ 0 & 0 & -1 & 0 & 0 & 0 & 0 & 1 & 0 & 0 & -1 & 0 & 0 \\ 0 & 0 & 1 & -1 & 0 & 0 & 0 & 0 & 1 & 0 & 0 & -1 & 0 \\ 0 & 0 & 0 & 1 & 0 & 0 & 0 & 0 & 0 & 1 & 0 & 0 & -1 \end{bmatrix}.$$

Note that the transpose of this matrix is also used in the constitutive relation.

8.6. Mass matrix

The mass matrix is referred to the equations in this formulation where the stress components themselves act as the Lagrange multipliers. Specifically, this is one of the mass matrices, which is used to enforce the constitutive law.

Because there are 4 stress components in the two-dimensional formulation, there are also 4 equations enforcing the constitutive relation. In general, the mass matrix can be written as $\left[(\widetilde{\boldsymbol{\sigma}}^h)^T \mathbb{M}_\sigma \boldsymbol{\sigma}^h\right]$. To make it easier to write it down, $\mathbb{M}_\sigma$ can be separated into 4 horizontal matrices, representing each of the constitutive equations, as

$$\mathbb{M}_\sigma = \begin{bmatrix} \mathbb{M}_1 \\ \mathbb{M}_2 \\ \mathbb{M}_3 \\ \mathbb{M}_4 \end{bmatrix}.$$

Let us look at how the different components are written down as.

8.6.1. Constitutive relation 1

This relation has $\widetilde{\sigma_{\xi\xi}}$ as the test function. With this

$$(\mathbb{M}_{11})_{ijkl} = \sum_{r=1}^{N_x}\sum_{s=1}^{N_x} C'_{11}(\xi_r,\eta_s)\, h_i(\xi_r)\, e'_j(\eta_s)\, h_k(\xi_r)\, e'_l(\eta_s)\, w_r\, w_s, \tag{8.22}$$

where w_r and w_s are the integration weights associated with the nodes at ξ_r and η_s using Gaussian quadrature, and N_x denotes the number of Gauss-Lobatto nodes used for quadrature.

Similarly,

$$(\mathbb{M}_{12})_{ijkl} = \sum_{r=1}^{N_x}\sum_{s=1}^{N_x} C'_{12}(\xi_r,\eta_s)\, e_i(\xi_r)\, h'_j(\eta_s)\, h_k(\xi_r)\, e'_l(\eta_s)\, w_r\, w_s. \tag{8.23}$$

$$(\mathbb{M}_{13})_{ijkl} = \sum_{r=1}^{N_x}\sum_{s=1}^{N_x} C'_{13}(\xi_r,\eta_s)\, h'_i(\xi_r)\, e_j(\eta_s)\, h_k(\xi_r)\, e'_l(\eta_s)\, w_r\, w_s. \tag{8.24}$$

$$(\mathbb{M}_{14})_{ijkl} = \sum_{r=1}^{N_x}\sum_{s=1}^{N_x} C'_{14}(\xi_r,\eta_s)\, e'_i(\xi_r)\, h_j(\eta_s)\, h_k(\xi_r)\, e'_l(\eta_s)\, w_r\, w_s. \tag{8.25}$$

Once these matrices are formed $\mathbb{M}_1 = [\mathbb{M}_{11}\ \ \mathbb{M}_{12}\ \ \mathbb{M}_{13}\ \ \mathbb{M}_{14}]$. The coefficients are those derived in (8.2.1).

8.6.2. Constitutive relation 2

A similar method to the way the matrices are derived can be used to determine the matrices for the second constitutive relation, with the test function being $\widetilde{\sigma_{\eta\xi}}$. The expressions are given below.

$$(\mathbb{M}_{21})_{ijkl} = \sum_{r=1}^{N_x}\sum_{s=1}^{N_x} C'_{21}(\xi_r,\eta_s)\, h_i(\xi_r)\, e'_j(\eta_s)\, e_k(\xi_r)\, h'_l(\eta_s)\, w_r\, w_s. \tag{8.26}$$

$$(\mathbb{M}_{22})_{ijkl} = \sum_{r=1}^{N_x}\sum_{s=1}^{N_x} C'_{22}(\xi_r,\eta_s)\, e_i(\xi_r)\, h'_j(\eta_s)\, e_k(\xi_r)\, h'_l(\eta_s)\, w_r\, w_s. \tag{8.27}$$

$$(\mathbb{M}_{23})_{ijkl} = \sum_{r=1}^{N_x}\sum_{s=1}^{N_x} C'_{23}(\xi_r,\eta_s)\, h'_i(\xi_r)\, e_j(\eta_s)\, e_k(\xi_r)\, h'_l(\eta_s)\, w_r\, w_s. \tag{8.28}$$

$$(\mathbb{M}_{24})_{ijkl} = \sum_{r=1}^{N_x}\sum_{s=1}^{N_x} C'_{24}\,(\xi_r,\eta_s)\,e'_i(\xi_r)\;h_j(\eta_s)\;e_k(\xi_r)\;h'_l(\eta_s)\,w_r\,w_s. \tag{8.29}$$

where the components of $\underline{\underline{\boldsymbol{C'}}}$ are what were derived in (8.2.1).
Then we get $\mathbb{M}_2 = [\mathbb{M}_{21}\;\;\mathbb{M}_{22}\;\;\mathbb{M}_{23}\;\;\mathbb{M}_{24}]$.

8.6.3. Constitutive relation 3

The third constitutive relation has $\widetilde{\sigma_{\xi\eta}}$ as the test function. The expressions are given below.

$$(\mathbb{M}_{31})_{ijkl} = \sum_{r=1}^{N_x}\sum_{s=1}^{N_x} C'_{31}\,(\xi_r,\eta_s)\,h_i(\xi_r)\;e'_j(\eta_s)\;h'_k(\xi_r)\;e_l(\eta_s)\,w_r\,w_s. \tag{8.30}$$

$$(\mathbb{M}_{32})_{ijkl} = \sum_{r=1}^{N_x}\sum_{s=1}^{N_x} C'_{32}\,(\xi_r,\eta_s)\,e_i(\xi_r)\;h'_j(\eta_s)\;h'_k(\xi_r)\;e_l(\eta_s)\,w_r\,w_s. \tag{8.31}$$

$$(\mathbb{M}_{33})_{ijkl} = \sum_{r=1}^{N_x}\sum_{s=1}^{N_x} C'_{33}\,(\xi_r,\eta_s)\,h'_i(\xi_r)\;e_j(\eta_s)\;h'_k(\xi_r)\;e_l(\eta_s)\,w_r\,w_s. \tag{8.32}$$

$$(\mathbb{M}_{34})_{ijkl} = \sum_{r=1}^{N_x}\sum_{s=1}^{N_x} C'_{34}\,(\xi_r,\eta_s)\,e'_i(\xi_r)\;h_j(\eta_s)\;h'_k(\xi_r)\;e_l(\eta_s)\,w_r\,w_s. \tag{8.33}$$

where the components of $\underline{\underline{\boldsymbol{C'}}}$ are what were derived in (subsection 8.2.1).
Then we get $\mathbb{M}_3 = [\mathbb{M}_{31}\;\;\mathbb{M}_{32}\;\;\mathbb{M}_{33}\;\;\mathbb{M}_{34}]$.

8.6.4. Constitutive relation 4

The third constitutive relation has $\widetilde{\sigma_{\eta\eta}}$ as the test function. The expressions are given below.

$$(\mathbb{M}_{41})_{ijkl} = \sum_{r=1}^{N_x}\sum_{s=1}^{N_x} C'_{41}\,(\xi_r,\eta_s)\,h_i(\xi_r)\;e'_j(\eta_s)\;e'_k(\xi_r)\;h_l(\eta_s)\,w_r\,w_s. \tag{8.34}$$

$$(\mathbb{M}_{42})_{ijkl} = \sum_{r=1}^{N_x}\sum_{s=1}^{N_x} C'_{42}\,(\xi_r,\eta_s)\,e_i(\xi_r)\;h'_j(\eta_s)\;e'_k(\xi_r)\;h_l(\eta_s)\,w_r\,w_s. \tag{8.35}$$

$$(\mathbb{M}_{43})_{ijkl} = \sum_{r=1}^{N_x}\sum_{s=1}^{N_x} C'_{43}\,(\xi_r,\eta_s)\,h'_i(\xi_r)\;e_j(\eta_s)\;e'_k(\xi_r)\;h_l(\eta_s)\,w_r\,w_s. \tag{8.36}$$

$$(\mathbb{M}_{44})_{ijkl} = \sum_{r=1}^{N_x}\sum_{s=1}^{N_x} C'_{44}\,(\xi_r,\eta_s)\,e'_i(\xi_r)\;h_j(\eta_s)\;e'_k(\xi_r)\;h_l(\eta_s)\,w_r\,w_s. \tag{8.37}$$

where the components of $\underline{\underline{\boldsymbol{C'}}}$ are what were derived in (subsection 8.2.1).
Then we get $\mathbb{M}_4 = [\mathbb{M}_{41}\;\;\mathbb{M}_{42}\;\;\mathbb{M}_{43}\;\;\mathbb{M}_{44}]$.
With these components, the mass matrix can be set up by vertically stacking $\mathbb{M}_1, \mathbb{M}_2, \mathbb{M}_3$ and $\mathbb{M}_4$ respectively.

8.7. Rotation matrix

The rotation matrix can be represented as

$$\mathbb{R} = \begin{bmatrix} 0 \\ \mathbb{R}_{\eta\xi} \\ \mathbb{R}_{\xi\eta} \\ 0 \end{bmatrix}$$

where,

$$(\mathbb{R}_{\eta\xi})_{ijkl} = -\sum_{r=1}^{N_x}\sum_{s=1}^{N_x} \det\mathcal{J}(\xi_r,\eta_s) e_i(\xi_r)\;h'_j(\eta_s)\;h'_k(\xi_r)\;h'_l(\eta_s)\,w_r\,w_s. \tag{8.38}$$

and

$$(\mathbb{R}_{\xi\eta})_{ijkl} = \sum_{r=1}^{N_x}\sum_{s=1}^{N_x} \det \mathcal{J}(\xi_r,\eta_s) h_i'(\xi_r)\, e_j(\eta_s)\, h_k'(\xi_r)\, h_l'(\eta_s)\, w_r\, w_s. \tag{8.39}$$

8.8. Boundary conditions

The boundary conditions can be enforced using a trick arising from the definition of the dual basis functions themselves. Let us see this in more detail.

8.8.1. Normal displacements for the Constitutive relation

The boundary condition for the constitutive relation with $\widetilde{\sigma_{\xi\xi}}$ shall be considered first. When looking at the reference domain, the displacement in the $\xi-$direction is prescribed on the left and right boundaries in the reference domain.

On the boundary, the prescribed $x-$displacement is expanded as

$$\int_{\partial\hat{\Omega}} u_\xi^{ex}(\xi,\eta)\,\mathrm{d}\eta \approx \int_{\partial\hat{\Omega}} \sum_{l=1}^{N+1} ((u_\xi)_P)_l h_l(\eta)\,\mathrm{d}\eta.$$

Using the dual polynomials, this integral can be reformulated as

$$\int_{\partial\hat{\Omega}} \sum_{j=1}^{N+1}\sum_{l=1}^{N+1} ((u_\xi)_P)_l h_l(\eta) e_j'(\eta)\mathrm{d}\eta \approx \int_{\partial\hat{\Omega}} \sum_{j=1}^{N+1} u_\xi^{ex}(\xi,\eta) e_j'(\eta)\mathrm{d}\eta = (u_\xi)_{a,j},$$

where $a=0$ or $a=N+1$ depending on whether it is the left or the right boundary.

Thus, the boundary condition becomes

$$\int_{\partial\hat{\Omega}} (u_\xi)_P \widetilde{\sigma_{\xi\xi}} n_\xi \mathrm{d}\Gamma = \int_{\partial\hat{\Omega}} \sum_{j=1}^{N+1}\sum_{l=1}^{N+1} (\widetilde{\sigma_{\xi\xi}})_{a,l} (u_\xi)^{ex}(\xi,\eta)\, e_j'(\eta)\mathrm{d}\eta = \sum_{j=1}^{N+1}\sum_{l=1}^{N+1} (\widetilde{\sigma_{\xi\xi}})_{a,l} (u_\xi)_{a,j}. \tag{8.40}$$

In a similar manner, the $y-$displacement is prescribed to the constitutive relation with $\widetilde{\sigma_{\eta y}}$ on the bottom and top boundaries in the *reference* domain, as

$$\int_{\partial\hat{\Omega}} (u_\eta)_P \widetilde{\sigma_{\eta\eta}} n_\eta \mathrm{d}\Gamma = \int_{\partial\hat{\Omega}} \sum_{j=1}^{N+1}\sum_{l=1}^{N+1} (\widetilde{\sigma_{\eta\eta}})_{l,a} (u_\eta)^{ex}(\xi,\eta)\, e_j'(\xi)\mathrm{d}\xi = \sum_{j=1}^{N+1}\sum_{l=1}^{N+1} (\widetilde{\sigma_{\eta\eta}})_{l,a} (u_\eta)_{j,a}. \tag{8.41}$$

where $a=0$ and $a=N+1$ for the bottom and top boundaries respectively.

An observation to be made here is that these displacements are the normal displacements to the physical boundaries, which are prescribed at all the boundaries. This is one of the reasons this approach was tested (where both the stress components and the displacement components are resolved into their reference domain counterparts), so that with the normal displacements at the boundaries, the constitutive laws also act as equations which conserve fluxes through the boundaries of the element.

Also, note that both these boundary conditions are independent of basis functions, and only involve the degrees of freedom. This is another strength of this approach.

8.8.2. Shear stresses for conservation of linear momentum

Considering the conservation of linear momentum for the stresses along the $\xi-$direction (for which $\widetilde{u_\xi}$ is the Lagrange multiplier), the stress component $\sigma_{\eta\xi}$ needs to be prescribed at the top and bottom boundaries in the reference domain.

This stress component can be expanded as

$$\int_{\partial\hat{\Omega}} \sigma_{\eta\xi}^{ex}(\xi,\eta)\,\mathrm{d}\xi \approx \int_{\partial\hat{\Omega}} \sum_{l=1}^{N} (\sigma_{\eta\xi})_P e_l(\xi)\mathrm{d}\xi.$$

Using dual polynomials, this can be modified as

$$\int_{\partial\hat{\Omega}} \sum_{j=1}^{N}\sum_{l=1}^{N}(\sigma_{\eta\xi})_P e_l(\xi)h'_j(\xi)\mathrm{d}\xi \approx \int_{\partial\hat{\Omega}} \sum_{j=1}^{N} \sigma^{ex}_{\eta\xi}(\xi,\eta)\, h'_j(\xi)\mathrm{d}\xi = (\sigma_{\eta\xi})_{j,a},$$

where $a = 0$ and $a = N+1$ respectively for the bottom and top boundaries.
Thus, the boundary integral can be reformulated as

$$\int_{\partial\hat{\Omega}} \widetilde{u_\xi}\,(\sigma_{\eta\xi})_P\, n_\eta \mathrm{d}\Gamma = \int_{\partial\hat{\Omega}} \sum_{j=1}^{N}\sum_{l=1}^{N}(\widetilde{u_\xi})_{l,a}\sigma^{ex}_{\eta\xi}(\xi,\eta)\, h'_j(\xi)\mathrm{d}\xi = \sum_{j=1}^{N}\sum_{l=1}^{N}(\widetilde{u_\xi})_{l,a}(\sigma_{\eta\xi})_{j,a}. \tag{8.42}$$

Similarly, considering the conservation of linear momentum for the stresses along the $\eta-$direction (with $\widetilde{u_\eta}$ as the Lagrange multiplier), the stress component $\sigma_{\xi\eta}$ needs to be prescribed at the left and right boundaries. The integral can be simplified as

$$\int_{\partial\hat{\Omega}} \widetilde{u_\eta}\,(\sigma_{\xi\eta})_P\, n_\xi \mathrm{d}\Gamma = \int_{\partial\hat{\Omega}} \sum_{j=1}^{N}\sum_{l=1}^{N}(\widetilde{u_\eta})_{a,l}\sigma^{ex}_{\xi\eta}(\xi,\eta)\, h'_j(\eta)\mathrm{d}\eta = \sum_{j=1}^{N}\sum_{l=1}^{N}(\widetilde{u_\eta})_{a,l}(\sigma_{\xi\eta})_{a,j}. \tag{8.43}$$

An observation with these boundary conditions is that these stress components are the components of traction that is always tangential to the physical boundaries. As mentioned before, these boundary conditions also do not involve the use of basis functions, only the degrees of freedom, which is another strong point of this formulation.

8.9. Contributions from the forcing function

The forcing function in both directions needs to have the same basis as the derivatives of the stresses, i.e.

$$\overline{f_\xi} = \sum_{i=1}^{N}\sum_{j=1}^{N+1}(f_\xi)_{i,j}e_i(\xi)e'_j(\eta),$$

$$\overline{f_\eta} = \sum_{i=1}^{N+1}\sum_{j=1}^{N}(f_\eta)_{i,j}e'_i(\xi)e_j(\eta).$$

Similar to the boundary conditions, the degrees of freedom for the body forces can be computed using the property of the dual basis functions.

$$\begin{aligned}(f_\xi)_{k,l} &= \int_{\hat{\Omega}} \sum_{i=1}^{N}\sum_{j=1}^{N+1}(f_\xi)_{i,j}e_i(\xi)e'_j(\eta)h'_k(\xi)h_l(\eta)\mathrm{d}\xi\wedge\mathrm{d}\eta \\ &= \int_{\hat{\Omega}} \left[\left(\frac{\partial y}{\partial\eta}\right) f^{ex}_x(x(\xi,\eta),y(\xi,\eta)) - \left(\frac{\partial x}{\partial\eta}\right) f^{ex}_y(x(\xi,\eta),y(\xi,\eta))\right] h'_k(\xi)h_l(\eta)\mathrm{d}\xi\wedge\mathrm{d}\eta.\end{aligned}$$

$$\begin{aligned}(f_\eta)_{k,l} &= \int_{\hat{\Omega}} \sum_{i=1}^{N+1}\sum_{j=1}^{N}(f_\eta)_{i,j}e'_i(\xi)e_j(\eta)h_k(\xi)h'_l(\eta)\mathrm{d}\xi\wedge\mathrm{d}\eta \\ &= \int_{\hat{\Omega}} \left[-\left(\frac{\partial y}{\partial\xi}\right) f^{ex}_x(x(\xi,\eta),y(\xi,\eta)) + \left(\frac{\partial x}{\partial\xi}\right) f^{ex}_y(x(\xi,\eta),y(\xi,\eta))\right] h_k(\xi)h'_l(\eta)\mathrm{d}\xi\wedge\mathrm{d}\eta.\end{aligned}$$

Note that these transformations derived are the same ones mentioned in subsection 8.1.5.

8.10. Hybridized system

With the current formulation, it is possible to hybridize the physical domain. This makes the method attractive when looking at it from a computational perspective.

The idea behind the hybridized system is that the physical domain is divided into various subdomains, and this formulation is applied individually to each element as if it were an independent problem on its own. The reference domain remains the same for each element and is the same reference domain used for formulations

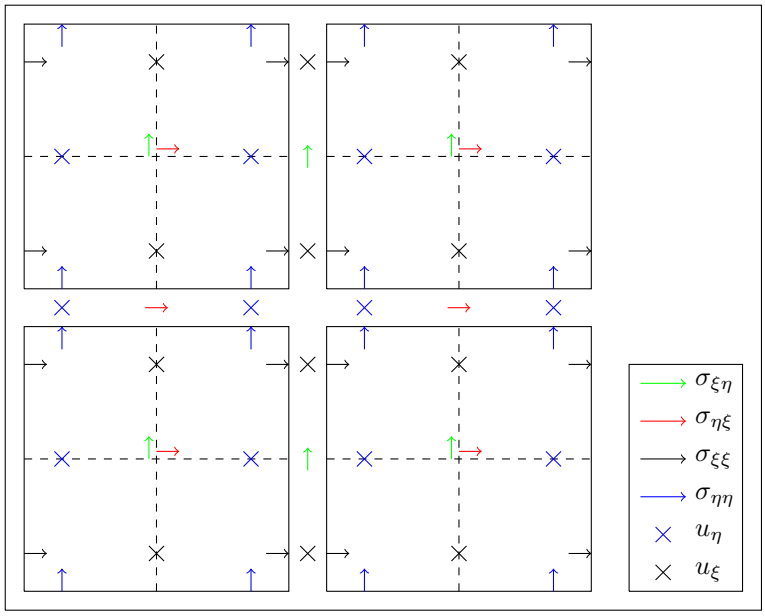

Figure 8.1: Degrees of freedom of quantities for the hybrid formulation on the reference domain with $K_x = K_y = 2$, $N = 1$

with a single element, shown in Figure 4.2. This makes each element have its own function map between the physical and the reference domains.

In order to not overdefine the problem, the Lagrange multipliers at the internal boundaries of different elements are used to constrain the values on neighbouring elements to be the same. This will result in a system matrix of the form

$$\begin{bmatrix} \mathbb{A} & \mathbb{B}^T \\ \mathbb{B} & 0 \end{bmatrix} \begin{bmatrix} \mathbf{x}^h \\ \boldsymbol{\lambda}^h \end{bmatrix} = \begin{bmatrix} \mathbf{f}^h \\ 0 \end{bmatrix}. \tag{8.44}$$

$\mathbb{A}$ contains the elemental stiffness matrix, with elements arranged in (again) lexicographic order. This enables it to be a block-diagonal matrix.

$\mathbb{B}$ contains the relations which enforce the continuity of the quantities in the reference domain, at the element boundaries. With this formulation, the relations used at the *horizontal* boundaries are

$$\widetilde{\sigma_{\xi\xi}}\,|_l = \widetilde{\sigma_{\xi\xi}}\,|_r$$
$$\widetilde{u_\eta}\,|_l = \widetilde{u_\eta}\,|_r,$$

where l and r indicate the left and right boundaries respectively. At the *vertical* boundaries,

$$\widetilde{\sigma_{\eta\eta}}\,|_b = \widetilde{\sigma_{\eta\eta}}\,|_t$$
$$\widetilde{u_\xi}\,|_b = \widetilde{u_\xi}\,|_t.$$

where b and t indicate the bottom and top boundaries respectively. How the hybridized domain looks like, in terms of degrees of freedom in the reference domain is shown in Figure 8.1.

8.11. Results

This formulation is tested against a manufactured solution. The manufactured solution is the same one tested in Section 7.9

8.11.1. Domain

A trapezoid domain is chosen for this problem. In order to quantify the effects of the ”skewness”, the slope of the skewed edge (m) is chosen to be a variable, and studies are conducted over multiple m, each of which results in a different domain. A sample domain with $m = 2$ is shown in Figure 5.2.

The points on this domain are mapped onto the points in the reference domain (Figure 4.2) using bilinear transfinite mapping. The Gauss-Lobatto points on the reference domain are then mapped onto the physical domain. When the domain is divided into several elements, the boundaries of the elements are first calculated using a bilinear transfinite mapping, and using these maps the Gauss-Lobatto points are mapped onto the physical domain. Note that the maps for each element can be different. These can be visualised in Figure 5.3

On these domains, the displacement u_{ξ}^{ex} and the stress component $\sigma_{\xi\eta}^{ex}$ are prescribed on the left and right boundary, and the displacement u_{η}^{ex} and $\sigma_{\eta\xi}^{ex}$ is prescribed at the bottom and top boundary.

8.11.2. Observations and Conclusions

Looking at the results, it is great to see that even when the unknowns are calculated in the reference domain, the solution obtained on reconstruction and transformation back to the physical domain seems to be consistent for u_x, u_y, σ_{xx}, σ_{yy} and even ω, as long as the solution is resolved well, as seen in Figure 8.2, Figure 8.3, Figure 8.4, Figure 8.5 and Figure 8.7. Even the symmetry of the Cauchy stress tensor is strongly enforced, as seen in Figure 8.8. However, there is something erratic seen in Figure 8.6, the shear stresses themselves show a significant error, that does not go away on increasing the refinement, considering that the exact solution for the shear stresses is also exactly zero. A similar trend is observed when looking at errors with respect to the exact solution for all other quantities too which seemed to be consistent, as observed in Figure 8.9 for u_x and u_y, Figure 8.10 for the normal stresses and Figure 8.11.

Further examination reveals that, with the use of hybrid elements, the surprising story is that there are very minimal discontinuities observed at the boundaries of the element, when looking at the quantities $u_x, u_y, \sigma_{xx}, \sigma_{yy}$ and even ω. The exception to this is when the solution is not resolved well enough within the element, for example when $N = 1$, which should also be the cause for the observed discontinuities. However, the discontinuities are more readily observed in the solution for quantities σ_{xy} and σ_{yx}, even when the solution is well-resolved for all the other quantities. The physical shear stresses also show a high error that does not seem to go away with refinement.

To confirm this, we can look at Figure 8.12, which is the convergence plot on increasing the number of elements. This indicates there is a limiting error that is not related to the refinement in the element width. A look at Figure 8.13 reveals the same story, this error does not go away with polynomial refinement. This shows there might be an error in the formulation, and that the tangential stress at the boundaries may not be the right Lagrange multiplier to couple elements when using this formulation.

The aim of developing this formulation in the first place was to eliminate the problems caused by the Lagrangian formulations, where the symmetry of the Cauchy stress tensor could not be enforced. With both the forms and the vector value for the stress components in the reference domain, the shear stresses in the reference domain can be used to enforce the symmetry in the reference domain, as well as in the physical domain. However, this formulation has a different error encoded into it, rather than a numerical problem.

The main problem with this formulation lies with how ω is used. By its definition, ω is defined as the antisymmetric part of the displacement gradient tensor. What is implicit, but not mentioned so far is that this also means that ω depends on what the undeformed state of the body. This means that $\omega(x, y)$ is a better representation of the rotation tensor. However, as $x(\xi, \eta)$ and $y(\xi, \eta)$ are functions of the reference coordinates, the displacements u_x and u_y should be functions of (ξ, η). This can be viewed as the displacements of particles, indicated by the label (ξ, η) in the reference domain will move u_x and u_y along the x- and y-directions respectively. When you convert the displacements into their reference counterparts, (ξ, η) is no longer a label to the physical world, instead you are observing the displacement field in the directions in the reference domain, which will lead to this particle being in a new position (ξ', η'). However, the rotation tensor is still defined with respect to the undeformed state of the body, which is a function of (x, y). This means that the antisymmetric part of the displacement gradient with respect to the undeformed domain can be decomposed into two parts, calculating how the undeformed domain looks from the reference domain and its labels, and then calculating the displacement gradient taking into consideration how the configuration changes from the undeformed domain. In this formulation, while the (antisymmetric part) of the displacement gradient is calculated, how the configuration changes with respect to the undeformed domain is not taken into consideration. This is why there is an error in this formulation.

Another point of view for this formulation is that while the definition of the stress components in this domain is symmetric with the definition of ω, the strain tensor does not account for the antisymmetric displacement gradient in the reference domain. The strain tensor is symmetric, but this symmetry is enforced by ω, which is the rotation tensor in the physical domain. The antisymmetric displacement gradient in the reference domain, which is $\frac{\partial u_\eta}{\partial \xi} - \frac{\partial u_\xi}{\partial \eta}$ is not accounted for in this formulation. This tensor field should generate an unbalanced rotational force in the reference domain, which does not appear in the equilibrium of forces. This unbalanced

force is added on to the shear stress component in the reference domain as a result, because the normal stresses in the reference domain are already defined because of the normal displacement boundary conditions.

To have another perspective on the error, let us look at what happens when you transform the value parts into the reference domain. In the physical domain, at each point, there is a different value for ξ and η, and hence is a continuous variable. When the form parts were converted onto the reference domain, the only change happened in the quantities we associate to the geometries. Because the geometry/domain changes under transformation from the physical to the reference (or vice versa) components should also reflect this change under transformation. However, the vector directions along which forces are balanced for example remain the same, which means the exterior derivative related to the geometrical components will still be accurate, along that direction. When you transform the directions, how ξ and η vary across the physical domain also needs to be taken into account. A simple exterior covariant derivative is not enough to get the complete variation of the physical quantity in the reference coordinates.

This means that the system only converges until a limiting value, and there is a limiting error value for each system. A similar result is observed when a different skewed domain is used, mentioned in section B.4.

8.12. Summary

In this section, a formulation is tested with all stress and displacement components transformed into their respective components in a reference domain. With the stresses written as vector-valued forms, the conservation of linear momentum is again topological, with the forces balanced in terms of reference components. The displacements are now written as covector-valued forms in the reference domain, thus (again) nullifying the value parts. With this formulation, the stress tensor is made symmetric by equating the shear components in the reference domain. This formulation can also be hybridized. This results in linear momentum being conserved up to machine precision, and even the symmetry of the stress tensor maintained up to machine precision. However, the shear stresses show an inherent error, which is confirmed by the convergence studies in both polynomial degree and the mesh width. This is due to the rotation not being taken into consideration in the reference domain, as the rotation tensor is defined with respect to the undeformed physical domain. This means that when you are writing down the rotation tensor in the reference domain, it should be with respect to the undeformed reference domain, which is not done in this formulation. This results in freedom for the reference domain to rotate, which is seen as an error in shear stresses in the final formulation.

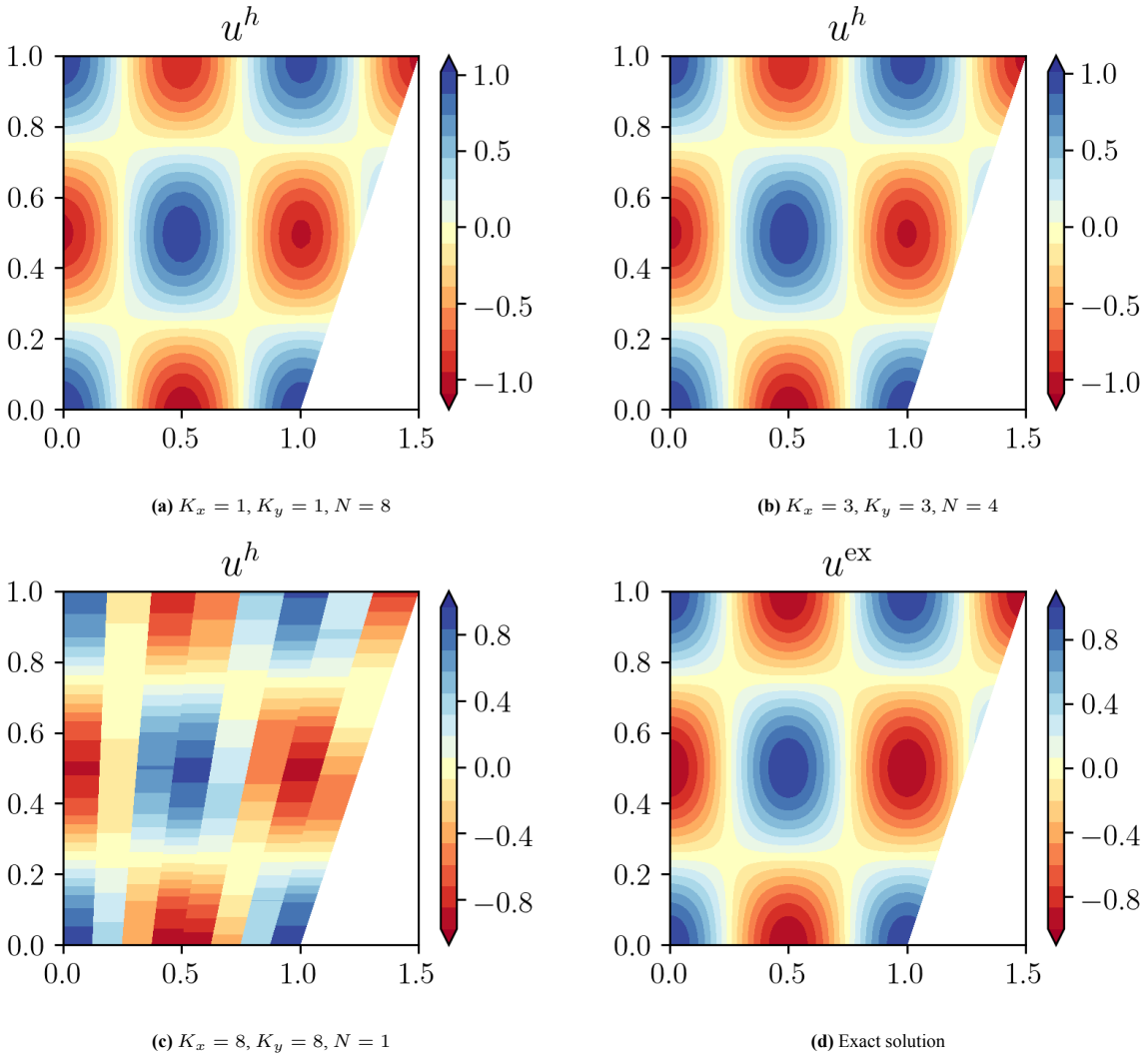

(a) $K_x = 1, K_y = 1, N = 8$

(b) $K_x = 3, K_y = 3, N = 4$

(c) $K_x = 8, K_y = 8, N = 1$

(d) Exact solution

Figure 8.2: Results for u^h in the physical domain

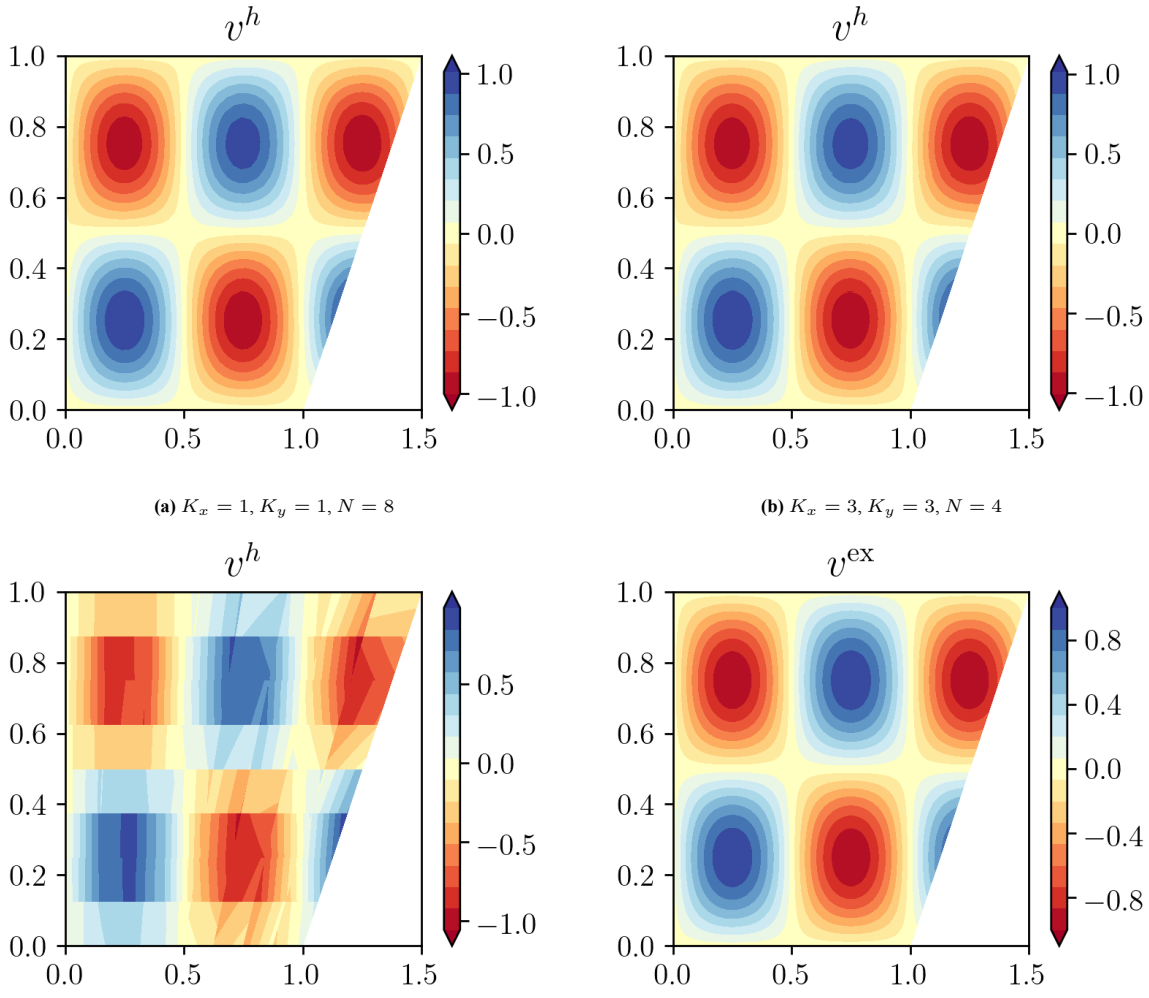

(a) $K_x = 1, K_y = 1, N = 8$

(b) $K_x = 3, K_y = 3, N = 4$

(c) $K_x = 8, K_y = 8, N = 1$

(d) Exact solution

Figure 8.3: Results for v^h in the physical domain

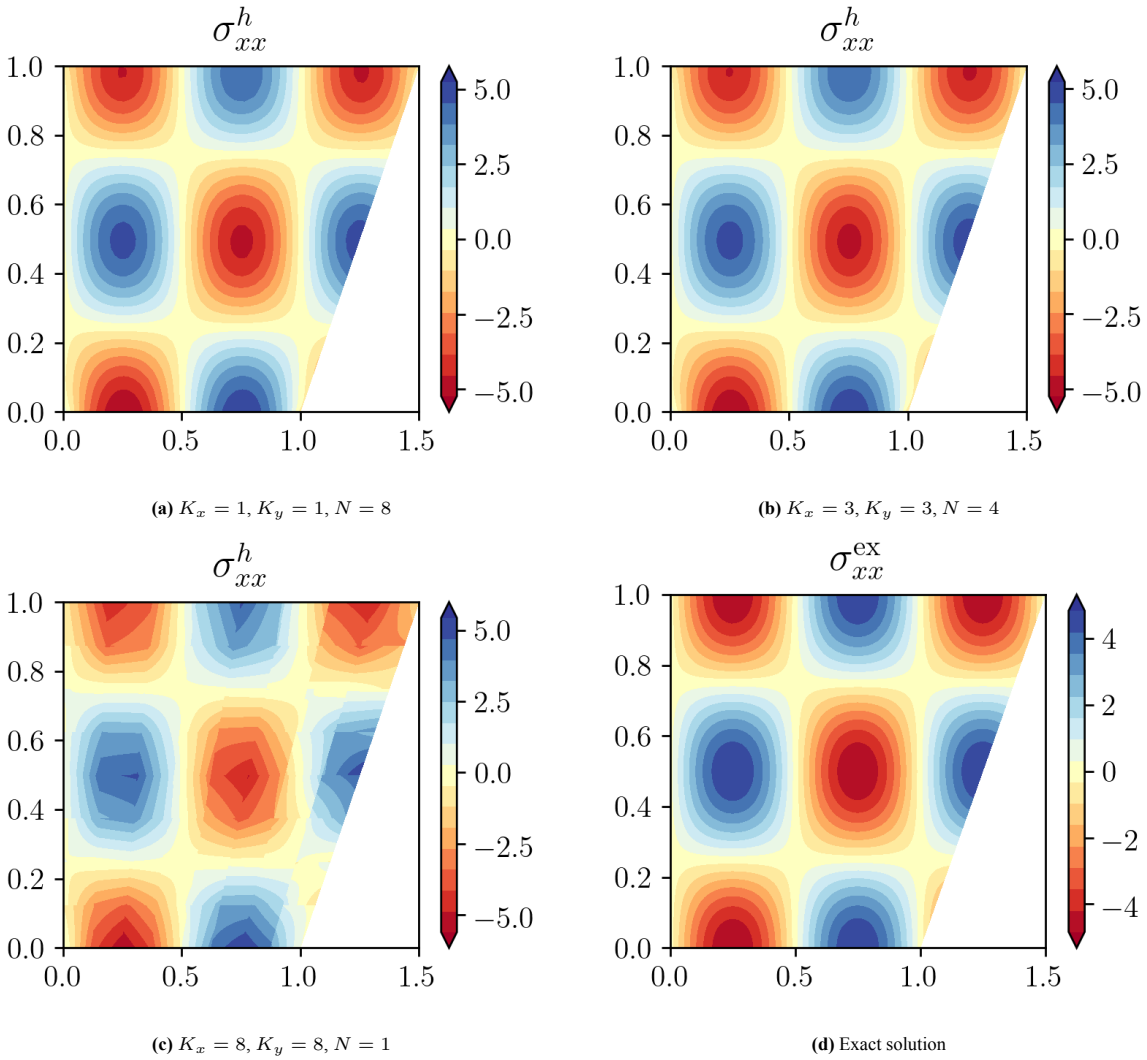

(a) $K_x = 1, K_y = 1, N = 8$

(b) $K_x = 3, K_y = 3, N = 4$

(c) $K_x = 8, K_y = 8, N = 1$

(d) Exact solution

Figure 8.4: Results for σ^h_{xx} in the physical domain

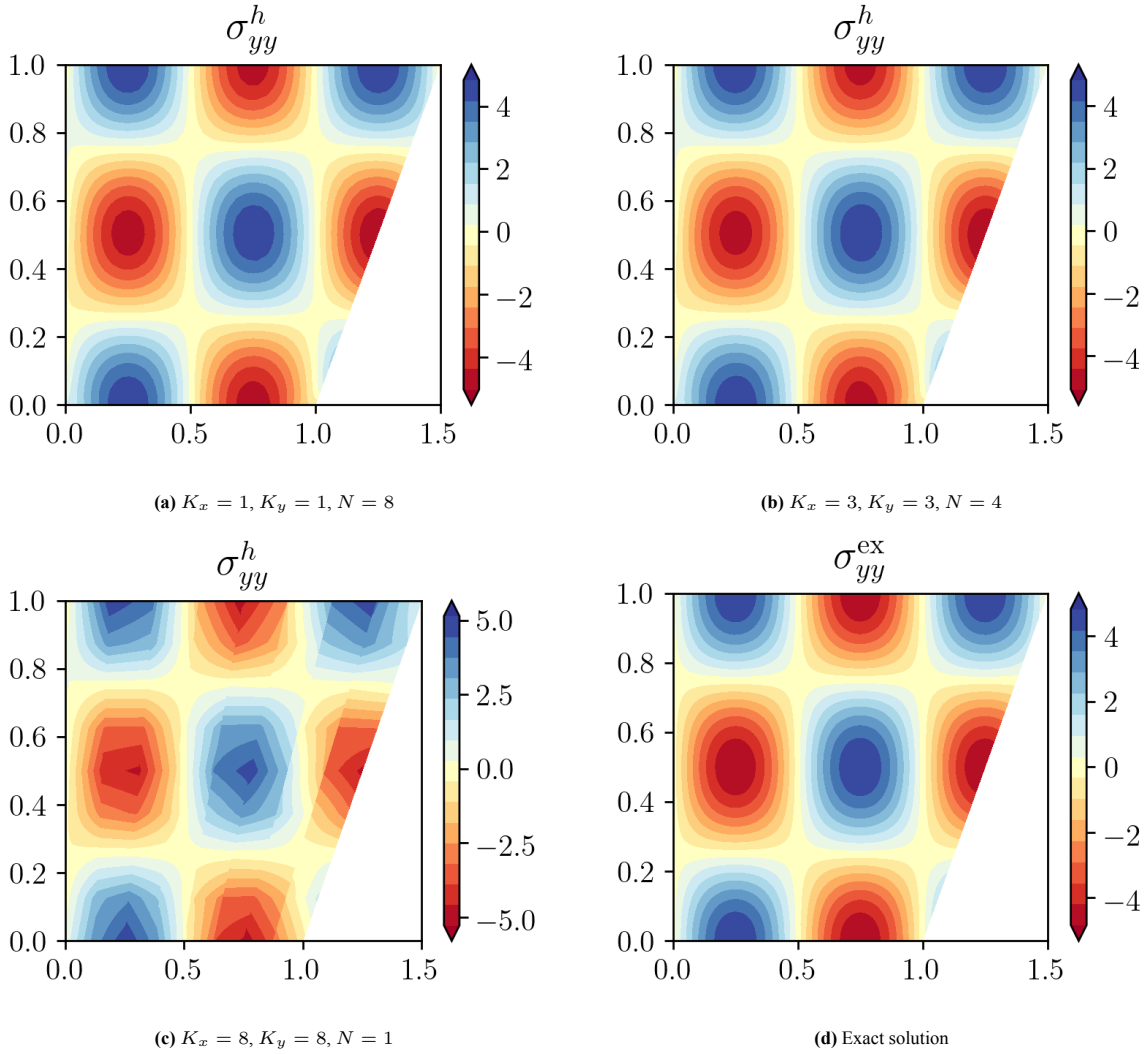

(a) $K_x = 1, K_y = 1, N = 8$

(b) $K_x = 3, K_y = 3, N = 4$

(c) $K_x = 8, K_y = 8, N = 1$

(d) Exact solution

Figure 8.5: Results for σ^h_{yy} in the physical domain

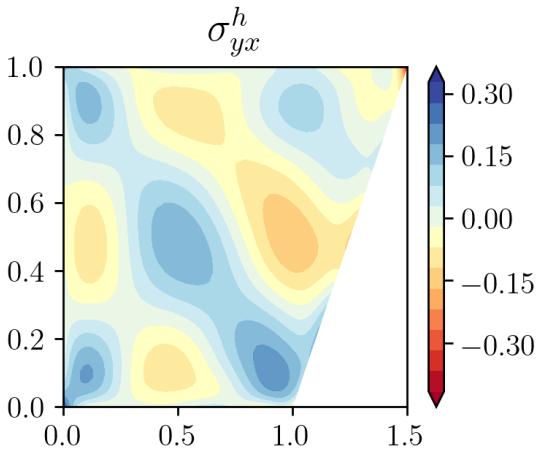

(a) σ^h_{yx} for $K_x = 1, K_y = 1, N = 8$

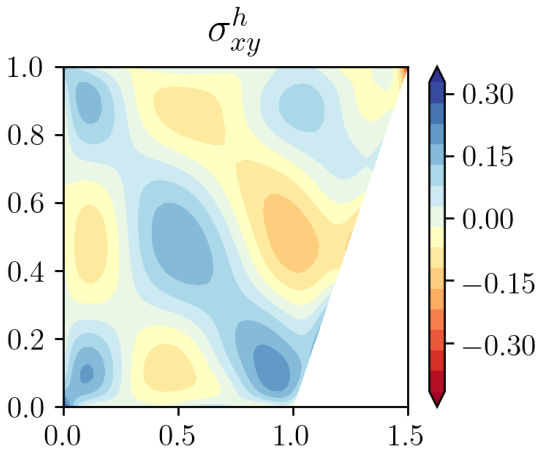

(b) σ^h_{xy} for $K_x = 1, K_y = 1, N = 8$

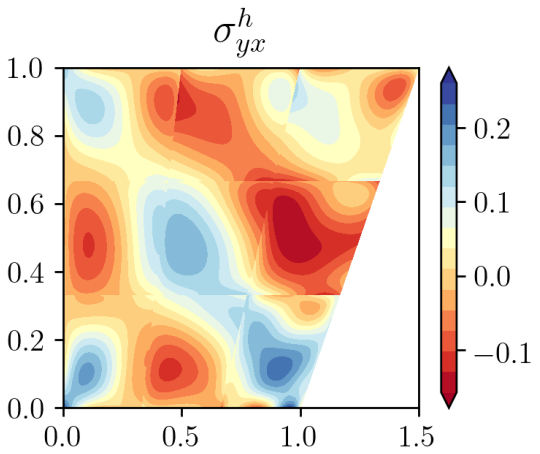

(c) σ^h_{yx} for $K_x = 3, K_y = 3, N = 4$

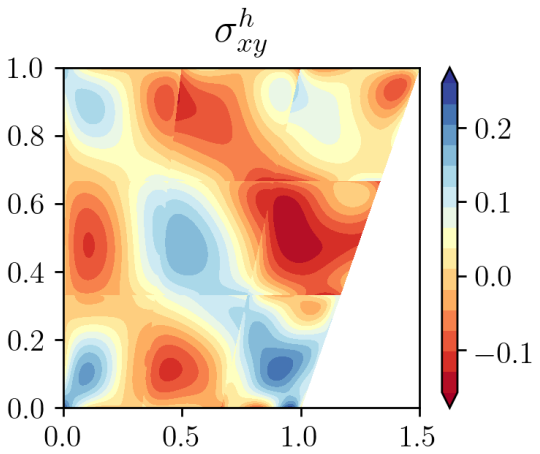

(d) σ^h_{xy} for $K_x = 3, K_y = 3, N = 4$

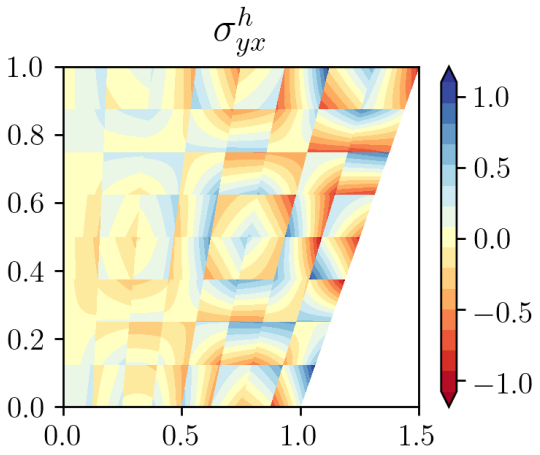

(e) σ^h_{yx} for $K_x = 8, K_y = 8, N = 1$

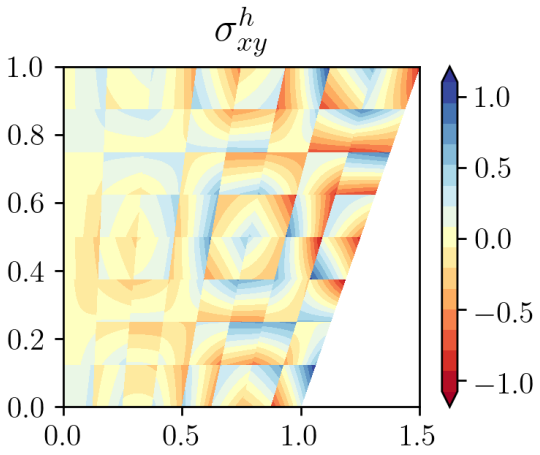

(f) σ^h_{xy} for $K_x = 8, K_y = 8, N = 1$

Figure 8.6: Results for σ^h_{xy} and σ^h_{yx} in the physical domain

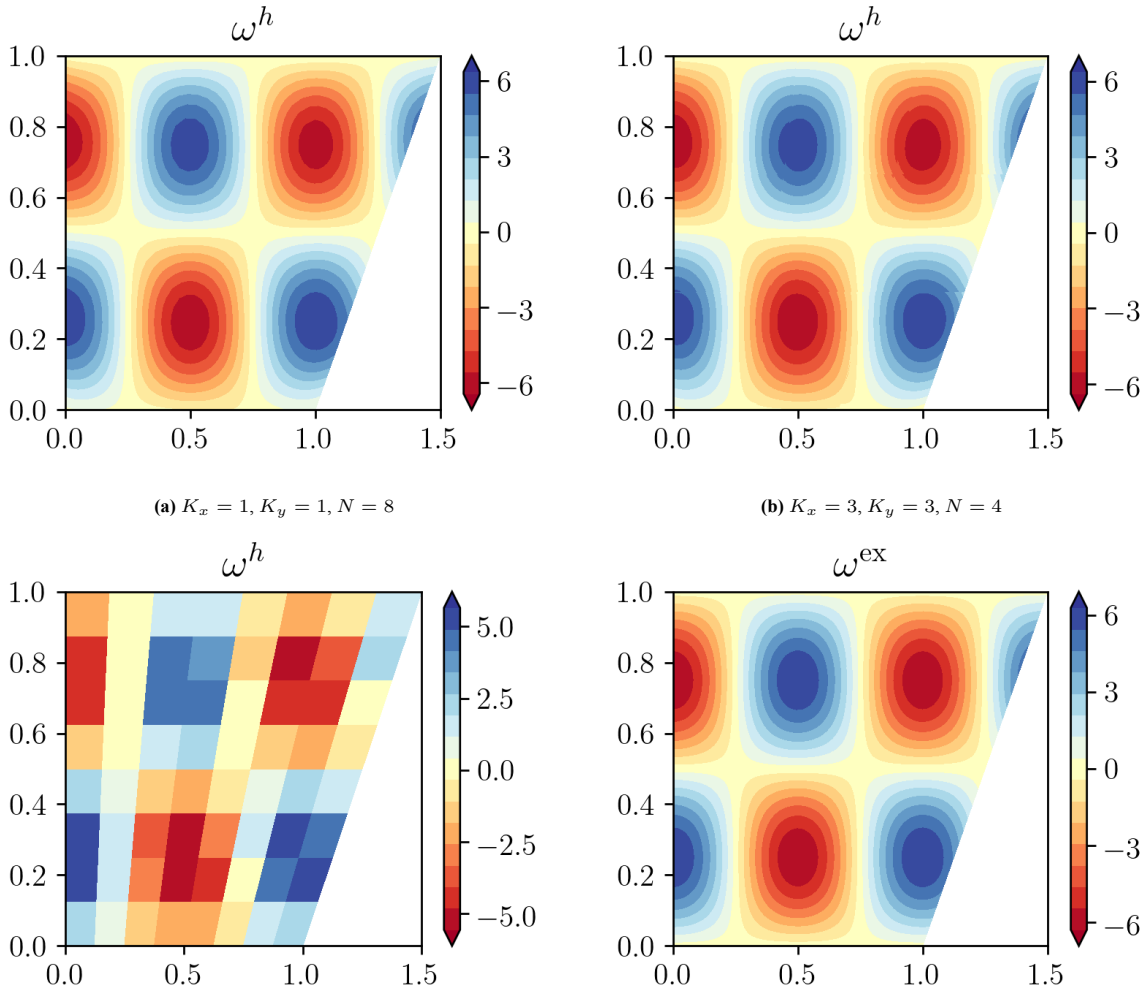

(a) $K_x = 1, K_y = 1, N = 8$

(b) $K_x = 3, K_y = 3, N = 4$

(c) $K_x = 8, K_y = 8, N = 1$

(d) Exact solution

Figure 8.7: Results for ω^h in the physical domain

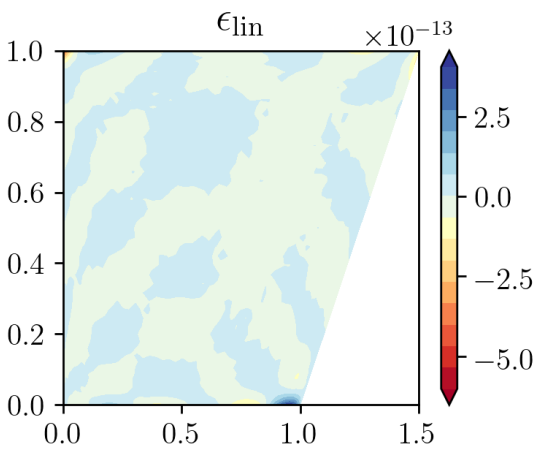

(a) Error in equilibrium of forces for $K_x = 1$, $K_y = 1$, $N = 8$

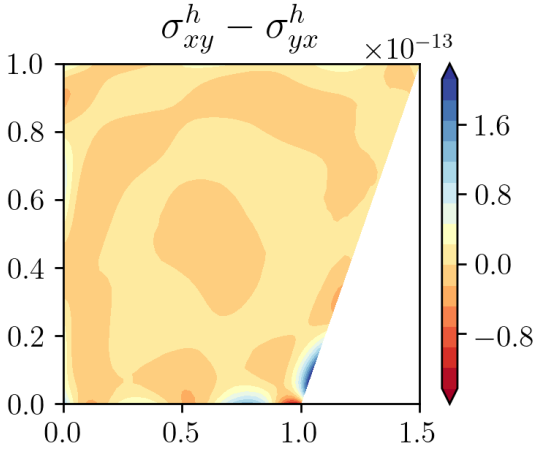

(b) $\sigma^h_{xy} - \sigma^h_{yx}$ for $K_x = 1$, $K_y = 1$, $N = 8$

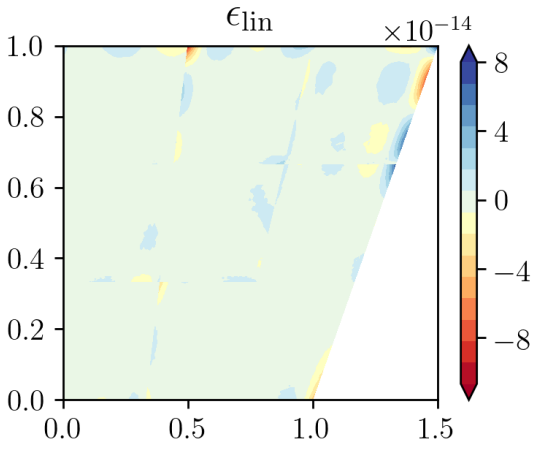

(c) Error in equilibrium of forces for $K_x = 3$, $K_y = 3$, $N = 4$

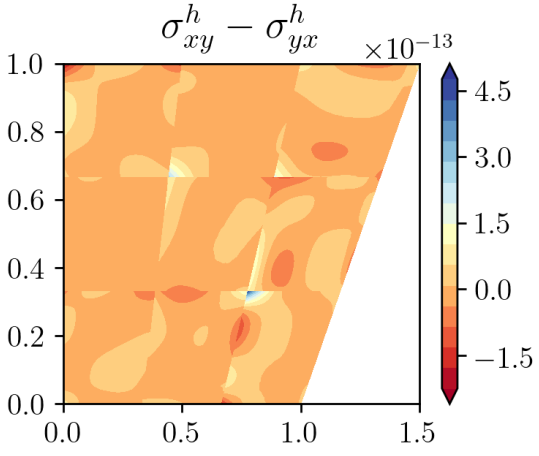

(d) $\sigma^h_{xy} - \sigma^h_{yx}$ for $K_x = 3$, $K_y = 3$, $N = 4$

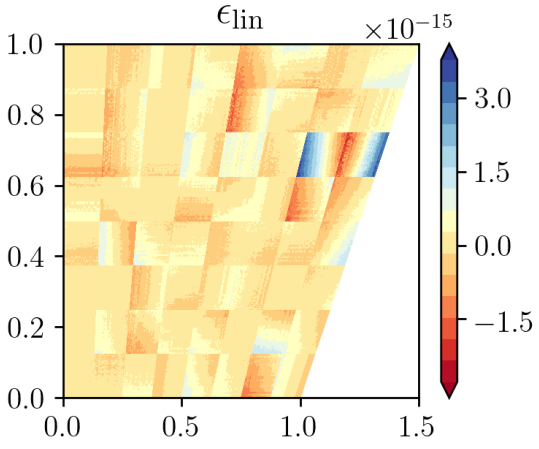

(e) Error in equilibrium of forces for $K_x = 8$, $K_y = 8$, $N = 1$

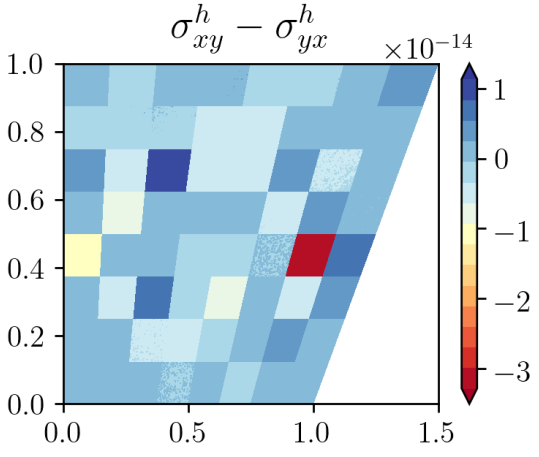

(f) $\sigma^h_{xy} - \sigma^h_{yx}$ for $K_x = 8$, $K_y = 8$, $N = 1$

Figure 8.8: Error in the conservation of linear momentum and symmetry of the Cauchy stress tensor

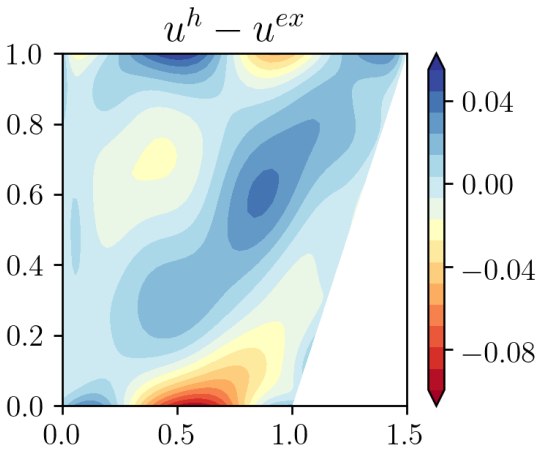

(a) $u_x^h - u_x^{ex}$ for $K_x = 1, K_y = 1, N = 8$

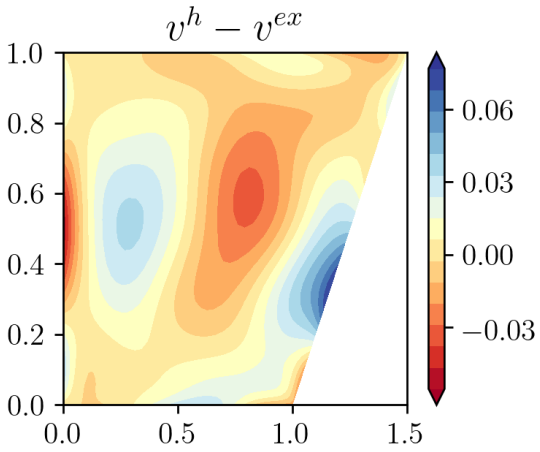

(b) $u_y^h - u_y^{ex}$ for $K_x = 1, K_y = 1, N = 8$

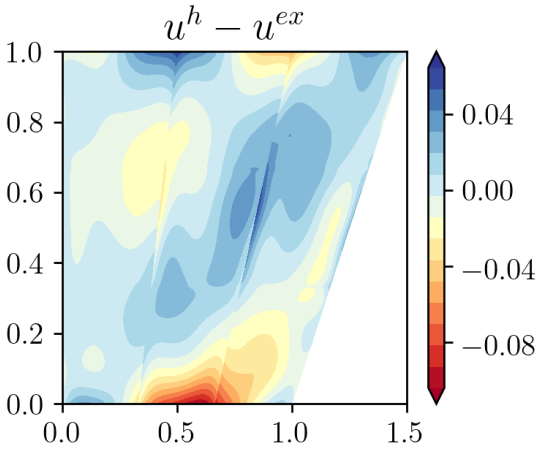

(c) $u_x^h - u_x^{ex}$ for $K_x = 3, K_y = 3, N = 4$

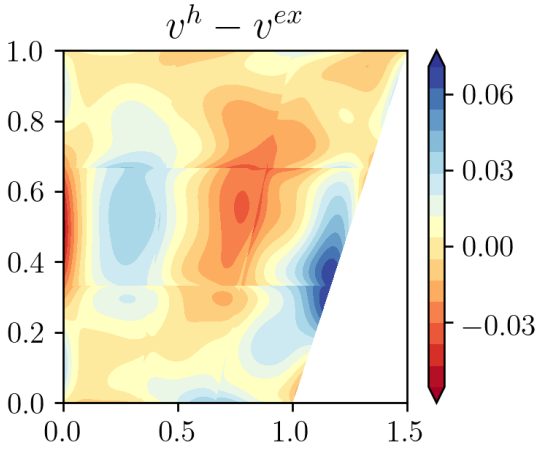

(d) $u_y^h - u_y^{ex}$ for $K_x = 3, K_y = 3, N = 4$

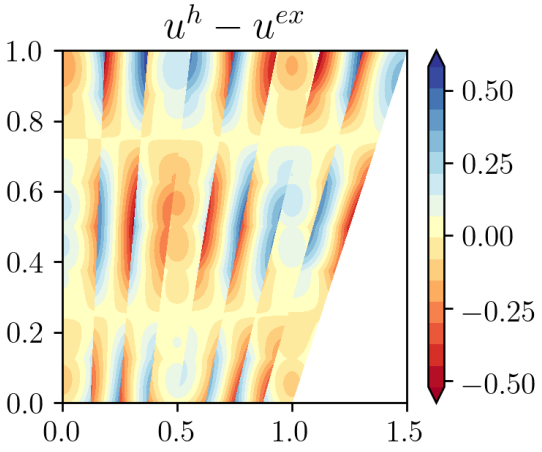

(e) $u_x^h - u_x^{ex}$ for $K_x = 8, K_y = 8, N = 1$

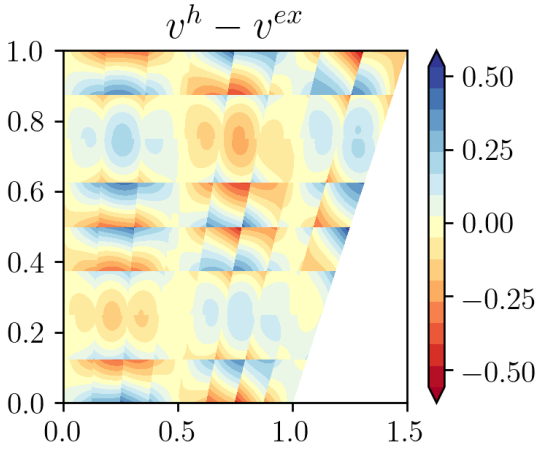

(f) $u_y^h - u_y^{ex}$ for $K_x = 8, K_y = 8, N = 1$

Figure 8.9: $u_x^h - u_x^{ex}$ and $u_y^h - u_y^{ex}$ in the physical domain

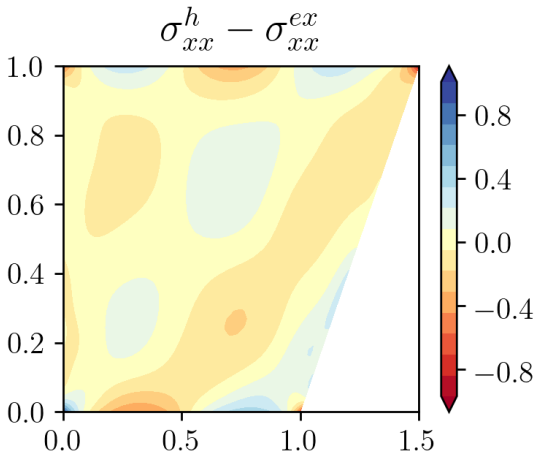

(a) $\sigma^h_{xx} - \sigma^{ex}_{xx}$ for $K_x = 1, K_y = 1, N = 8$

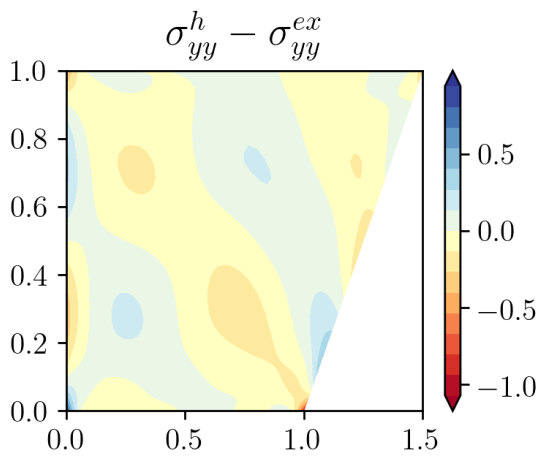

(b) $\sigma^h_{yy} - \sigma^{ex}_{yy}$ for $K_x = 1, K_y = 1, N = 8$

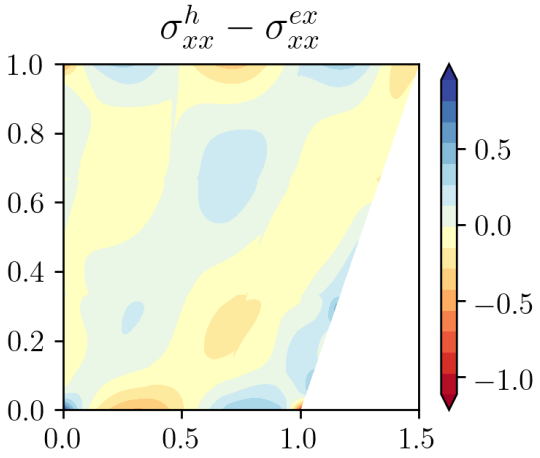

(c) $\sigma^h_{xx} - \sigma^{ex}_{xx}$ for $K_x = 3, K_y = 3, N = 4$

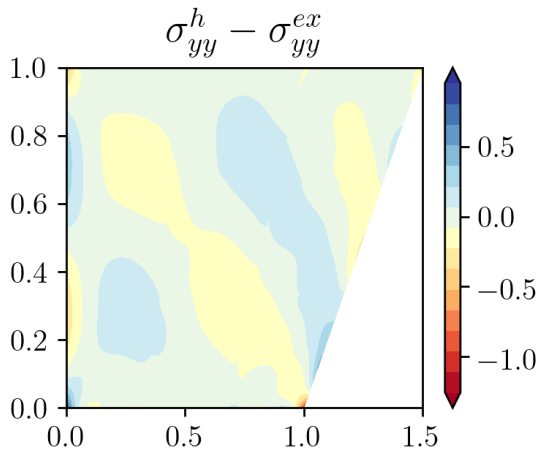

(d) $\sigma^h_{yy} - \sigma^{ex}_{yy}$ for $K_x = 3, K_y = 3, N = 4$

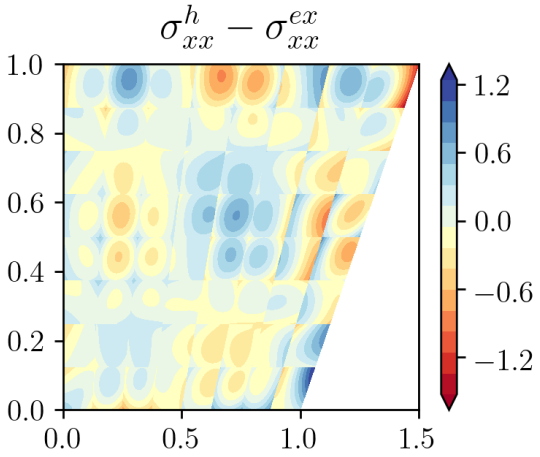

(e) $\sigma^h_{xx} - \sigma^{ex}_{xx}$ for $K_x = 8, K_y = 8, N = 1$

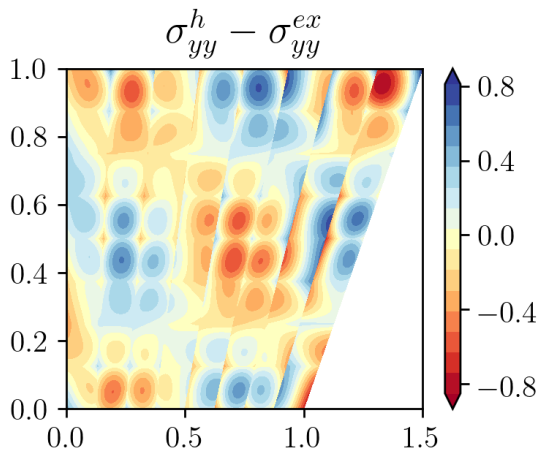

(f) $\sigma^h_{yy} - \sigma^{ex}_{yy}$ for $K_x = 8, K_y = 8, N = 1$

Figure 8.10: $\sigma^h_{xx} - \sigma^{ex}_{xx}$ and $\sigma^h_{yy} - \sigma^{ex}_{yy}$ in the physical domain

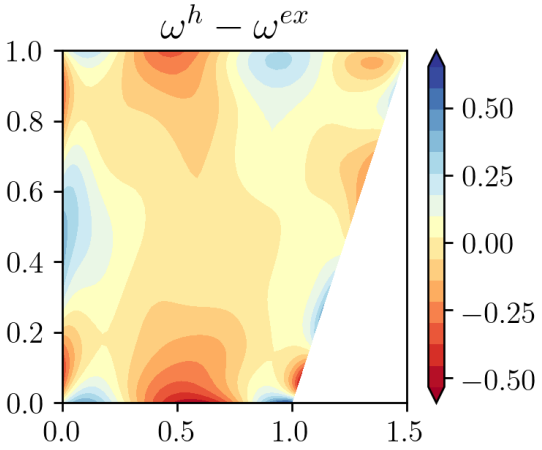

(a) $\omega^h - \omega^{ex}$ for $K_x = 1, K_y = 1, N = 8$

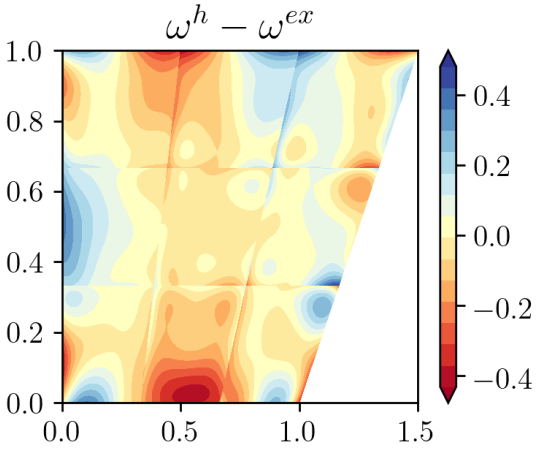

(b) $\omega^h - \omega^{ex}$ for $K_x = 3, K_y = 3, N = 4$

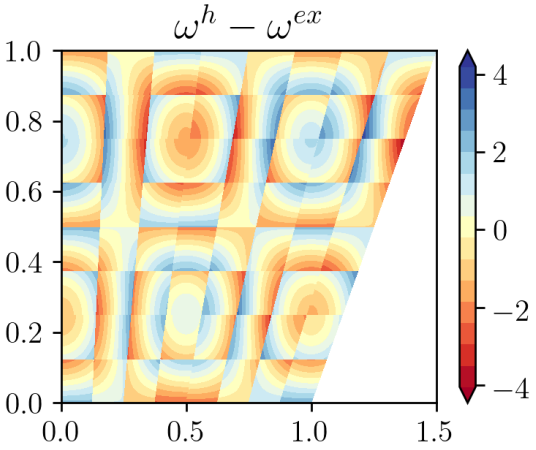

(c) $\omega^h - \omega^{ex}$ for $K_x = 8, K_y = 8, N = 1$

Figure 8.11: $\omega^h - \omega^{ex}$ in the physical domain

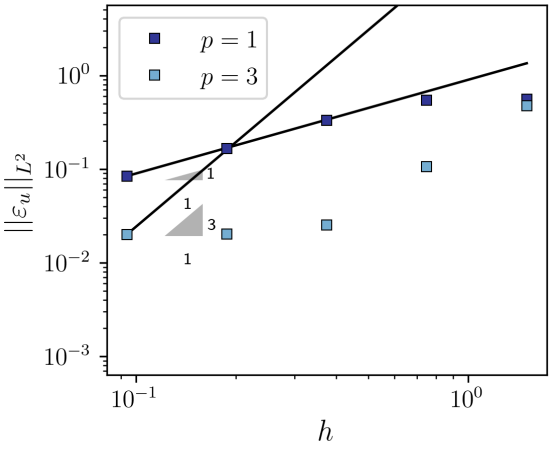

(a) Convergence with mesh width of L^2 error for u^h

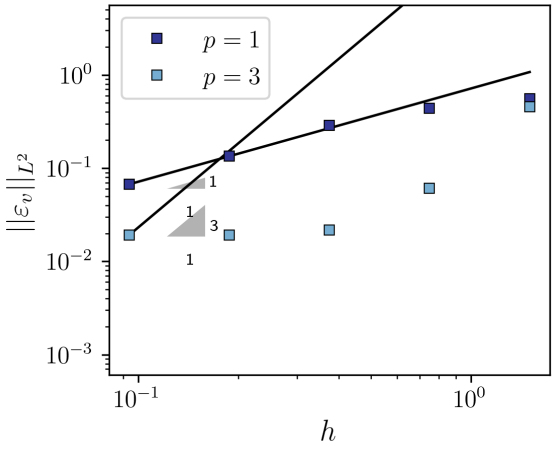

(b) Convergence with mesh width of L^2 error for v^h

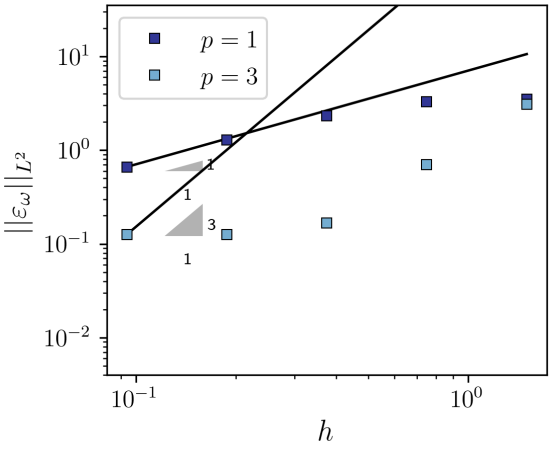

(c) Convergence with mesh width of L^2 error for ω^h

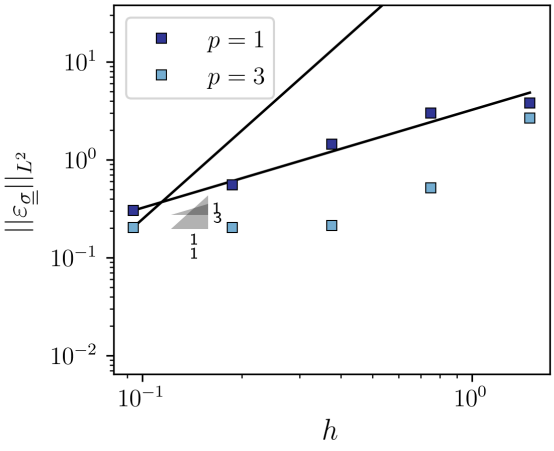

(d) Convergence with mesh width of L^2 error for $\underline{\underline{\boldsymbol{\sigma}}}^h$

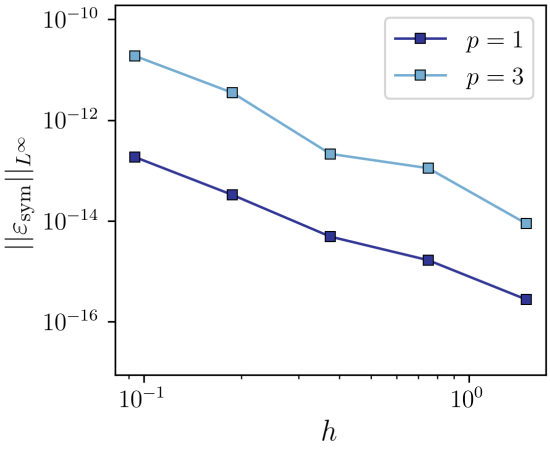

(e) Convergence with mesh width of L^∞ error for conservation of angular momentum

Figure 8.12: Results from the h-convergence study

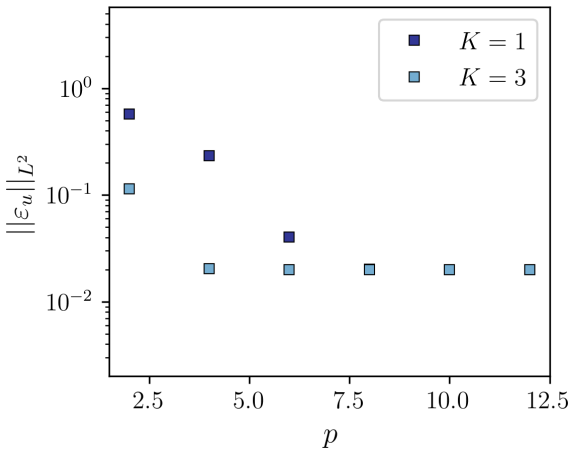

(a) L^2 error for u^h

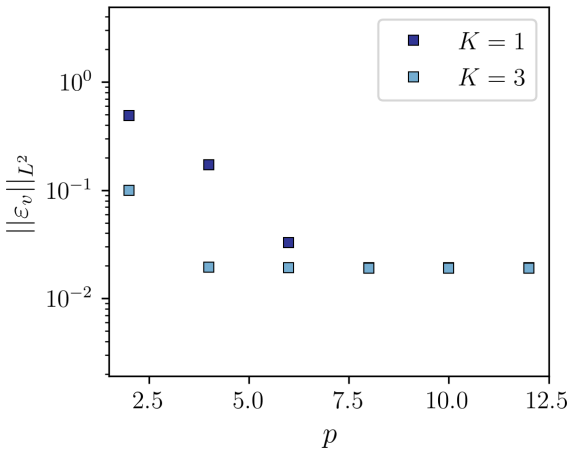

(b) L^2 error for v^h

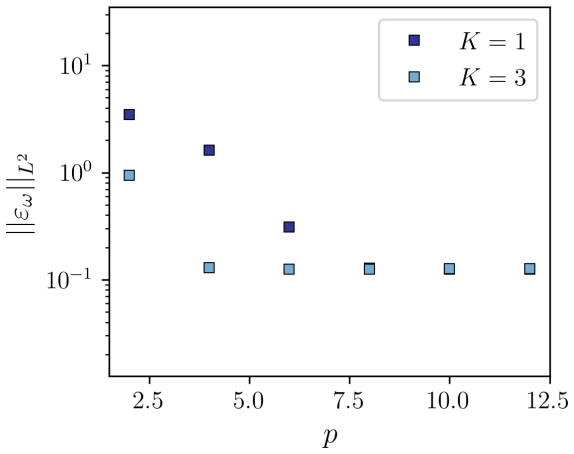

(c) L^2 error for ω^h

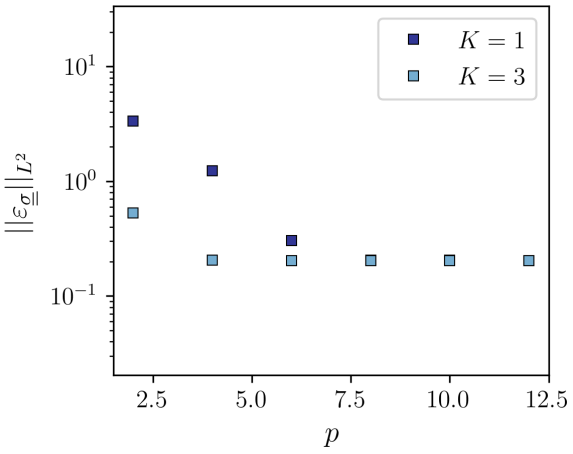

(d) L^2 error for $\underline{\underline{\boldsymbol{\sigma}}}^h$

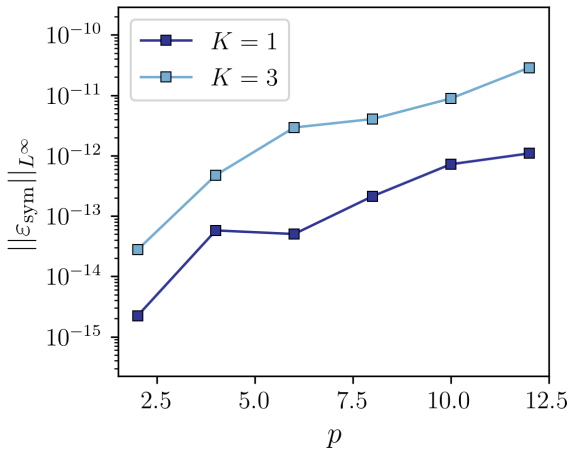

(e) L^∞ error in conservation of angular momentum

Figure 8.13: Results from the polynomial convergence study

9

Conclusions and Recommendations

The mimetic spectral element method had already been applied to solve the Poisson problem and the Linear elasticity problem. However, they were restricted to working in an orthogonal domain, where the coordinates in the physical domain were only related to the coordinates in the reference domain with a diagonal relationship. To account for arbitrary domains, with the goal being that the computations should still be in the reference domain, a new formulation must be devised, taking into different parameters for computation. With this motivation, several formulations were put forward and analysed. While the symmetry of the stress tensor was not maintained in all these methods, there was point-wise conservation of linear momentum in all these methods for an arbitrary domain. An extension of the Poisson problem was put forward too, that serves as an alternative to the previous formulations for an arbitrary domain.

The motivation to use and the understanding of the mimetic methods were derived from completing the literature review. This begins with trying to have a geometric description of physics, an idea that came together from combining mathematical ideas of exterior calculus with the insights of Tonti. When concepts from algebraic topology work together with geometric descriptions, it results in a natural discretisation which is able to describe physics. The most important aspect of this discretisation is that the metric and topological aspects of a physical problem can be distinguished easily, leading to better choices for the representation of physical variables and the separation of errors in numerical computation. With the mimetic spectral method, a high-order solution can be obtained with the ability to be extended to hybrid formulations and exact conservation of angular momentum.

This thesis aims to prepare the mixed hybrid mimetic spectral element method for Fluid-Structure Interaction when it could be used to simultaneously ensure the symmetry of the Cauchy stress tensor and the equilibrium of forces. The first step in this endeavour would be to look at unsteady Linear elasticity and how the conservation of angular and linear momentum would work. However, this revealed that we had to take some steps back in order to find the right formulation. For this, a new Lagrangian functional was proposed, such that the minimisation of this functional would lead to the constitutional laws and topological relations separately, with a constitutional relation used to couple the rate of change of displacement with the momentum. The spectral bases used in the literature were extended to the time domain as well, such that the conservation of linear momentum would remain topological even with the introduction of unsteady force due to changes in momentum over time. However, all of these led to a formulation that would diverge as soon as there was some deformation introduced into the otherwise rectangular domain. The conclusion was that the spectral bases, which were constructed on the reference domain, could not tackle the deformation because then the mapping from the reference domain to the physical domain would not be a simple diagonal mapping, instead, a coordinate in the physical domain will need a linear operator that relates the coordinates in the reference domain to them.

With this, the decision was to devise a novel formulation that would solve the Poisson problem when the physical domain is skewed, in this case, a trapezium. With the help of the transformation of differential forms, the quantities in the physical domain are mapped to the reference domain, and the linear elasticity formulation was modified to solve a diffusion equation using mixed spectral bases. Again, a Lagrangian functional was constructed such that the minimisation of this functional in the reference domain would lead to multiple equations that would model the Poisson problem. The modification from previous studies that were in the domain, was that the mass matrix in the constitutive equation also contains the pull-back operator within it, apart from the constitutional law itself. This means that even in the reference domain, the divergence equation is topological, and the results for the physical quantities converge on further refinement. Additionally, the formulation was hybridized, and optimal

results were obtained.

This meant the step-up to linear elasticity could be made, as it is essentially Poisson equations in two different directions, coupled together using the conservation of angular momentum. This would mean that while the Poisson problem could be tackled with differential forms, the vector-valued and covector-valued forms were used to represent displacements and stress components, respectively. The stress components were consequently chosen to have covector-values in the physical domain, while the forms would be transformed to their equivalents in the reference domain. Another Lagrangian functional was written in such a way that its minimisation would model the linear elasticity problem in the reference domain, with the mass matrix containing contributions from both the constitutive law and the pull-back operation, with the value parts of the quantities playing no part due to duality pairing. While the conservation of linear momentum was point-wise, angular momentum could not be conserved point-wise like in a rectangular domain. However, all physical quantities (and the error in conservation of angular momentum) did converge on further refinement. The difference in this formulation from the one on the orthogonal domain is that the symmetry of the Cauchy stress tensor requires enforcing a linear relation between all four stress components when it is converted in the reference domain, which all have different degrees of freedom. This formulation did not result in spurious kinematic modes.

In an attempt to solve this problem, an alternative formulation was developed, in which the spectral bases representing the stress components in the 'shear' directions would have higher degrees of freedom compared to the 'normal' stresses, while the opposite was true in the previous formulation. The rotation, which had the same degrees of freedom as the 'shear' components in previous formulations, also followed suit. The idea was to ensure that to ensure the symmetry of the Cauchy shear stresses in the reference domain, those stress components which are multiplied by the diagonal components of the mapping would have higher degrees of freedom. The result was that while the error in the symmetry of the Cauchy tensor was lower than in the previous formulation, the point-wise equality seen on rectangular domains was again not observed. The results again showed optimum convergence, apart from when the degree of the polynomial degree is one, where spurious modes are observed at the corners of the element.

In further pursuit of strong conservation of angular momentum, all the quantities were transformed into the reference domain, and another formulation was set up. The stress components were vector-valued this time, while the displacements were covector-valued. With this ensuring another topological formulation for the conservation of linear momentum and the symmetry of shear components in the reference domain, the requirement for the conservation of angular momentum, the Lagrangian functional was set up for these components. However, the results obtained were not converging and had an inherent error in the formulation itself. This was chalked down to an error in defining the rotation tensor, meaning that the reference domain was free to rotate about its axis. This results in the shear stress in the reference domain not being balanced, meaning that linear momentum is not conserved, and more terms need to be accounted for. Another explanation for this behaviour was that with the change in directions (from the physical coordinate directions to the reference coordinate directions), there was also a change in the quantities themselves, which could not be modelled only through operations on associated geometries. This means that one should also take into account how the reference coordinate directions will vary by location in the physical domain.

While the goal with this thesis was regarded as too ambitious, there were several steps taken to extend the thesis towards the goal, although the goal itself was not reached. With more continuum mechanics to tackle, the future holds promise for working with vector- and covector-valued forms in these applications. Future avenues for development include:

- Understand how the formulation with full transformation to the reference domain can be implemented such that there is convergence. Specifically, the formulation should maintain the point-wise conservation of linear and angular momentum.
- All studies conducted here are based on the same isotropic linear elastic material, which means that the compliance tensor in the physical domain (which relates the Cauchy stress tensor to the Cauchy-Green strain tensor) is the same. A replication of these studies using other constitutive relations (and thus, different compliance tensors) will help in understanding how the reference domain can capture changing constitutive relations.
- With the Lagrangian formulation for solids developed, where the values remain in the physical domain, the idea is to extend these studies to develop a Lagrangian method for fluids. This avoids the use of non-linear terms in the conservation of linear momentum as particles are tracked in this method, like in [17].
- Extending the study for solids in deformed domains into the formulation for unsteady solid simulations. This would mean extending this study into the time domain as well.

- A three-dimensional implementation for linear elasticity can be studied as well. Although it should be straightforward for the cases with partial transformation of stress components, the changes in the mapping with the addition of an extra dimension need to be taken into account.
- All of these case studies are conducted on a trapezoidal domain, where domain decomposition is easily achieved, and the element's boundaries can be modelled exactly as a linear function. It would be interesting to see if the same results are seen when the mapping is a polynomial function of the reference coordinates, not just linear, like in a circular domain. It should also be noted to look at domains where the transformation from the physical domain to the reference domain involves all non-zero components of the deformation gradient.
- This implementation was done using a high-level programming language. Another extension would be to look at the performance of this algorithm when it is implemented in parallel with multiple elements.

References

[1] Douglas N Arnold and Lizao Li. “Finite element exterior calculus with lower-order terms”. In: *Mathematics of Computation* 86.307 (Oct. 2017), pp. 2193–2212. ISSN: 0025-5718.

[2] Douglas N. Arnold, Richard S. Falk, and Ragnar Winther. “Finite element exterior calculus, homological techniques, and applications”. In: *Acta Numerica* 15 (2006). ISSN: 09624929.

[3] Douglas N. Arnold, Richard S. Falk, and Ragnar Winther. “Finite element exterior calculus: From hodge theory to numerical stability”. In: *Bulletin of the American Mathematical Society* 47.2 (2010). ISSN: 02730979.

[4] Douglas N. Arnold et al. “Unified Analysis of Discontinuous Galerkin Methods for Elliptic Problems”. In: *SIAM journal of numerical analysis* 39.5 (July 2002), pp. 1749–1779. ISSN: 00361429.

[5] Pavel B. Bochev and James M. Hyman. “Principles of Mimetic Discretizations of Differential Operators”. In: *Compatible Spatial Discretizations*. Springer New York, Jan. 2007, pp. 89–119.

[6] Pavel. B Bochev. “A discourse on variational and geometric aspects of stability of discretizations”. In: *33rd Computational Fluid Dynamics Lecture Series, VKI LS,* 5 (2003).

[7] Daniele Boffi, Franco Brezzi, and Michel Fortin. *Mixed Finite Element Methods and Applications*. Vol. 44. Springer Series in Computational Mathematics. Berlin, Heidelberg: Springer Berlin Heidelberg, 2013. ISBN: 978-3-642-36518-8.

[8] Jérôme Bonelle and Alexandre Ern. “Analysis of Compatible Discrete Operator schemes for elliptic problems on polyhedral meshes”. In: *ESAIM: Mathematical Modelling and Numerical Analysis* 48.2 (Mar. 2014), pp. 553–581. ISSN: 0764-583X.

[9] Alain Bossavit. “Computational electromagnetism and geometry: Building a finite-dimensional ”Maxwell’s house”. In: *J Japan Soc Appl Elctromagn & Mech* 7 (July 1999).

[10] Alain Bossavit. “Whitney forms: A class of finite elements for three-dimensional computations in electromagnetism”. In: *IEE Proceedings A: Physical Science. Measurement and Instrumentation. Management and Education. Reviews* 135 pt A.8 (1988). ISSN: 0143702X.

[11] Mick Bouman et al. “A conservative spectral element method for curvilinear domains”. In: *Lecture Notes in Computational Science and Engineering* 76 LNCSE (2011), pp. 111–119. ISSN: 14397358.

[12] F. Brezzi, Richard S. Falk, and L. Donatella Marini. “Basic principles of mixed Virtual Element Methods”. In: *ESAIM: Mathematical Modelling and Numerical Analysis* 48.4 (July 2014), pp. 1227–1240. ISSN: 0764-583X.

[13] Franco Brezzi, Annalisa Buffa, and Konstantin Lipnikov. “Mimetic finite differences for elliptic problems”. In: *Mathematical Modelling and Numerical Analysis* 43.2 (2009). ISSN: 0764583X.

[14] A. Buffa, C. De Falco, and G. Sangalli. “IsoGeometric Analysis: Stable elements for the 2D Stokes equation”. In: *International Journal for Numerical Methods in Fluids* 65.11-12 (Apr. 2011), pp. 1407–1422. ISSN: 1097-0363.

[15] Bernardo Cockburn. “Static condensation, hybridization, and the devising of the HDG methods”. In: *Building bridges: connections and challenges in modern approaches to numerical partial differential equations* (2016), pp. 129–177.

[16] Bernardo Cockburn, George E. Karniadakis, and Chi-Wang Shu. “The Development of Discontinuous Galerkin Methods”. In: (2000), pp. 3–50.

[17] Joey Dekker. *The Lagrangian Mimetic Spectral Element Method: Solving (non-)Linear Advection Problems with a Mimetic Method*. 2022.

[18] Leszek F. Demkowicz and Jay Gopalakrishnan. “An Overview of the Discontinuous Petrov Galerkin Method”. In: (2014), pp. 149–180.

[19] Mathieu Desbrun et al. “Discrete Exterior Calculus”. In: (2005).

[20] Jozef Dodziuk. “Finite-Difference Approach to the Hodge Theory of Harmonic Forms”. In: *American Journal of Mathematics* 98.1 (1976). ISSN: 00029327.

[21] Jérôme Droniou et al. “A unified approach to Mimetic Finite Difference, Hybrid Finite Volume and Mixed Finite Volume methods”. In: *https://doi.org/10.1142/S0218202510004222* 20.2 (Apr. 2012), pp. 265–295. ISSN: 02182025.

[22] John A. Evans and Thomas J.R. Hughes. “Isogeometric divergence-conforming B-splines for the unsteady Navier–Stokes equations”. In: *Journal of Computational Physics* 241 (May 2013), pp. 141–167. ISSN: 0021-9991.

[23] Joël Marius Fisser. *Advancing the Mimetic Spectral Element Method: Towards Continuum Mechanics Applications*. 2019.

[24] Harley. Flanders. “Differential forms with applications to the physical sciences.” In: (1963), p. 203.

[25] Harley. Flanders. *Differential forms with applications to the physical sciences.* Academic Press, 1963, p. 203. ISBN: 978-0486661698.

[26] Theodore Frankel. *The Geometry of Physics*. 2011.

[27] Marc Gerritsma. “An introduction to a compatible spectral discretization method”. In: *Mechanics of Advanced Materials and Structures* 19.1-3 (2012). ISSN: 15376494.

[28] Marc Gerritsma. “Edge functions for spectral element methods”. In: *Lecture Notes in Computational Science and Engineering*. Vol. 76 LNCSE. 2011.

[29] Marc Gerritsma, Jeroen Kunnen, and Boudewijn de Heij. “Discrete lie derivative”. In: *Lecture Notes in Computational Science and Engineering* 112 (2016), pp. 635–643. ISSN: 14397358.

[30] Marc Gerritsma et al. “Algebraic Dual Polynomials for the Equivalence of Curl-Curl Problems”. In: *Lecture Notes in Computational Science and Engineering* 132 (2020), pp. 307–320. ISSN: 21977100.

[31] William J. Gordon and Charles A. Hall. “Construction of curvilinear co-ordinate systems and applications to mesh generation”. In: *International Journal for Numerical Methods in Engineering* 7.4 (Jan. 1973), pp. 461–477. ISSN: 1097-0207.

[32] William J. Gordon and Charles A. Hall. “Transfinite element methods: Blending-function interpolation over arbitrary curved element domains”. In: *Numerische Mathematik 1973 21:2* 21.2 (Apr. 1973), pp. 109–129. ISSN: 0945-3245.

[33] R. R. Hiemstra et al. “High order geometric methods with exact conservation properties”. In: *Journal of Computational Physics* 257.PB (Jan. 2014), pp. 1444–1471. ISSN: 0021-9991.

[34] R. Hiptmair. “Discrete Hodge operators”. In: *Numerische Mathematik* 90.2 (Dec. 2001), pp. 265–289. ISSN: 0029599X.

[35] Thomas J.R. Hughes et al. “The Continuous Galerkin Method Is Locally Conservative”. In: *Journal of Computational Physics* 163.2 (Sept. 2000), pp. 467–488. ISSN: 0021-9991.

[36] J. M. Hyman and M. Shashkov. “Natural discretizations for the divergence, gradient, and curl on logically rectangular grids”. In: *Computers & Mathematics with Applications* 33.4 (Feb. 1997), pp. 81–104. ISSN: 0898-1221.

[37] V. Jain et al. “Construction and application of algebraic dual polynomial representations for finite element methods on quadrilateral and hexahedral meshes”. In: *Computers & Mathematics with Applications* 95 (Aug. 2021), pp. 101–142. ISSN: 08981221.

[38] J. van (Jos van) Kan, A. (Guus) Segal, and F. (Fred) Vermolen. *Numerical methods in scientific computing*. Delft Academic Press, 2008. ISBN: 9789071301506.

[39] Jasper Kreeft and Marc Gerritsma. “Mixed mimetic spectral element method for Stokes flow: A pointwise divergence-free solution”. In: *Journal of Computational Physics* 240 (2013). ISSN: 10902716.

[40] Jasper Kreeft, Artur Palha, and Marc Gerritsma. “Mimetic spectral element method for generalized convection-diffusion problems”. In: (July 2010), pp. 14–17.

[41] Konstantin Lipnikov, Gianmarco Manzini, and Mikhail Shashkov. “Mimetic finite difference method”. In: *Journal of Computational Physics* 257.PB (2014). ISSN: 10902716.

[42] G Manzini et al. “The tensor-train mimetic finite difference method for three-dimensional Maxwell’s wave propagation equations”. In: *Mathematics and Computers in Simulation* 210 (2023), pp. 615–639.

[43] Claudio Mattiussi. “A reference discretization strategy for the numerical solution of physical field problems”. In: *Advances in Imaging and Electron Physics* 121.C (2002). ISSN: 10765670.

[44] R. A. Nicolaides and K. A. Trapp. “Covolume Discretization of Differential Forms”. In: *Compatible Spatial Discretizations* (Jan. 2006), pp. 161–171.

[45] K. Olesen et al. “A higher-order equilibrium finite element method”. In: *International Journal for Numerical Methods in Engineering* 114.12 (2018). ISSN: 10970207.

[46] A Palha, J Kreeft, and M Gerritsma. “Numerical solution of advection equations with the discretization of the Lie derivative”. In: (2010).

[47] Artur Palha, Pedro Pinto Rebelo, and Marc Gerritsma. “Mimetic Spectral Element advection”. In: (Apr. 2013).

[48] Artur Palha et al. “Physics-compatible discretization techniques on single and dual grids, with application to the Poisson equation of volume forms”. In: *Journal of Computational Physics* 257 (2014), pp. 1394–1422.

[49] J Blair Perot and Christopher J Zusi. “Differential forms for scientists and engineers”. In: *Journal of Computational Physics* 257 (2014), pp. 1373–1393.

[50] J. Blair Perot. “Discrete conservation properties of unstructured mesh schemes”. In: *Annual Review of Fluid Mechanics* 43 (2011). ISSN: 00664189.

[51] A. Quarteroni and A. Valli. “Theory and Application of Steklov-Poincaré Operators for Boundary-Value Problems”. In: *Applied and Industrial Mathematics* (1991), pp. 179–203.

[52] Ramy Rashad et al. “Intrinsic nonlinear elasticity: An exterior calculus formulation”. In: 2023.

[53] P A Raviart and J Thomas. “Primal hybrid finite element methods for 2nd order elliptic equations”. In: *Mathematics of Computation* 31 (1977), pp. 391–413.

[54] Nicolas Robidoux and Stanly Steinberg. “A discrete vector calculus in tensor grids”. In: *Computational Methods in Applied Mathematics* 11.1 (2011), pp. 23–66. ISSN: 16099389.

[55] Christopher J. Roy. “Review of code and solution verification procedures for computational simulation”. In: *Journal of Computational Physics* 205.1 (May 2005), pp. 131–156. ISSN: 0021-9991.

[56] Mikhail Shashkov and Stanly Steinberg. “Solving Diffusion Equations with Rough Coefficients in Rough Grids”. In: *Journal of Computational Physics* 129.2 (Dec. 1996), pp. 383–405. ISSN: 0021-9991.

[57] Deepak Suryavanshi and Rahul Dehiya. “A Mimetic Finite-Difference Method for Two-Dimensional DC Resistivity Modeling”. In: *Mathematical Geosciences* (May 2023), pp. 1–28. ISSN: 18748953.

[58] Timo Tarhasaari, Lauri Kettunen, and Alain Bossavit. “Some realizations of a discrete Hodge operator: A reinterpretation of finite element techniques”. In: *IEEE Transactions on Magnetics* 35.3 PART 1 (1999). ISSN: 00189464.

[59] Michael E. Taylor. *Partial Differential Equations I*. Vol. 115. Applied Mathematical Sciences. New York, NY: Springer New York, 2011. ISBN: 978-1-4419-7054-1.

[60] Wouter Tonnon and Ralf Hiptmair. “Semi-Lagrangian Finite-Element Exterior Calculus for Incompressible Flows”. In: (Jan. 2023).

[61] E. Tonti. “On the Mathematical Structure of a Large Class of Physical Theories”. In: (1971).

[62] Enzo Tonti. “The Mathematical Structure of Classical and Relativistic Physics”. In: Modeling and Simulation in Science, Engineering and Technology (2013).

[63] Enzo Tonti. “Why starting from differential equations for computational physics?” In: *Journal of Computational Physics* 257 (2014), pp. 1260–1290.

[64] Deepesh Toshniwal, R. H.M. Huijsmans, and M. I. Gerritsma. “A Geometric Approach Towards Momentum Conservation”. In: *Lecture Notes in Computational Science and Engineering* 95 (Apr. 2013), pp. 393–402. ISSN: 14397358.

[65] Yi Zhang, Joël Fisser, and Marc Gerritsma. "A hybrid mimetic spectral element method for three-dimensional linear elasticity problems". In: *Journal of Computational Physics* 433 (May 2021), p. 110179. ISSN: 0021-9991.

[66] Yi Zhang et al. "A high order hybrid mimetic discretization on curvilinear quadrilateral meshes for complex geometries". In: *Proceedings of the 6th European Conference on Computational Mechanics: Solids, Structures and Coupled Problems, ECCM 2018 and 7th European Conference on Computational Fluid Dynamics, ECFD 2018* (2020), pp. 426–437.

[67] Yi Zhang et al. "A mass-, kinetic energy- and helicity-conserving mimetic dual-field discretization for three-dimensional incompressible Navier-Stokes equations, part I: Periodic domains". In: *Journal of Computational Physics* 451 (Feb. 2022), p. 110868. ISSN: 0021-9991.

[68] Yi Zhang et al. "Discrete equivalence of adjoint neumann–dirichlet div-grad and grad-div equations in curvilinear 3d domains". In: *Lecture Notes in Computational Science and Engineering*. Vol. 134. 2020.

A

Experimental setup and other choices

This chapter consists of further explanations of the choices made in plotting as well as brief explanation of the repository that helps investigate bundle-valued forms for Linear elasticity problems.

A.1. Element width

One important measure that needs to be considered while plotting is the measure of the element width. Because physically the elements are skewed, it is necessary to make a good estimate of the element width to see how computed solutions behave on refinement.

The first step taken is to ensure that all results were plotted for equal number of elements along the coordinate directions, i.e. $K_x = K_y$. This enables us to consider the skewness only in one of the directions, and not to be influenced by how the elements themselves are divided.

For all skewed domains, the idea was that if L_t is the length of the top boundary, with K_x indicating how many elements are along the x-direction, then the element width is assumed to be

$$h = \frac{L_t}{K_x}$$

Do note that this was chosen as the representative width for each element would be different, and thus it was necessary to come up with a unique value for the purpose of analysis.

A.2. Experimental setup

The choices for the experimental setup, including how the repository is maintained is explained here.

A.2.1. Hardware

The machine on which this thesis will be carried out has an Intel i7-9750H CPU, with 16GB RAM. The computational setup consists of running codes on a Python environment and consists of many files of code grouped in folders based on their use. In general, these sets of codes depend on the `numpy` and `scipy` open-source libraries. The `pickle` library is also used to store and read solution data and the `matplotlib.pyplot` library is used for plotting results. In addition, the `os` library is used as a means to automate the opening and closing of files with the help of their addresses. Python 3.7 is used for running the experiments, which is part of an Anaconda installation on Ubuntu 22.04 operating system. This setup is selected as everything is open source and is widely used, meaning it is also well documented.

A.2.2. Code methodology

The settings for the simulation is mentioned in `settings.py` file. The method used, along with the domain that should be used for the simulation. Along with this, the exact solution (when analysing the results where the manufactured solution is known) and the initial conditions (for unsteady linear elasticity) are prescribed in the files `exact_solution.py` and `initial_conditions.py` respectively.

In the `Problems/` folder, there is a code which calls functions from other folders to solve a specific problem. A typical problem file will do everything from assembling the matrices and running the postprocessing routine. All

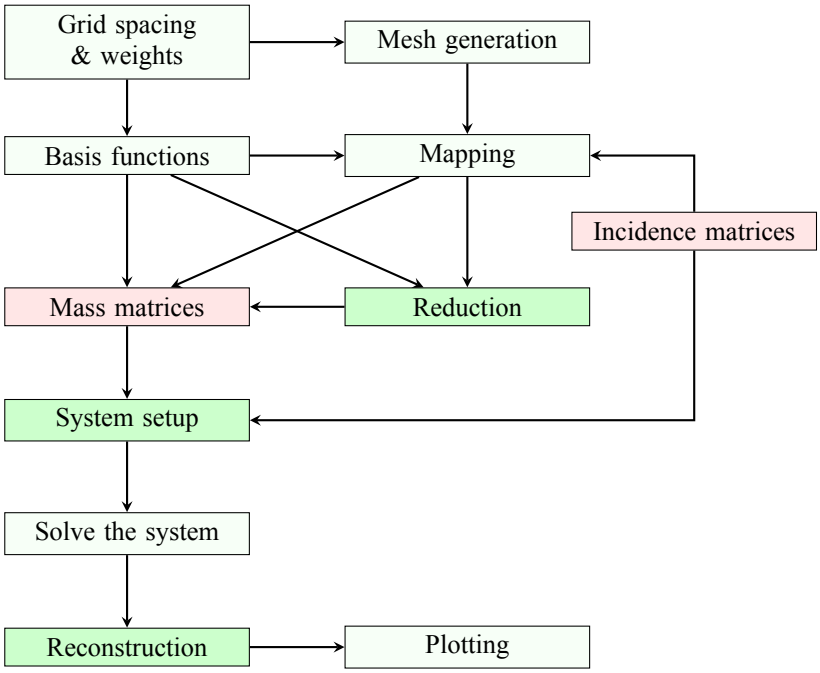

Figure A.1: Schematic diagram of the implementation of the hybrid mimetic spectral element method

of these tasks of actually specifying the details of the matrices, the vectors etc are imported from their definitions in the other files, and this file only assembles it such that the correct system for this problem formulation is solved. For example, the `Problems.Linear_Elasticity_Lagrangian` file contains details about how the Original Linear Elasticity formulation in the Lagrangian method is assembled.

The `Defs` folder contains the descriptions of several programs which are essential to MSEM. From the spectral bases for the method to the assembly of the system and the construction of various matrices are in various files in this folder, and each file has a specific purpose. For example, `Defs.mapping` is used to mention details of the mappings between the reference domain and the deformed/undeformed domain, and `Defs.matrices` contains functions to make the various Hodge and incidence matrices that will be used in other files. `Defs.grid` is used to generate both the reference domain and the mesh for the physical domain. `Defs.quad` contains details about quadrature and are where the basis functions are generated. `Defs.reduction` is the main file where reduction operations take place, including generation of the vectors for the boundary conditions and the forcing function. Additionally, `Defs.index` is a library that assists in the global and local indexing of variables while setting up and generating matrices.

In addition, the `Data/` and `Plots/` folders contain data and plots generated of previous experiments. The visual representation of the repository is done in Figure A.2, while how the repository is used is depicted in Figure A.1.

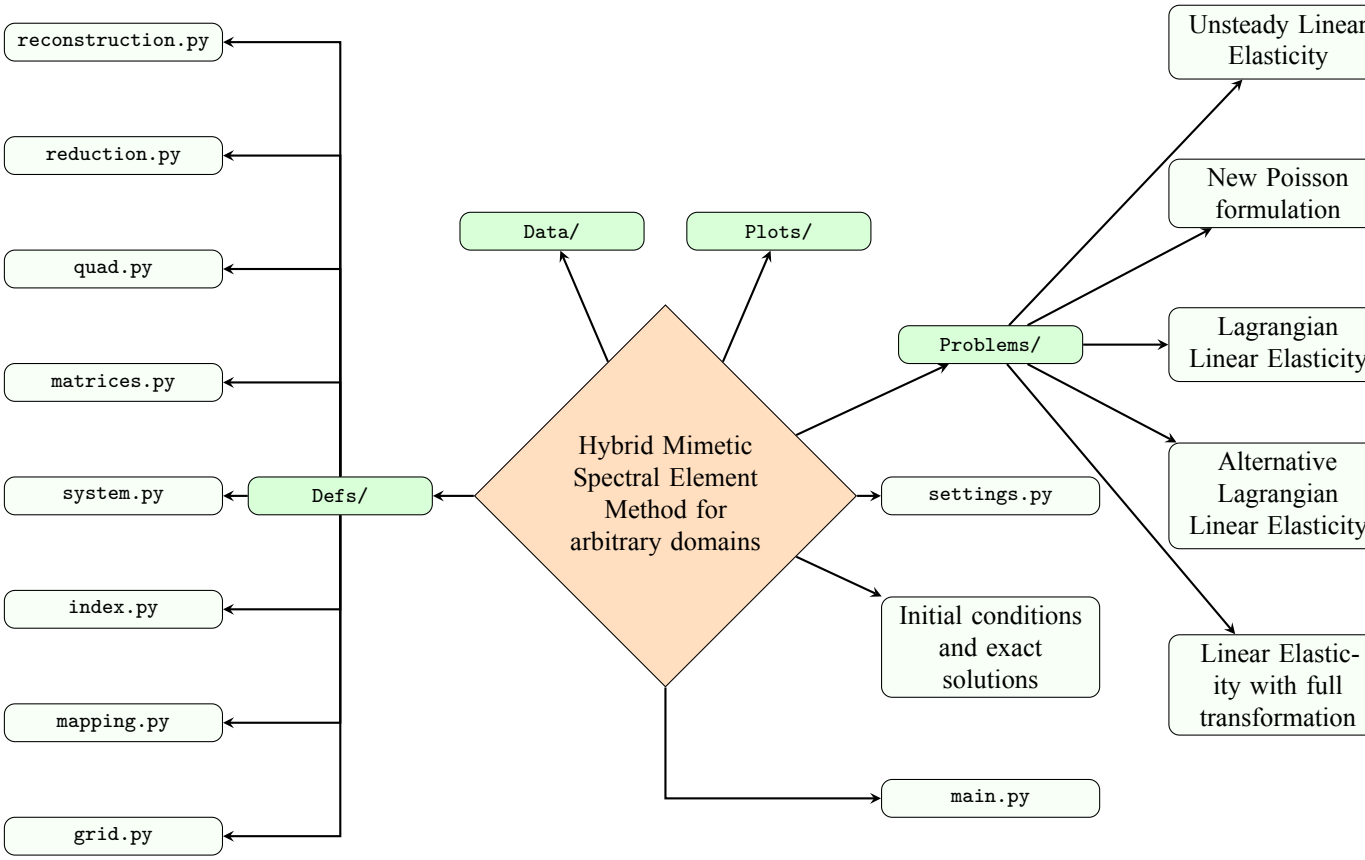

Figure A.2: Visualisation of the repository

B

Results for other domains

This section contains the results from sections with arbitrary domains which are skewed differently.

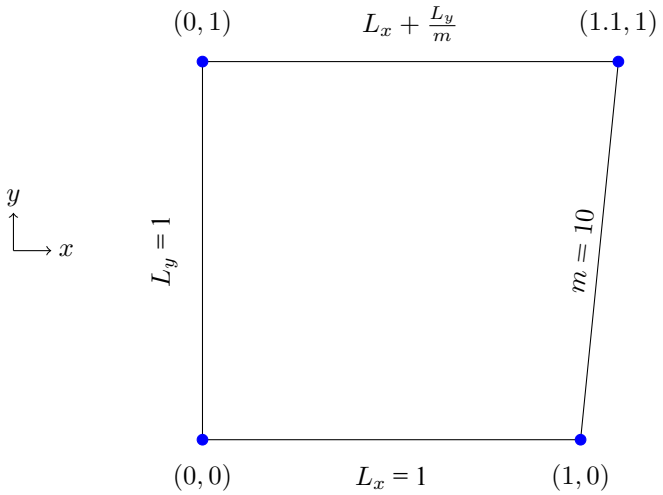

Figure B.1: Domain with $m = 10$

B.1. New Poisson formulation

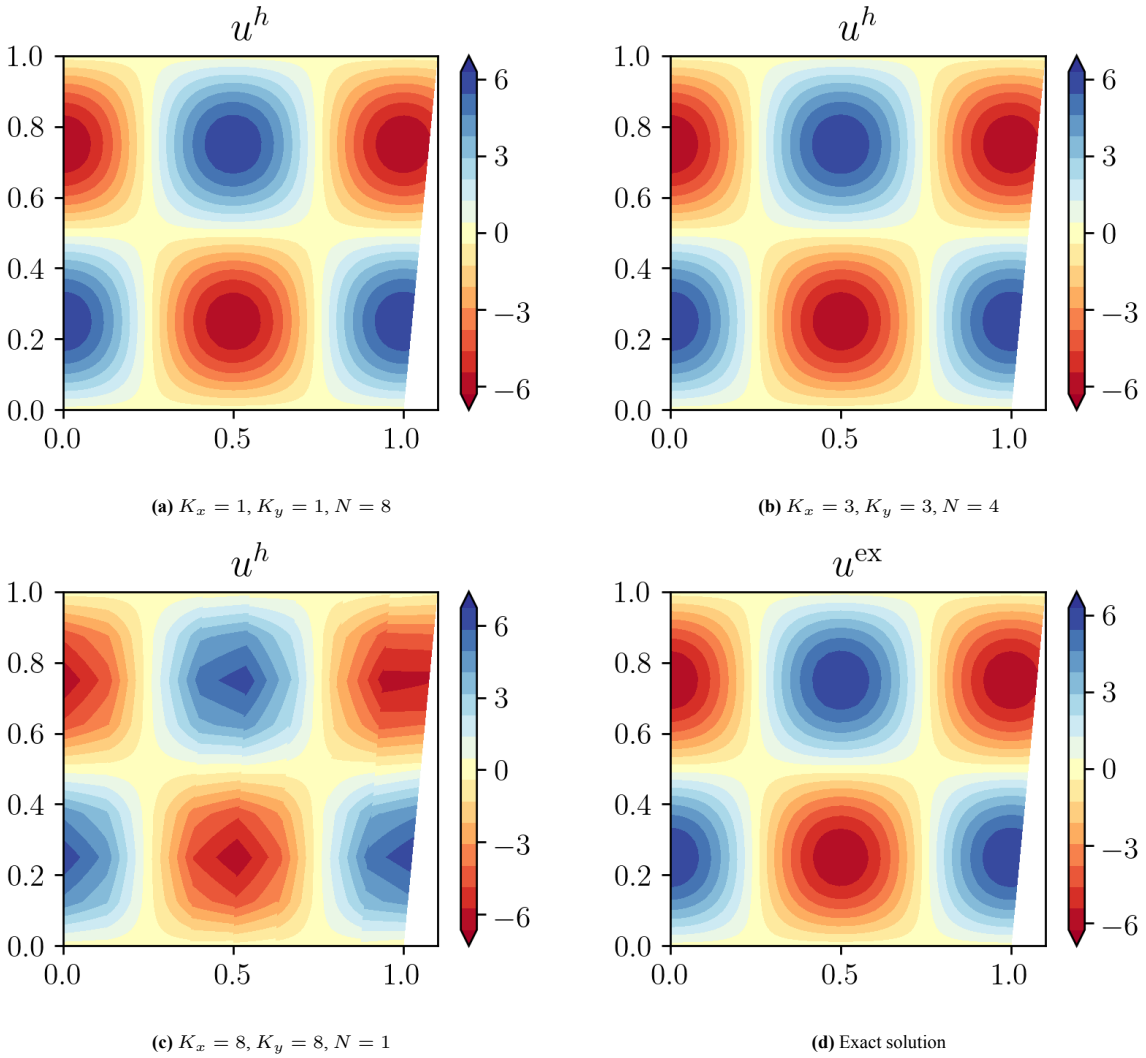

(a) $K_x = 1, K_y = 1, N = 8$

(b) $K_x = 3, K_y = 3, N = 4$

(c) $K_x = 8, K_y = 8, N = 1$

(d) Exact solution

Figure B.2: Results for u^h in the physical domain

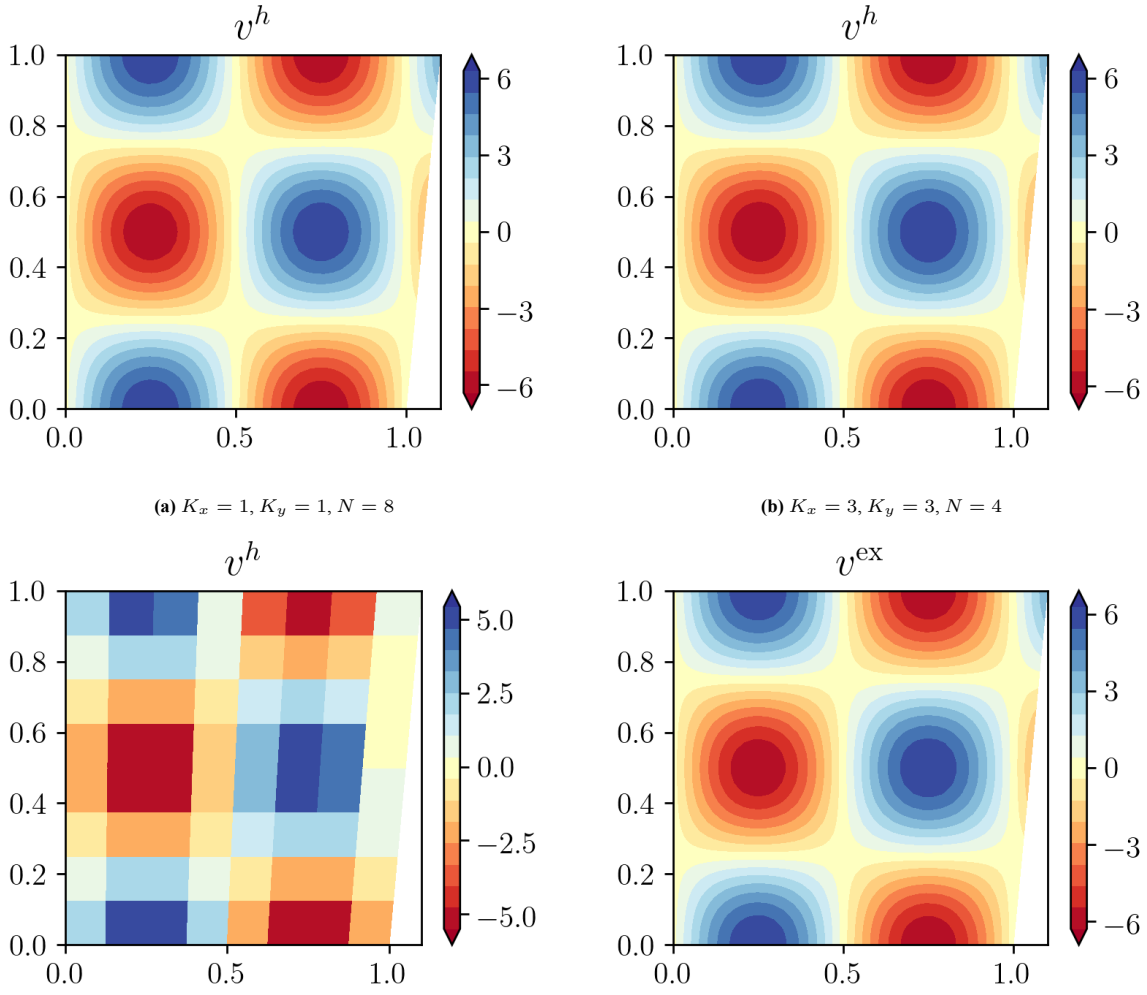

(a) $K_x = 1, K_y = 1, N = 8$

(b) $K_x = 3, K_y = 3, N = 4$

(c) $K_x = 8, K_y = 8, N = 1$

(d) Exact solution

Figure B.3: Results for v^h in the physical domain

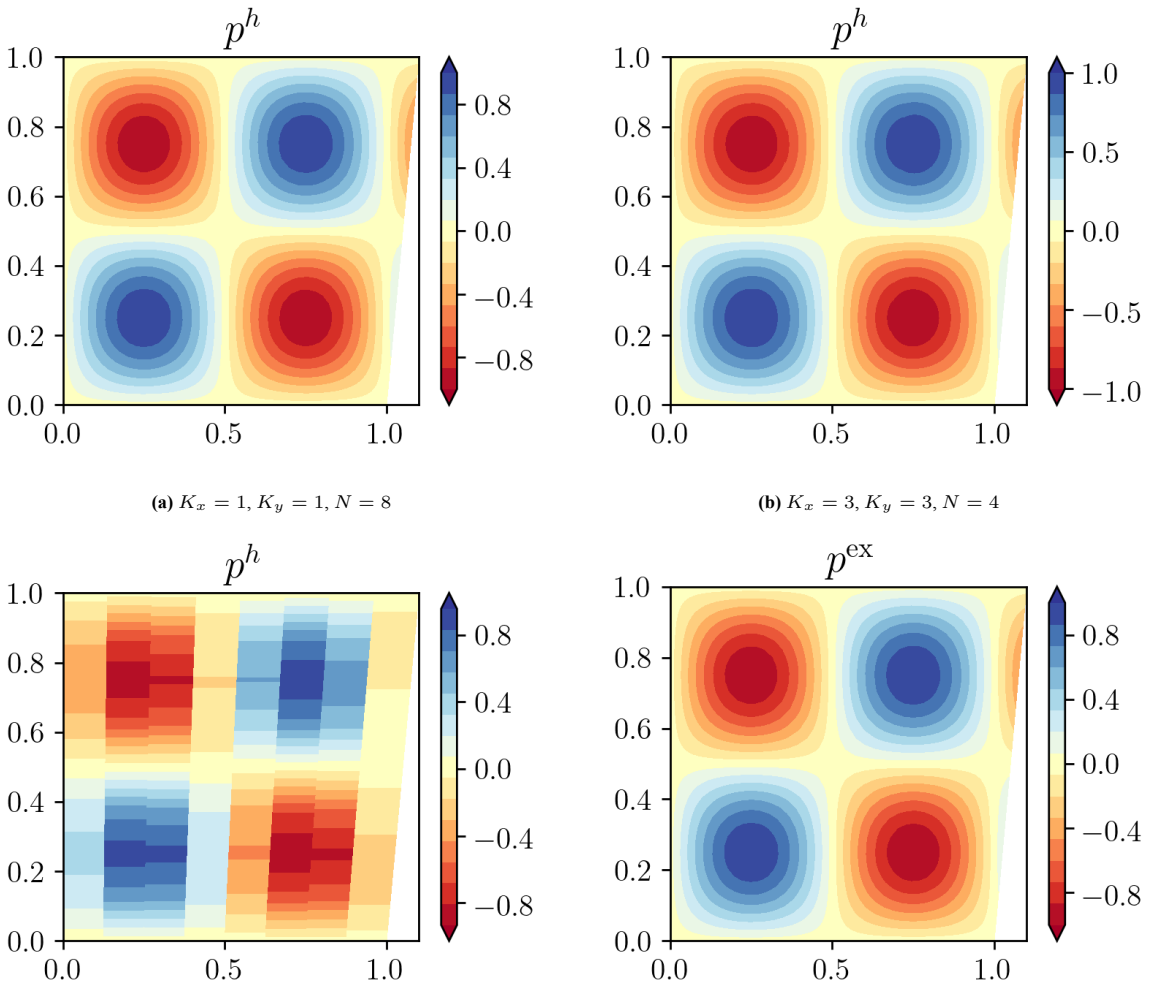

(a) $K_x = 1, K_y = 1, N = 8$

(b) $K_x = 3, K_y = 3, N = 4$

(c) $K_x = 8, K_y = 8, N = 1$

(d) Exact solution

Figure B.4: Results for p^h in the physical domain

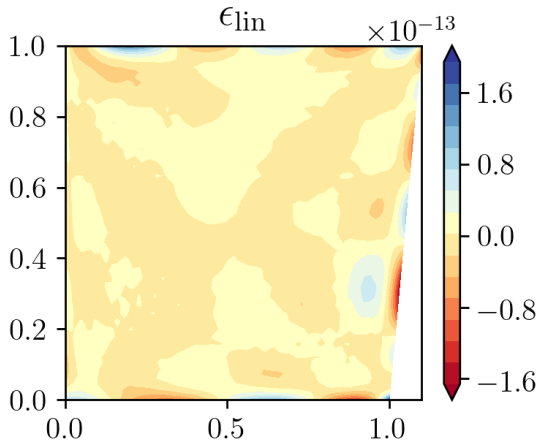

(a) $K_x = 1, K_y = 1, N = 8$

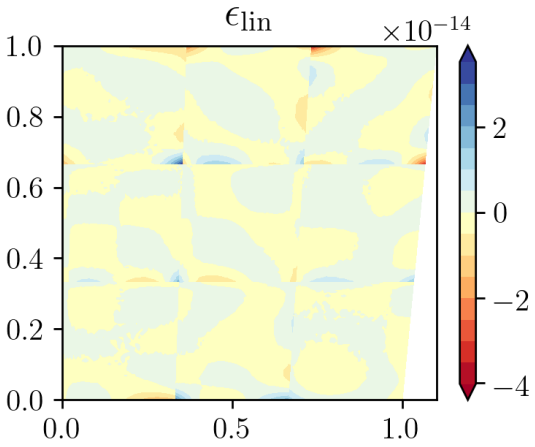

(b) $K_x = 3, K_y = 3, N = 4$

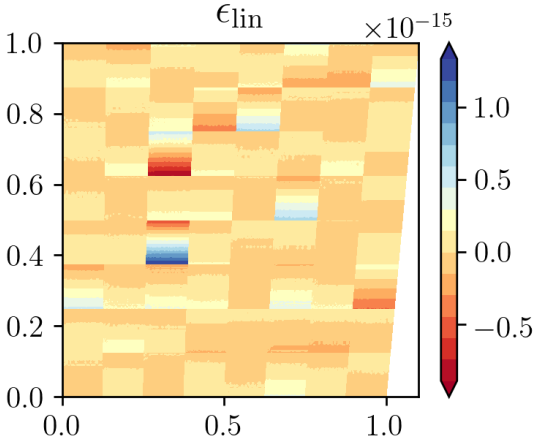

(c) $K_x = 8, K_y = 8, N = 1$

Figure B.5: Results for the error in the diffusion equation in the physical domain

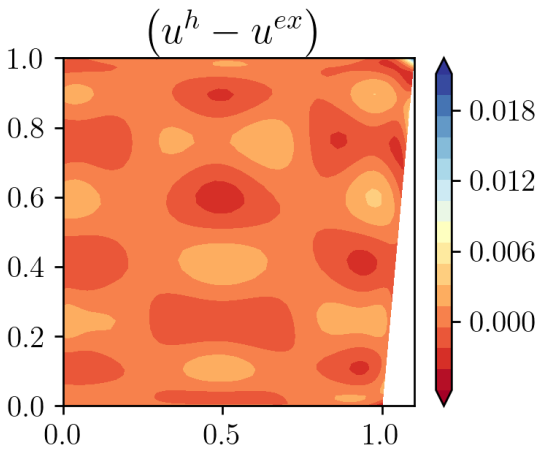

(a) $u_x^h - u_x^{ex}$ for $K_x = 1, K_y = 1, N = 8$

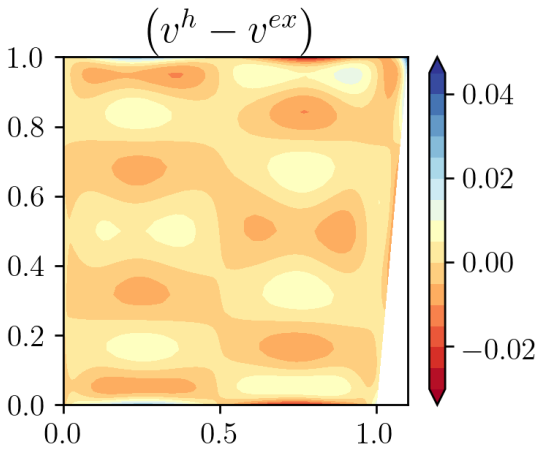

(b) $u_y^h - u_y^{ex}$ for $K_x = 1, K_y = 1, N = 8$

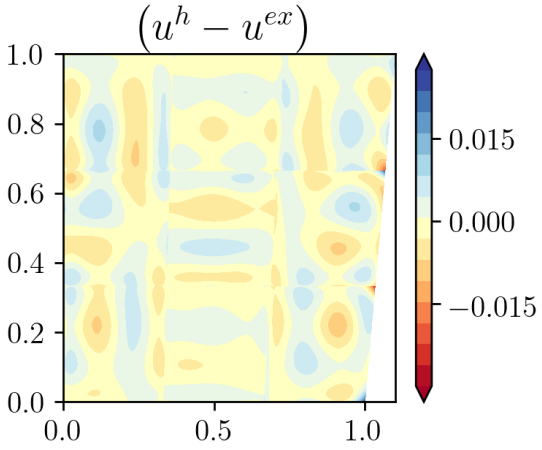

(c) $u_x^h - u_x^{ex}$ for $K_x = 3, K_y = 3, N = 4$

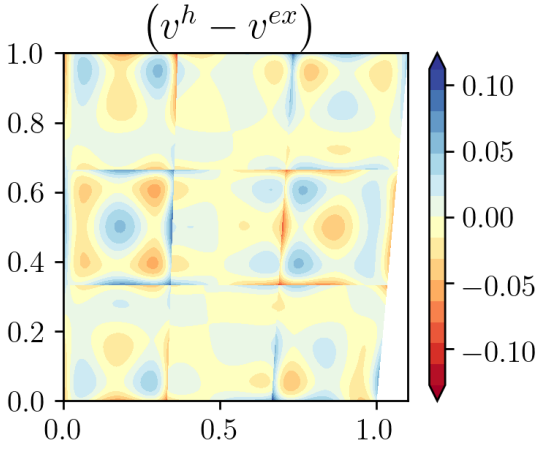

(d) $u_y^h - u_y^{ex}$ for $K_x = 3, K_y = 3, N = 4$

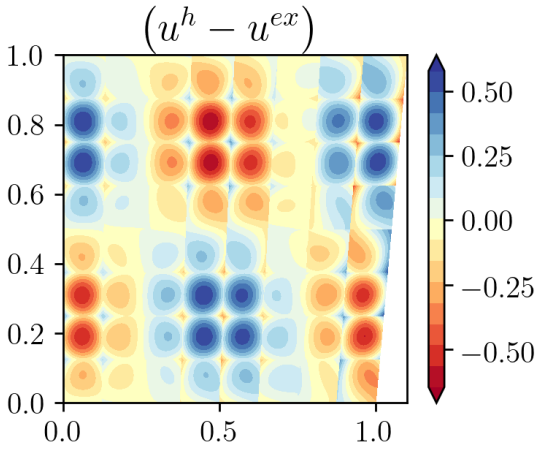

(e) $u_x^h - u_x^{ex}$ for $K_x = 8, K_y = 8, N = 1$

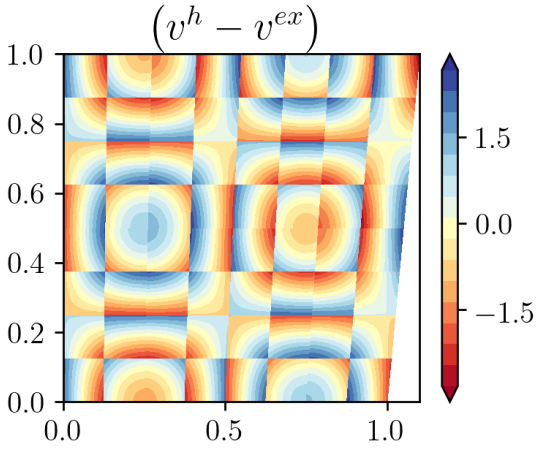

(f) $u_y^h - u_y^{ex}$ for $K_x = 8, K_y = 8, N = 1$

Figure B.6: Errors in u_y and u_x for different configurations

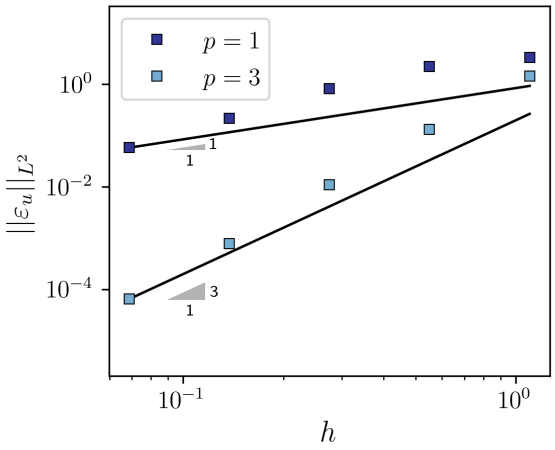

(a) Convergence with mesh width of L^2 error for u^h

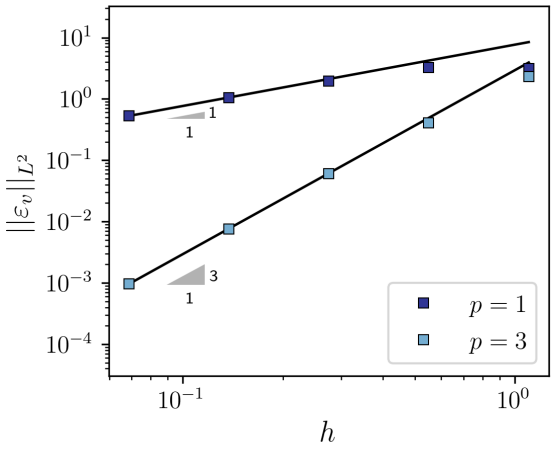

(b) Convergence with mesh width of L^2 error for v^h

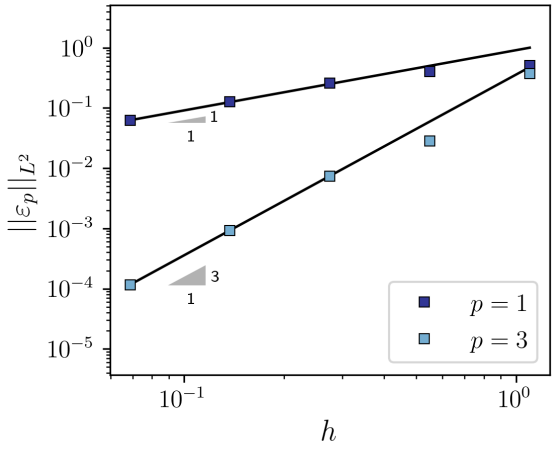

(c) Convergence with mesh width of L^2 error for p^h

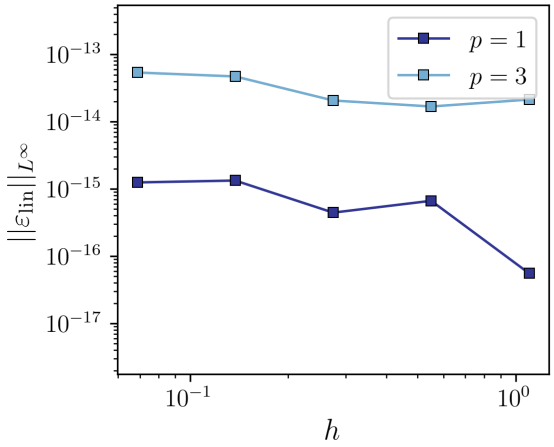

(d) Convergence with mesh width of L^∞ error for the error in the diffusion equation

Figure B.7: Results from the h-convergence study

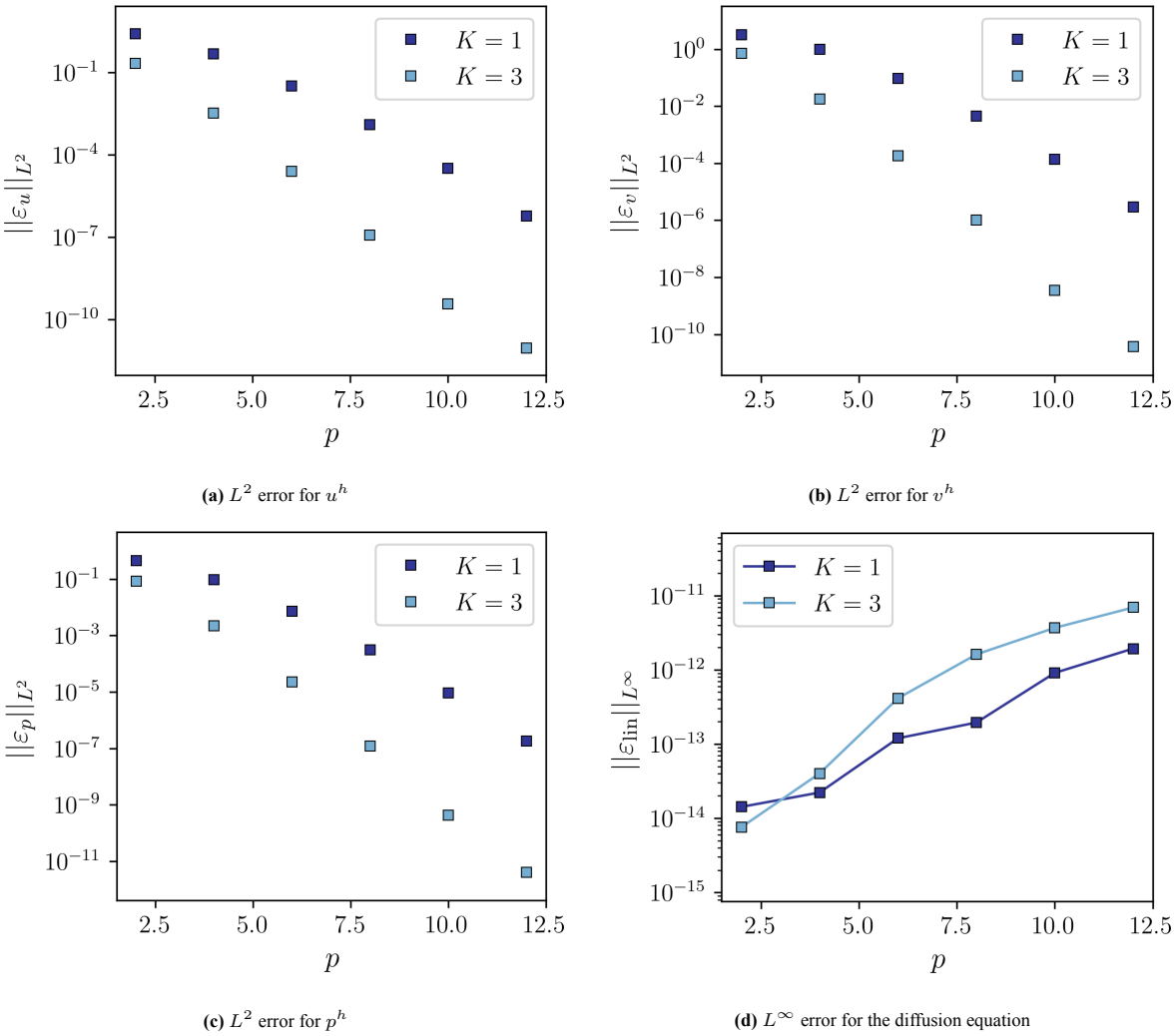

(a) L^2 error for u^h

(b) L^2 error for v^h

(c) L^2 error for p^h

(d) L^∞ error for the diffusion equation

Figure B.8: Results from the polynomial convergence study

B.2. Lagrangian formulation

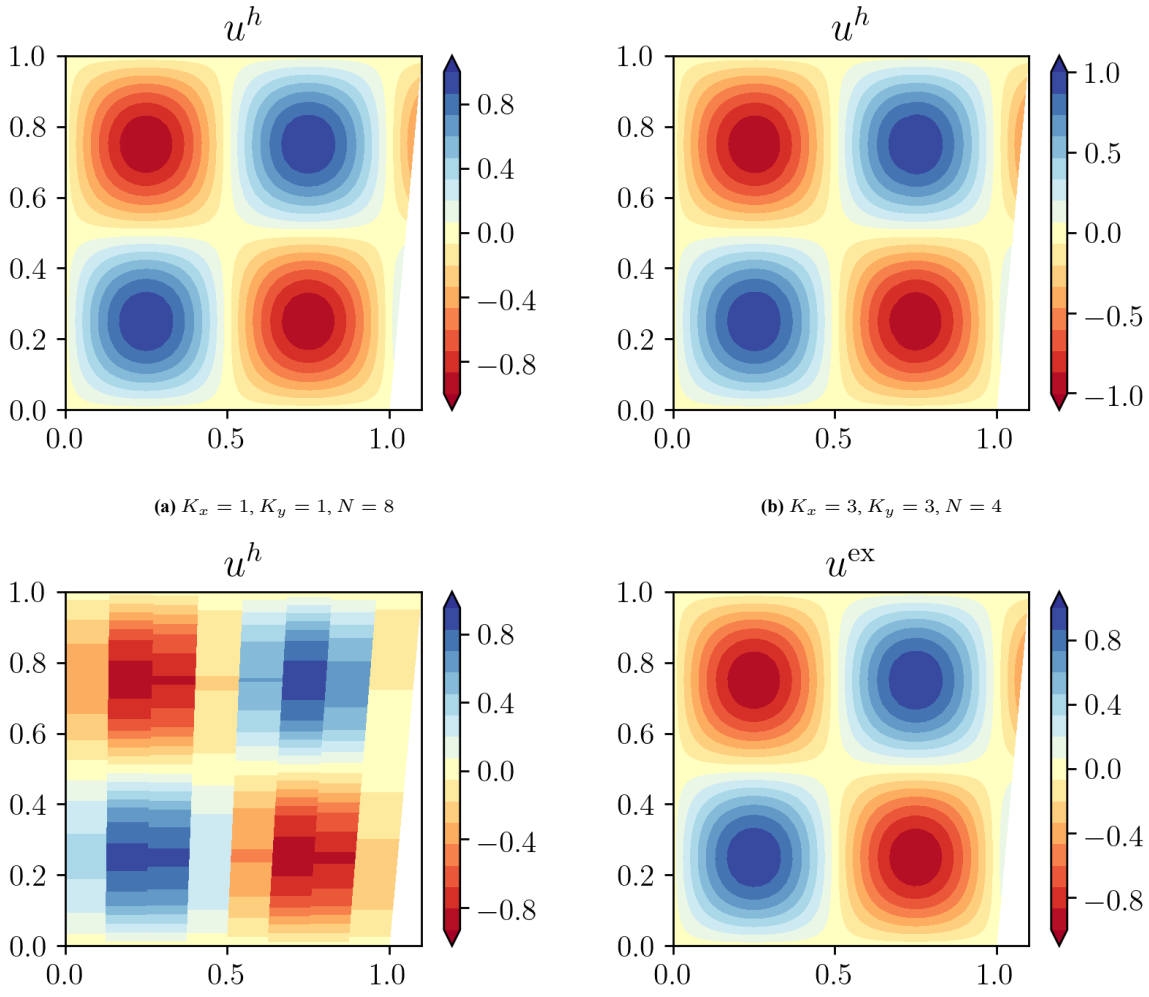

(a) $K_x = 1, K_y = 1, N = 8$

(b) $K_x = 3, K_y = 3, N = 4$

(c) $K_x = 8, K_y = 8, N = 1$

(d) Exact solution

Figure B.9: Results for u^h in the physical domain

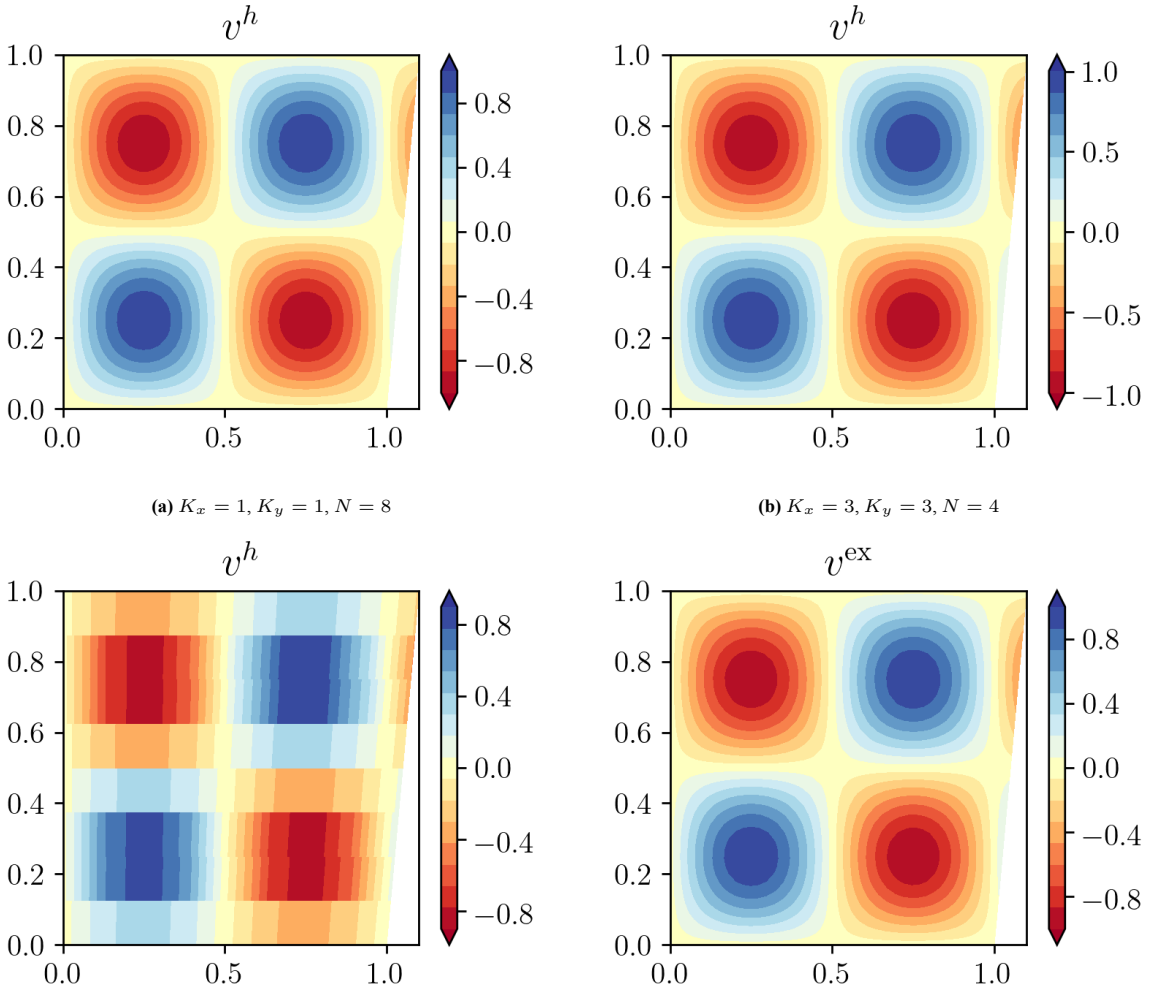

(a) $K_x = 1, K_y = 1, N = 8$

(b) $K_x = 3, K_y = 3, N = 4$

(c) $K_x = 8, K_y = 8, N = 1$

(d) Exact solution

Figure B.10: Results for v^h in the physical domain

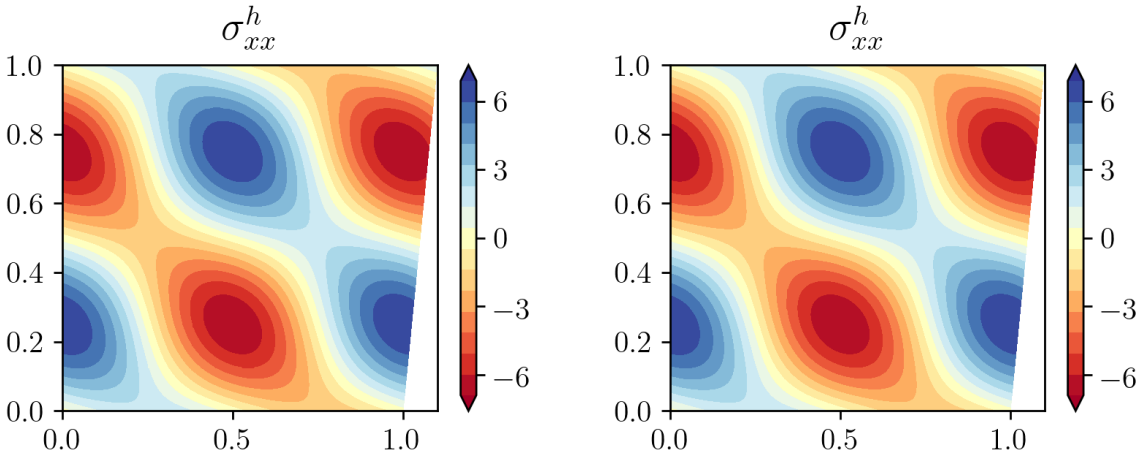

(a) $K_x = 1, K_y = 1, N = 8$

(b) $K_x = 3, K_y = 3, N = 4$

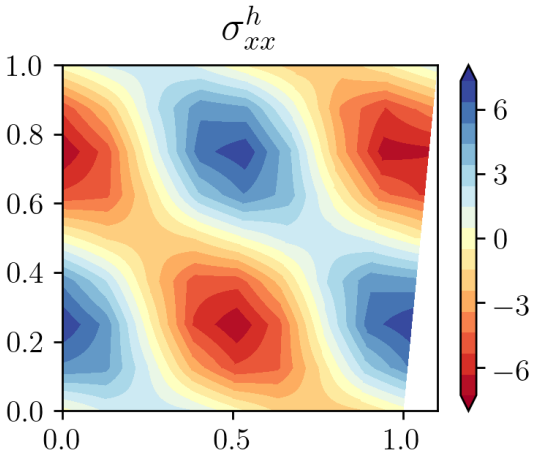

(c) $K_x = 8, K_y = 8, N = 1$

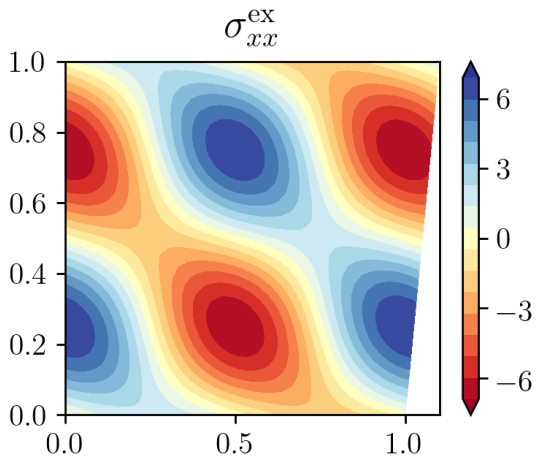

(d) Exact solution

Figure B.11: Results for σ^h_{xx} in the physical domain

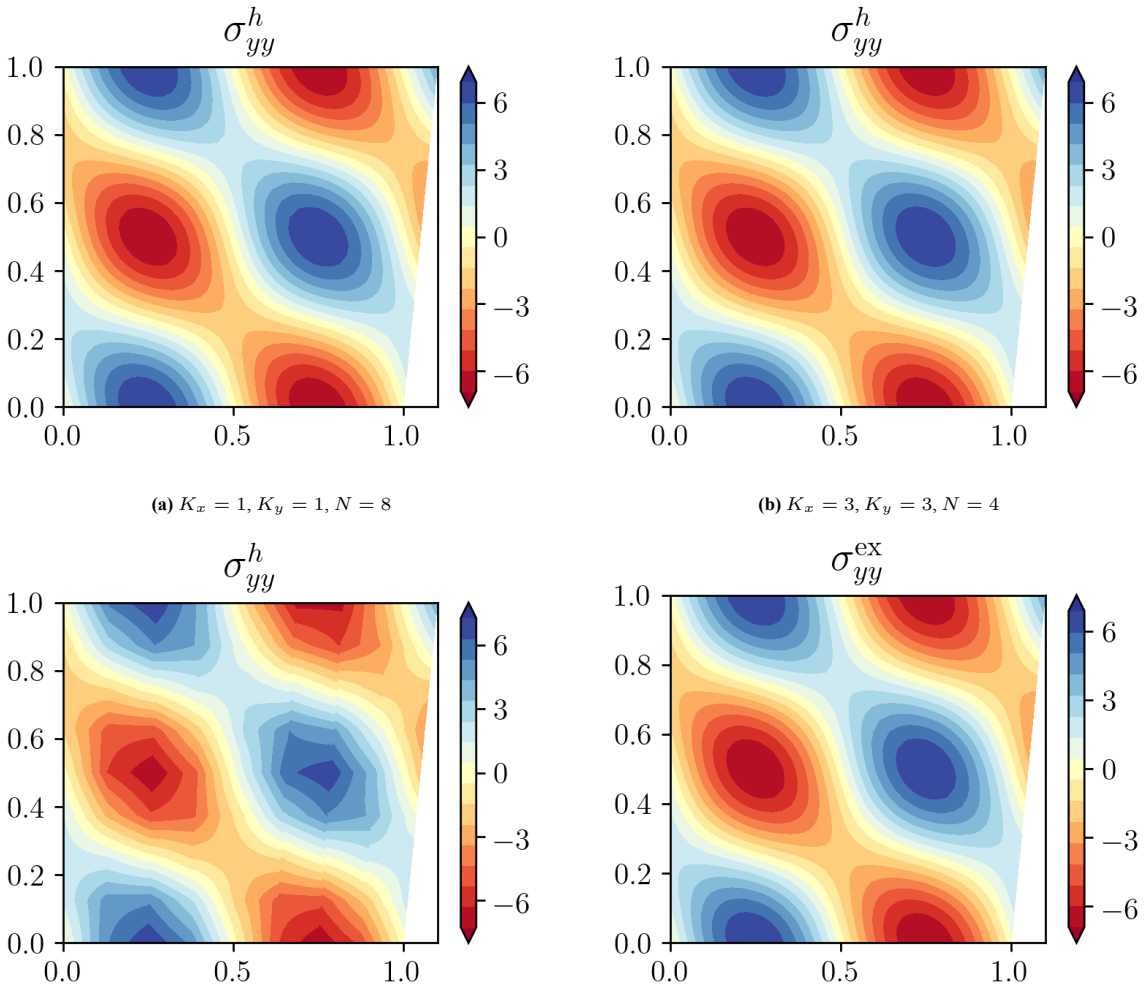

(a) $K_x = 1, K_y = 1, N = 8$

(b) $K_x = 3, K_y = 3, N = 4$

(c) $K_x = 8, K_y = 8, N = 1$

(d) Exact solution

Figure B.12: Results for σ^h_{yy} in the physical domain

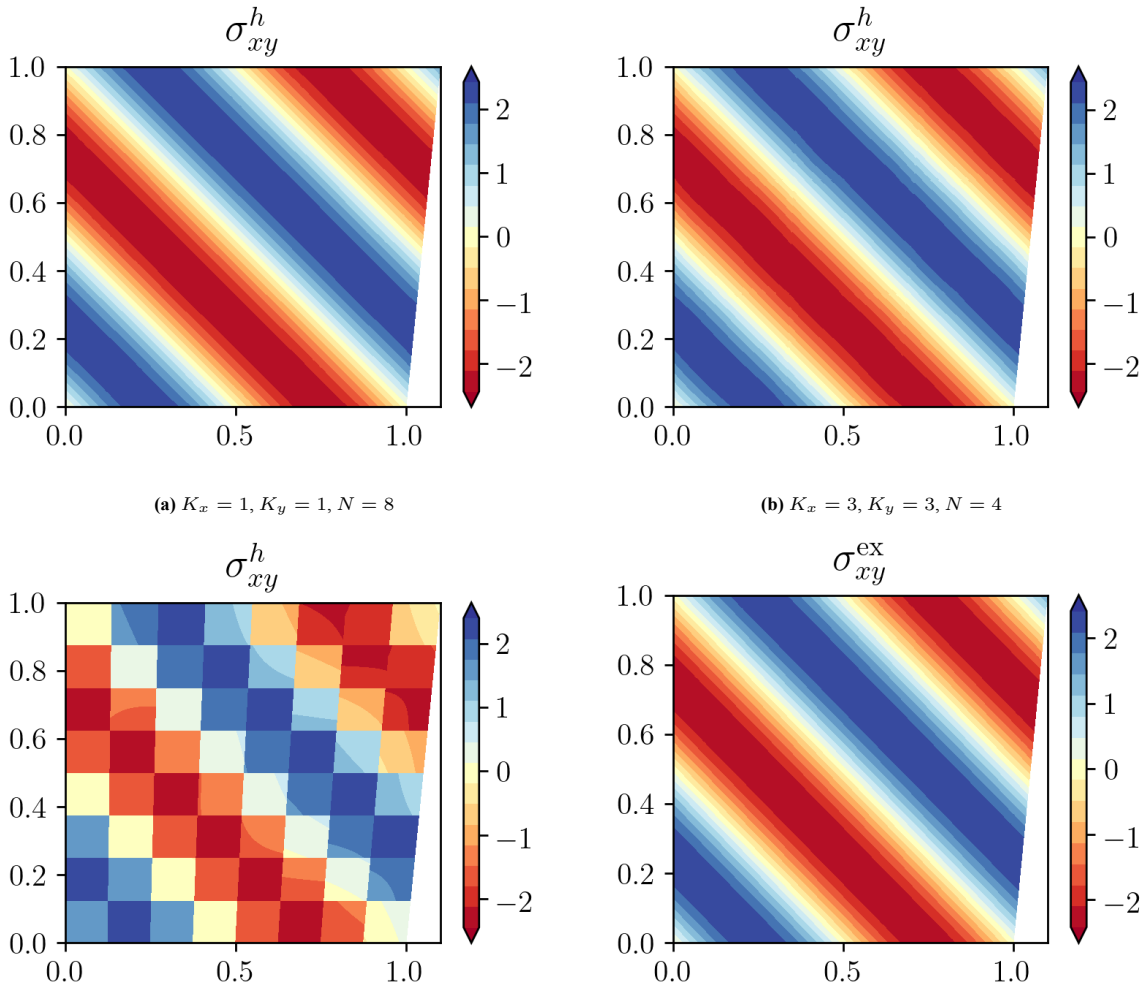

(a) $K_x = 1, K_y = 1, N = 8$

(b) $K_x = 3, K_y = 3, N = 4$

(c) $K_x = 8, K_y = 8, N = 1$

(d) Exact solution

Figure B.13: Results for σ^h_{xy} in the physical domain

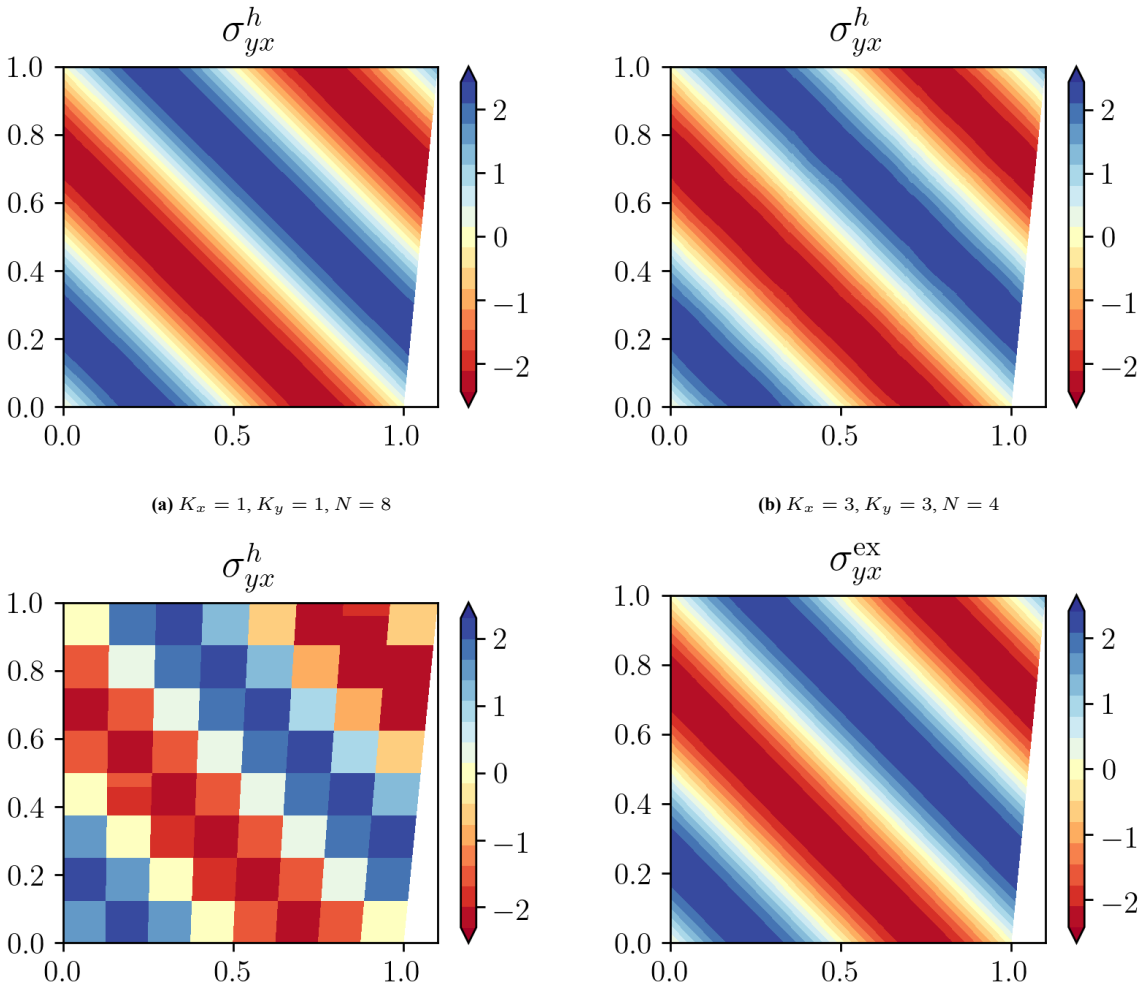

(a) $K_x = 1, K_y = 1, N = 8$

(b) $K_x = 3, K_y = 3, N = 4$

(c) $K_x = 8, K_y = 8, N = 1$

(d) Exact solution

Figure B.14: Results for σ^h_{yx} in the physical domain

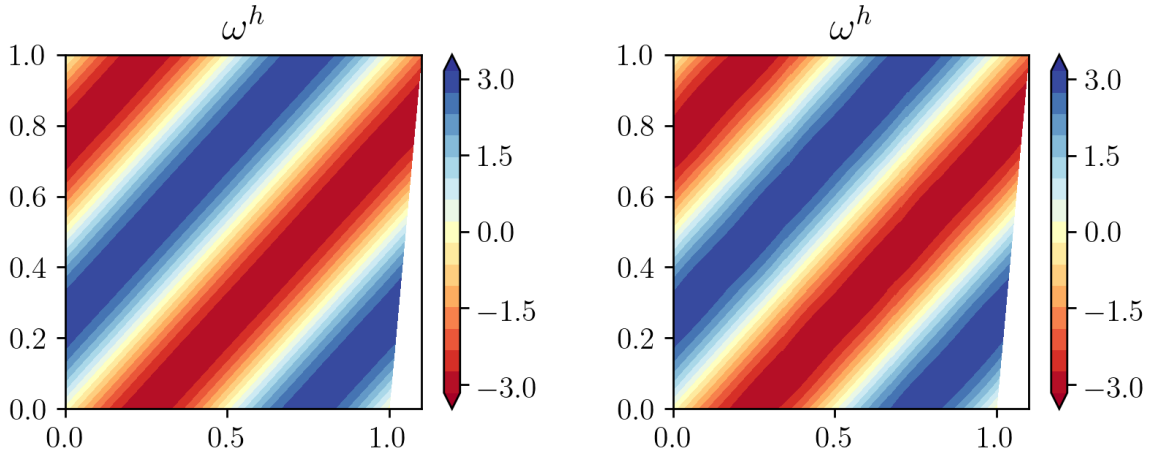

(a) $K_x = 1, K_y = 1, N = 8$

(b) $K_x = 3, K_y = 3, N = 4$

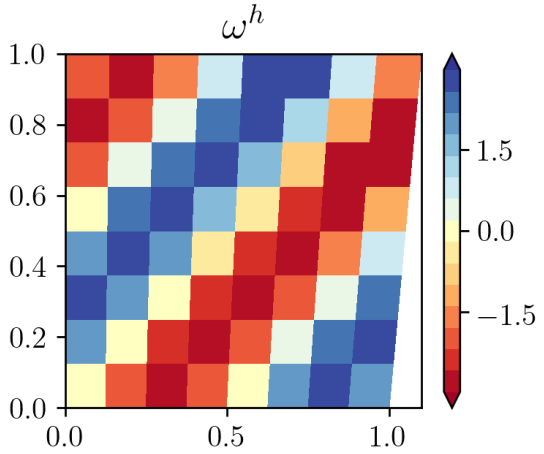

(c) $K_x = 8, K_y = 8, N = 1$

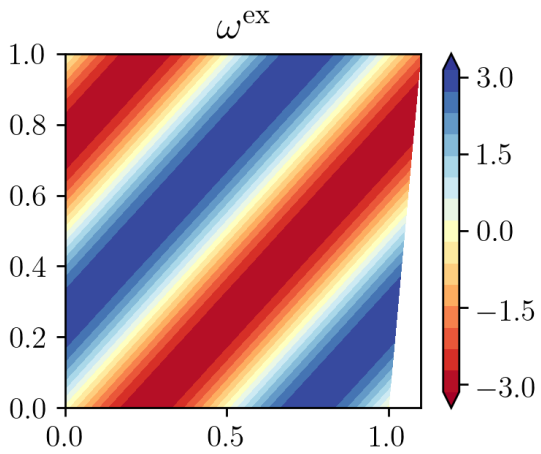

(d) Exact solution

Figure B.15: Results for ω^h in the physical domain

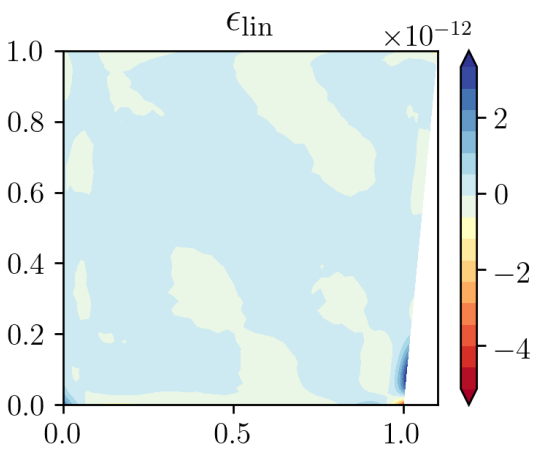

(a) Error in conservation of linear momentum for $K_x = 1$, $K_y = 1$, $N = 8$

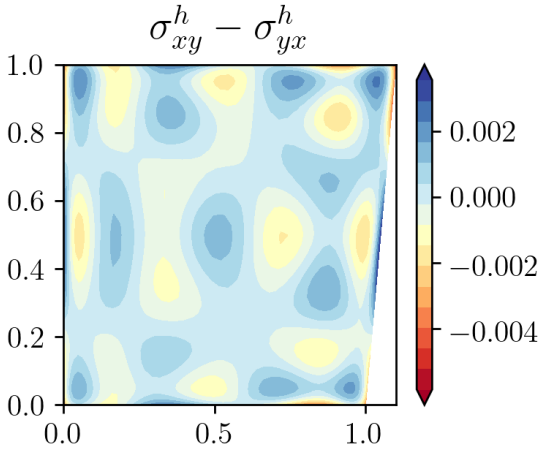

(b) Error in symmetry of stress tensor for $K_x = 1$, $K_y = 1$, $N = 8$

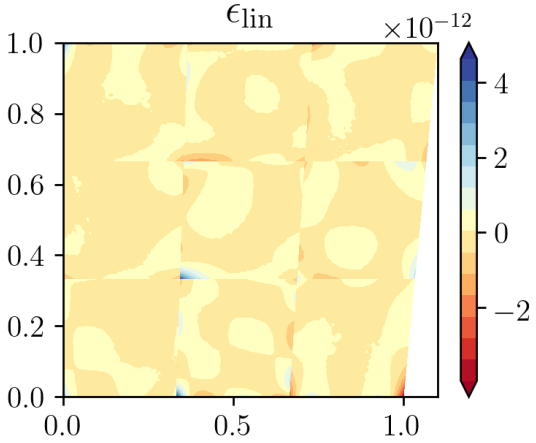

(c) Error in conservation of linear momentum for $K_x = 3$, $K_y = 3$, $N = 4$

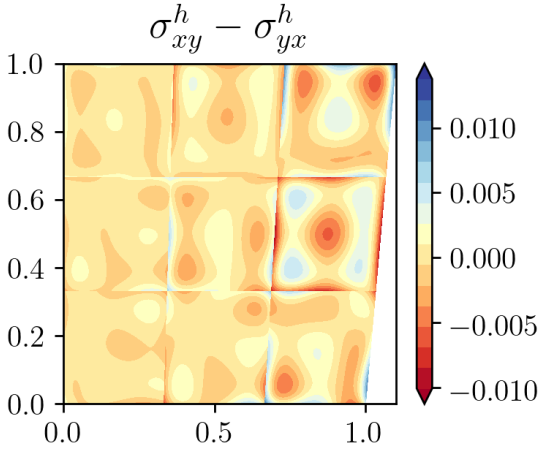

(d) Error in symmetry of stress tensor for $K_x = 3$, $K_y = 3$, $N = 4$

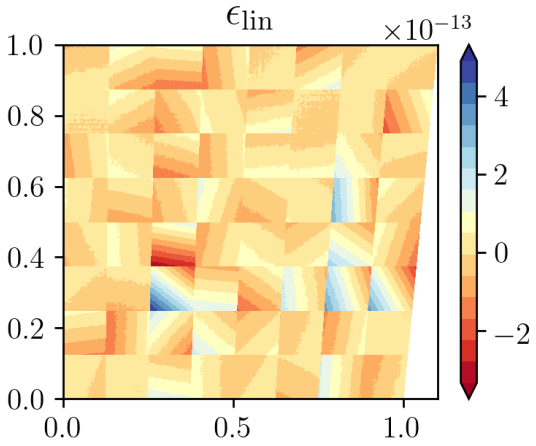

(e) Error in conservation of linear momentum for $K_x = 8$, $K_y = 8$, $N = 1$

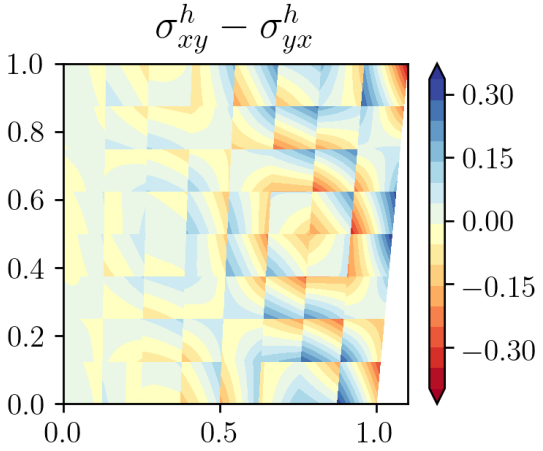

(f) Error in symmetry of stress tensor for $K_x = 8$, $K_y = 8$, $N = 1$

Figure B.16: Results for errors in conservation of linear momentum and angular momentum

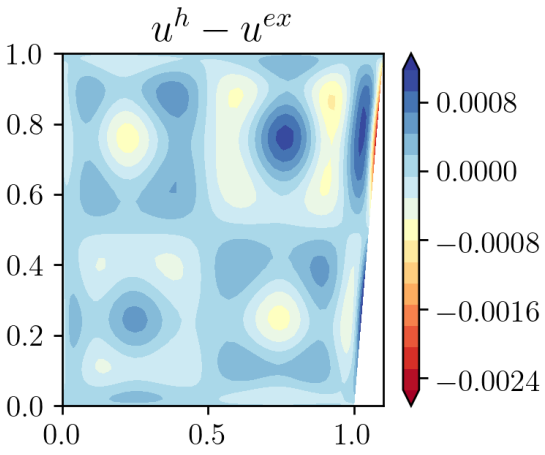

(a) $u_x^h - u_x^{ex}$ for $K_x = 1, K_y = 1, N = 8$

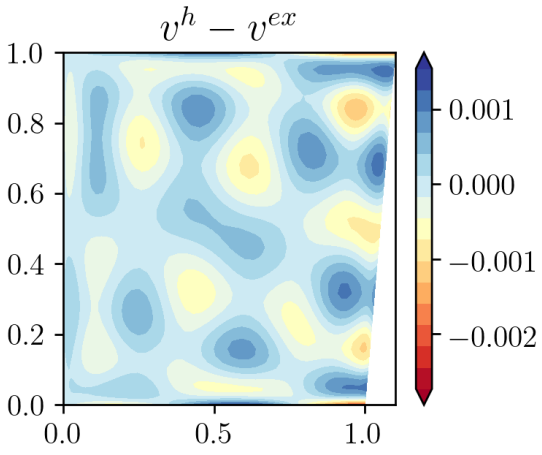

(b) $u_y^h - u_y^{ex}$ for $K_x = 1, K_y = 1, N = 8$

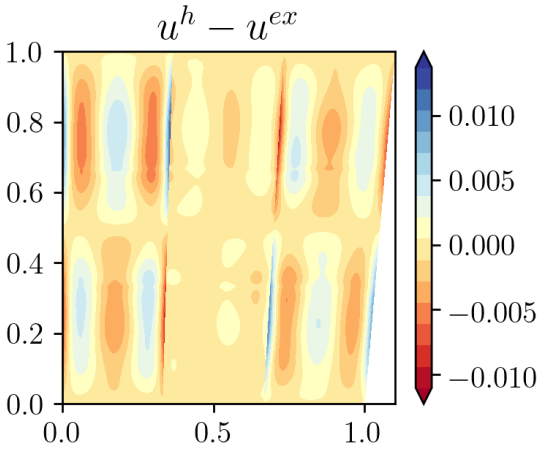

(c) $u_x^h - u_x^{ex}$ for $K_x = 3, K_y = 3, N = 4$

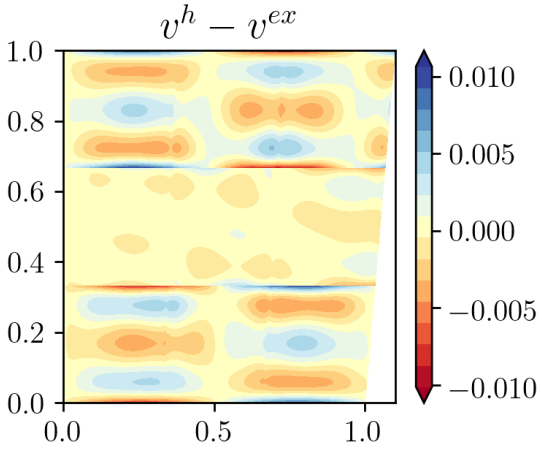

(d) $u_y^h - u_y^{ex}$ for $K_x = 3, K_y = 3, N = 4$

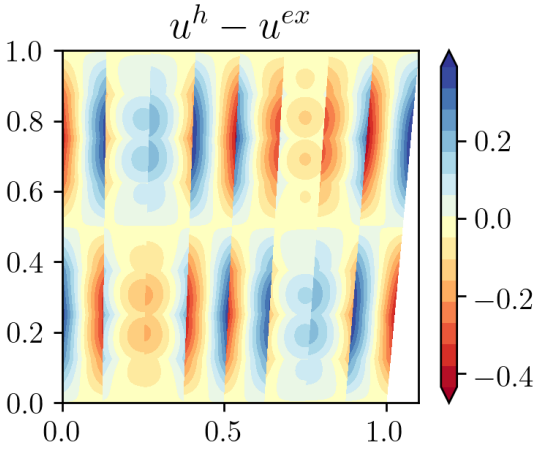

(e) $u_x^h - u_x^{ex}$ for $K_x = 8, K_y = 8, N = 1$

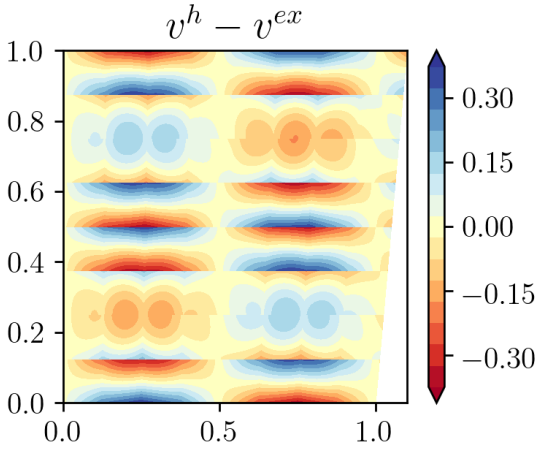

(f) $u_y^h - u_y^{ex}$ for $K_x = 8, K_y = 8, N = 1$

Figure B.17: Results for errors in u_x^h and u_y^h from the exact solutions

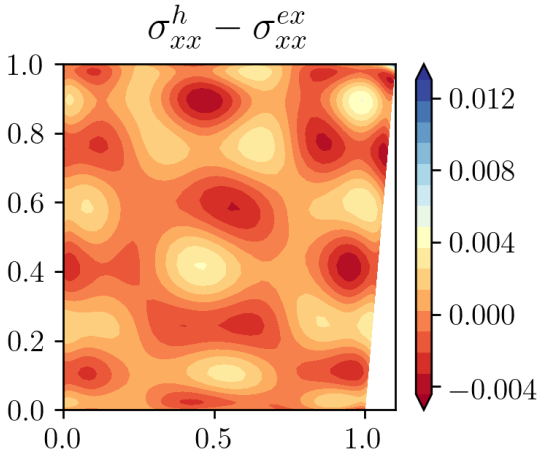

(a) $\sigma^h_{xx} - \sigma^{ex}_{xx}$ for $K_x = 1, K_y = 1, N = 8$

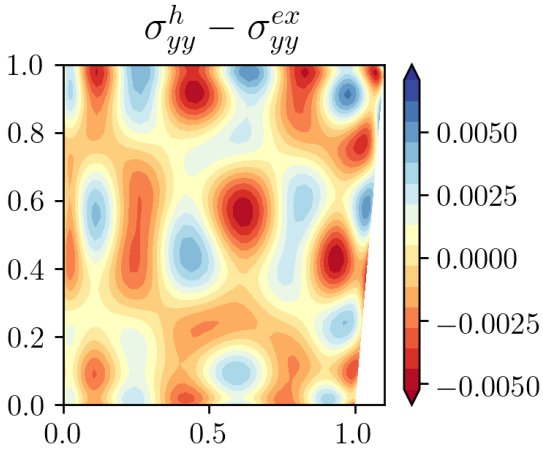

(b) $\sigma^h_{yy} - \sigma^{ex}_{yy}$ for $K_x = 1, K_y = 1, N = 8$

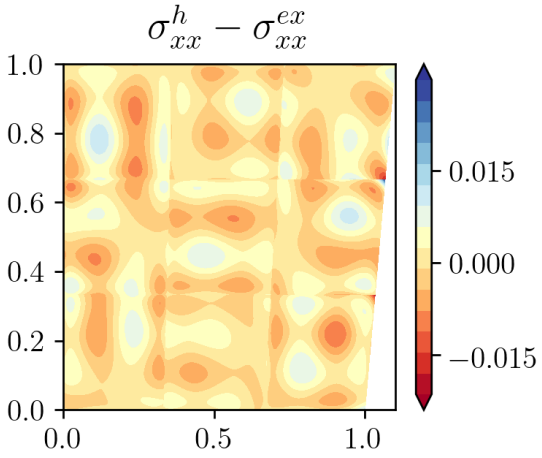

(c) $\sigma^h_{xx} - \sigma^{ex}_{xx}$ for $K_x = 3, K_y = 3, N = 4$

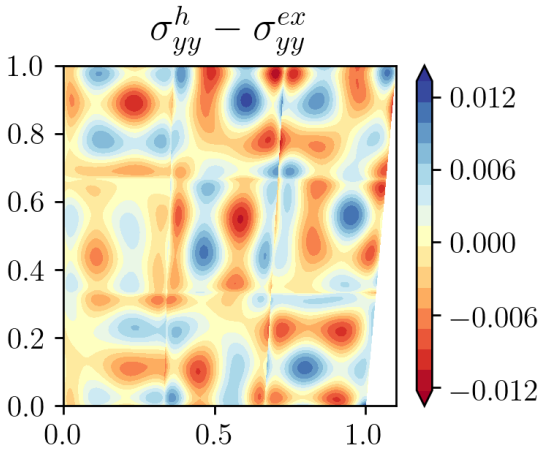

(d) $\sigma^h_{yy} - \sigma^{ex}_{yy}$ for $K_x = 3, K_y = 3, N = 4$

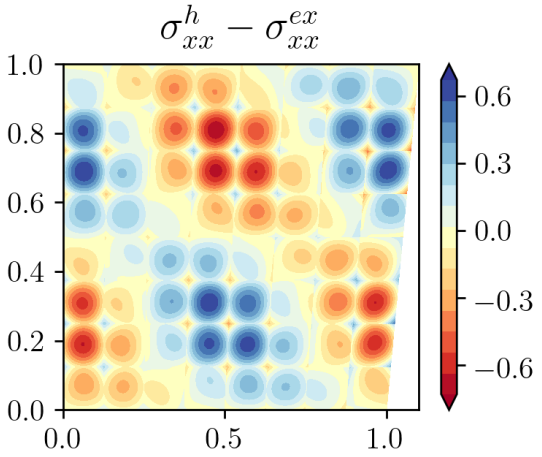

(e) $\sigma^h_{xx} - \sigma^{ex}_{xx}$ for $K_x = 8, K_y = 8, N = 1$

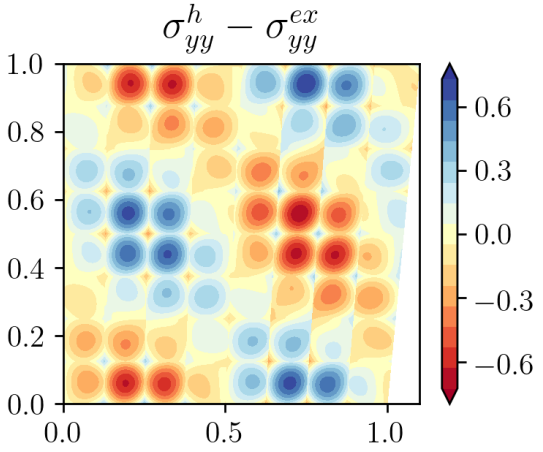

(f) $\sigma^h_{yy} - \sigma^{ex}_{yy}$ for $K_x = 8, K_y = 8, N = 1$

Figure B.18: Results for errors in σ^h_{xx} and σ^h_{yy} from the exact solutions

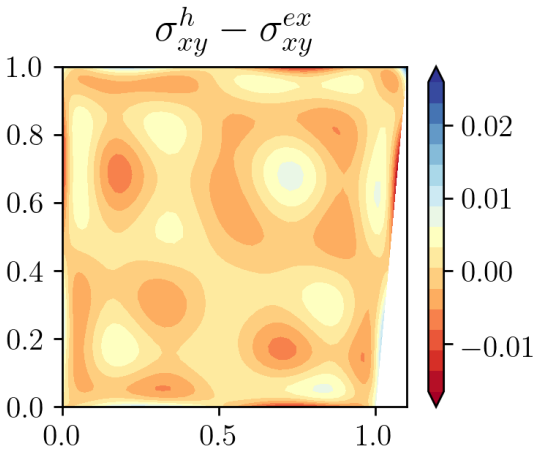

(a) $\sigma^h_{xy} - \sigma^{ex}_{xy}$ for $K_x = 1, K_y = 1, N = 8$

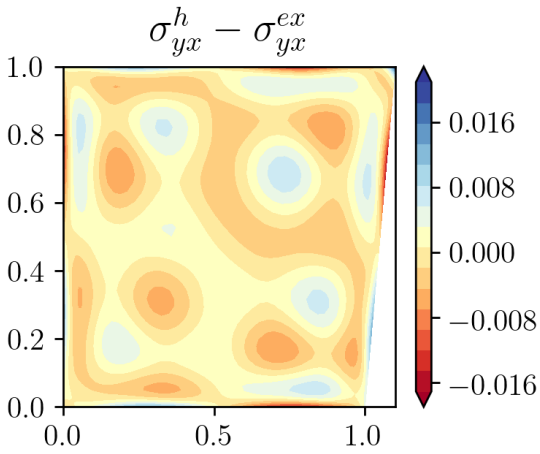

(b) $\sigma^h_{yx} - \sigma^{ex}_{yx}$ for $K_x = 1, K_y = 1, N = 8$

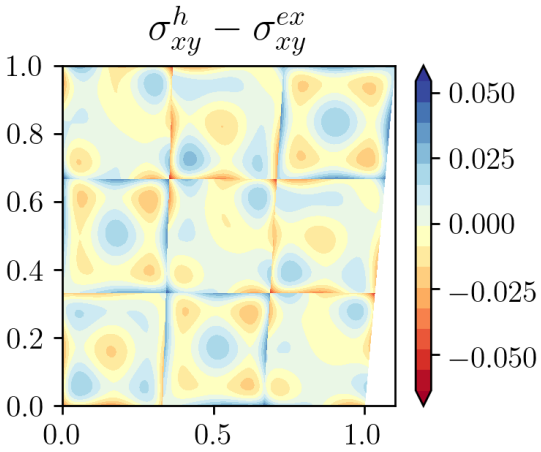

(c) $\sigma^h_{xy} - \sigma^{ex}_{xy}$ for $K_x = 3, K_y = 3, N = 4$

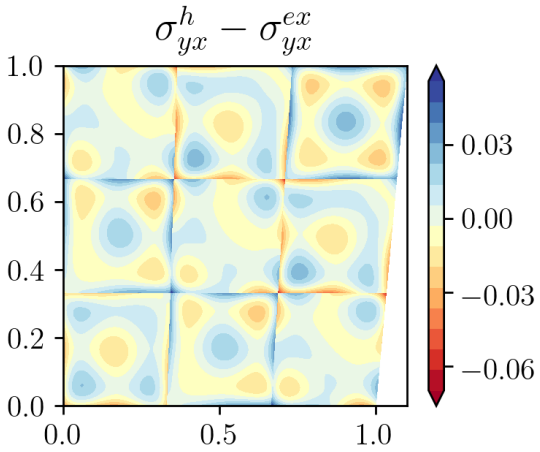

(d) $\sigma^h_{yx} - \sigma^{ex}_{yx}$ for $K_x = 3, K_y = 3, N = 4$

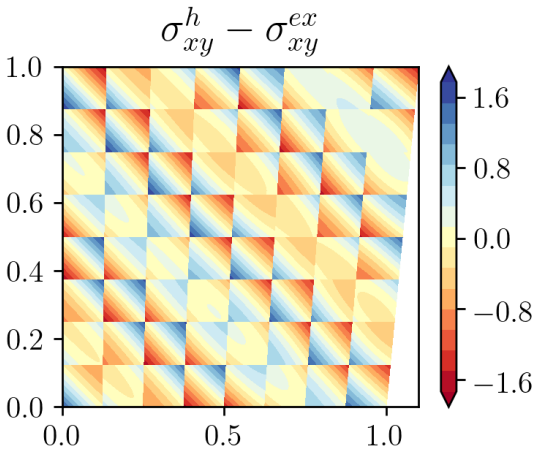

(e) $\sigma^h_{xy} - \sigma^{ex}_{xy}$ for $K_x = 8, K_y = 8, N = 1$

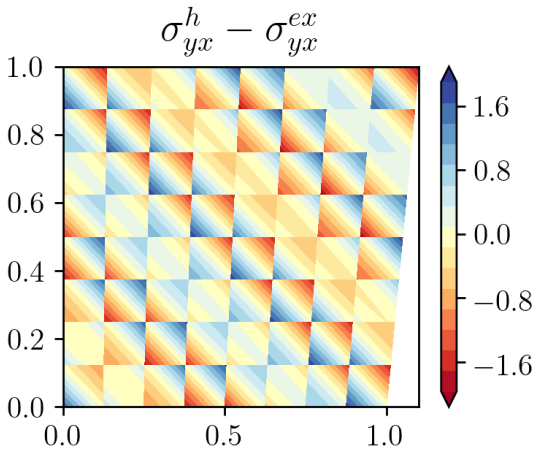

(f) $\sigma^h_{yx} - \sigma^{ex}_{yx}$ for $K_x = 8, K_y = 8, N = 1$

Figure B.19: Results for errors in σ^h_{xy} and σ^h_{yx} from the exact solutions

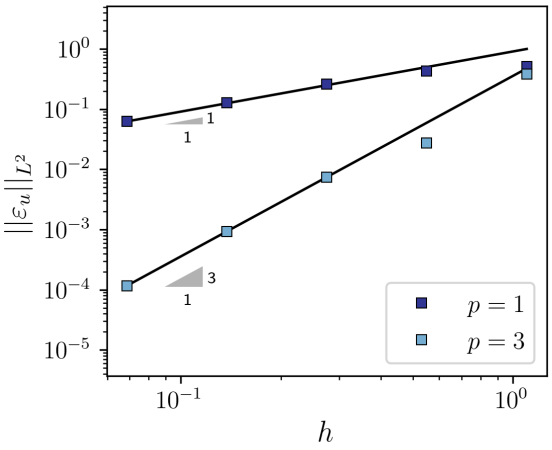

(a) Convergence with mesh width of L^2 error for u^h

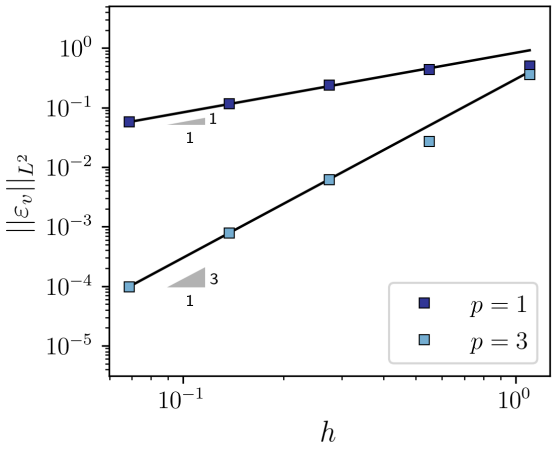

(b) Convergence with mesh width of L^2 error for v^h

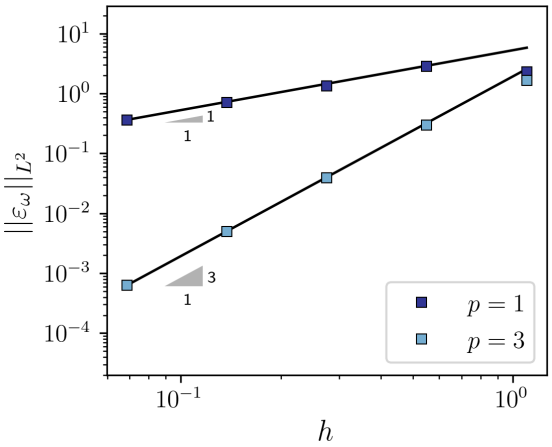

(c) Convergence with mesh width of L^2 error for ω^h

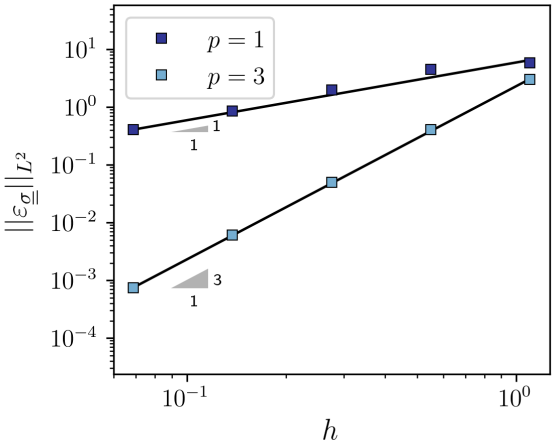

(d) Convergence with mesh width of L^2 error for $\underline{\underline{\boldsymbol{\sigma}}}^h$

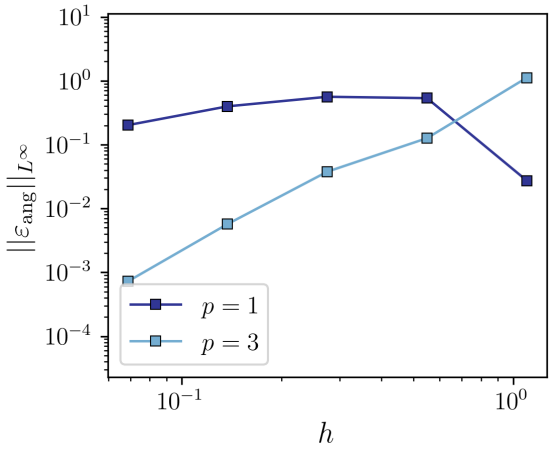

(e) Convergence with mesh width of L^∞ error for conservation of angular momentum

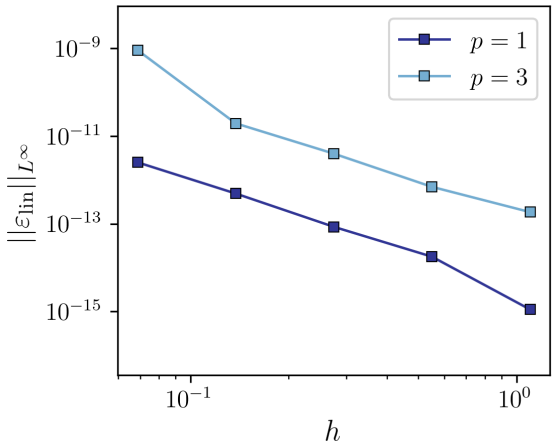

(f) Convergence with mesh width of L^∞ error for conservation of linear momentum

Figure B.20: Results from the h-convergence study

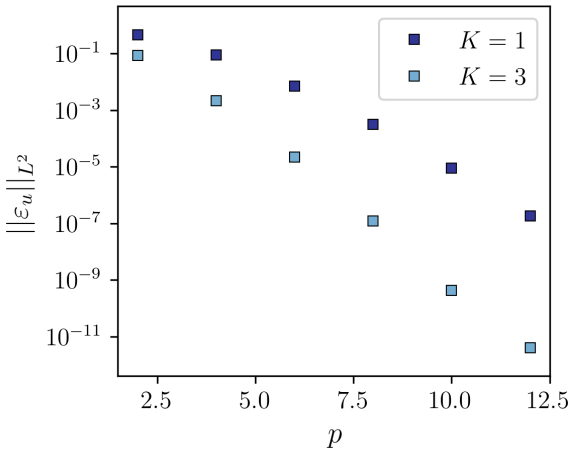

(a) L^2 error for u^h

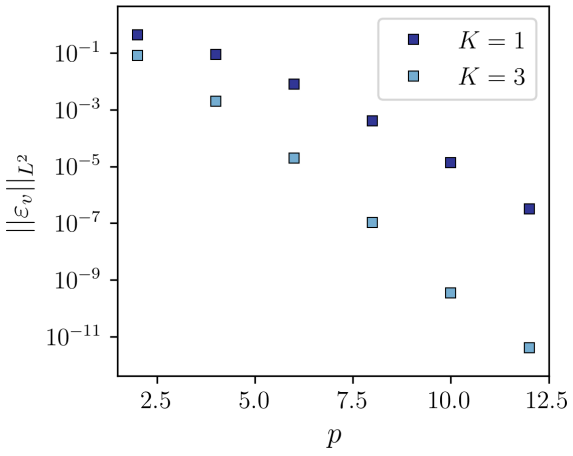

(b) L^2 error for v^h

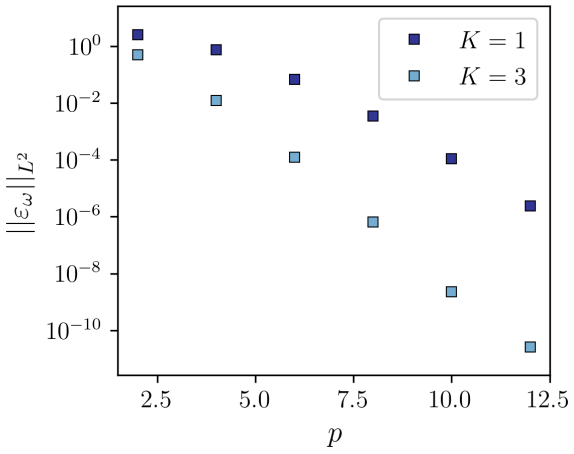

(c) L^2 error for ω^h

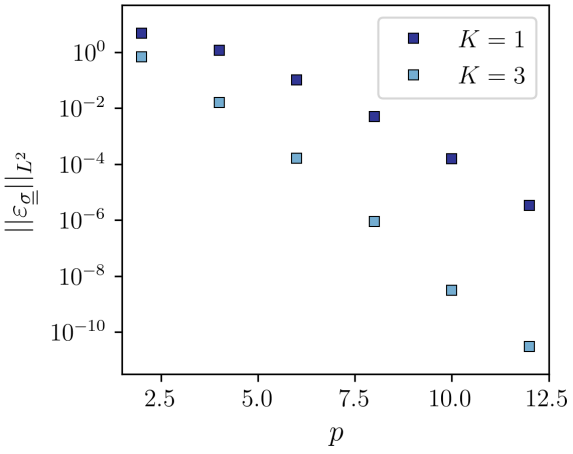

(d) L^2 error for $\underline{\underline{\boldsymbol{\sigma}}}^h$

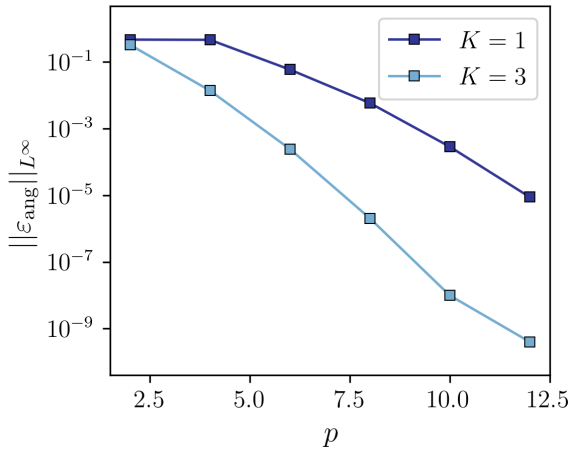

(e) L^∞ error in conservation of angular momentum

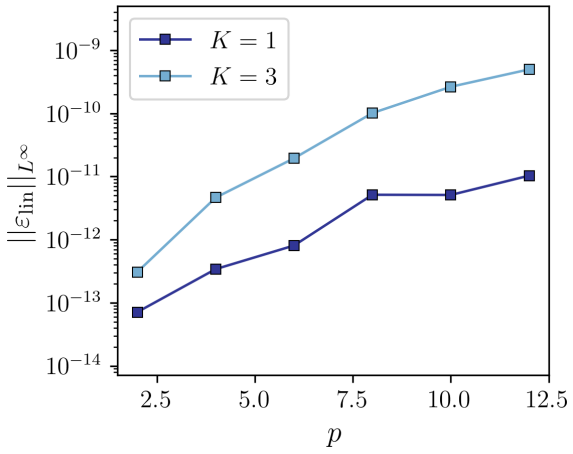

(f) L^∞ error in conservation of linear momentum

Figure B.21: Results from the polynomial convergence study

B.3. Dual Lagrangian formulation

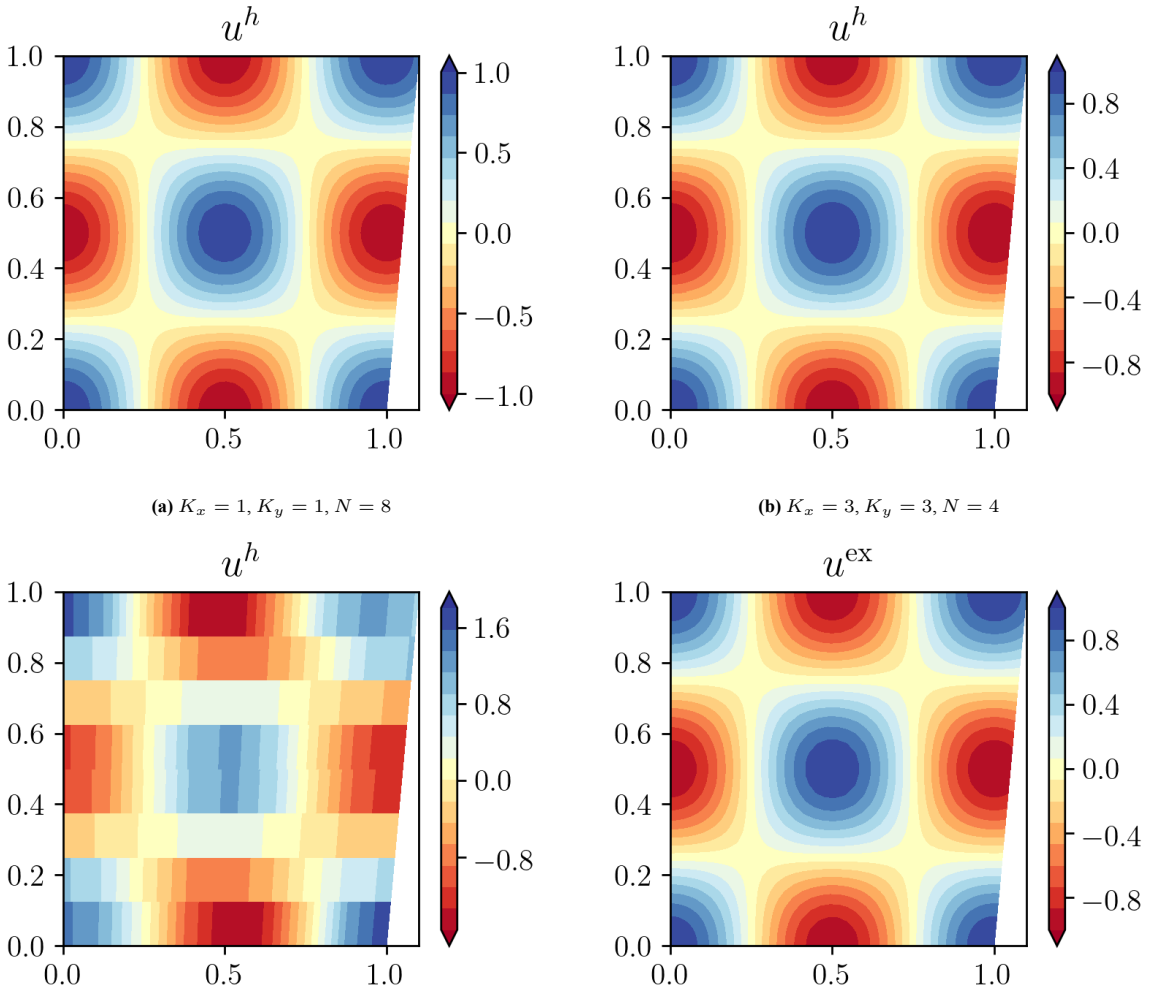

(a) $K_x = 1, K_y = 1, N = 8$

(b) $K_x = 3, K_y = 3, N = 4$

(c) $K_x = 8, K_y = 8, N = 1$

(d) Exact solution

Figure B.22: Results for u^h in the physical domain

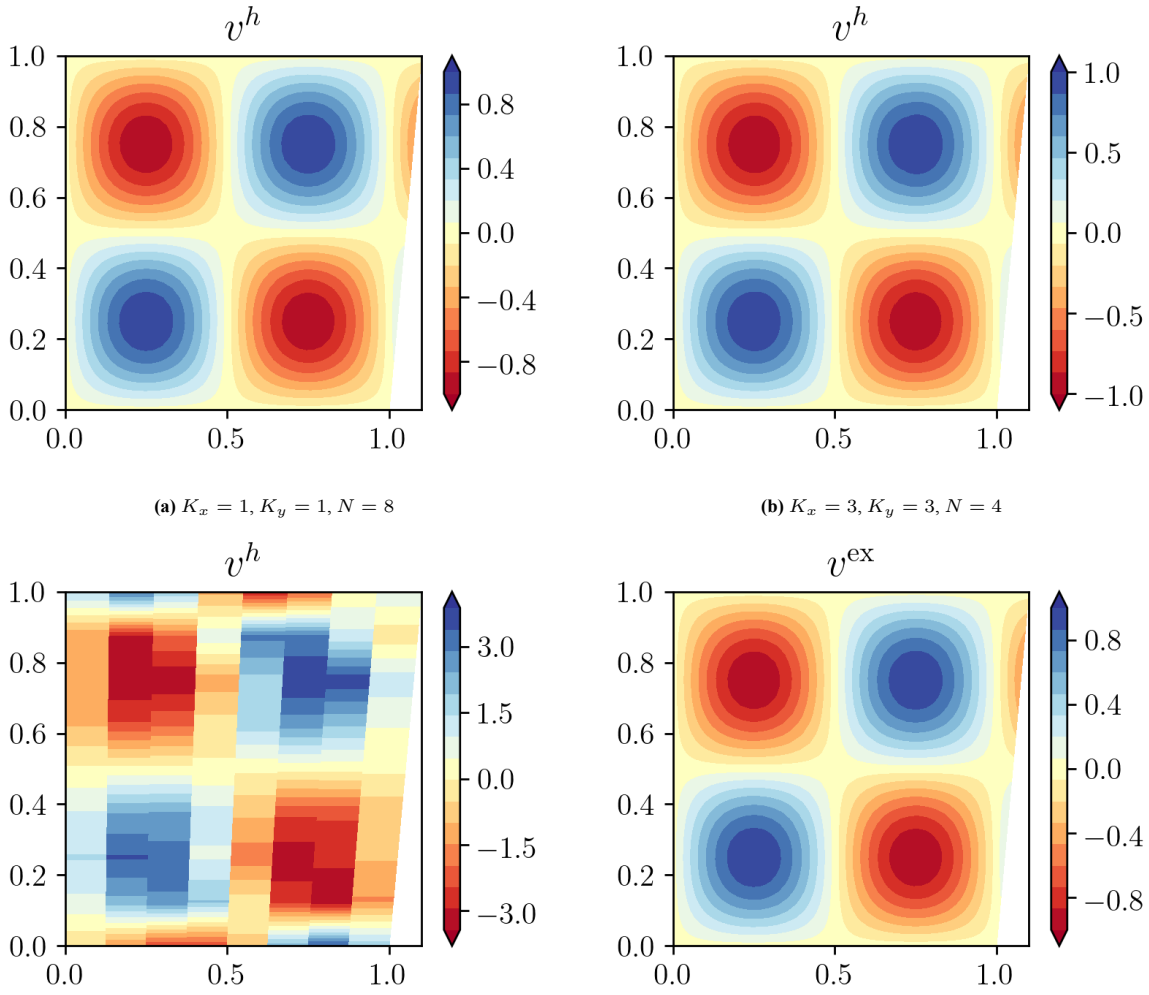

(a) $K_x = 1, K_y = 1, N = 8$

(b) $K_x = 3, K_y = 3, N = 4$

(c) $K_x = 8, K_y = 8, N = 1$

(d) Exact solution

Figure B.23: Results for v^h in the physical domain

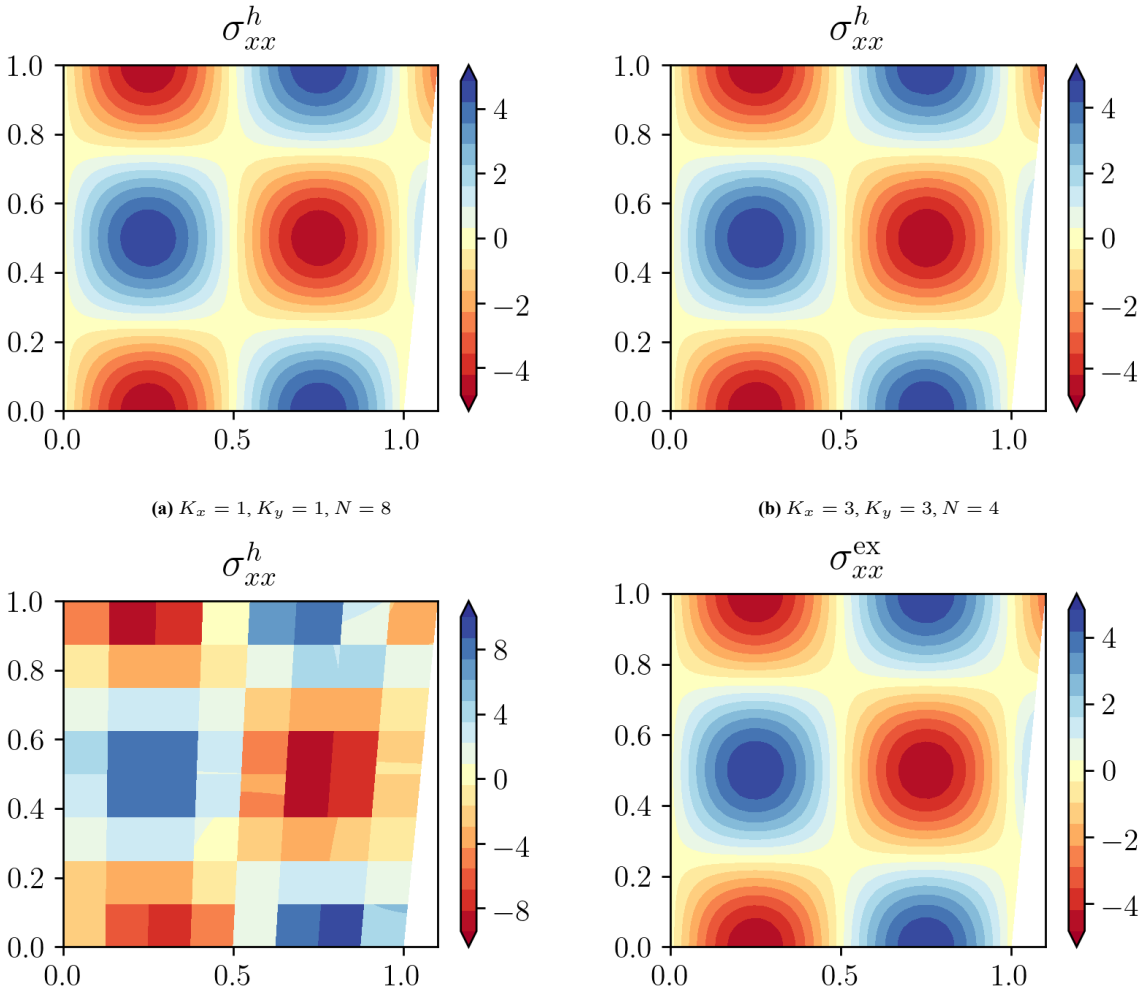

(a) $K_x = 1, K_y = 1, N = 8$

(b) $K_x = 3, K_y = 3, N = 4$

(c) $K_x = 8, K_y = 8, N = 1$

(d) Exact solution

Figure B.24: Results for σ^h_{xx} in the physical domain

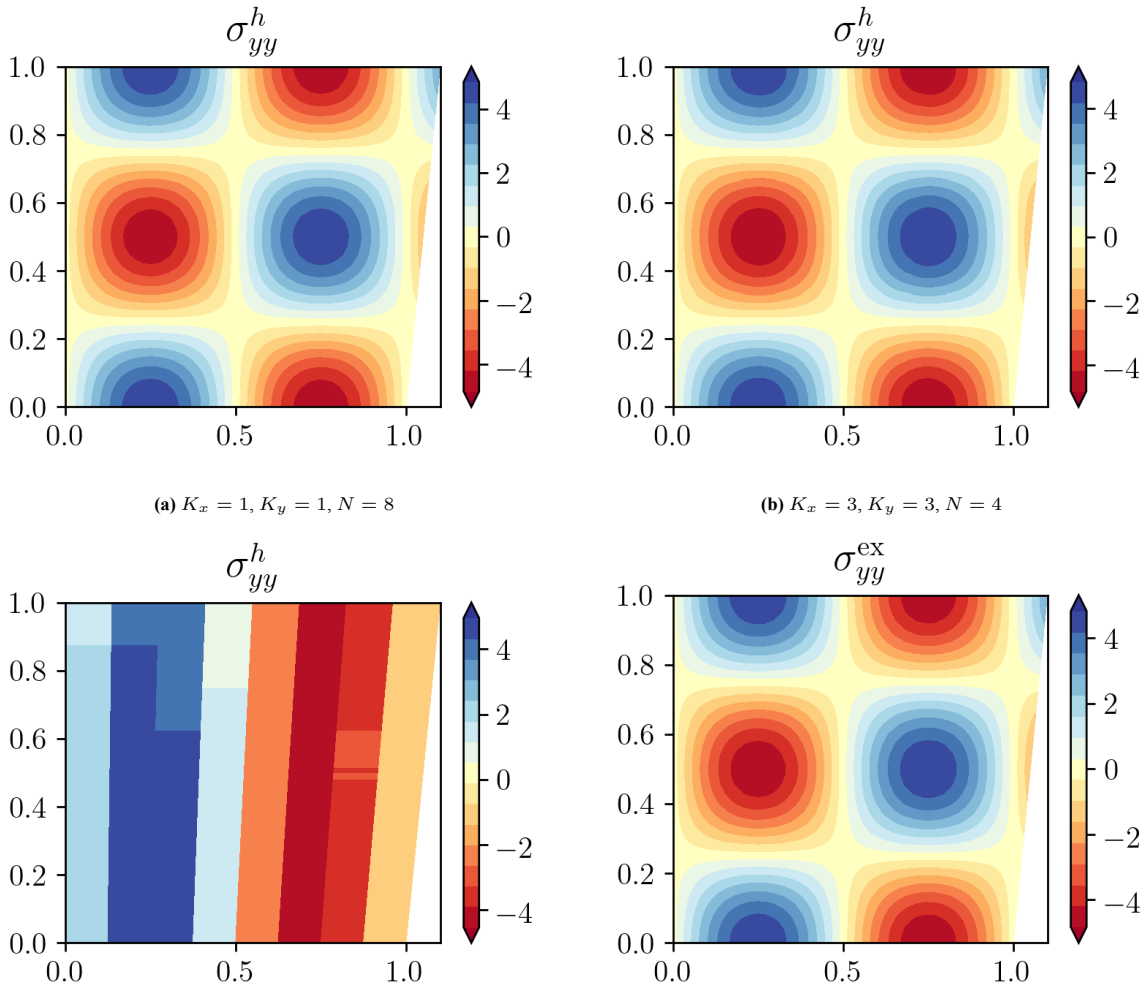

(a) $K_x = 1, K_y = 1, N = 8$

(b) $K_x = 3, K_y = 3, N = 4$

(c) $K_x = 8, K_y = 8, N = 1$

(d) Exact solution

Figure B.25: Results for σ^h_{yy} in the physical domain

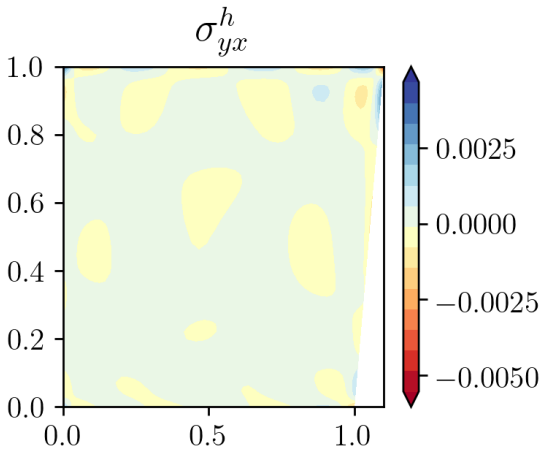

(a) σ^h_{yx} for $K_x = 1, K_y = 1, N = 8$

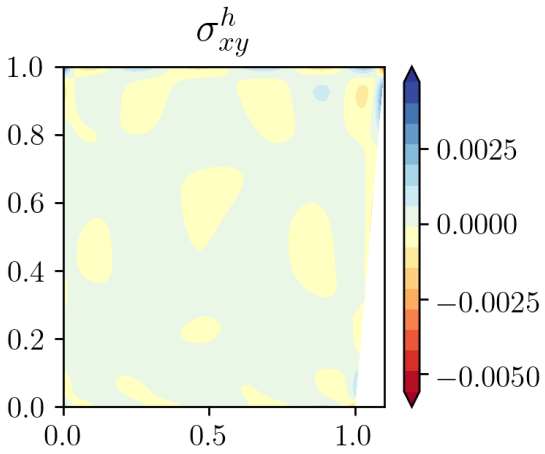

(b) σ^h_{xy} for $K_x = 1, K_y = 1, N = 8$

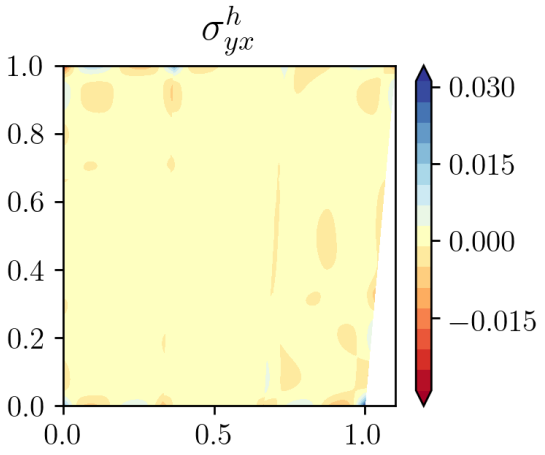

(c) σ^h_{yx} for $K_x = 3, K_y = 3, N = 4$

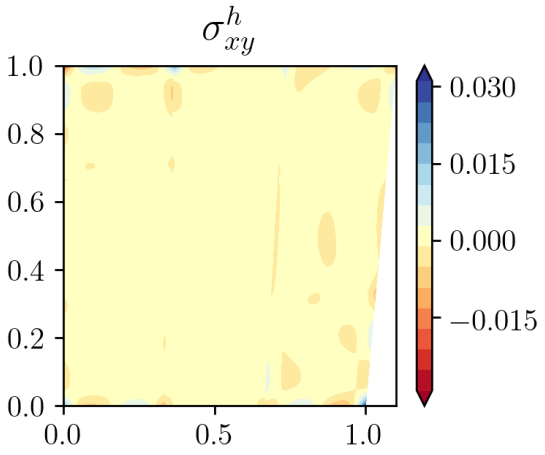

(d) σ^h_{xy} for $K_x = 3, K_y = 3, N = 4$

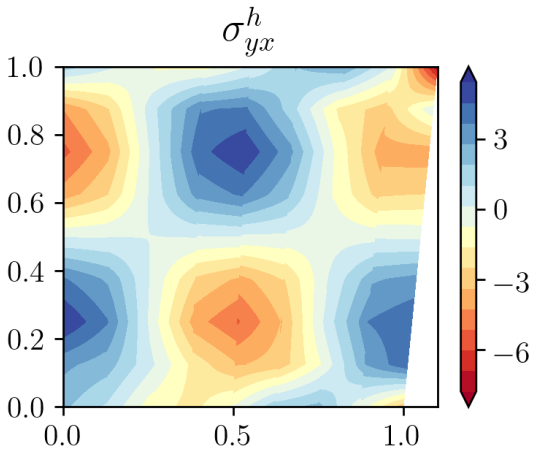

(e) σ^h_{yx} for $K_x = 8, K_y = 8, N = 1$

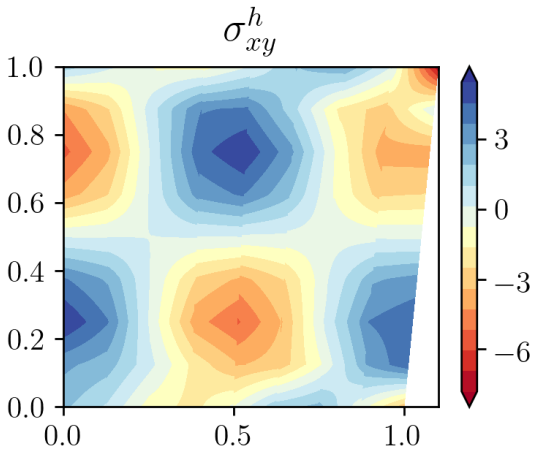

(f) σ^h_{xy} for $K_x = 8, K_y = 8, N = 1$

Figure B.26: Results for σ^h_{yx} and σ^h_{xy} in the physical domain

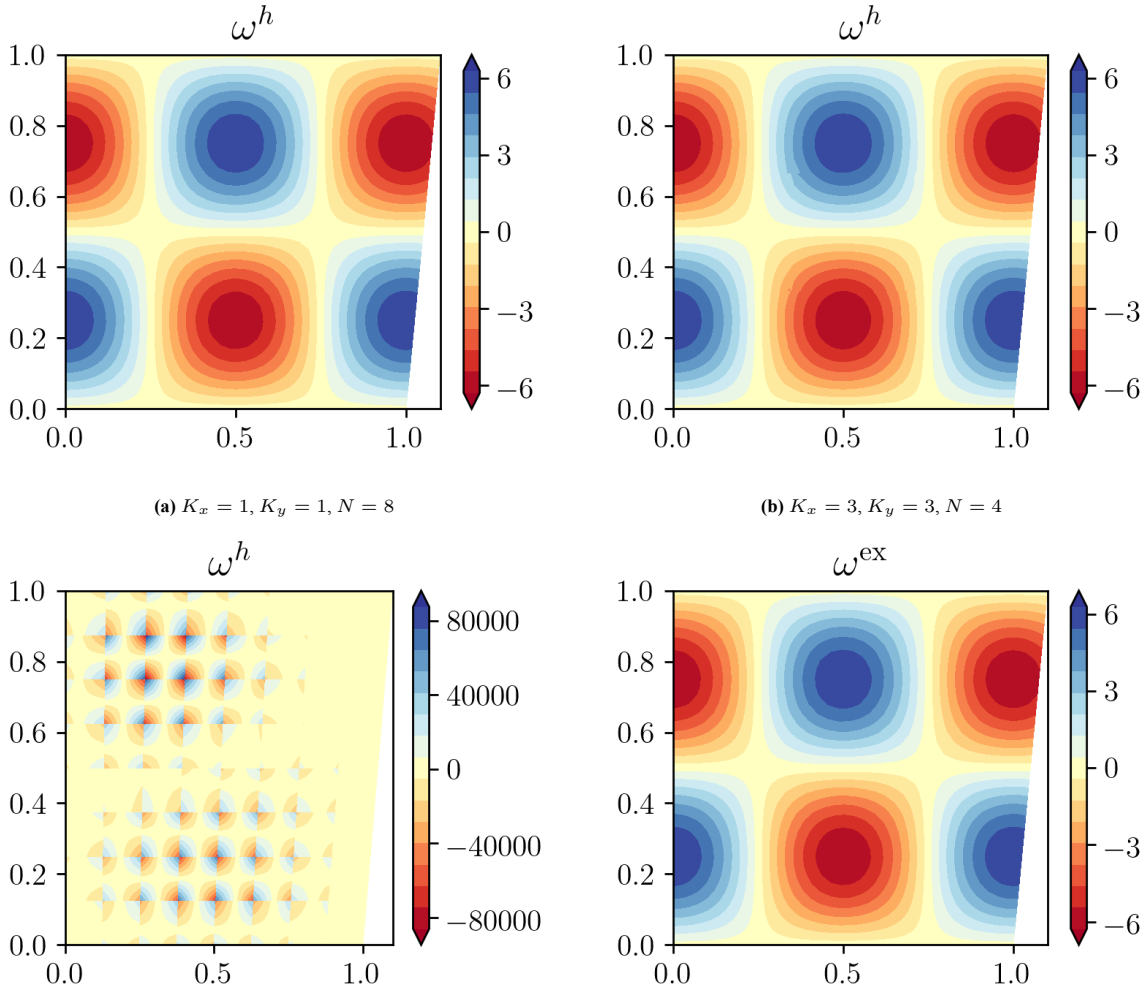

(a) $K_x = 1, K_y = 1, N = 8$

(b) $K_x = 3, K_y = 3, N = 4$

(c) $K_x = 8, K_y = 8, N = 1$

(d) Exact solution

Figure B.27: Results for ω^h in the physical domain

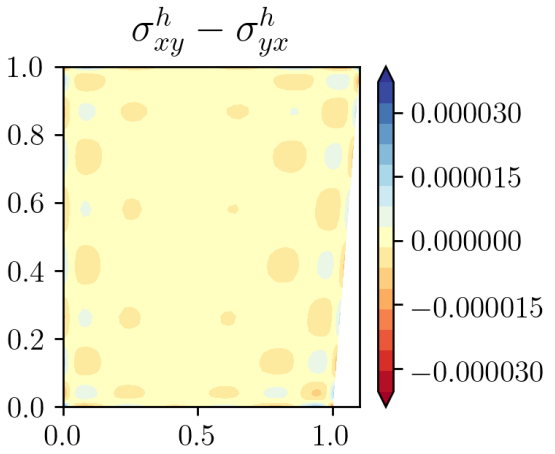

(a) $K_x = 1, K_y = 1, N = 8$

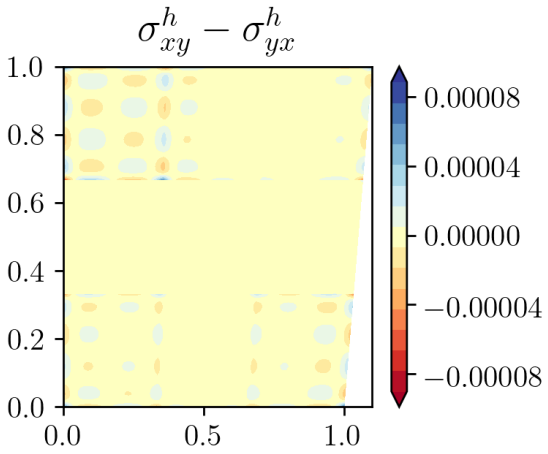

(b) $K_x = 3, K_y = 3, N = 4$

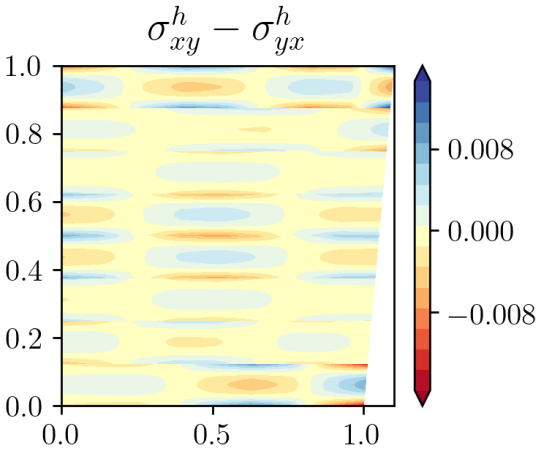

(c) $K_x = 8, K_y = 8, N = 1$

Figure B.28: Error in the symmetry of the Cauchy stress tensor

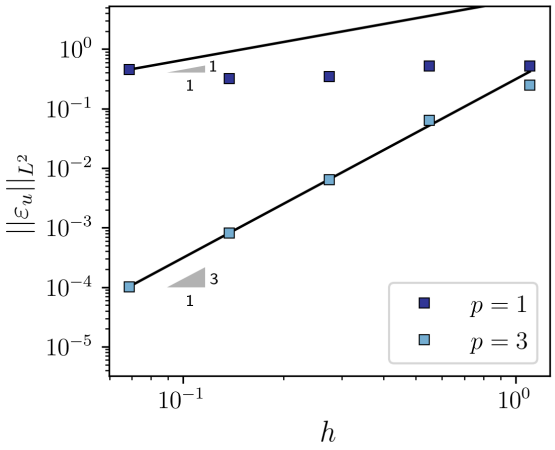

(a) Convergence with mesh width of L^2 error for u^h

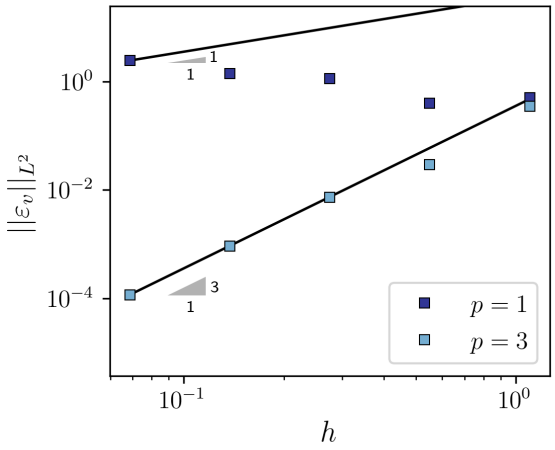

(b) Convergence with mesh width of L^2 error for v^h

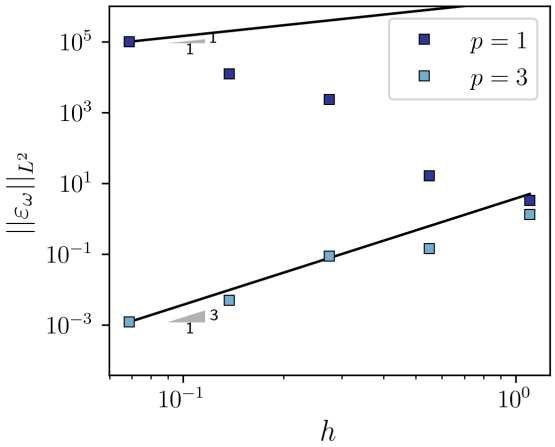

(c) Convergence with mesh width of L^2 error for ω^h

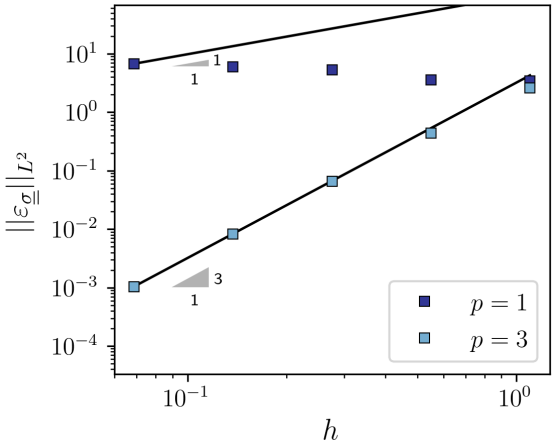

(d) Convergence with mesh width of L^2 error for $\underline{\underline{\boldsymbol{\sigma}}}^h$

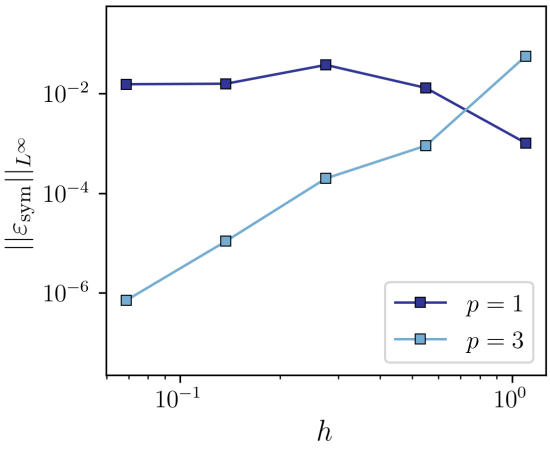

(e) Convergence with mesh width of L^∞ error for conservation of angular momentum

Figure B.29: Results from the h-convergence study

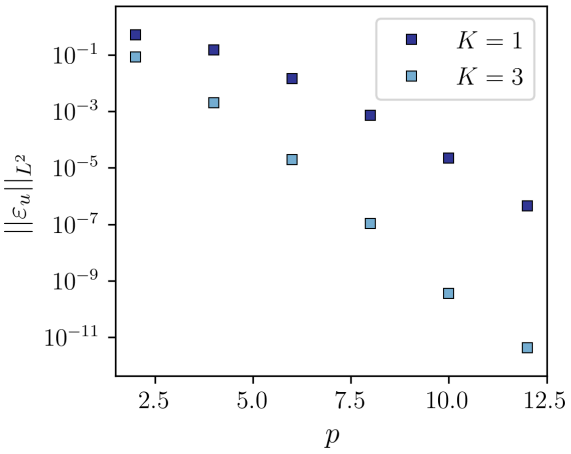

(a) L^2 error for u^h

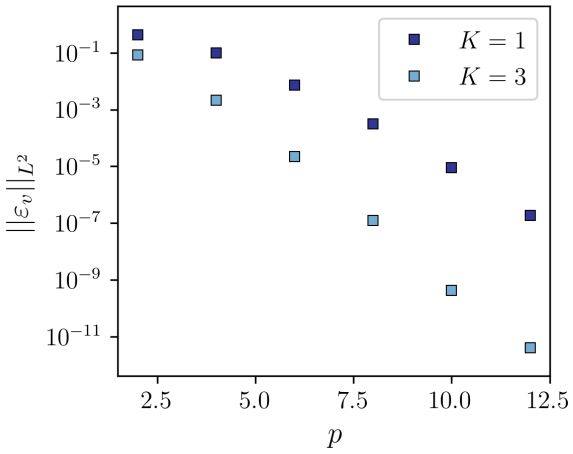

(b) L^2 error for v^h

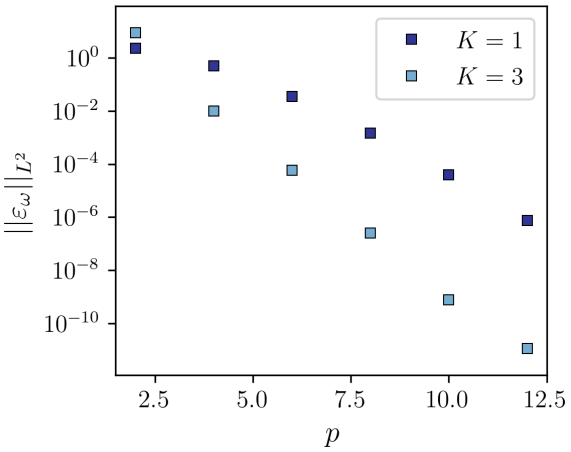

(c) L^2 error for ω^h

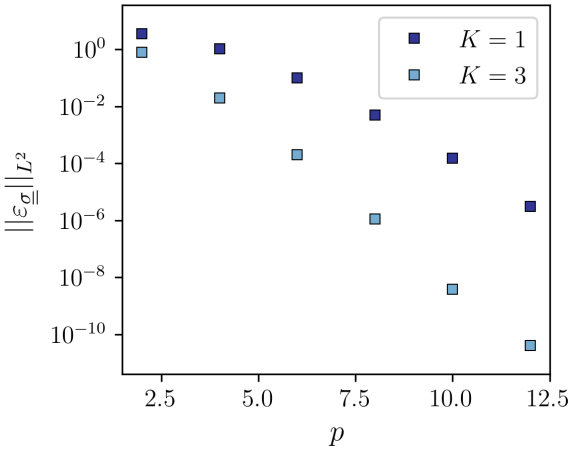

(d) L^2 error for $\underline{\underline{\boldsymbol{\sigma}}}^h$

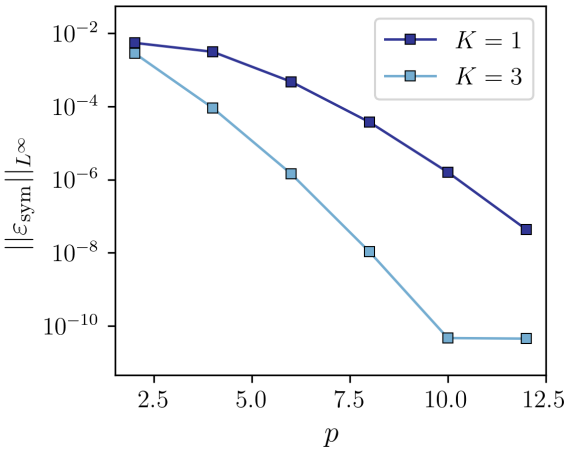

(e) L^∞ error in conservation of angular momentum

Figure B.30: Results from the polynomial convergence study

B.4. Completely transformed formulation

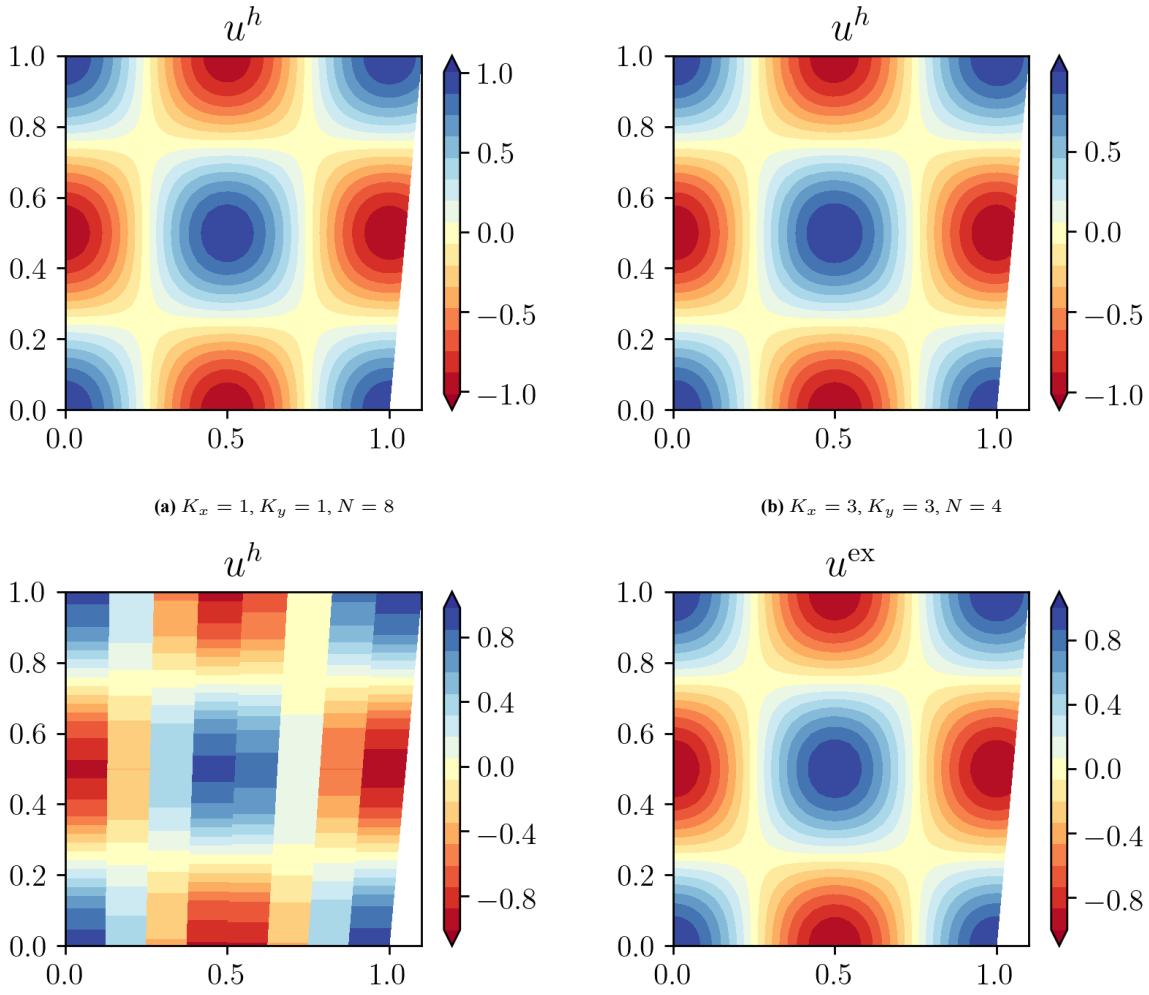

(a) $K_x = 1, K_y = 1, N = 8$

(b) $K_x = 3, K_y = 3, N = 4$

(c) $K_x = 8, K_y = 8, N = 1$

(d) Exact solution

Figure B.31: Results for u^h in the physical domain

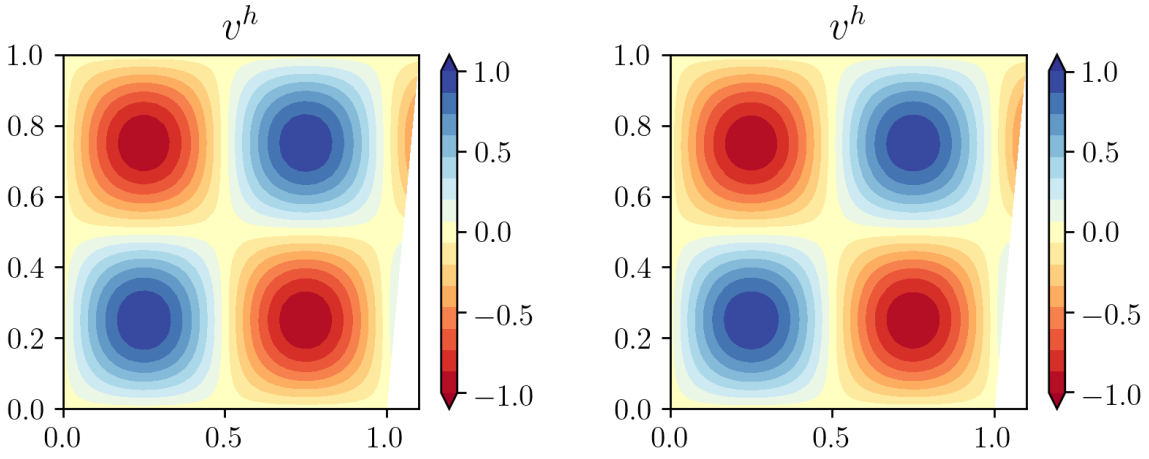

(a) $K_x = 1, K_y = 1, N = 8$

(b) $K_x = 3, K_y = 3, N = 4$

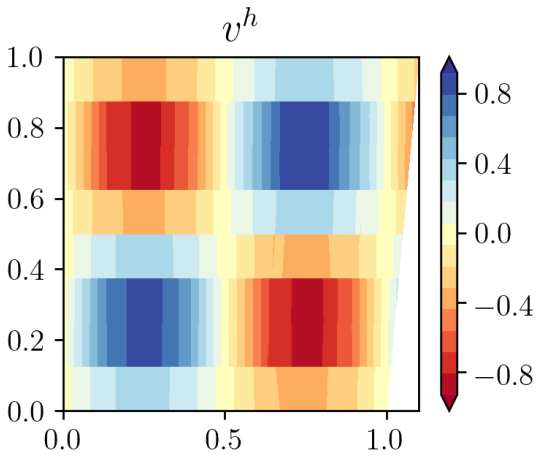

(c) $K_x = 8, K_y = 8, N = 1$

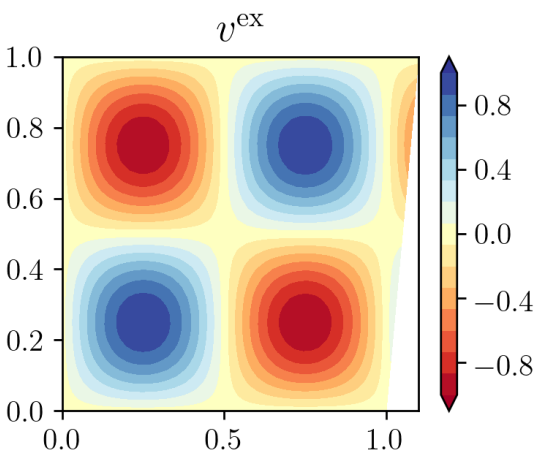

(d) Exact solution

Figure B.32: Results for v^h in the physical domain

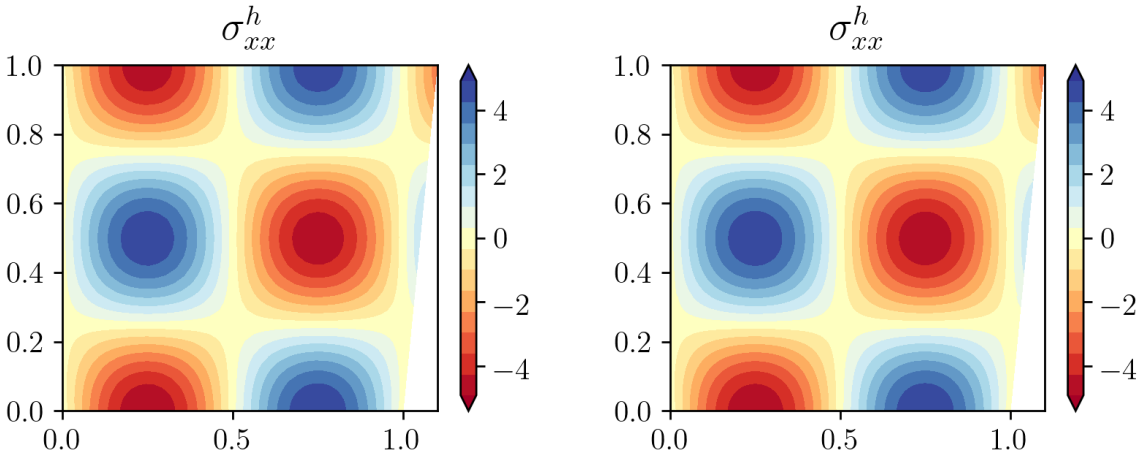

(a) $K_x = 1, K_y = 1, N = 8$

(b) $K_x = 3, K_y = 3, N = 4$

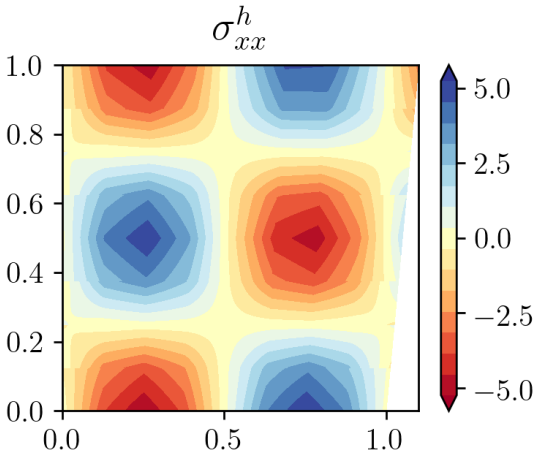

(c) $K_x = 8, K_y = 8, N = 1$

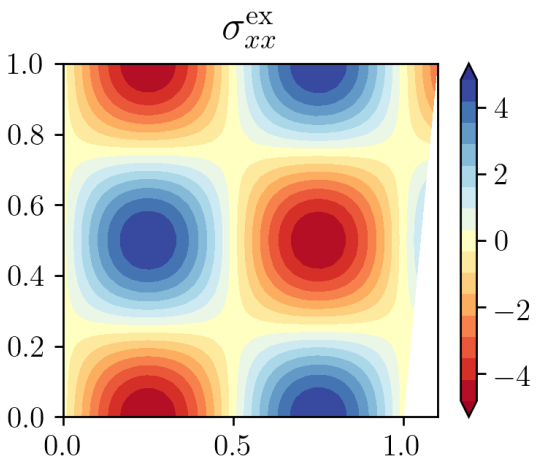

(d) Exact solution

Figure B.33: Results for σ^h_{xx} in the physical domain

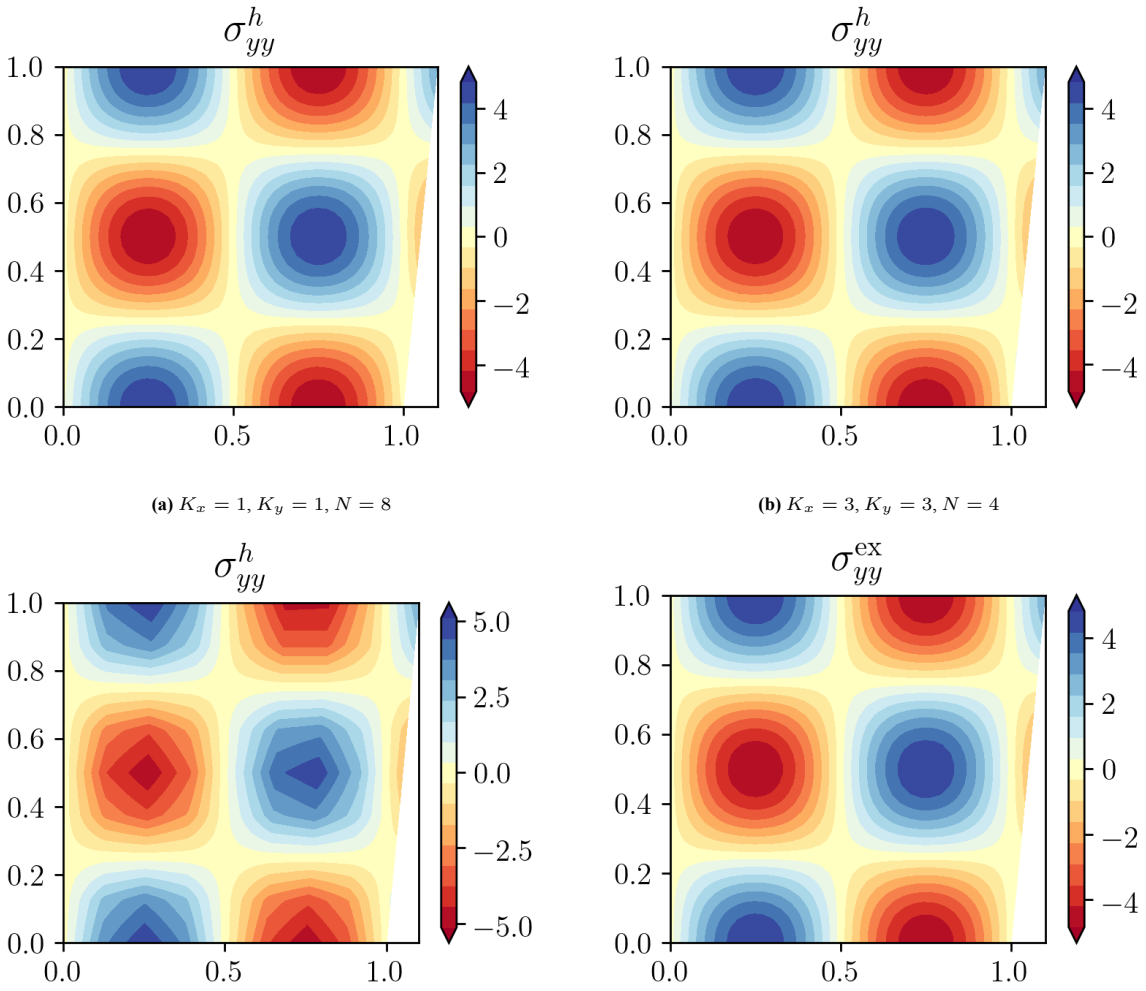

(a) $K_x = 1, K_y = 1, N = 8$

(b) $K_x = 3, K_y = 3, N = 4$

(c) $K_x = 8, K_y = 8, N = 1$

(d) Exact solution

Figure B.34: Results for σ^h_{yy} in the physical domain

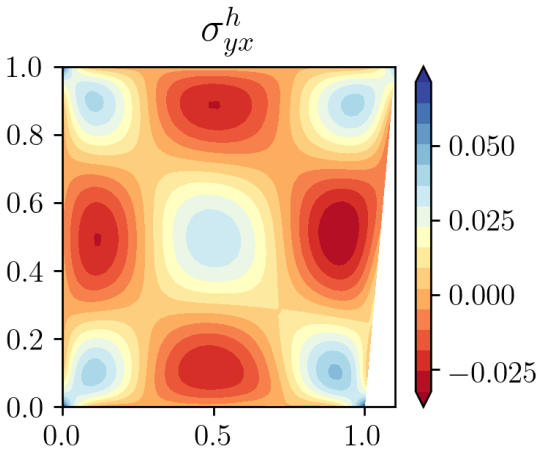

(a) σ^h_{yx} for $K_x = 1, K_y = 1, N = 8$

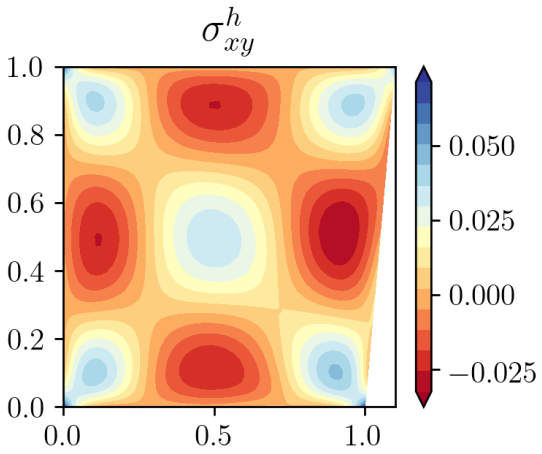

(b) σ^h_{xy} for $K_x = 1, K_y = 1, N = 8$

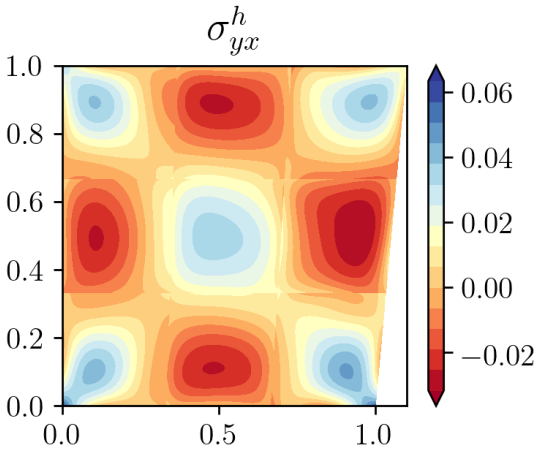

(c) σ^h_{yx} for $K_x = 3, K_y = 3, N = 4$

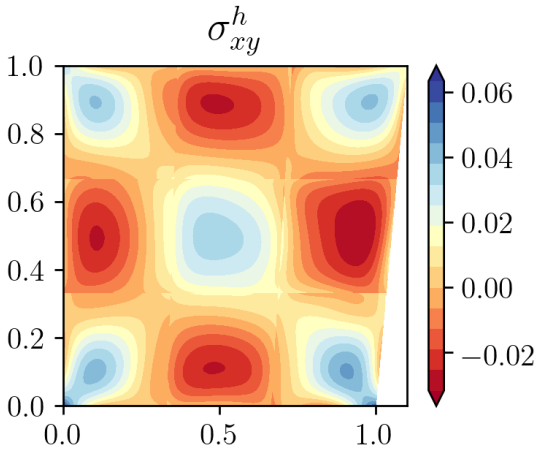

(d) σ^h_{xy} for $K_x = 3, K_y = 3, N = 4$

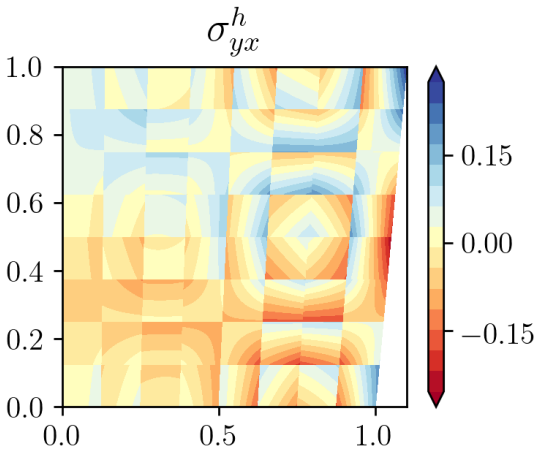

(e) σ^h_{yx} for $K_x = 8, K_y = 8, N = 1$

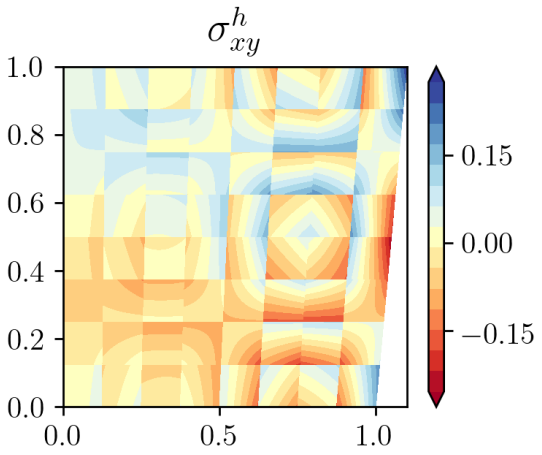

(f) σ^h_{xy} for $K_x = 8, K_y = 8, N = 1$

Figure B.35: Results for σ^h_{xy} and σ^h_{yx} in the physical domain

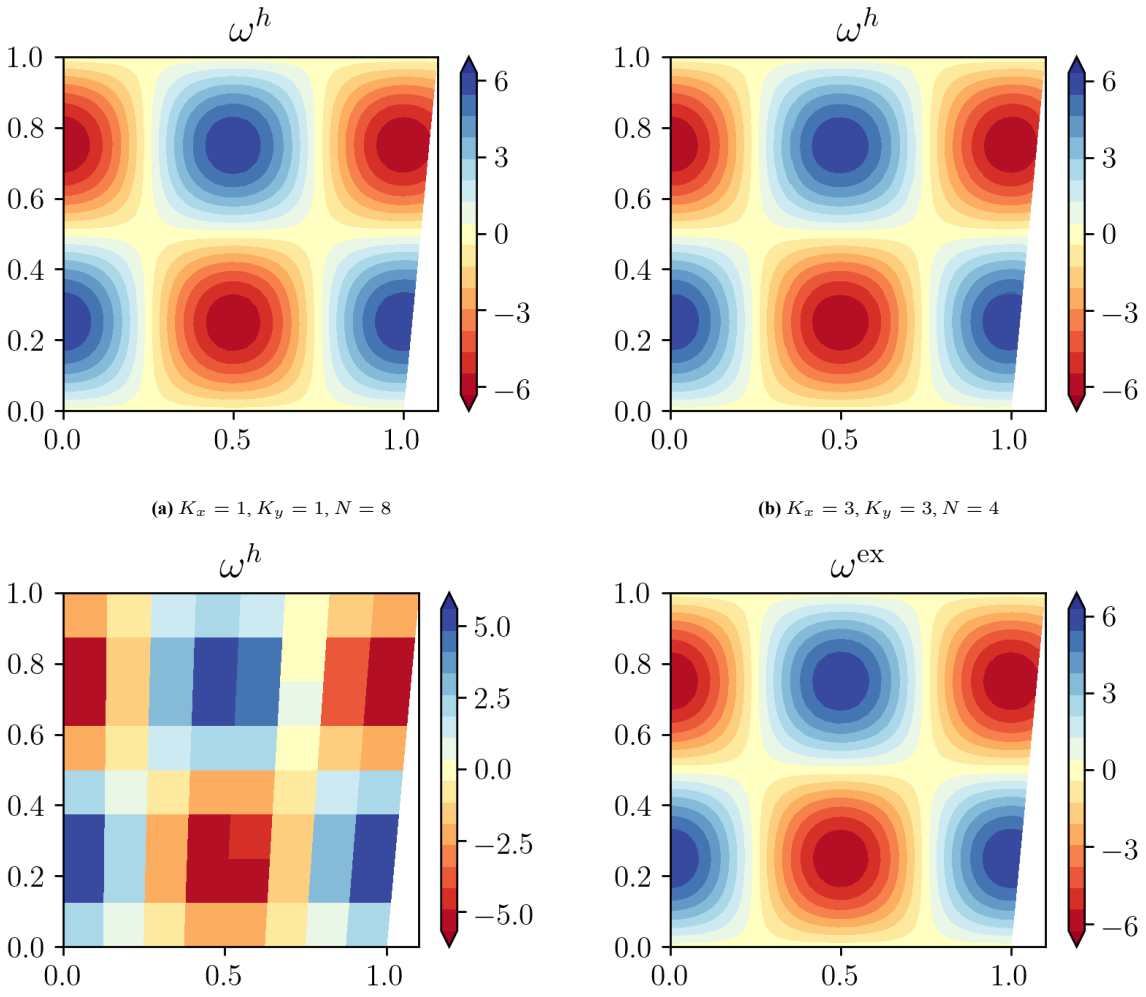

(a) $K_x = 1, K_y = 1, N = 8$

(b) $K_x = 3, K_y = 3, N = 4$

(c) $K_x = 8, K_y = 8, N = 1$

(d) Exact solution

Figure B.36: Results for ω^h in the physical domain

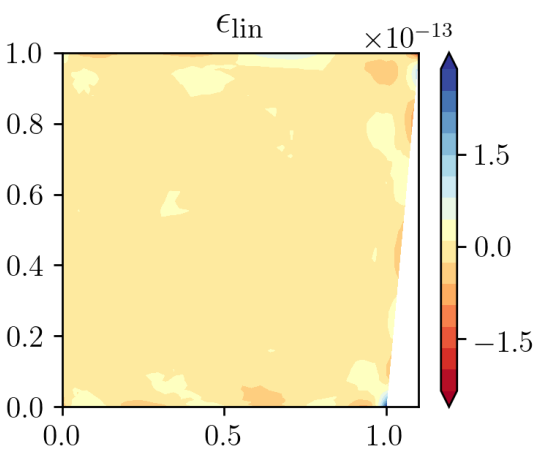

(a) Error in equilibrium of forces for $K_x = 1$, $K_y = 1$, $N = 8$

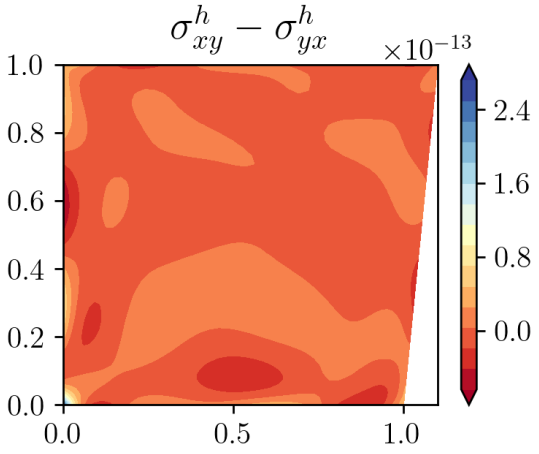

(b) $\sigma^h_{xy} - \sigma^h_{yx}$ for $K_x = 1$, $K_y = 1$, $N = 8$

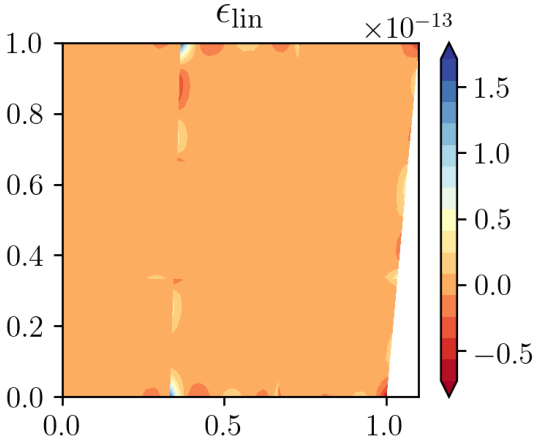

(c) Error in equilibrium of forces for $K_x = 3$, $K_y = 3$, $N = 4$

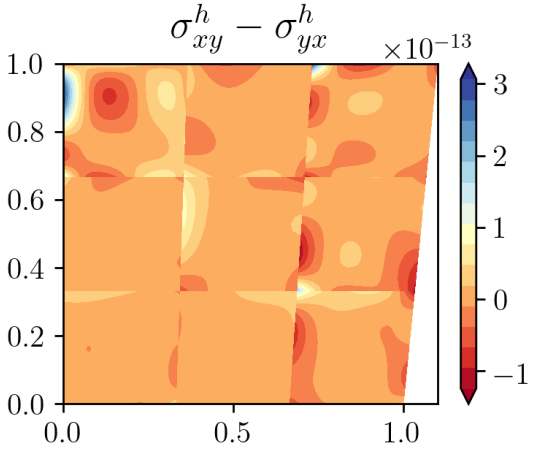

(d) $\sigma^h_{xy} - \sigma^h_{yx}$ for $K_x = 3$, $K_y = 3$, $N = 4$

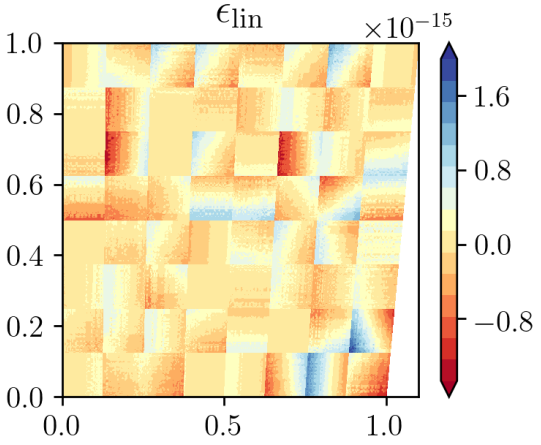

(e) Error in equilibrium of forces for $K_x = 8$, $K_y = 8$, $N = 1$

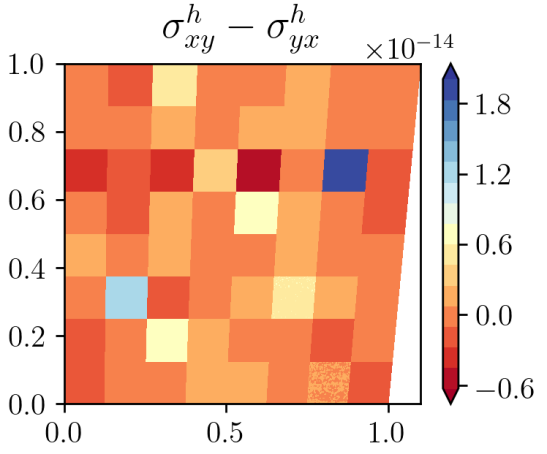

(f) $\sigma^h_{xy} - \sigma^h_{yx}$ for $K_x = 8$, $K_y = 8$, $N = 1$

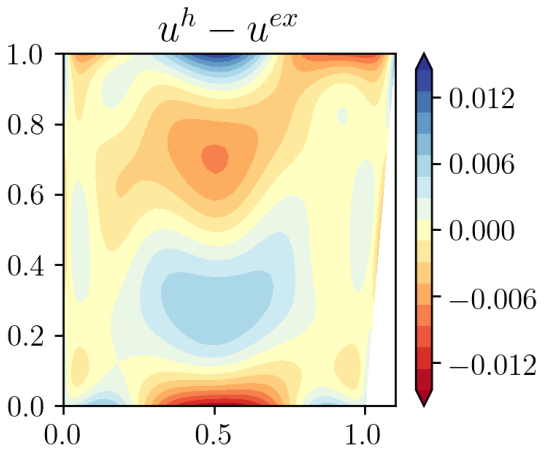

(a) $u_x^h - u_x^{ex}$ for $K_x = 1, K_y = 1, N = 8$

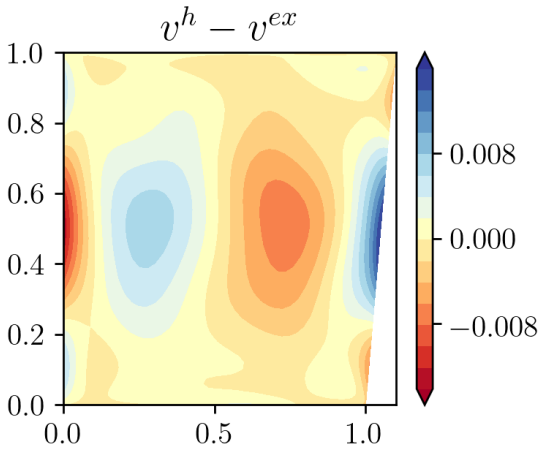

(b) $u_y^h - u_y^{ex}$ for $K_x = 1, K_y = 1, N = 8$

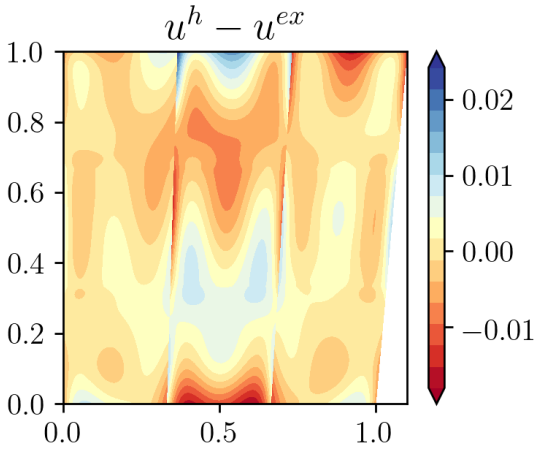

(c) $u_x^h - u_x^{ex}$ for $K_x = 3, K_y = 3, N = 4$

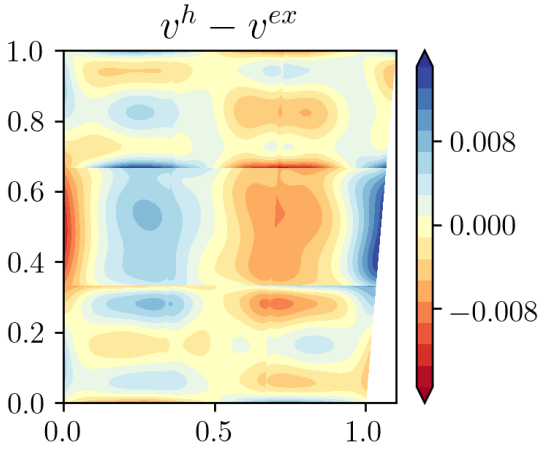

(d) $u_y^h - u_y^{ex}$ for $K_x = 3, K_y = 3, N = 4$

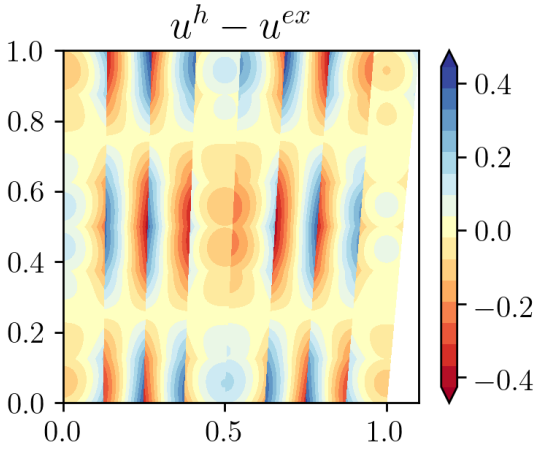

(e) $u_x^h - u_x^{ex}$ for $K_x = 8, K_y = 8, N = 1$

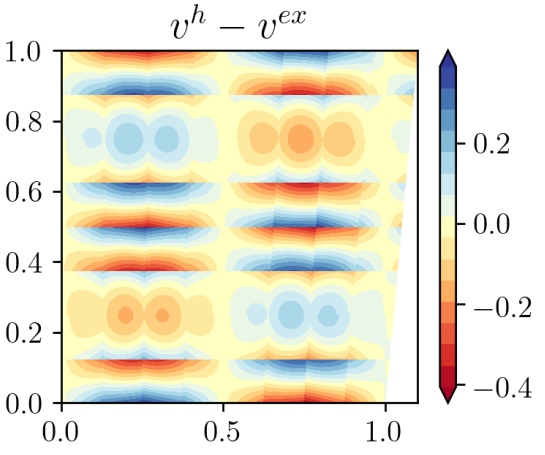

(f) $u_y^h - u_y^{ex}$ for $K_x = 8, K_y = 8, N = 1$

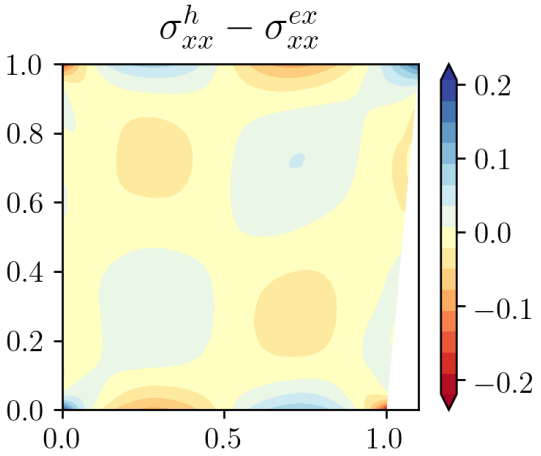

(a) $\sigma^h_{xx} - \sigma^{ex}_{xx}$ for $K_x = 1, K_y = 1, N = 8$

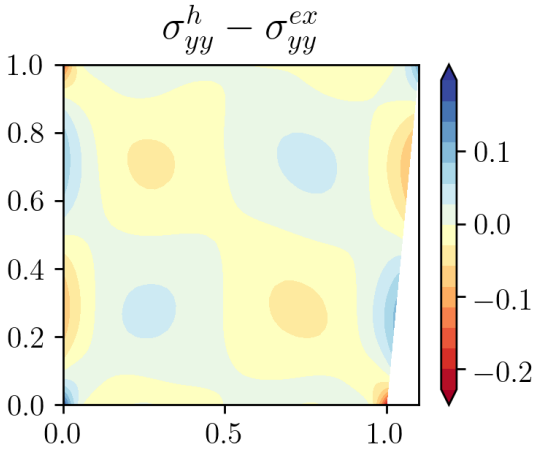

(b) $\sigma^h_{yy} - \sigma^{ex}_{yy}$ for $K_x = 1, K_y = 1, N = 8$

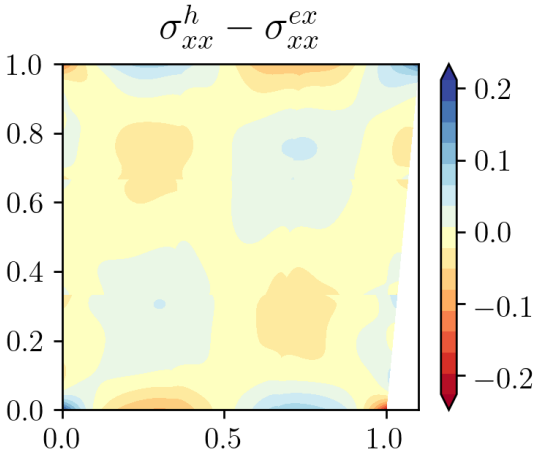

(c) $\sigma^h_{xx} - \sigma^{ex}_{xx}$ for $K_x = 3, K_y = 3, N = 4$

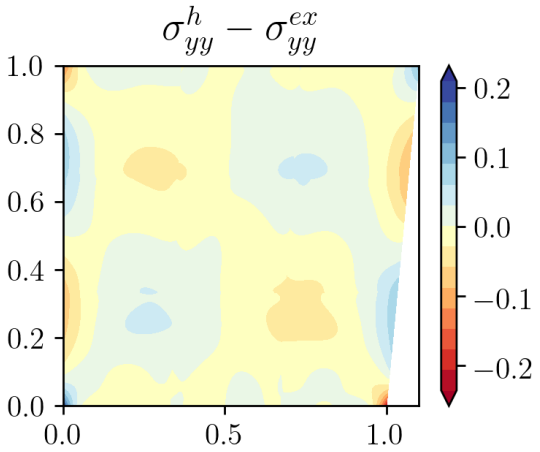

(d) $\sigma^h_{yy} - \sigma^{ex}_{yy}$ for $K_x = 3, K_y = 3, N = 4$

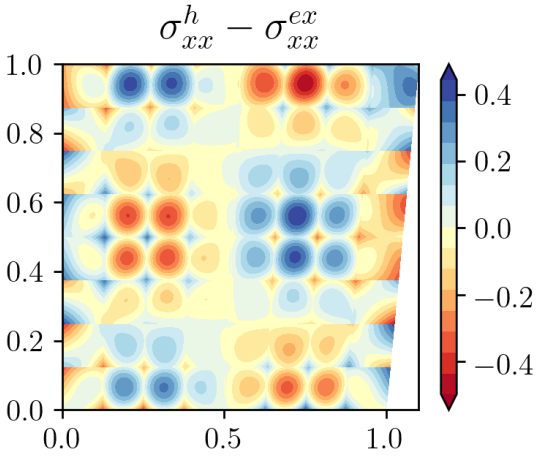

(e) $\sigma^h_{xx} - \sigma^{ex}_{xx}$ for $K_x = 8, K_y = 8, N = 1$

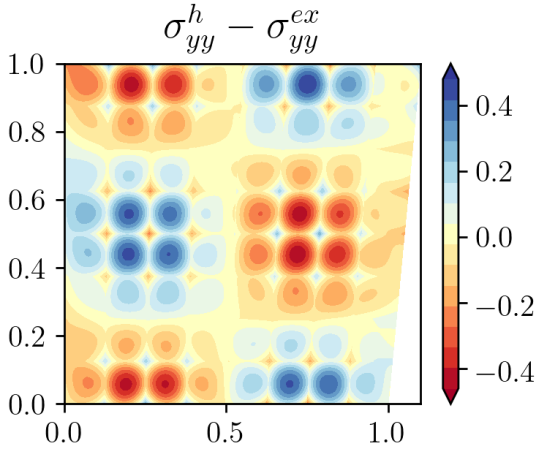

(f) $\sigma^h_{yy} - \sigma^{ex}_{yy}$ for $K_x = 8, K_y = 8, N = 1$

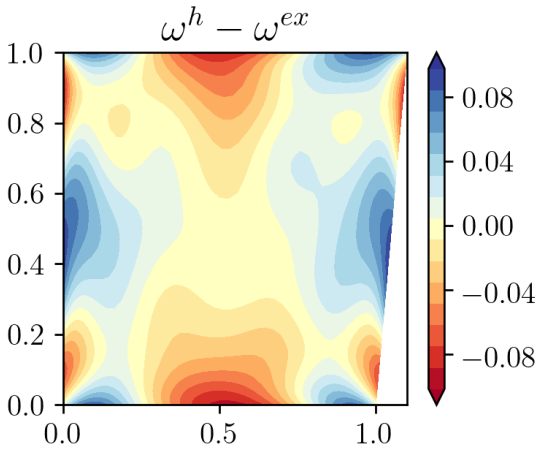

(a) $\omega^h - \omega^{ex}$ for $K_x = 1, K_y = 1, N = 8$

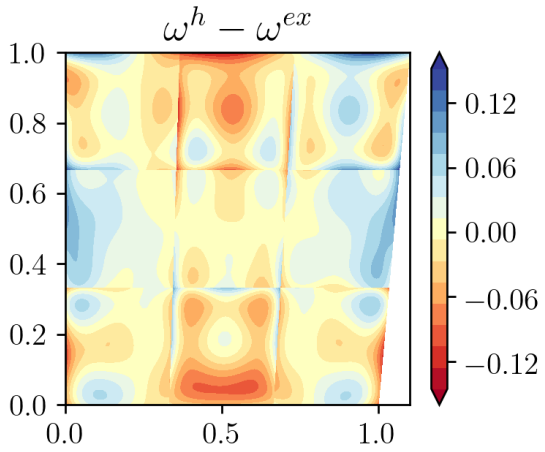

(b) $\omega^h - \omega^{ex}$ for $K_x = 3, K_y = 3, N = 4$

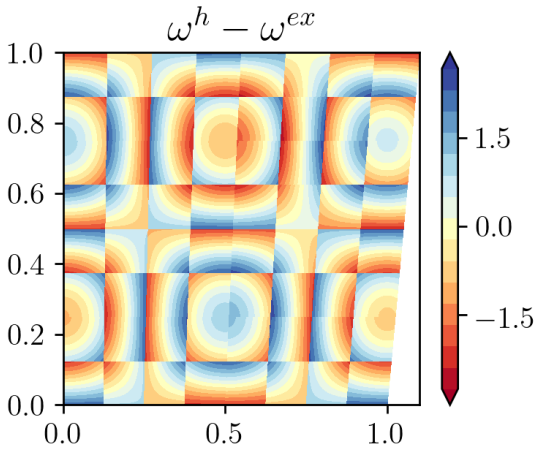

(c) $\omega^h - \omega^{ex}$ for $K_x = 8, K_y = 8, N = 1$

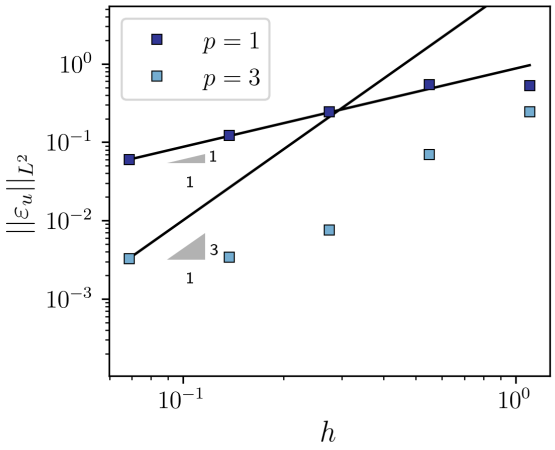

(a) Convergence with mesh width of L^2 error for u^h

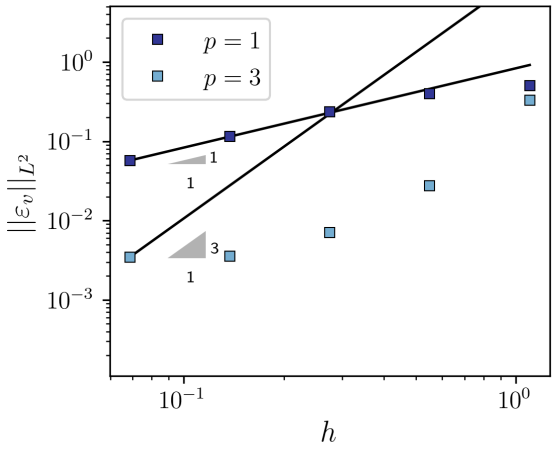

(b) Convergence with mesh width of L^2 error for v^h

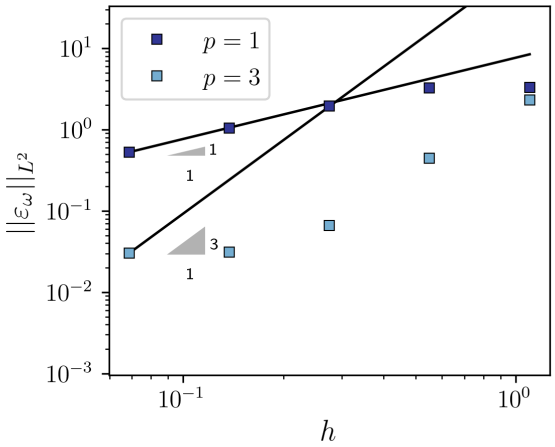

(c) Convergence with mesh width of L^2 error for ω^h

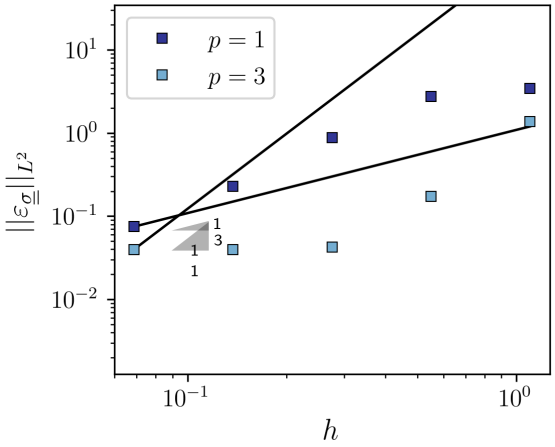

(d) Convergence with mesh width of L^2 error for $\underline{\underline{\boldsymbol{\sigma}}}^h$

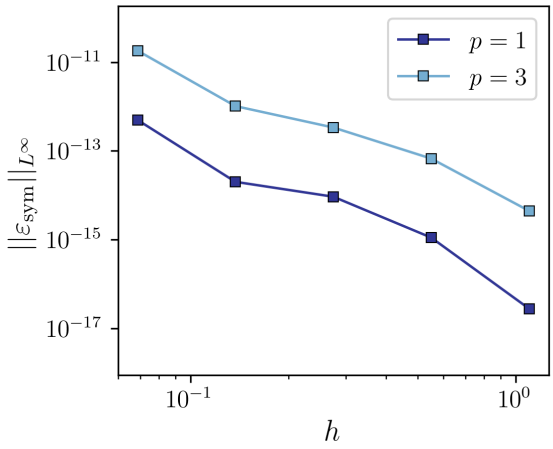

(e) Convergence with mesh width of L^∞ error for conservation of angular momentum

Figure B.41: Results from the h-convergence study

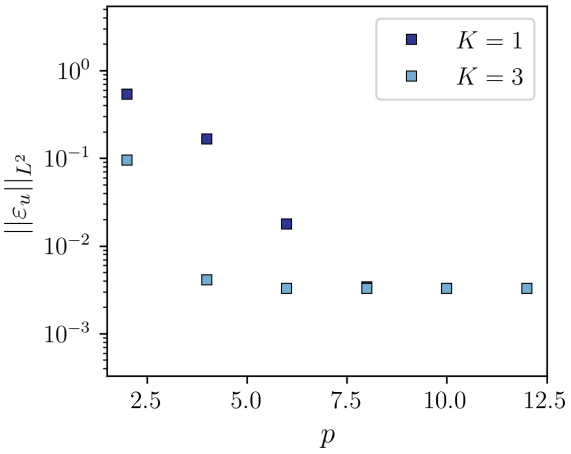

(a) L^2 error for u^h

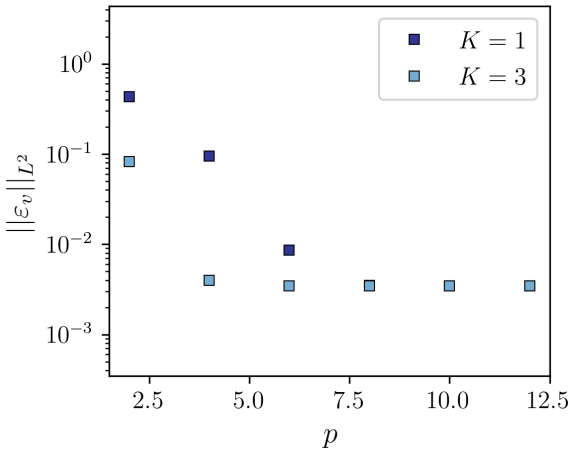

(b) L^2 error for v^h

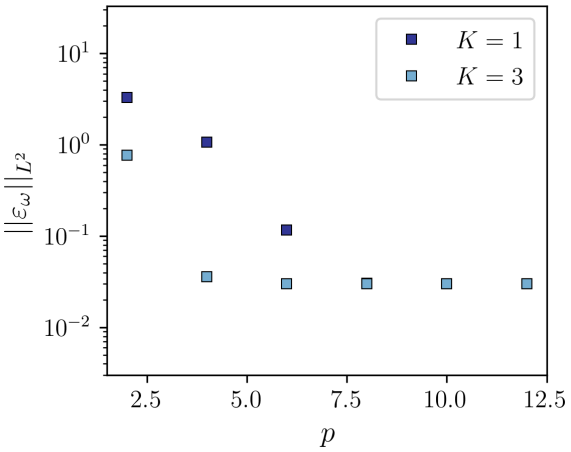

(c) L^2 error for ω^h

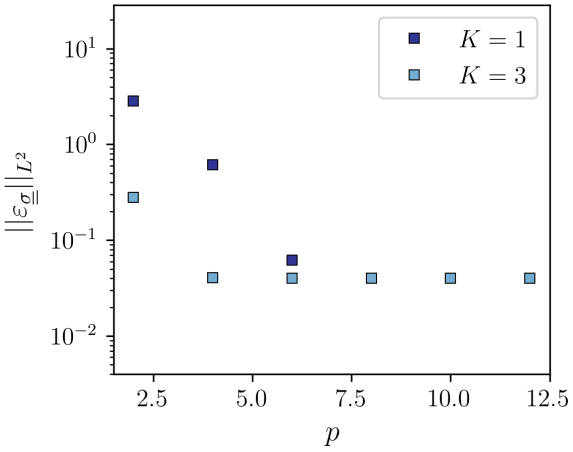

(d) L^2 error for $\underline{\underline{\boldsymbol{\sigma}}}^h$

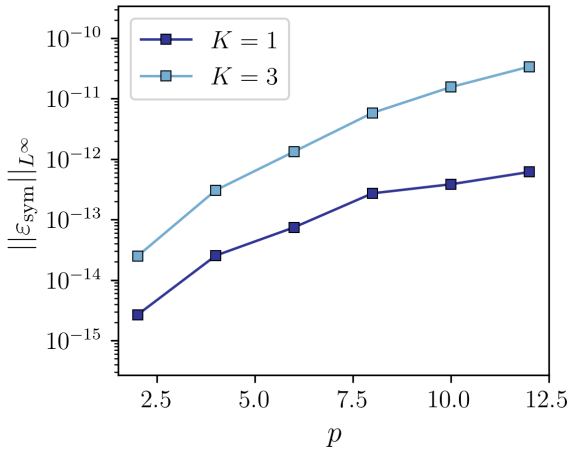

(e) L^∞ error in conservation of angular momentum

Figure B.42: Results from the polynomial convergence study